
UNIVERSITY OF BIRMINGHAM

# EVALUATION OF THE SEABED TEMPERATURE CORROSION AND SULPHIDE STRESS CRACKING (SSC) RESISTANCE OF WELDABLE MARTENSITIC 13% CHROMIUM STAINLESS STEEL (WMSS)

**By**

**Philip Nigel Dent**
**893319**

**A thesis submitted to the**
**University of Birmingham**
**for the degree of**
**MASTER OF PHILOSOPHY (MPhil)**

Metallurgy and Materials
College of Engineering and
Physical Science
University of Birmingham
February 2014

# ABSTRACT

Weldable martensitic 13% Chromium Stainless Steels (WMSSs) are used for mildly sour welded flow lines in the oil and gas industry, as an alternative to inhibited carbon steel or lined pipe. For most material selection and qualification programmes for sour applications the material is tested in accordance with NACE MR0175 / ISO 15156-1 [1] at the maximum design temperature and at ambient temperature (i.e. 24 ± 3°C). A testing programme conducted by Exova [2] in 2005 indicated that the material could be more susceptible to cracking at temperatures below ambient temperature. Consequently qualification to the requirements of NACE MR0175 / ISO 15156-3 [3] may show acceptable results, whereas in service cracking could occur, due to exposure to temperatures below ambient. This may not be relevant for all applications, however for sub-sea pipelines the typical sea-bed temperature is in the region of 5°C and therefore the material could be exposed to these low temperature conditions.

Sulphide Stress Cracking (SSC) and electrochemical testing has been undertaken on parent grade LC80-130S (API 5CT [4]) weldable martensitic 13% chromium stainless steel (WMSS) pipe, supplied by Nippon Steel & Sumitomo Metal Corporation (NSSMC). SSC tests have been conducted at the ambient (24°C) and at seabed (5°C) temperatures in condensed water (CW) and produced water (PW) solutions with 35 mbara $H_2S$ and 69 mbara $H_2S$ (PW only) with specimens in the as-received and 600 SiC ground conditions. In addition corrosion potential measurements and anodic potentiodynamic polarisation scans have been carried out to correlate the SSC behaviour with the passivity of the material.

In the PW environment the material was found to be more susceptible to SSC at 5°C compared to ambient temperature and the cracking performance was influenced by the surface condition; with the 600 grit SiC ground surface having a detrimental effect on the SSC resistance.

The electrochemical investigations did not reveal a correlation between the passivity of the material and the increased cracking susceptibility at 5°C, although differences in the electrochemical behaviour between the as-received and 600 SiC ground surfaces were observed.

# ACKNOWLEDGEMENTS

I would like to thank Exova plc. for their financial support and for the use of the laboratory facilities at Exova Corrosion Centre for the experimental work. I am also grateful to Nippon Steel & Sumitomo Corporation (NSSMC) for providing the test material and in particular to Dr. Amaya and to Dr. Takabe from NSSMC for their support.

I am grateful for the support, guidance and patience of my academic supervisor Dr. Brian Connolly and my industrial mentor at Exova Dr. Chris Fowler.

I would also like to thank the Department of Metallurgy & Materials at the University of Birmingham for the use of their laboratory facilities and to Dr. Chris Cooper, from the University of Birmingham and Matthew Walters, formerly of Exova, for their assistance with the experimental work.

# Contents

## Chapter 1: Introduction



## Chapter 2: Literature Review

## Chapter 6: Results & Discussion; SSC Testing



## Chapter 7: Results & Discussion; Electrochemical Testing

# List of Figures

# List of Tables

# List of Abbreviations

| | |
|---|---|
| α | Ferrite |
| $\alpha^{-}$ | Martensite |
| AFM | Atomic Force Microscopy |
| API | American Petroleum institute |
| AYS | Actual Yield Strength |
| bct | body centred tetragonal |
| C | Carbon |
| $CH_3COOH$ | Acetic acid |
| $CH_3COONa$ | Sodium acetate |
| $Cl^-$ | Chloride ion |
| $CO_2$ | Carbon Dioxide |
| CP | Cathodic Protection |
| Cr | Chromium |
| CRAs | Corrosion Resistant Alloys |
| Cu | Copper |
| CW | Condensed Water |
| CSSRT | Cyclic Slow Strain rate Test |
| DBTT | Ductile-Brittle Transition Temperature |
| DCB | Double Cantilever Beam |
| DL-EPR | Double loop Electrochemical Potentiokinetic Reactivation |
| DOS | Degree of Sensitisation |
| E | Modulus of Elasticity |
| ε | Strain |
| $E_{bd}$ | Break-down or Pitting Potential |
| $E_{corr}$ | Corrosion Potential |
| EDSD | Electron Back Scattered Diffraction |
| EFC | European Federation of Corrosion |
| FPB | Four Point Bent |
| fcc | face centred cubic |
| FFS | Fitness for Service |
| FW | Formation Water |
| γ | Austenite |
| $H_2S$ | Hydrogen Sulphide |
| $H_2SO_4$ | Sulphuric Acid |
| HAZ | Heat Affected Zone |
| HCl | Hydrochloric acid |
| HF | Hydrofluoric acid |
| HIC | Hydrogen Induced Cracking |
| HISC | Hydrogen Induced Stress Cracking |
| $HNO_3$ | Nitric Acid |
| HRc | Rockwell C Hardness |
| Hv | Vickers Hardness |
| IGC | Intergranular Corrosion |
| IGSCC | Intergranular Stress Corrosion Cracking |
| $i_{pass}$ | Passive Current Density |
| ISO | International Standards Organisation |
| $K_{ISCC}$ | Stress Intensity Factor for SCC |
| KSCN | Potassium Thiocyanate |
| LPR | Linear Polarisation Resistance |
| Mo | Molybdenum |
| MPhil | Master of Philosophy |
| $M_s$ | Martensite start temperature |
| $N_2$ | Nitrogen gas |

| | |
|---|---|
| NaCl | Sodium chloride |
| Nb | Niobium |
| $NH_4CNS$ | Ammonium Thiocyanate |
| Ni | Nickel |
| NPL | National Physical Laboratory |
| NSSMC | Nippon Steel & Sumitomo Metal Corporation |
| $O_2$ | Oxygen |
| OCP | Open Circuit Potential |
| OCTG | Oil Country Tubular Goods |
| OES | Optical Emission Spectrography |
| $pCO_2$ | Partial pressure of Carbon dioxide |
| $pH_2S$ | Partial pressure of Hydrogen Sulphide |
| PW | Produced Water |
| PWHT | Post Weld Heat Treatment |
| RDE | Rotating Disc Electrode |
| RT | Room Temperature |
| SCC | Stress Corrosion Cracking |
| SCE | Saturated Calomel Electrode |
| SEM | Scanning Electron Microscope |
| SiC | Silicon Carbide |
| SMSS | Super Martensitic Stainless Steel |
| SMYS | Specified Minimum Yield Strength |
| SOHIC | Stress Orientated Hydrogen Induced Cracking |
| Sr | Repeatability standard deviation |
| SSC | Sulphide Stress Cracking |
| SSRT | Slow Strain Rate Test |
| SZC | Soft Zone Cracking |
| TDS | Thermal Dispersion Spectroscopy |
| Ti | Titanium |
| WMSS | Weldable Martensitic Stainless Steel |
| UNS | Unified Numbering System |
| XRD | X-ray Diffraction |
| 95%CI | 95% Confidence Interval (1.96 x Sr, i.e. 2 standard deviations). |

# CHAPTER 1: INTRODUCTION

## 1.1 Background

Weldable 13%Cr martensitic stainless steels (WMSSs) are corrosion resistant alloys commonly used for welded pipelines in the oil and gas industry as an alternative to inhibited carbon steel or lined pipe. These pipelines are used for transporting sweet (carbon dioxide-containing) and mildly-sour (carbon dioxide and low levels of hydrogen sulphide) production fluids from the wellhead to the platform or on-shore. An example of an off-shore sub-sea system is shown in Figure 1.1; the pipeline is part of a fixed installation on the seabed floor that can operate at depths in excess of 1,000 meters. Down-hole tubular pipes connect the wellhead to the reservoir and are typically made of carbon steel, medium strength (80 ksi SMYS) and high strength (up to 125 ksi) non-weldable grades of martensitic stainless steels (i.e. 13%Cr, 15%Cr & 17%Cr), or other corrosion resistant alloys (CRAs). For WMSS in operating conditions, the internal pipe temperature can be as high as 130°C, but during shut-down conditions the pipe will be at the same temperature as the seabed (which can be as low as 5°C, depending on depth).

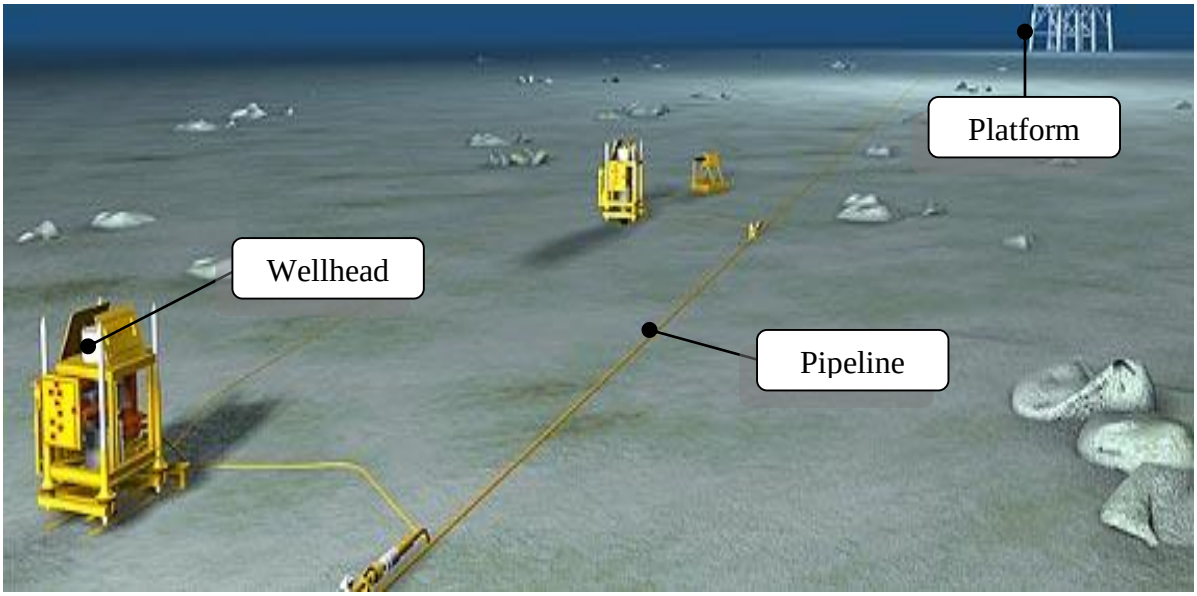


**Figure 1.1** Subsea pipelines transporting production fluids from wellheads to the oil platform [5]

## 1.2 Industrial Problem

Weldable 13%Cr martensitic stainless steel (WMSS) has experienced reported service-related problems due to external hydrogen induced stress cracking (HISC) and elevated temperature (i.e. >65°C) internal intergranular stress corrosion cracking (IGSCC) in the vicinity of seam and girth welds. In addition the material can be susceptible to pitting, at low and elevated temperatures and low temperature (i.e. <65°C) sulphide stress cracking (SSC).

As a result of the service-related problems developments in the processing of the material and the installation have been implemented, in particular to prevent HISC by cathodic protection (CP) control and to prevent 'sensitised' intergranular stress corrosion cracking (IGSSC) by post weld heat treatment (PWHT).

For most material selection and qualification programmes for sour applications the material is tested in accordance with NACE MR0175/ISO15156 [3] at the maximum design temperature and at room temperature (RT). A testing programme conducted by Bodycote in 2005 [2] indicated that the material could be more susceptible to cracking at temperatures below room temperature. Consequently qualification to the requirements of NACE MR0175 / ISO 15156 [3] could show acceptable results whereas in service cracking may occur by exposure to temperatures below ambient. This may not be applicable for some applications, however for sub-sea pipelines typical seabed temperatures in the region of 4°C can be experienced during 'shut-in' conditions.

It should also be noted that the possibility of in-situ cracking at low temperatures is complicated by the possibility that RT or low temperature cracking may be eliminated by prior 'conditioning' of the surface at the higher operating temperatures. This is an important practical consideration, since pipelines would not normally see a low temperature corrosive environment until after first being exposed to the production fluids at a higher temperature.

## 1.3 Project Objectives

Nippon Steel & Sumitomo Metal Corporation (Former Nippon Steels and Sumitomo Metal Industries) commissioned Exova (Former Bodycote) to undertake an investigation on the low temperature (seabed temperature) sulphide stress cracking (SSC) resistance of grade LC80-130S (API 5LC) 13%Cr weldable martensitic stainless steel pipe, manufactured by Sumitomo Metals.

It was agreed that as part of the program of work being conducted by Exova this MPhil thesis would be supported by Nippon Steel & Sumitomo Metal Corporation (NSSMC). The two primary objectives of this MPhil thesis program are detailed below:

1. To undertake sulphide stress cracking (SSC) tests on the parent material supplied by NSSMC in condensed water (CW) and produced water (PW) environments at room temperature (24°C) and at a seabed temperature (5°C), to establish if the cracking susceptibility was Influenced by the low temperature conditions.

   An additional objective was to examine the Influence of the surface condition (i.e. as-received v 600 SiC ground) on the SSC resistance at the two test temperatures.

2. To undertake electrochemical corrosion tests at the two test temperatures (i.e. 24°C & 5°C) under the same conditions as the SSC tests to establish if the passive film was Influenced by the variation in the test temperature.

   Additional objectives of the electrochemical test program were to

   a) investigate the Influence of surface finish (i.e. as-received v 600 SiC ground) and

   b) determine the effect of the initial purge gas (i.e. $N_2$ v $CO_2$) on the electrochemical behaviour.

# CHAPTER 2: LITERATURE REVIEW

## 2.1 Introduction

Martensitic stainless steels are widely used in the oil and gas industry, predominately for their strength and corrosion resistance. A variety of alloys are used depending on the combination of strength and corrosion resistance required for a particular application. The combination of sufficient chromium to impart corrosion resistance and a maximum chromium content to achieve a predominately martensitic structure lies between 12%Cr and 15%Cr. Below approximately 12%Cr a stable chromium oxide film will not be formed and consequently the corrosion resistance will be compromised and above approximately 15%Cr the ferrite content will increase and impact the mechanical properties. In the review a 17%Cr alloy is included, which has recently been developed with a dual phase martensite-ferrite structure.

In the review the alloys have been classified into conventional 13%Cr, modified 13%Cr, super 13%Cr, higher alloy grades (i.e. 15%Cr and 17%Cr) and weldable grades. The materials within each grade will have a unique interaction between their composition, mechanical properties and corrosion resistance, which can also be influenced by the manufacturing route and the individual manufacturer.

For down-hole tubular and well-head applications the conventional, modified, super and high alloyed grades are not considered to be weldable, without post weld heat treatment, whereas the weldable grades, used for line pipe applications are welded with the inclusion of a 5 minute post weld heat treatment cycle to prevent intergranular stress corrosion cracking (IGSCC).

In the oil and gas industry martensitic stainless steels are used in applications requiring corrosion resistance in sweet (i.e. $CO_2$ corrosion) and sour (i.e. $H_2S$ corrosion) environments at temperatures generally below 175°C for the '13%Cr' grades and below 230°C for the high alloyed 17%Cr grade. The service limit of each particular grade is governed by the chloride concentration, the partial pressure of

$CO_2$, the partial pressure of $H_2S$, the pH, the temperature and the hardness and yield stress of the material.

## 2.2 Scope

This literature survey covers a review of martensitic stainless steels used for oil and gas transportation to include materials used for well-head, down-hole tubular and line pipe applications.

## 2.3 Material Grades and Classification

The family of martensitic Stainless Steel pipe-line and down-hole tubular products used in the oil and gas industry can be broadly classified into five groups, as discussed below.

### 2.3.1 Conventional 13%Cr grades (13Cr)

'Conventional' 13%Cr martensitic stainless steels, containing ≤0.22%C, 11.5 – 14%Cr and up to 0.5%Ni have been in use for oil country tubular goods (OCTG) in down-hole tubular applications (i.e. down-hole tubing and casing) since the early 1980s. These grades were introduced predominately to offer an increased resistance to $CO_2$ corrosion over the un-alloyed or low-alloyed carbon steel grades and they are typically used in $CO_2$ service up to 125°C, depending on the chloride concentration. However they additionally exhibit a resistance to SSC and SCC in the presence of $H_2S$, and the following grades are currently listed in ISO 15156 / NACE MR0175 [3] as being suitable for down-hole tubular applications:

**Table 2.1** Summary on 'Conventional' 13Cr Grades in ISO 15156 / NACE MR0175 [3]

| Specification / Individual alloy UNS number | Temperature Max. °C (F) | Partial Pressure $pH_2S$ kPa (psia) | Chloride conc. Max. mg/L | pH | Hardness Max. (HRc) | Remarks |
|---|---|---|---|---|---|---|
| UNS S41000 | See 'Remarks' column | 10 (1.5) | See 'Remarks' column | ≥3.5 | 22 | Any combination of temperature and chloride concentration occurring in production environments are acceptable. |
| UNS S42000 | | | | | 22 | |
| ISO 11960 L-80 13Cr | | | | | 23* | |
| **maximum hardness specified in API Specification 5CT / ISO 11960* [4], [33] | | | | | | |

### 2.3.2 Modified 13%Cr Grades (Modified 13Cr)

During the 1990s the 'modified' grades were developed, primarily to increase the high temperature corrosion resistance in $CO_2$ environments and to increase the strength from the 80—85 ksi range of the conventional 13Cr grade up to a maximum of 110 ksi. For these 'modified' grades the increased corrosion resistance is achieved by the addition of nickel (2 – 6%) and molybdenum (0.2 – 1.2%). These grades exhibit similar or inferior (dependent on the strength grade) SSC resistance to the conventional grades, but show an increase in the maximum service temperature from ≤125°C up to ≤175°C. The 'modified 13Cr' grades, currently listed in ISO 15156 / NACE MR0175 [3], are shown in Table 2.2.

**Table 2.2** Summary on 'Modified' 13Cr Grades in ISO 15156 / NACE MR0175 [3]

| Specification / Individual alloy UNS number | Temperature Max. °C (F) | Partial Pressure $pH_2S$ kPa (psia) | Chloride conc. Max. mg/L | pH | Hardness Max. (HRc) | Remarks |
|---|---|---|---|---|---|---|
| UNS S41429 | See 'Remarks' column | 10 (1.5) | See 'Remarks' column | ≥4.5 | 27 (120 ksi max.) | Any combination of temperature and chloride concentration occurring in production environments are acceptable. |
| UNS S41500 | | | | ≥3.5 | 23 | |
| UNS S42400 | | | | | 23 | |

### 2.3.3 'Super' 13%Cr Grades (Super 13Cr)

During the 1990s the 'super' grades were developed, primarily to increase the high temperature pitting corrosion resistance in $CO_2$ environments, containing high chloride concentrations. For these grades the increased corrosion resistance is achieved by the addition of nickel (4 – 7%) and molybdenum (1.5 - 3%). These grades exhibit improved stress corrosion cracking (SCC) resistance compared to the conventional grades and also show an increase in the maximum service temperature from ≤150°C up to ≤175°C. These 'super' grades were introduced into the ISO 15156 / NACE MR0175 [3] document from 2000 – 2003 and are commonly referred to as '13-5-2', referring to the nominal concentrations of chromium, nickel and molybdenum.

As with the modified grades the higher strength 110 ksi grades will exceed the hardness restriction in ISO 15156 / NACE MR0175 [3] and therefore qualification testing would be a requirement for sour service applications. The 'Super 13Cr' grades currently listed in ISO 15156 / NACE MR0175 [3] are shown in Table 2.3.

**Table 2.3** Summary on 'Super' 13Cr Grades in ISO 15156 / NACE MR0175 [3]

| Specification / Individual alloy UNS number | Temperature Max. °C (F) | Partial Pressure $pH_2S$ kPa (psia) | Chloride conc. Max. mg/L | pH | Hardness Max. (HRc) | Remarks |
|---|---|---|---|---|---|---|
| UNS S41425 | See 'Remarks' column | 10 (1.5) | See 'Remarks' column | ≥3.5 | 28 | Any combination of temperature and chloride concentration occurring in production environments are acceptable. |
| UNS S41426 | | | | | 27 (105 ksi max) | |

The use of the above alloys in the 110 ksi strength grade is currently not covered by the limits in the ISO 15156 / NACE MR0175 [3] document. However discussions held at the maintenance panel meeting at the Eurocorr 2011 conference in Stockholm [34] indicated that the tube manufacturers will be submitting a future ballot to include these high strength grades in the document.

### 2.3.4 Higher Cr Grades (15%Cr & 17%Cr)

'New' higher alloyed grades with chromium concentrations of 15% and 17% have recently been developed by JFE [21] and Nippon Steel & Sumitomo Metal Corporation (NSSMC) [35] respectively to increase the strength threshold up to 125 ksi and also to increase the maximum service temperature in $CO_2$ environments, up to 200°C, in the case of the 15%Cr grades and 200°C - 230°C in the case of the 17%Cr grade. The composition, strength and hardness of these new 15%Cr and 17%Cr grades are presented in Table 2.4.

**Table 2.4** Composition (wt.%), Strength and Hardness of new 15%Cr and 17%Cr grades.

| Grade | Strength | %C | %Cr | %Ni | %Mo | %Cu | %W | Hardness (HRc) |
|---|---|---|---|---|---|---|---|---|
| 15%Cr | 125 ksi | ≤0.04 | 14 – 16 | 6 – 7 | 1.8 – 2.5 | ≤1.5 | -- | 37 |
| 17%Cr | 110 ksi | ≤0.04 | 16 – 18 | 3.5 – 4.5 | 2 - 3 | ≤1 | ≤1 | -- |
| 17%Cr | 125 ksi | | | | | | | -- |

In the case of the 15%Cr grades increasing the chromium content promotes the formation of delta ferrite and also austenite and therefore close compositional control of Cr, Ni, Mo and Cu is required to maintain the predominately martensitic structure, in order to achieve the correct balance of strength and corrosion resistance.

In the case of the new 17%Cr steels it is not possible to maintain a martensitic structure and therefore in order to achieve the high strength (i.e. 125 ksi) and corrosion resistance these steels have a dual phase structure comprising of martensite and ferrite (see Figure 2.1).

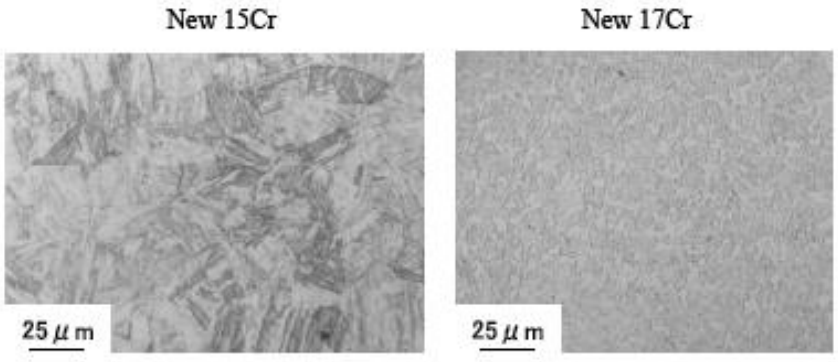


**Figure 2.1** Photomicrographs showing the microstructures of the new 15%Cr and new 17%Cr stainless steels [6]

NSSMC (Dr Amaya) presented data on their new 125 ksi grade 17%Cr alloy (SM17CRS-125) at the ISO 15156 / NACE MR0175 maintenance panel meeting in Stockholm (Sept 2011) [34]. The material was reported to exhibit acceptable SSC performance in a 180 000 mg/L chloride solution at 0.1 bara (1.5 psia) $pH_2S$ at a pH of 5.0 and at 0.03 (0.45 psia) bara $pH_2S$ at a pH of 3.5. Additionally the SCC performance was acceptable at 200°C and at 0.01 bara $pH_2S$ / 30 bara $CO_2$ in a 180,000 mg/L chloride solution, at a pH of 4.5 and in a 70,000 mg/L chloride solution, at a pH of 4.0.

Neither of these new 15%Cr and 17%Cr grades is currently listed in ISO 15156 / NACE MR0175 [3]. However a 15%Cr martensitic steel (UNS S42500) is listed, which is generally used for equipment or components in lower strength (i.e. 80 ksi) grades, with a maximum hardness restriction of 28 HRc.

### 2.3.5 Weldable Martensitic Stainless Steel (WMSS)

The concept of WMSS was developed by Zingg & Greiger in the late 1950s (0.07% max. C) and in the mid-late 1980s WMSSs were developed with low C (<0.03) & N, 4 – 6%Ni and <2.5%Mo. Further advances in steel-making technology in the 1990s led to the developments of ultra-low carbon (<0.01%C) grades, containing Ti and Nb, which are currently being used today.

During the early developments of 13%Cr WMSSs for oil & gas environments, three grades were available, based on the Ni and Mo concentrations and often categorised [36] as 'lean' (1 – 2.5%Ni / < 1%Mo), 'medium' (2.5 – 4.5%Ni / 1 - 2%Mo) and 'fat' (4.5 – 6.5%Ni / >2%Mo). However due to service failures [36] the 'lean' and 'medium' grades are rarely used and the 'fat' 13%Cr / 4.5 – 6.5%Ni / >2%Mo WMSS has been adopted as the 'industry standard'.

The low C enables the material to be welded (without conventional post weld heat treatment (PWHT) and increases effective Cr (in solution), thus improving the resistance to $CO_2$ corrosion. The addition of Mo improves resistance to local corrosion (i.e. pitting and crevice) and improves the susceptibility to SSC/SCC. The Mo content also increases the critical Ac1 temperature and reduces susceptibility to retained austenite formation during tempering. The addition of Ti stabilises the C to reduce hardness and refines the grain size in the HAZ and the addition of Nb increases the strength (NbC) and improves the SSC / SCC resistance.

The family of WMSSs were first used for flow-lines in the mid-1990s in the north Sea (UK) and they are currently being specified and used for $CO_2$ service in mild $H_2S$ (up to 40 mbara) environments at temperatures generally ≤140°C. The materials are considered to be an alternative to inhibited carbon steel, clad/lined 316L stainless steel or solid 22%Cr duplex stainless steel for mildly sour environments.

The more widespread use of these materials for welded flow-lines was restricted by early service failures due to intergranular stress corrosion cracking (IGSCC) in the fusion-line region (see Figure 2.2) and hydrogen induced stress cracking (HISC) from cathodic protection in areas of high plastic strain (i.e. at anode connections).

The likelihood of further failures due to these two problems has now been mitigated by conducting a localised PWHT (i.e. 5min @ 650°C) and by ensuring cathodic potentials from Cathodic Protection (CP) are controlled and stresses in the vicinity of anode connections are kept low. Diodes have been used to control the applied potentials and 25%Cr super duplex pup pieces have been used to attach the anode connections.

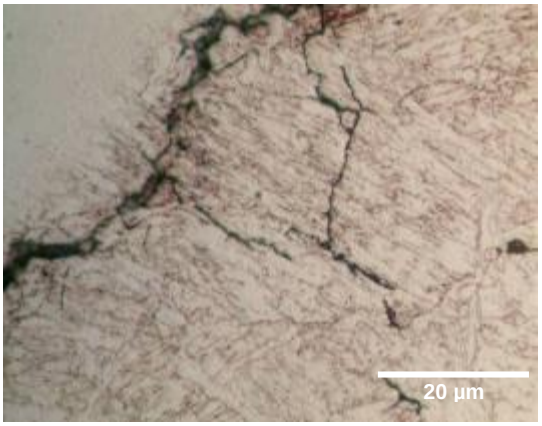


**Figure 2.2** Photomicrographs showing IGSCC in the fusion line region of a weldable martensitic stainless steel. *(Ref: Exova archive)*

The weldable grades are currently not covered in the ISO 15156 / NACE MR0175 [3] document and are normally tested on a fitness for service basis (FFS).

### 2.3.6 Down-hole Tubular Martensitic Proprietary Grades and Manufacturers

Martensitic grades of OCTG are manufactured and available in a variety of compositional and strength grades, depending on the specific application. The currently available proprietary grades from the major manufacturers are shown in Table 2.5.

**Table 2.5** Down-hole Tubular (OCTG) and Weldable Line-pipe Proprietary Grades and Manufacturers*

| Classification | Strength (ksi) | Hardness (HRc) | Manufacturer / Grade | | | |
|---|---|---|---|---|---|---|
| | | | JFE | NSSMC | TenarisNKK Tubes | Vallourec & Mannesmann |
| **Conventional** | | | | | | |
| '13Cr' | 80 | 23 | JFE-13CR-80 | SM13CR-80 | TN80Cr13 | VM8013Cr |
| | 85 | 24 | JFE-13CR-85 | SM13CR-85 | TN85Cr13 | |
| | 90 | 26 | | | | VM9013Cr |
| | 95 | 27 | JFE-13CR-95 | | TN95Cr13 | VM9513Cr |
| **Modified** | | | | | | |
| '13Cr-4Ni-1Mo' | 95 | 28 | JFE-HP1-13CR-95 | SM13CRM-95 | TN 95Cr13M | |
| | 110 | 31-32 | JFE-HP1-13CR-110 | SM13CRM-110 | TN 110Cr13M | |
| **Super** | | | | | | |
| '13Cr-5Ni-2Mo' | 95 | 29-30 | JFE-HP2-13CR-95 | SM13CRS-95 | TN 95Cr13S | VM 95 13CrSS |
| | 110 | 31-32 | JFE-HP2-13CR-110 | SM13CRS-110 | TN 110Cr13S | VM 110 13CrSS |
| **15Cr & 17Cr** | | | | | | |
| 15%Cr | 125 | 37 | JFE-UHP-15CR-125 | | | |
| 17%Cr | 110 | | | | | |
| 17%Cr | 125 | | | SM17CRS-125 | | |
| **Weldable** | | | | | | |
| 12%Cr | 80 | 31 | JFE-12HP1-X80 | | | |
| 13Cr-5Ni-0.7Mo | 80 | | | 13Cr-M | | |
| 12Cr-6Ni-2.5Mo | 80 | | | 13Cr-S | | |
| *Information taken from the respective manufactures data sheets [37];[38];[39];[40] | | | | | | |

## 2.4 Metallurgy & Material Properties

### 2.4.1 Microstructure

Martensitic stainless steels owe their high strength to their tempered martensitic microstructure (Figure 2.3). The martensite phase is produced by diffusionless transformation of a fully austenitic single phase (γ-iron) cooled to room temperature. Since the transformation is diffusionless, there is no compositional change from austenite to martensite.

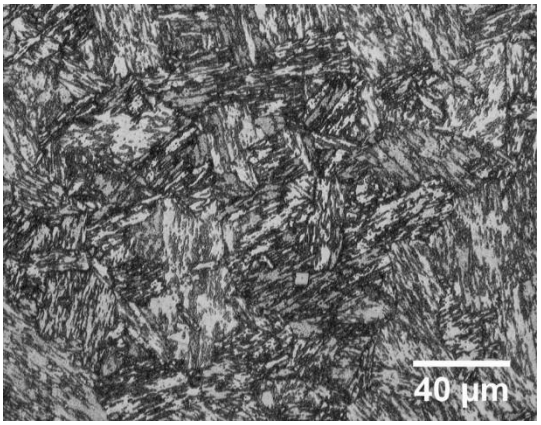


**Figure 2.3** Photomicrograph showing the tempered martensitic microstructure of a low-carbon weldable martensitic stainless steel. *(Ref: Exova archiv*e)

The unit cell of the austenite phase is face-centered cubic (f.c.c.). On cooling, austenite transforms to martensite at approximately the speed of sound. This rapid phase change means there is no time for carbon atoms to diffuse out of the austenite phase, so the crystal lattice distorts to form body-centered tetragonal (b.c.t.) martensite. To minimize elastic strain energy during transformation, martensite forms as thin plate or lath shapes on crystallographic planes called habit planes, constrained in the prior austenite grain boundaries. The austenite-martensite transformation is athermal, since the amount of martensite formed depends not on the amount of time at a given temperature, but on the amount of cooling below the martensite start temperature ($M_s$). The $M_s$ is approximately 200°C for 13%Cr martensitic steels and the exact value will be dependent on the steel composition and the specific heat treatment schedule. For example for a SMSS, containing 0.105%C, 12.34%Cr, 5.66%Ni, 2.02%Mo, 0.42%Mn, 0.22%Si and 0.18%V the Ms temperature has been determined by Bojack et. al. [41] using magnetic measurements to be 230°C.

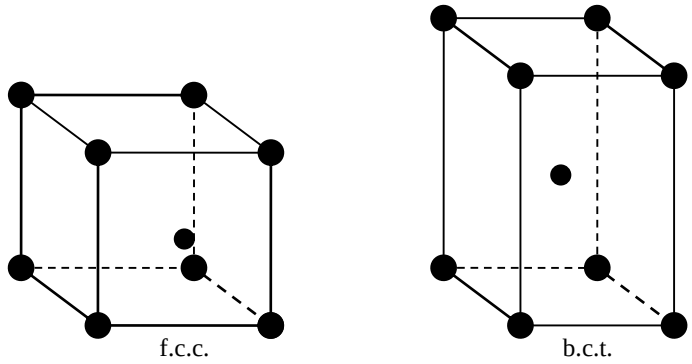


**Figure 2.4** Schematic of f.c.c. austenite and b.c.t. martensite structures.

When a martensitic stainless steel is cooled from a liquid (approximately 1500°C) to room temperature, the following phase changes occur: firstly, the liquid solidifies to δ-ferrite at approximately 1450°C. At approximately 1250°C, δ-ferrite transforms to austenite (γ-iron), and the γ-iron starts to transform to martensite at the $M_s$ temperature, which is significantly below the $A_1$ temperature on the Fe-C equilibrium phase diagram, since the transition from austenite to martensitic is a non-equilibrium transformation. In 13%Cr martensitic stainless steels the austenite to martensite transformation is not complete at ambient temperature, due to the relatively low martensite finish ($M_f$) temperature, hence a percentage of austenite is retained in the steel.

### 2.4.2 Alloying Elements

Since a predominately martensitic microstructure is required to achieve the desired properties of martensitic stainless steels, alloying elements are carefully selected, together with the heat treatment schedule in order to control the final phase balance. It is desirable not to retain delta-ferrite as this reduces strength and SSC resistance. Retained austenite will be present in the structure and the % present will predominately be dependent on the composition of the steel.

Conventional, modified, super and weldable martensitic stainless steels typically have chromium contents ranging from 12-15%. This is a fundamental element, as it gives the steel its ‘stainless’ property by means of a thin surface chromium oxide film that protects against corrosion. If chromium is added above 15%, delta-ferrite forms at the solution temperature and will remain in the microstructure on cooling.

Molybdenum is added to improve the stability of this passive film for improved resistance against pitting corrosion and SSC [42]. The concentrations are limited to a maximum of 3% since above this level, molybdenum starts to precipitate with iron to form intermetallic phases such as $Fe_2Mo$ reducing the effectiveness of the alloy on the corrosion resistance [43].

The effect of molybdenum on SSC resistance was quantified by Hashizume *et al.* [7] in terms of depassivation pH (figure 2.5). The research showed that increasing the molybdenum content of the steel decreased its depassivation pH. This is important because when the solution pH falls below the depassivation pH of the material, the passive film breaks down and atomic hydrogen generated from the corrosion process can diffuse into the steel. Therefore a lower depassivation pH suggests higher SSC resistance. Although this is not the whole story; regardless of the depassivation pH, pitting corrosion may still occur, and this will provide another route for hydrogen entry. When the solution pH is above the depassivation pH, the SSC resistance of the material depends upon $H_2S$ partial pressure and chloride concentration.

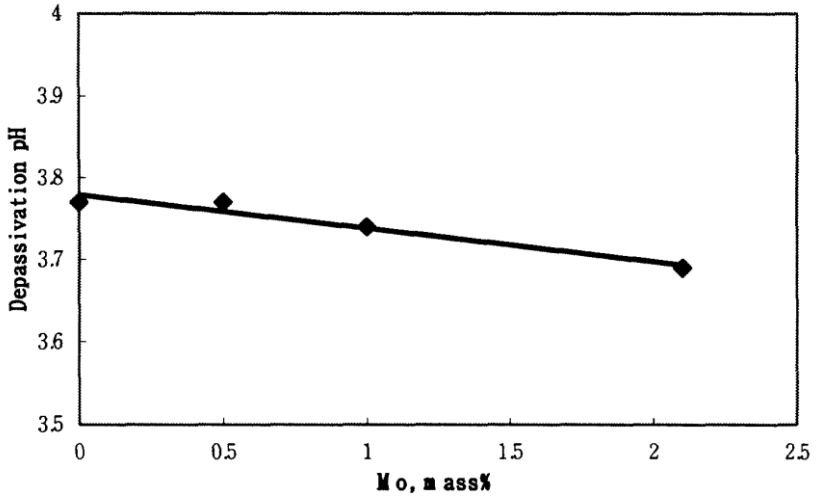


**Figure 2.5** Effect of Mo on depassivation pH in martensitic stainless steels [7]

At elevated solution temperatures, additions of chromium and molybdenum tend to stabilize the ferrite field rather than the austenite field; so austenite-stabilizing elements such as nickel are added to counteract this. Nickel also improves toughness. However if too much nickel is added then the austenite field becomes too stable, resulting in high levels of retained austenite in the microstructure. This happens because $M_f$ is depressed below room temperature so the austenite to martensite transformation cannot be completed.

Other austenite-stabilizing elements include carbon, nitrogen and manganese. In the case of the modified, super and weldable grades carbon and nitrogen contents are kept low (<0.01%), since they can form precipitates with chromium and molybdenum, diminishing the effective chromium and molybdenum concentrations in the matrix, that are required for effective corrosion resistance.

The low carbon content keeps hardness levels down which benefits SSC resistance and facilitates welding of the weldable grades. Manganese can be included up to 2% and is used as a deoxidizer and as a cheaper substitute for the more expensive nickel.

Titanium is a ferrite stabiliser; it is added to form stable Ti (C, N) inclusions in preference to the precipitation of chromium or molybdenum carbo-nitrides. The solubility of Ti (C, N) inclusions is low even near the melting point of the metal and this has a pinning effect that restricts grain growth in weld heat affected zones [44]. This is beneficial as a refined grain size improves SSC resistance.

## 2.5 Corrosion & Cracking Resistance

### 2.5.1 Introduction

The corrosion and cracking resistance of martensitic stainless steels is dependent on material and environmental factors. Material factors include; the composition (grade), retained delta ferrite concentration, amount of retained austenite, strength level, hardness, passive film stability and the surface condition. The amount of retained delta ferrite and retained austenite, together with the strength and hardness are dependent on the product size and heat treatment. The environmental factors include; the applied stress, pH, temperature, partial pressure of $H_2S$, partial pressure of $CO_2$ and the chloride concentration.

### 2.5.2 Influence of Material on Corrosion & Cracking Resistance

2.5.2.1 Strength and hardness

Since high hardness reduces SSC resistance, so does high material strength. In general, high strength super martensitics are more susceptible to SSC than lower strength grades with a similar composition. Therefore, it would be expected that the lower strength 80 ksi grade weldable martensitic stainless steel would produce pH-$H_2S$ domain diagrams with larger 'acceptable' areas.

2.5.2.2 Passive Film Stability

The passive chromium oxide film provides an effective barrier to hydrogen entering the steel, so providing this film remains intact, hydrogen uptake is low and the material is resistant to cracking by hydrogen embrittlement. When the passive film breaks down, which can happen by dissolution during active corrosion and localized pitting, or film rupture from plastic straining, hydrogen is free to enter the steel. Film rupture by plastic straining could occur in service by pipe movement, or in the case of welded joints, by stress concentration generated by the shape of the weld root profile.

The condition of the surface oxide film determines the pitting susceptibility of the material and its hydrogen uptake. Stress been, particularly at the root of welded surfaces can cause local plastic straining that can rupture this film. When the as-received pipe surfaces have been grit blasted, it is likely that residual stresses are present. Surface treatments such as grit blasting will induce a residual compressive stress at the surface that would act in opposition to any applied tensile stress, reducing the likelihood of crack initiation. This could explain the observations made by Enerhaug *et al*. [45] on weldable martensitic stainless steel who reported that all corrosion and cracking that occurred during SSC testing were found in the HAZ on the machined edges of the four-point bend specimens, with no SSC on the 'as-received' inner pipe surface. Olsen *et al.* [46] also observed that machined surfaces are more susceptible to cracking than specimens with the oxide film intact.

2.5.2.3 Delta Ferrite

Delta-ferrite (δ-ferrite)is likely to be present in the martensitic microstructure of super-martensitic stainless steels and research suggests that it does Influence the corrosion and cracking susceptibility of this material when the volume fraction exceeds 5% [47]. Hara & Asahi [8] examined the influence of delta-ferrite on the ambient temperature corrosion potential and SSC resistance of 13%Cr martensitic stainless steels in a 5 wt.% NaCl solution, saturated with 0.01 bara $H_2S$ at a pH of 3.5 and revealed 10% volume fraction delta ferrite, reduced the corrosion potential ($E_{corr}$), de-passivated the surface (see Figure 2.6) and led to SSC: The reduction in $E_{corr}$ and the de-passivation of the surface was attributed to a local decrease in the Cr and Mo concentrations and the precipitation of chromium carbides near the delta ferrite grain boundaries. Whether the delta ferrite was present as stringers or along the prior austenite grain boundaries was not found to influence $E_{corr}$ [8].

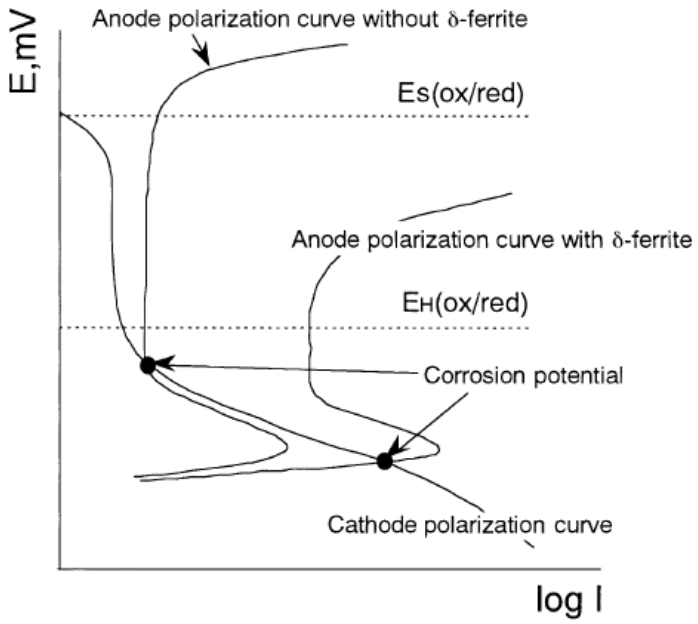


**Figure 2.6** Effect of delta-ferrite on the corrosion potential and anodic polarisation curves for two 13%Cr martensitic stainless steels, one without delta ferrite and one with a volume fraction of 10% delta ferrite [8].

2.5.2.4 Retained Austenite

Austenite can be retained in the microstructure by tempering above the Ac1 transformation temperature (approximately 550°C), which promotes the precipitation of finely distributed austenite along the martensite inter-lath boundaries and prior austenite grain boundaries [48], [49], [50], [51].

Reports show that the presence of retained austenite is not harmful to the material's corrosion resistance since Cr and Mo do not concentrate in the austenite phase, which would otherwise lead to localised corrosion [52], [53], [10], [9]. Although a study by Kimura *et al*. [10] showed that the corrosion potential and the pitting potential were independent of the retained austenite content, a later study by Bilmes [54] showed that pitting and re-passivation potentials shift towards the noble direction as retained austenite content increases, thus improving pitting resistance. Kimura *et al*. [10] showed that the pitting potential increase was due to a decrease in precipitated Cr and Mo in the matrix, and this is a consequence of an increase in retained austenite content.

Various tests have shown that retained austenite improves the SSC resistance of supermartensitic stainless steels. Nose and Asahi [53] showed that a 'fat' grade[1] supermartensitic, with more than 10% retained austenite, showed better SSC resistance than the same steel with lower levels of retained austenite under the same test conditions. Their SSC tests were carried out according to NACE TM0177 method A [55] (at 90% AYS, 25°C, pH 4) at 10 mbara, 40 mbara and 100 mbara $H_2S$ partial pressures. The test samples were normalised at 950°C for 30 mins. air cooled, then received varying amounts of heat treatment (from 300°C to 720°C) for 30 mins. to give levels of retained austenite ranging from 0% to 18%. Whilst none of the samples failed at 10 mbara $H_2S$, the best SSC resistance (at 100 mbara $H_2S$) was achieved by the samples containing the highest levels of retained austenite (13% & 18%). Although SSC resistance is related to strength, the improved SSC resistance could not

[1]Grades based on the Ni and Mo concentrations and often categorised [36] as 'lean' (1 – 2.5%Ni / < 1%Mo), 'medium' (2.5 – 4.5%Ni / 1 - 2%Mo) and 'fat' (4.5 – 6.5%Ni / >2%Mo). However due to service failures [36] the 'lean' and 'medium' grades are rarely used and the 'fat' 13%Cr / 4.5 – 6.5%Ni / >2%Mo WMSS has been adopted as the 'industry standard'.

be attributed solely to the reduced tensile strength of the samples with high retained austenite content. This was due to one sample with lower tensile strength and only 4% retained austenite failing at (see section 2.3.5) 100 mbara $H_2S$. Kimura *et al*. [10] did similar tests to NACE TM0177 method A [55] on a 'fat' grade supermartensitic showing that steels with 4.8% and 17.8% retained austenite failed by SSC whilst steel with 37.3% retained austenite did not fail, even at 100 mbara $H_2S$.

The improved SSC resistance associated with retained austenite content can be attributed to the austenite phase reducing the amount of hydrogen in the martensitic matrix when the passive film is broken [10], [9]. It has been stated that hydrogen trapping occurs at the interface between the austenite and martensite phase. Kondo *et al.*[9] showed this for a weldable martensitic stainless steel using Thermal Dispersion Spectroscopy (TDS) after a corrosion test to determine the absorbed hydrogen content. Specimens were tested in 10 mbara $H_2S$ in 5% NaCl and stressed to 100% of the Specified Minimum Yield Stress (SMYS). The solution pH was 2.7 (below the de-passivation pH) to generate excess hydrogen to enter the specimens. The results are given in figures 2.7 to 2.9, showing that hydrogen trapped in the martensitic matrix (P1) reduces as the retained austenite content increases (i.e. more austenite-martensite interfaces).

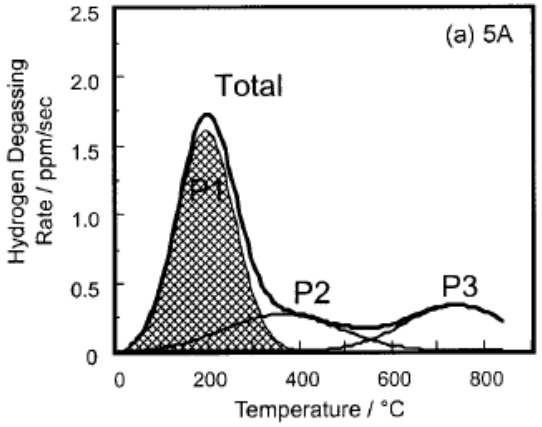


**Figure 2.7** 0% retained austenite: P1 is hydrogen in martensite; P2 & P3 are non-diffusible hydrogen [9].

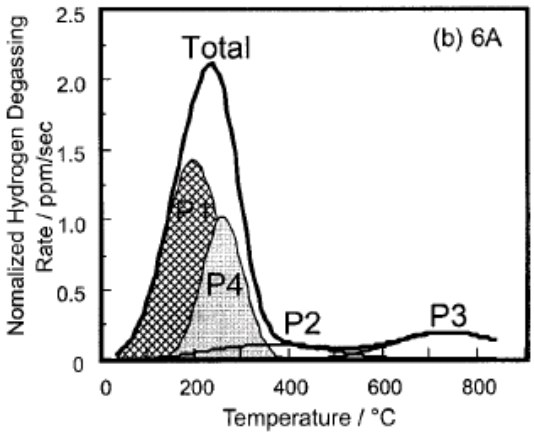


**Figure 2.8** 4.9% retained austenite: P1 is hydrogen in martensite; P4 is hydrogen in retained austenite [9].

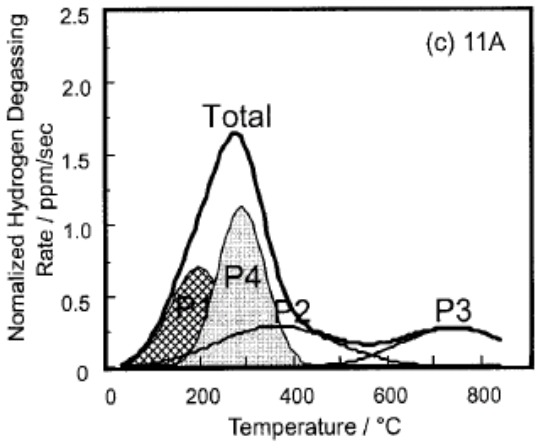


**Figure 2.9** 13.4% retained austenite: P1 is hydrogen in martensite; P4 is hydrogen in retained austenite [9].

Kimura *et al*. [10] described SSC susceptibility in terms of maximum hydrogen permeation rate. Figure 2.10 shows how the maximum hydrogen permeation rate decreases with increase in retained austenite; the retained austenite reducing the hydrogen content in the steel. However, Nose *et al*. [53] suggests that retained austenite may only be effective in preventing SSC when hydrogen entry is intermittent, such as when a corrosion pit re-passivates. If hydrogen entry is continuous, then trapping sites are not effective in preventing SSC.

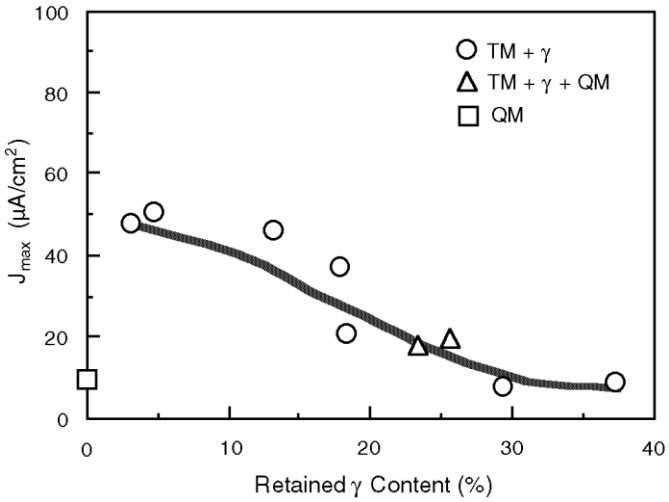


**Figure 2.10** Maximum hydrogen permeation rate versus retained austenite content [10].

Figure 2.11 shows how retained austenite content Influences the tensile strength of the material; after a threshold of around 10%, tensile strength tends to fall with increased retained austenite content.

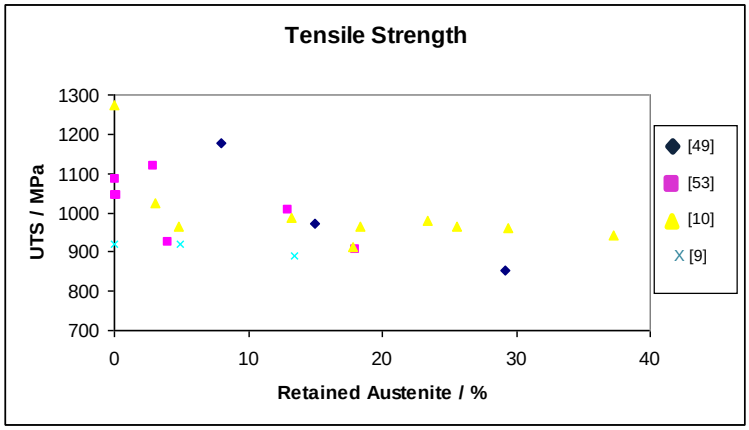


**Figure 2.11** Literature data of tensile strength versus retained austenite content.

2.5.2.5 Effects of Cold Work on Retained Austenite

Kondo *et al*. [9] investigated the effects of cold work reduction on the amount of retained austenite for a weldable martensitic stainless steel following various tempering conditions. The results showed that some of the retained austenite transformed to martensite, as a result of cold work, but most remained as retained austenite, even when cold worked up to 10% in reduction. This investigation also showed that the yield stress increases more in specimens containing retained austenite compared to those that do not, due to simple work hardening in the retained austenite.

These results are illustrated in figure 2.12 below:

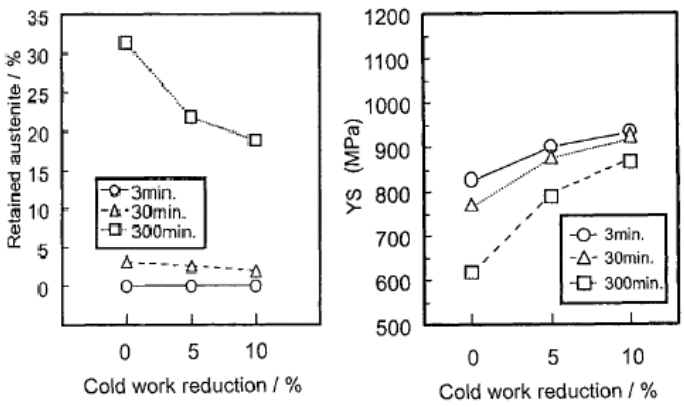


**Figure 2.12** Effect of cold work reduction on retained austenite content and yield strength when tempered at 600°C [9].

Smirnova*et al*. [56] measured the area fraction of retained austenite in a 0.01%C, 2.15%Mo, 5.9%Ni S13Cr steel using Electron Back Scattered Diffraction (EBSD) before and after deformation of the material by 0.4% strain. Their work suggest the area fraction of retained austenite fell from 19% (as-received) to 2.7% when strained to 100% of the yield stress (0.4% strain).

# 2.6 Influence of Environmental Factors on Corrosion & Cracking Resistance

### 2.6.1 Influence of pH on SSC Resistance

Solution pH is a measure of the concentration of hydrogen ions in the aqueous phase and this is influenced by the concentration of the 'acidic gases' $H_2S$ and $CO_2$ dissolved in solution. The solubility of $H_2S$ and $CO_2$ is also influenced by both temperature and salinity (chloride concentration). The $H_2S$ concentration in produced water and condensed water solutions, saturated with 1 bara $H_2S$ at temperatures ranging from 5°C to 25°C have been conducted by Exova [11] in accordance with the procedure in Appendix C of NACE TM0284 [57] and the results are given in Figure 2.13. The trend shows $H_2S$ solubility is higher at low temperature and in lower chloride solutions.

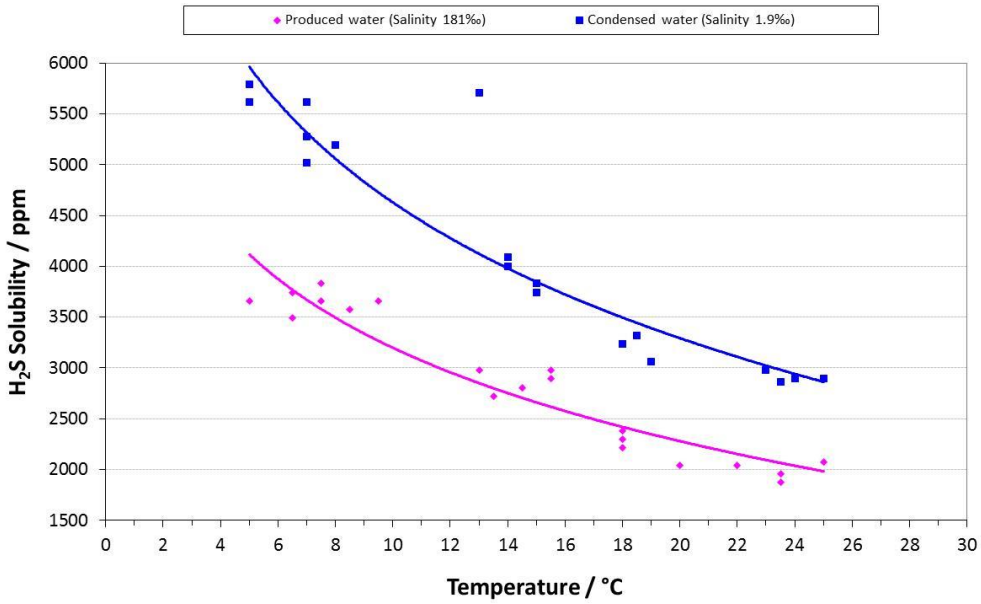


**Figure 2.13** Influence of temperature and chloride concentration (salinity) on $H_2S$ solubility [11].

$H_2S$ and $CO_2$ are 'acid gases', lowering the pH of the solution they are dissolved in. As described in section 2.4.2, when the solution pH falls below the de-passivation pH of the material, the protective oxide film breaks down and the material corrodes. This means the corrosion mechanism provides both a source of hydrogen ions and a route for hydrogen entry into the steel.

### 2.6.2 Influence of Chlorides

In general, high chloride concentration is seen to be more detrimental to the SSC resistance of martensitic stainless steels. This was shown by Takabe *et al.* [19] on tests on a '110 ksi' grade super martensitic, and also observed that the Influence of chlorides was larger for lower pH, or higher $H_2S$ partial pressure environments. The problem with chlorides is that they directly attack the passive film and this causes localised pitting corrosion and hydrogen entry. The base of corrosion pits are sites of high stress concentration, low pH and broken passive film; conditions ideal for SSC initiation.

Takabe *et al*. [19] showed the detrimental effect chlorides have on the depassivation pH in $H_2S/CO_2$ environments: At 24°C, the depassivation pH was 3 to 3.5 at 100,000 mg/L $Cl^-$, but increased to a pH of 4.4 at 181,000 mg/L $Cl^-$. Generally, resistance to SSC is greater in lower concentration chloride solutions (figure 2.14):

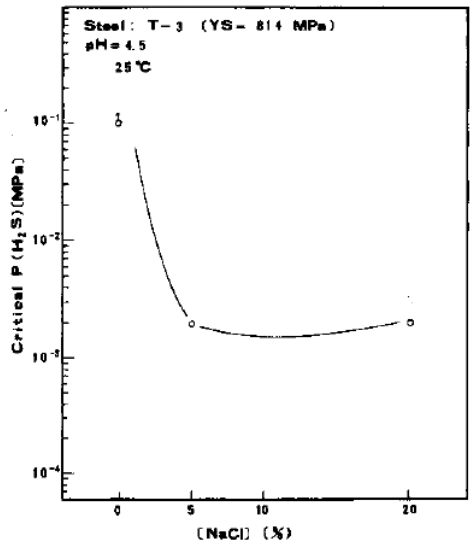


**Figure 2.14** Effect of [NaCl] on critical $H_2S$ partial pressure for cracking and pitting at 25°C [12].

SSC tests[2] performed by Cooling *et al*. [58] over a range of pH values (3.5 to 5.5) showed better SSC resistance in low chloride content condensed water environments (1,000 mg/L $Cl^-$) than higher chloride content produced water environments (120,000 mg/L $Cl^-$), suggesting that chloride content contributes to SSC more than pH alone.

The Åsgard Field qualification program on weldable martensitic stainless steels showed that the worst case of localised corrosion, followed by SSC, was at room temperature in high chloride containing (68,000 mg/L $Cl^-$) produced water (pH 4.5–5.0, 40 mbara $H_2S$), where the same material resisted SSC in lower pH (3.5) condensed water conditions with a low chloride ion concentration [45]. However, chlorides are far more detrimental to SSC resistance when combined with low pH (3.5) when compared to higher pH (4.5) solutions, as demonstrated by Takabe *et al.*[19] and Marchebois *et al.* [15].

### 2.6.3 Influence of Temperature

For carbon steels the risk of cracking in sour environments is greatest at ambient temperature and for corrosion resistant alloys (CRAs) the risk is generally accepted to be greater at elevated temperatures [36]. Although martensitic stainless steels are classed as a CRA, the risk of cracking, as a result of SSC, has been reported to be greatest at or near to room temperature [36], [45].

The Influence of temperature on the SSC / SCC resistance of the material have been well documented and an improvement in the resistance to initial pitting and subsequent cracking and the transformation from SSC to SCC has been reported at temperatures above 50°C by Sakamoto *et al.* [12] and Olsen *et al.* [46]. The improvement is reported to be attributable to the increased stability of the passive film leading to enhanced pitting resistance, which is relevant since pitting is recognised [59] to be the precursor to crack initiation at low temperatures (i.e. <50°C). Hence for martensitic stainless steels

[2]Tests were performed on 95 ksi and 110 ksi grade supermartensitics (0.01-0.04% C, 1-2% Mo, 4-6% Ni) at 20°C using NACE TM-0177 method A (tensile) and Slow Strain Rate Tests (SSRT).

SSC needs to be considered at temperatures below ~50°C and SCC at temperatures >50°C, with the likelihood of SCC increasing with increasing temperature above 60°C.

In addition, in $CO_2$ and $CO_2$-$H_2S$ environments seen in OCTG applications the corrosion rate and also the susceptibility to pitting and crevice corrosion need to be considered.

Consequently material selection needs to be based not only on the low temperature SSC resistance but on the resistance to SCC and general corrosion or pitting / crevice corrosion at the maximum service temperature. For the various classifications of martensitic OCTG pipes the limiting threshold temperatures for SCC are reported to be as follows:

| | |
|---|---|
| Conventional 13%Cr; | 100 – 125°C |
| Modified 13%Cr: | 150°C |
| Super 13%Cr: | 175°C |
| 15%Cr: | 200°C |
| 17%Cr: | 200 – 230°C |

It should be noted that the above threshold temperatures are also dependent on the partial pressure of $H_2S$, the pH and the chloride ion concentration.

It has been reported by Enerhaug *et al.* [45] that room temperature is the most critical temperature for SSC due to the 'weakness' of the passive film. However testing was not conducted at lower temperatures than 20°C and there is insufficient Information in the literature to support this statement. The inadequate data on susceptibility to SSC below room temperature were also noted by Cayard & Kane [16].

In the case of 13%Cr stainless steels the stability of the passive film at room temperature is related to the partial pressure of $H_2S$, the solution pH and the chloride ion concentration and Marchebois *et.al.* [27] reported that in the low pH (~3.5) condensed water environment the surface was active (active dissolution), whereas in the higher pH (~4.0) produced water environment the surface exhibited non-stable passive behaviour. Therefore in both environments pitting leading to cracking can occur, however due to the instability of the passive film, pitting leading to cracking is more likely in the produced water environment [45].

It is recognised that SSC is predominately a hydrogen embrittlement cracking mechanism and therefore the susceptibility to SSC is directly linked to the relationship between temperature, hydrogen uptake, diffusivity and trapping behaviour [60], with the tendency to cracking dominated by reversible trapped hydrogen. However the initiation of pitting is a critical factor since hydrogen permeation studies by Kimura et.al. [10] revealed that, at the high pH condition of 4.5, the hydrogen did not enter the steel from the surface but from the pit sites. Therefore in the case of corrosion at ambient or sub-ambient temperatures the hydrogen entry mechanism is from active corrosion at the site of pits and in the presence of $H_2S$ the pit growth rate can have an inverse relationship to temperature[61].

Both Hinds *et al*. [31] and Smirnova *et al.* [48] show that the effective diffusivity of super 13% Cr stainless steels increases with temperature and that the diffusivity of hydrogen is controlled by reversible trapping. Hinds *et al*. [31] also showed that the subsurface concentration of lattice hydrogen increases with temperature, whilst the concentration of reversibly trapped hydrogen does not vary significantly over the temperature range at a constant applied CP potential (see Table 2.6).

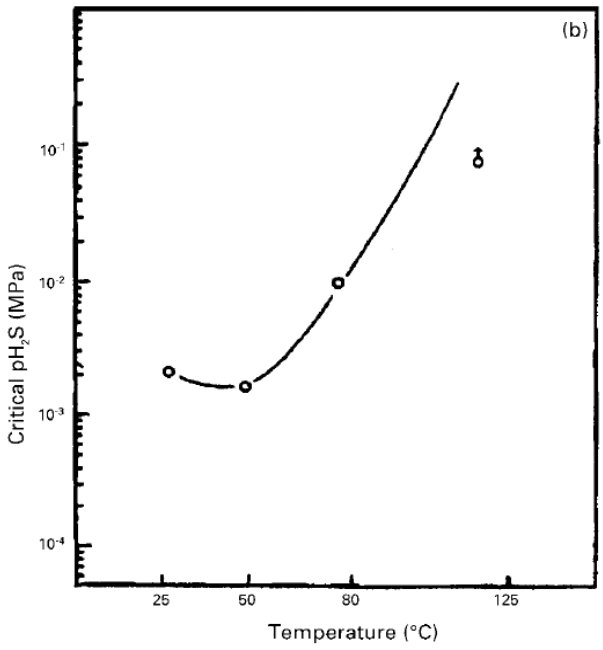


**Figure 2.15** Effect of temperature on the critical $H_2S$ partial pressure for cracking susceptibility [12].

**Table 2.6** Sub-surface concentration of hydrogen in super martensitic stainless steel with temperature at a constant applied CP potential (-1.0$V_{SCE}$) [31]

| Temperature (°C) | Subsurface concentration of lattice hydrogen (ppb) | Subsurface concentration of reversibly trapped hydrogen (ppm) |
|---|---|---|
| 5 | 0.12 | 23.3 |
| 23 | 0.43 | 23.9 |
| 40 | 0.76 | 14.8 |
| 70 | 5.5 | 21.6 |

When temperature is decreased, hydrogen is not mobile enough to reach trap sites effectively. This is why carbon steels are most susceptible to SSC at room temperature, however this trend has not yet been confirmed for the martensitic stainless steels and relatively few tests have been done to investigate this.

An investigation carried out by Exova Corrosion Centre in 2005 [2] suggested that an API 5LC grade LC80-130S weldable martensitic stainless steel was more susceptible to SSC at 7°C than at 25°C and 115°C[3]. It was reported that this may have been due to the increase in $H_2S$ solubility as temperature decreases. A higher susceptibility to SSC at 5°C compared to 24°C was also found under formation water conditions by Dent et al. [62]. In contrast, Chambers *et al.* [63] concluded that conventional 80 ksi grade and super martensitic 110 ksi grade stainless steels were less susceptible to SSC at 5°C compared to room temperature [46]. However, both of these tests were conducted using different test methods and using different grades of 13%Cr, hence they are not directly comparable: Chambers et al. [63] used tensile test specimens stressed to 90% AYS whereas Dent et al. [62] used the four-point bend method at 100% AYS. Chambers et al. used a higher chloride ion content produced water environment (100,000 mg/L $Cl^-$, pH 4.5) but at a lower level of $H_2S$ (38 mbara) compared to Dent et al. [62]. (30,000 mg/L $Cl^-$, pH 5 at 69 mbara $H_2S$). Interestingly, the results from Chambers et al. showed cracking at both room temperature and at 5°C for the 110 ksi grade super martensitic material but with no pitting corrosion in the simulated gas well tests (1,000 mg/L $Cl^-$, pH 3.5).

[3]Four-point loaded SSC tests performed in simulated produced water (30,000 mg/L $Cl^-$, pH 5) and condensed water (1000 mg/L $Cl^-$, pH 4) at 69 mbara $H_2S$ and 100% AYS

Work by Dent et.al. [62] on 80 ksi grade of weldable martensitic stainless steel in low pH (3.5), low chloride (i.e. 1,000 mg/L) condensed water and in high pH (4.5), high chloride ion content (i.e. 100,000 mg/L) produced water environments at 35 mbara and 69 mbara $pH_2S$ indicated a higher susceptibility to SSC at 5°C compared to 24°C. The results also demonstrated the importance of surface preparation and loading conditions on the initiation of SSC in laboratory tests.

### 2.6.4 Influence of Oxygen Contamination

Oxygen contamination is a serious problem when testing for SSC as this can lead to pitting corrosion. For this reason, EFC 17 guidelines recommend that oxygen levels are kept below 10 ppb in the liquid phase; however there is no evidence to prove that 10 ppb is the critical oxygen level below which there is no detrimental Influence. A study by Meng *et al.* [13] investigated the Influence of dissolved oxygen in sour (103 mbar $H_2S$) brine on the electrochemical behaviour of a 15%Cr martensitic stainless steel. The results showed (see Figure 2.16) that oxygen levels as low as 50 ppb increased the open circuit potential by 50 mV, increasing susceptibility to pitting and cracking [41].

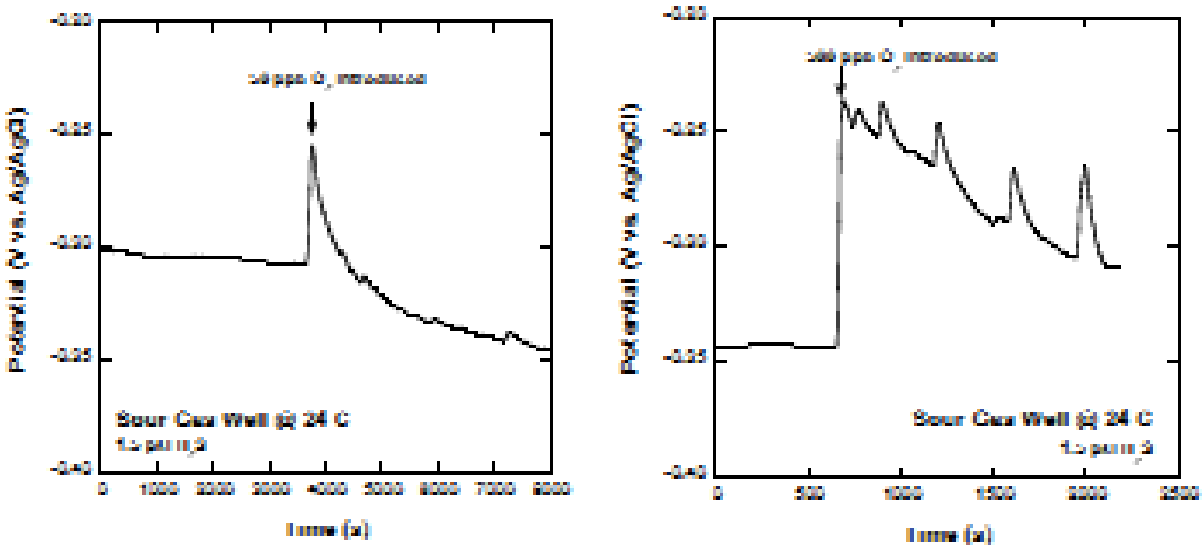


**Figure 2.16** Influence of oxygen ingress on the corrosion potential of modified 15%Cr stainless steel with 0.01 MPa (1.5 psia) $H_2S$ partial pressure (a) Above – Injection of 50 ppb $O_2$ in solution; (b) Below – injection of 500 ppb $O_2$ in solution [13].

### 2.6.5 Influence of Solution Buffer

Laboratory SSC testing is required to be conducted under controlled pH conditions to simulate service conditions and since the solution volumes are relatively small and the solution volume to specimen surface area ratio is generally in the range of 30 mL/cm$^2$ ± 10 mL/cm$^2$ buffers are normally used to control the pH within set limits.

The main function of the buffer is to maintain a stable pH, if possible, even under corroding conditions. However it is important that the selected buffer will not Influence the test result by influencing the stability of the passive film and in particular the use of acetate buffers have been the subject of extensive research since 1999 and a number of papers have been published in the literature [14], [64], [29], [46], [65], [66], [67], [68].

In a purely passive system buffering should not be required, however in the case of ambient pressure SSC testing of 13%Cr martensitic stainless steels, particularly under low pH (~3.5) condensed water conditions encountered in gas fields, the pH will tend to increase; with the rate of increase dependent on the amount of corrosion. The pH increases because the anodic dissolution and metal ion hydrolysis reaction is not balanced by the hydrogen ion reduction reactions. According to Turnbull [32] during a typical 30-day corrosion test with a relatively low passive current density of 1 µA/cm$^2$ about 1.7 x 10$^{-3}$ moles of hydrogen are consumed.

In the current editions of ISO 15156 / NACE MR0175 [3], NACE TM0177 [55] and EFC 17 [69] there are three options for the test solutions and respective buffers for ambient temperature or low temperature SSC testing of martensitic stainless steels, as detailed in sections 2.6.5.1 – 2.5.5.3.

2.6.5.1 Type 1 Environment

For this environment the in-situ pH is replicated by simulating the service conditions in terms of the actual $H_2S$ and $CO_2$ partial pressures, the chloride ion concentration and the presence of any bicarbonate ions. This solution is truly representative of the service environment, however it requires the use of autoclaves and the pH cannot be 'controlled' during the test, therefore pH drift may occur over the 720 hr test period. For this environment the pH is measured before and after testing at 1 bara $CO_2$ and at ambient pressure and any change in the pH is indicative of changes occurring during the test. There is no restriction on the 'drift' in the pH, however if the drift is >0.2 units this could be indicative of corrosion occurring during the test.

2.6.5.2 Type 2 Environment

This environment provides service simulation at ambient pressure using a 'natural' sodium bicarbonate buffering agent, but can only be applied for tests requiring an in-situ pH of 4.5 or greater. The solution pH is measured at the start and the end of the test and may be measured periodically during the test, with a restriction that the pH must be maintained to within ±0.2 units of the target pH.

A pH of 4.5 or greater can also be achieved using the acetate-HCl buffer system described for the type 3 environment in ISO 15156 / NACE MR0175 [3] (EFC17 [69]) and as solution C in NACE TM0177 [55]. Kimura et.al. [59] compared the pH stability of three 5 wt.% NaCl solutions at a pH of 4.5; one containing 4g/L sodium acetate with the pH adjusted by acetic acid and sodium bicarbonate (A), one containing 4g/L sodium acetate with the pH adjusted by hydrochloric acid and sodium bicarbonate (B), and one containing 65 ppm sodium acetate, with the pH adjusted by acetic acid and sodium bicarbonate (C). The work compared the pH response to acid additions of the three solutions and concluded that the pH was more stable in the higher buffered solution A than solutions B and C and that there was a greater susceptibility to SSC at the site of localised pitting (where the pH would be locally reduced) in the weakly buffered solution C compared to solution A.

Chambers et al. [63] also conducted SSC tests on 13%Cr OCTG material using the type 2 sodium bicarbonate natural buffer and the type 3 (NACE TM0177-solution C [55]) acetate-HCl buffer and found one of the three materials tested (13Cr-110) did not crack in the acetate-HCl buffered solution (type 3) but exhibited cracking in the type 2 solution, with the natural bicarbonate buffer. The difference between the natural bicarbonate buffer and acetate-HCl buffer on the pitting potential of a 15%Cr martensitic stainless steel was also investigated by Meng et al. [13] and the pitting potential was found to be higher in the acetate-HCl buffered solution compared to the natural bicarbonate buffered solution (see Figure 2.17).

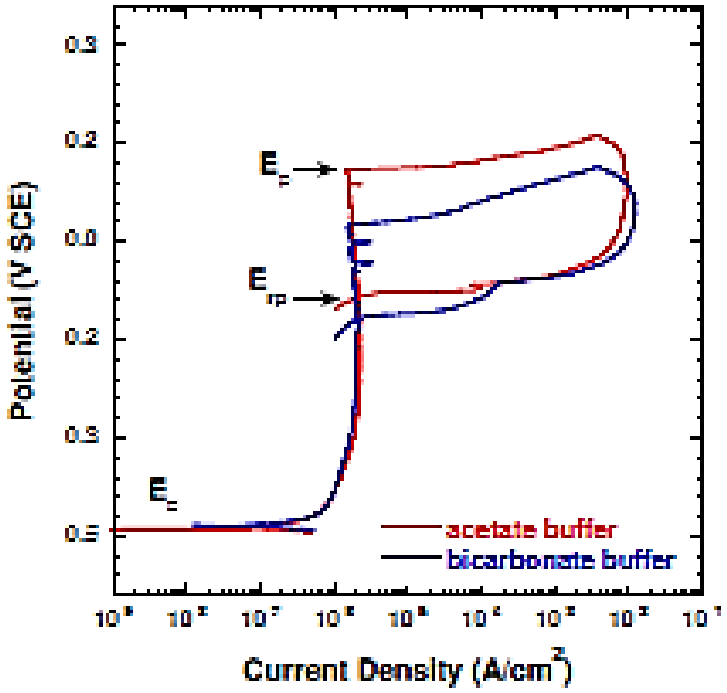


**Figure 2.17** Polarisation curves for 15%Cr steel in 100,000 mg/L chloride solution containing acetate or bicarbonate buffer with pH 4.5 at 24°C. The solutions were purged with $CO_2$ at ambient pressure. The potential scan rate was 0.2 mV/s [13].

In summary for pH values of 4.5 or greater the stronger buffered acetate-HCl solution would appear to provide more benign conditions over the weakly buffered bicarbonate solution by increasing the pitting potential and reducing the localised acidification within pits, thus reducing the chance of crack initiation from pits.

2.6.5.3 Type 3 Environment

This environment provides service simulation at ambient pressure using an 'artificial' acetic buffering agent. For testing martensitic stainless steels 0.4 g/L sodium acetate is added and the required in-situ pH is adjusted by the addition of HCl to the solution. Unlike the Type 2 environment this solution can be used over the full range of pH values encountered in oil and gas production. The solution pH is measured at the start and the end of the test and may be measured periodically during the test, with a restriction that the pH must be maintained to within ±0.2 units of the target pH. This solution is known as type 3a environment ISO 15156 / NACE MR0175 [3] and EFC17 [69] and test solution C in NACE TM0177 [55].

The use of the acetate buffer in test environment 3 has been the subject of research and discussion due to concerns that high acetate concentrations (i.e. 4 g/L) may de-passivate 13%Cr martensitic stainless steels at low pH values (i.e. ~3.5) and conversely that low acetate concentrations (i.e. 0.4 g/L) may not maintain the pH within acceptable limits. In the 1st edition of EFC17 [70], published in 1995, a sodium acetate buffer was specified with a concentration of 4 g/L and in the 1996 edition of NACE TM0177 [71] the only buffered test solution (solution B) was available containing 5 wt.% sodium chloride, 0.4 wt.% sodium acetate and 0.23 wt.% acetic acid. The Influence of the acetate concentration and solution composition was investigated by Amaya and Ueda [14] using the solutions shown in Table 2.7.

**Table 2.7** Test solution compositions and change in pH following saturation with $H_2S$ [14]

| | NaCl [wt%] | $CH_3COONa$ [wt%] | $CH_3COOH$ [wt%] | HCl (12N) [ml/l] | pH [-] |
|---|---|---|---|---|---|
| NACE TM0177 solution-B | 5.0 | 0.4 | 0.23 | - | 4.54 |
| EFC Publications | 5.0 | 0.4 | - | 4.0 | 3.44 |
| Solution-1 | 5.0 | 0.04 | 0.23 | - | 3.51 |
| Solution-2 | 5.0 | 0.4 | 2.30 | - | 3.55 |

pH measurements after $H_2S$ saturation using the four solutions revealed the NACE TM0177-96-Solution B [71] with 0.4 wt.% $CH_3COONa$ was not an effective buffer since the pH increased from 3.5 to 4.54. This solution was subsequently changed to the composition of solution-2 in the 2005 edition of the standard [55]. Amaya and Ueda also compared the Influence of solution composition on the SSC resistance of 13Cr-95 ksi grade four point bend specimens, the corrosion rate and the change in the pH over the 336 hr test period. The results, presented in Figures 2.18 – 2.20, showed that test solution 2 containing the relatively high 0.4 wt.% $CH_3COONa$ and 0.04 wt.% $CH_3COOH$ de-passivated the surface of the 13Cr-95 ksi material leading to relatively high weight loss values (1.87 – 2.32 g/m$^3$/hr) and associated SSC at 0.001 MPa $H_2S$ and at chloride ion concentrations of 0.1, 1.0 and 5.0 wt.%.

As a result of the active corrosion at the surface of the specimens the solution 2 environment, with the higher buffering capacity, was not effective in buffering the pH and as a consequence the solution pH increased from 3.50 to 4.02 over the 332 hr test period.

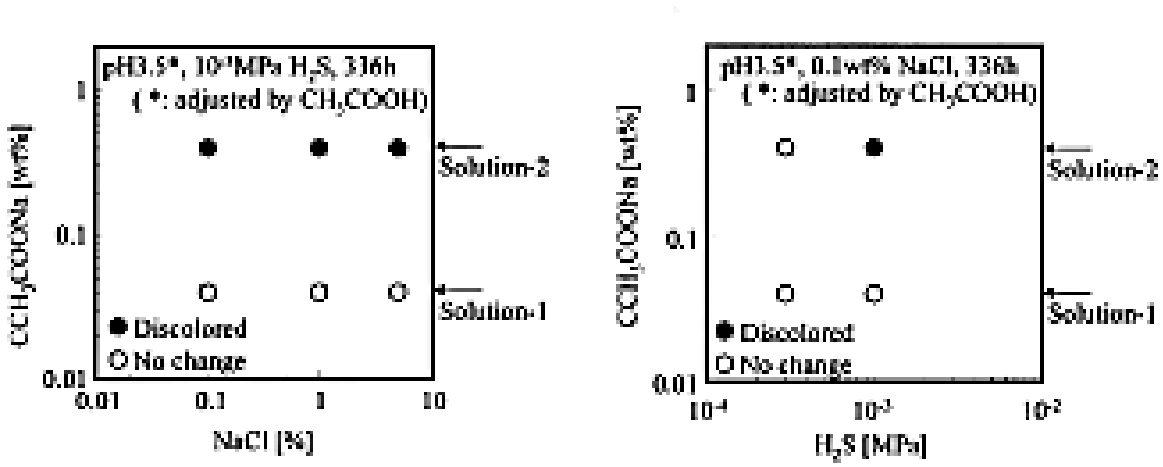


(a) –0.001 MPa $H_2S$ (b) – 0.1 wt.% NaCl

**Figure 2.18** Corrosion test results in each buffer solution with the variation of NaCl concentration [14].
(a) and $H_2S$ partial pressure (b).
(pH 3.5, four point bent beam, 336 hr, 25°C)

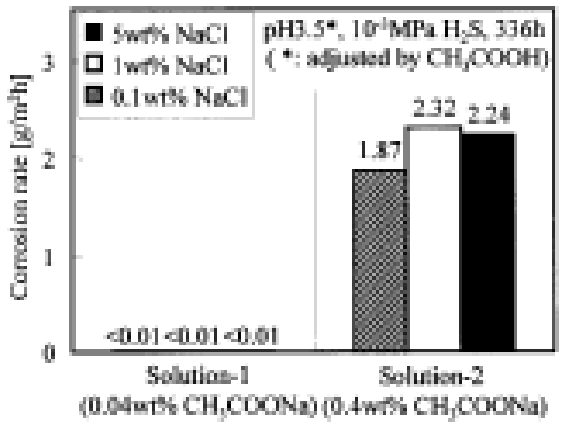


**Figure 2.19** Comparison of the corrosion rates in each buffer solution [14].
(pH 3.5, 0.001 MPa $H_2S$, four point bent beam, 336 hr, 25°C).

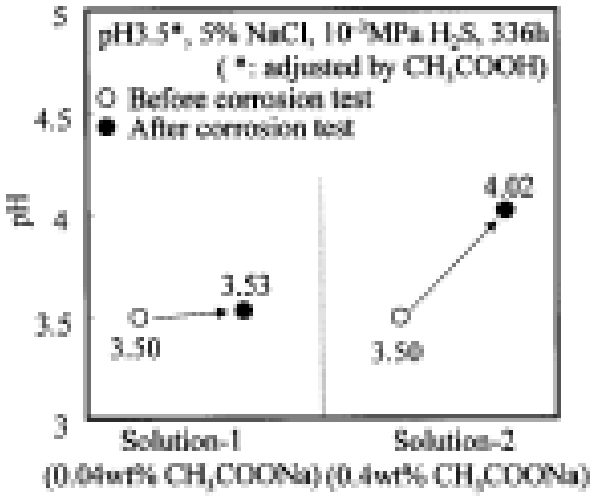


**Figure 2.20** Results of the pH measurements before and after corrosion tests in each buffer solution [14].
(pH 3.5, 0.001 MPa $H_2S$, four point bent beam, 336 hr, 25°C)

The authors also compared the stability of the passive film on the 13Cr-95 ksi material in the two buffered solutions using anodic polarisation scans and the results, shown in Figure 2.21, revealed the surface passivated in the low 0.04 wt.% $CH_3COONa$ / 0.23 wt.% $CH_3COOH$ solution but exhibited active corrosion in the relatively high 0.4 wt.% $CH_3COONa$ / 2.3 wt.% $CH_3COOH$ solution.

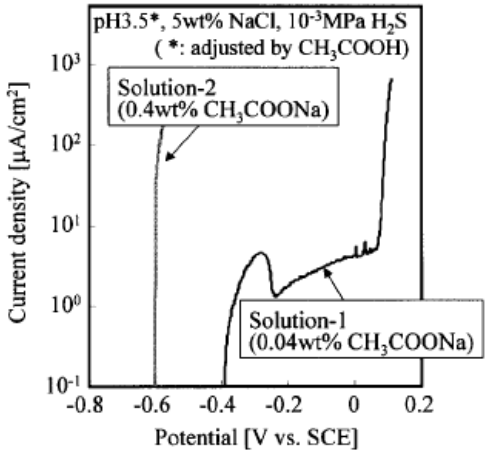


**Figure 2.21** Anodic polarisation curves of super 13Cr steels in each buffer solution [14]. (pH 3.5, 5 wt.% NaCl, 0.001 MPa $H_2S$, four point bent beam, 336 hr, 25°C)

In recognition of the potential damaging effect of the strongly buffered $CH_3COONa$ / $CH_3COOH$ test solution on the corrosion and cracking resistance of 13%Cr martensitic stainless steels in particular the 0.04 wt.% $CH_3COONa$ buffered solution (solution 3b) was included in the 2nd edition of EFC17 and a new test solution C was added to the 2005 edition of NACE TM0177. The solution was also changed to replace the $CH_3COOH$ with HCl.

The question of de-passivation of 13%Cr stainless steels in the presence of acetate species at relatively low pH values was reviewed and investigated by Turnbull [32] in the light of the previous publications [14], [65], [46]. Using an applied potential of -330 mV v SCE Turnbull compared the de-passivation pH of 13%Cr stainless steel in 5 wt.% NaCl, nitrogen de-aerated solutions containing an acetate-free HCl buffer, and a 4 g/L acetate buffer, acidified with HCl and acetic acid. The results of the studies, shown in Table 2.8, did not show any significant differences between the three solutions, so it was concluded that it would be prudent to use HCl only to achieve the low pH test conditions to avoid any potential issues with acetate buffers.

**Table 2.8**
Passive film destabilisation pH for super 13%Cr steel in 5% NaCl [32]

| Solution | Acid added | Destablisation pH |
|---|---|---|
| Acetate-free | HCl | 2.13≤pH<2.21 |
| 4g/L acetate | HCl | 2.16≤pH<2.45 |
| 4g/L acetate | Acetic acid | 2.19≤pH<2.30 |

The proposal by Turnbull [32] that it would be better to use just HCl to achieve low pH solutions without any buffer was supported by Crolet & Leyer [64]. Using just HCl without any acetate provides two potential issues to discuss; one is the Influence of the additional chloride concentration when testing under condensed water conditions with low NaCl additions and the other is how to minimise the drift in the pH during a typical 30-day SSC test.

When using the type 3b solution (or solution C of NACE TM0177 [55]) and a typical condensed water solution containing 1 g/L NaCl the $Cl^-$ ion concentration will be 0.017 M or 17 mM. To achieve a pH of 3.5, typically used for SSC testing in condensed water, approximately 4 ml of 12 M HCl will required to be added [14] which will increase the $Cl^-$ ion concentration by 0.048 M or 48 mM, leading to a significant increase, which would be even more pronounced at lower concentrations of NaCl sometimes used for testing. For this reason the alternative acetate-acetic acid buffer was proposed by Amaya & Ueda [14]. Crolet & Leyer [64] proposed only adding HCl for low pH condensed water conditions and stated that the chloride ion concentration would only increase from 17 mM to 18 mM for acidification of the solution down to a pH of 3, which was not considered to be significant in terms on the Influence of pitting and cracking of 13%Cr stainless steels.

The drift of the pH during SSC testing in low pH condensed water environments is a major concern since the conditions will become more benign during the typical 720 hr test period and as a consequence the tests may be invalidated. As previously discussed the pH of these low (i.e. ≤4.0) pH tests will tend to increase due to the decrease in the hydrogen ion concentration and dissolution of iron as a result of the passive film growth and localised pitting, resulting in an increase in the pH by 0.1 units for every 2.8 ppm of $Fe^{++}$ in solution [64].

In order to minimise the increase in pH for low pH test solutions the solution volume could be increased, HCl can be added during testing and the likelihood of localised corrosion can be minimised. The maximum solution volume to area ratio is currently restricted to a maximum value of 40 mL/cm$^2$ in the 2005 edition of NACE TM0177 [55], however there is no logical reason for this upper restriction and there is a proposal to remove this restriction in the next revision of NACE TM0177, as discussed during the NACE TG085 Task Group meeting in 2013. The addition of HCl to compensate for the reduction in the hydrogen ion concentration needs to be carefully controlled to avoid oxygen contamination and the increase in the chloride concentration needs to be considered when testing in low chloride ion content solutions, as previously discussed. Localised corrosion of specimens during laboratory testing can also add to problems in controlling the pH and measures can be taken to minimise these effects. For example epoxy coating of the sealing face of NACE TM0177-Method A [55] tensile specimens eliminates the risk of localised crevice corrosion at the seal surface.

2.6.5.4 Summary

The control of the pH during the laboratory SSC testing of 13%Cr stainless steels is critical and a number of methods are provided in the ISO 15156 / NACE MR0175 [3], NACE TM0177 [55] and EFC 17 [69] international standards. When testing at pH values of 4.5 and above a 'Natural' sodium bicarbonate or a sodium acetate-HCl buffer can be used, however there is evidence in the literature to suggest that the 'natural' bicarbonate buffer may provide more aggressive conditions with respect to localised corrosion and subsequent cracking.

At pH values below 4.5 the natural bicarbonate buffer is not an option and for ambient temperature testing sodium acetate-HCl and sodium acetate-acetic acid buffers have been used, although there is concern regarding the de-passivation of 13%Cr stainless steel by acetates, the effectiveness of pH control at low acetate concentrations (i.e. 0.4 g/L) and the Influence of HCl on low chloride solutions.

To avoid the use of acetate buffers one alternative is to control the pH using HCl additions which is not ideal due to the potential risk of oxygen ingress.

For all pH values the use of an autoclave enables the respective partial pressures of $H_2S$ and $CO_2$ occurring in the actual environment to be replicated together with the solution chemistry and this approach ensures the true in-situ pH is replicated under laboratory conditions. This approach does have the obvious benefit of avoiding the use of artificial buffers, however laboratory set up is more complicated than ambient pressure testing, the solution volume is often restricted and the pH cannot be easily monitored during the test.

## 2.7 SSC Application Limits

### 2.7.1 Conventional Grades

pH-$pH_2S$ domain diagrams provide a convenient method of expressing the application limits of 13%Cr OCTG in sour environments. In the case of SSC resistance the diagrams need to be plotted for different chloride concentrations, since as previously discussed the chloride concentration is one of the important parameters in determining the SSC resistance. Separate diagrams are also required for the different grades and strength levels of martensitic tubular products.

Comprehensive diagrams have been prepared by Marchebois et al. [15] for the conventional grades of 13%Cr at chloride levels of 1 g/L, 10 g/L and 100 g/L and these are presented in Figure 2.22. Additionally Cayard & Kane [16] plotted data for 80-95 ksi 13Cr from SSC tests conducted in chloride concentrations ranging from 30,000 – 60,000 mg/L (see Figure 2.23).

The diagrams show the reduction in the extent of the acceptable green zone with increasing chloride ion concentration and also show that the NACE MR0175 / ISO 15156 ‘safe’ condition of ≥3.5 pH / 10 kPa (0.1 bara) $pH_2S$ is only valid for relatively low chloride concentrations in the order of ≤10 g/L. At chloride levels of ≥100 g/L the conventional 13%Cr is likely to fail under the ‘NACE TM0177-Solution A’ conditions, as shown by Figure 2.22.

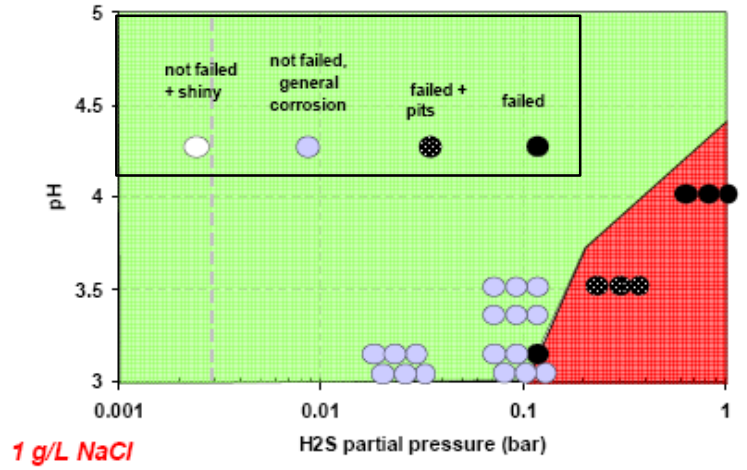


**(a)**

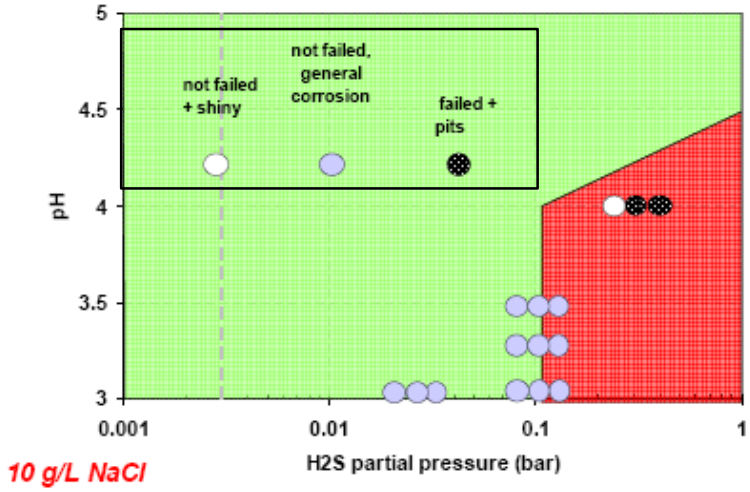


**(b)**

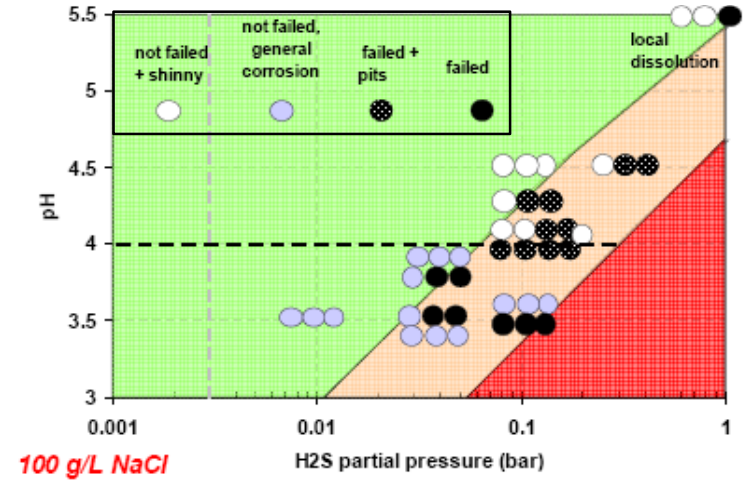


**(c.)**

**Figure 2.22** pH-$pH_2S$ domain diagrams for L80-13Cr stressed to 90% AYS (NACE TM0177-Method A) [15].

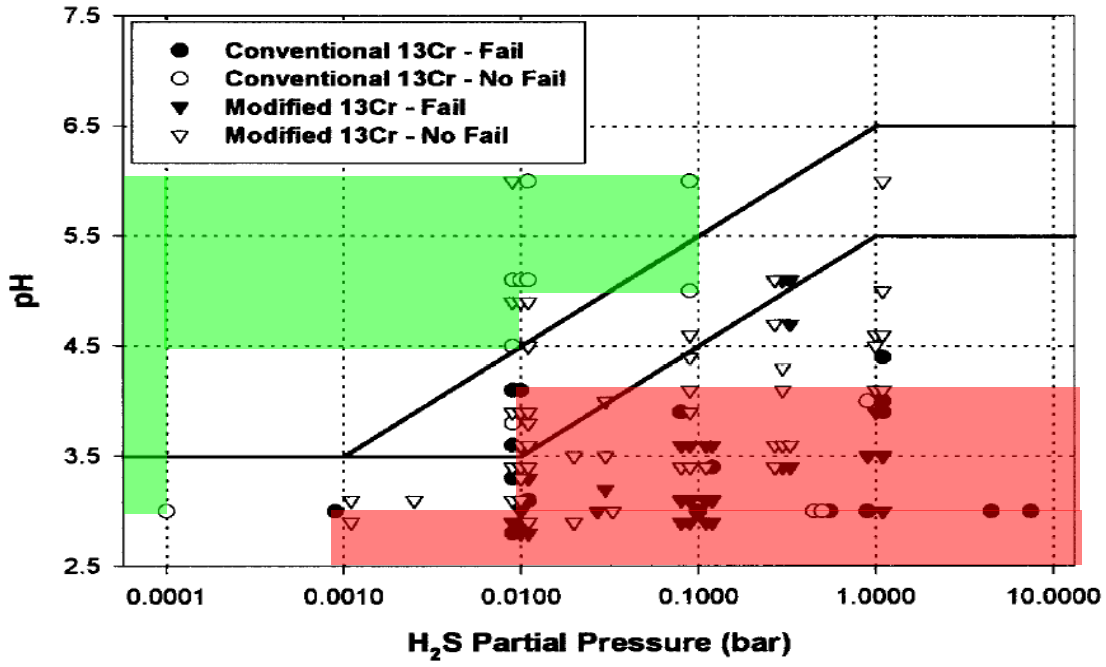


**Figure 2.23** pH-p$H_2S$ domain diagram for conventional 13Cr (80-95 ksi grades), stressed to 80-100% SMYS, 30,000 mg/L – 60,000 mg/L $Cl^-$ [16].

### 2.7.2 Modified 13% Cr Stainless Steels

Cayard & Kane [16] reviewed the literature in 1998 and plotted a pH-$H_2S$ domain diagram that included 'modified' 13%Cr (0.03% C, 1-2% Mo, 4-6% Ni), as shown in Figure 2.24. The data were based on specimens tested at 25°C, stressed from 80-100% SMYS in brine solutions containing 30,000 to 60,000 mg/L $Cl^-$. Safe threshold values can be taken as:

- 1 - 10 mbar $H_2S$ at pH 3.5
- 100 mbar $H_2S$ at pH 4.0-4.5

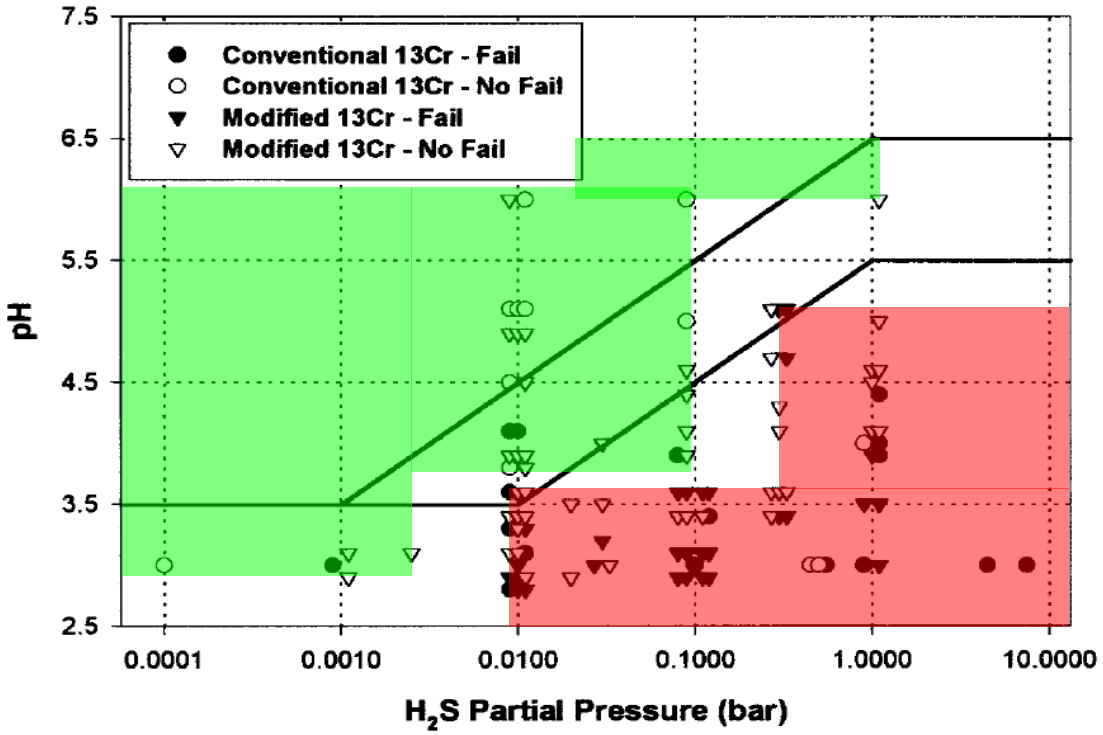


**Figure 2.24** pH-$pH_2S$ domain diagram for modified 13Cr (80-110 ksi grades), stressed to 80-100% SMYS, 30,000 mg/L – 60,000 mg/L $Cl^-$ [16].

Kane[17] presented results at the ISO 15156 maintenance panel meeting in 2007 in the form of pH-$pH_2S$ diagrams for modified 13Cr OCTG tube and bar stock, as shown in Figure 2.25.

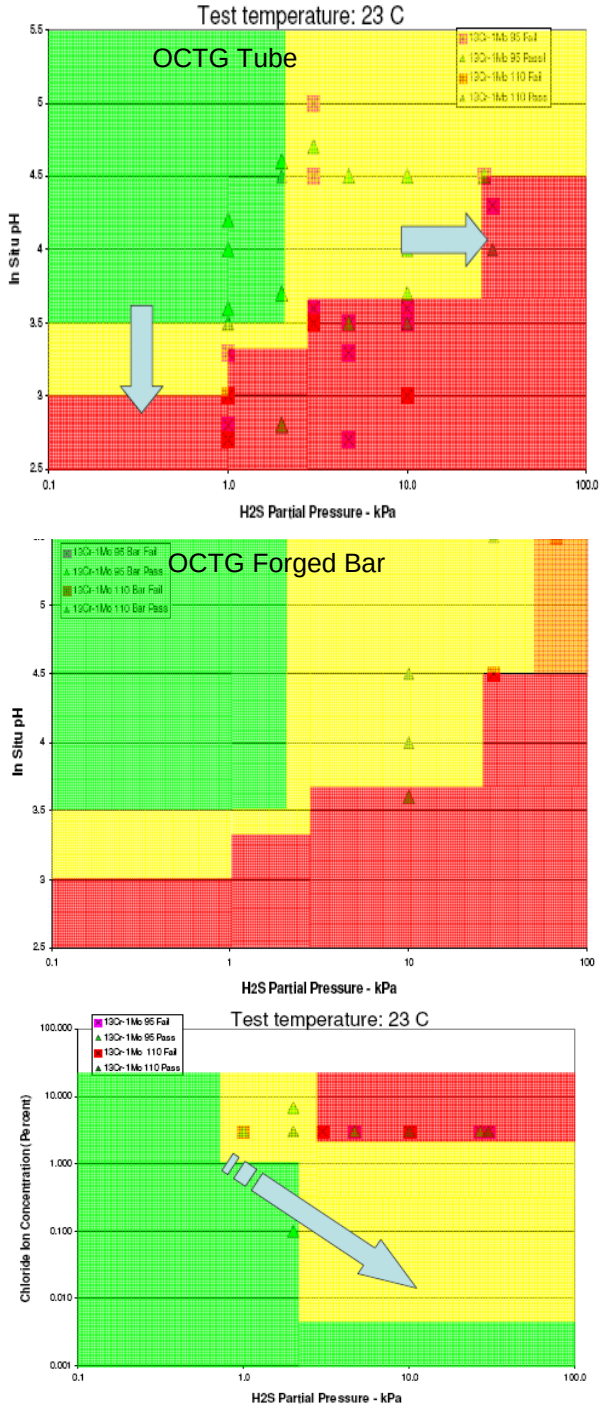


**Figure 2.25** pH-$pH_2S$ and chloride-$pH_2S$ domain diagrams for 95-110 ksi 13-5-1 modified martensitic stainless steels (OCTG Tube & Forged Bar), stressed to 80% SMYS – 90% AYS [17].

### 2.7.3 Super 13-5-2 Grades

pH-p$H_2S$ domain diagrams for the super martensitic grades in tube and bar form were presented by Kane at the ISO 15156 maintenance panel meeting in 2007, as shown in Figure 2.26. Comparison with Modified 13Cr results presented in Figure 2.25 shows application limits for the super grades are extended by the increase in the Mo concentration from 1% to 2.5%.

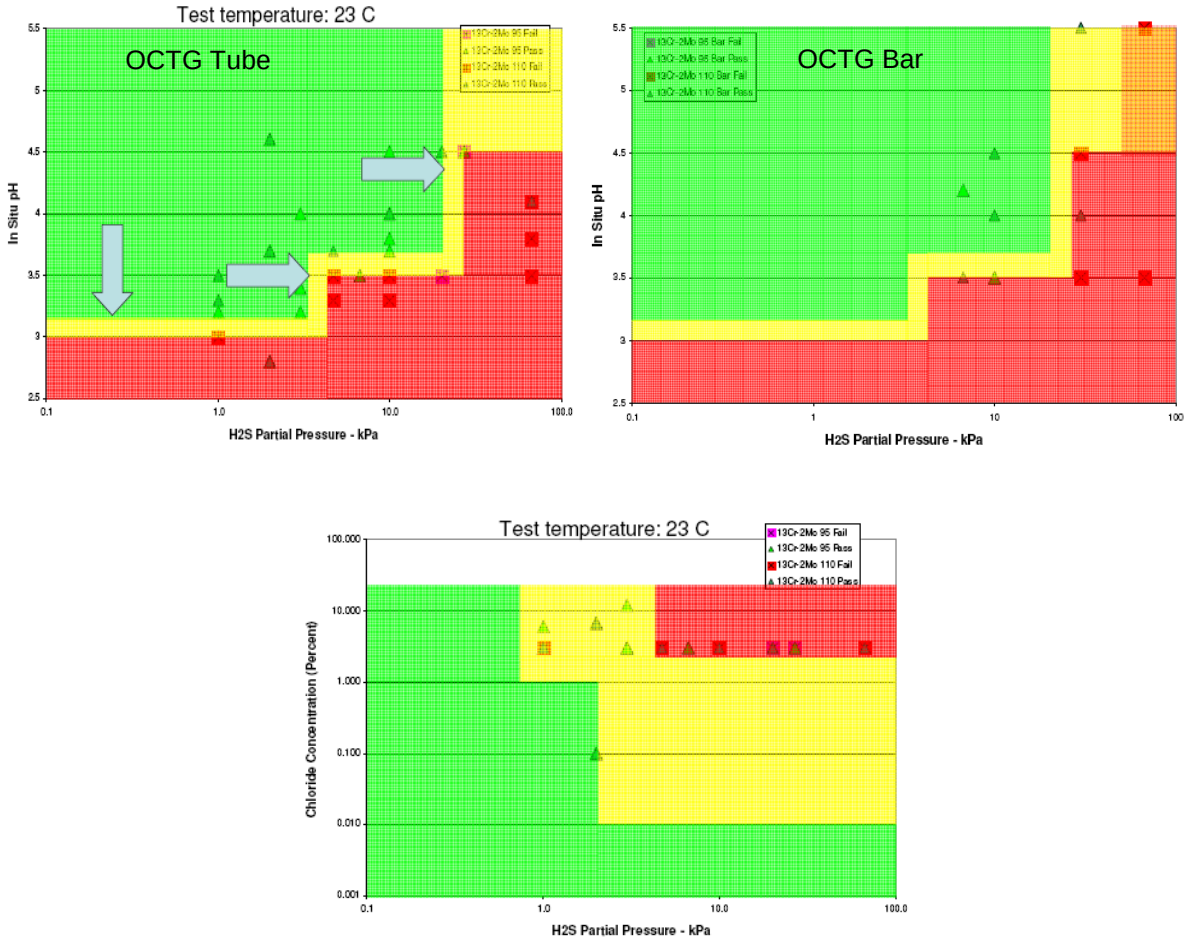


**Figure 2.26** pH-p$H_2S$ and chloride-p$H_2S$ domain diagrams for 95-110 ksi 13-5-2 super martensitic stainless steels (OCTG Tube and Forged Bar) stressed to 80% SMYS – 90% AYS. (Ref: Kane, Presentation to ISO 15156 Maintenance Panel, 9/9/2007 [17])

Data from NACE TM0177 tensile tests presented by Marchebois et al. [15], shown in Figure 2.27, were in general agreement with the data collated by Kane [17] and also clearly illustrated the Influence of chloride concentration on the SSC resistance.

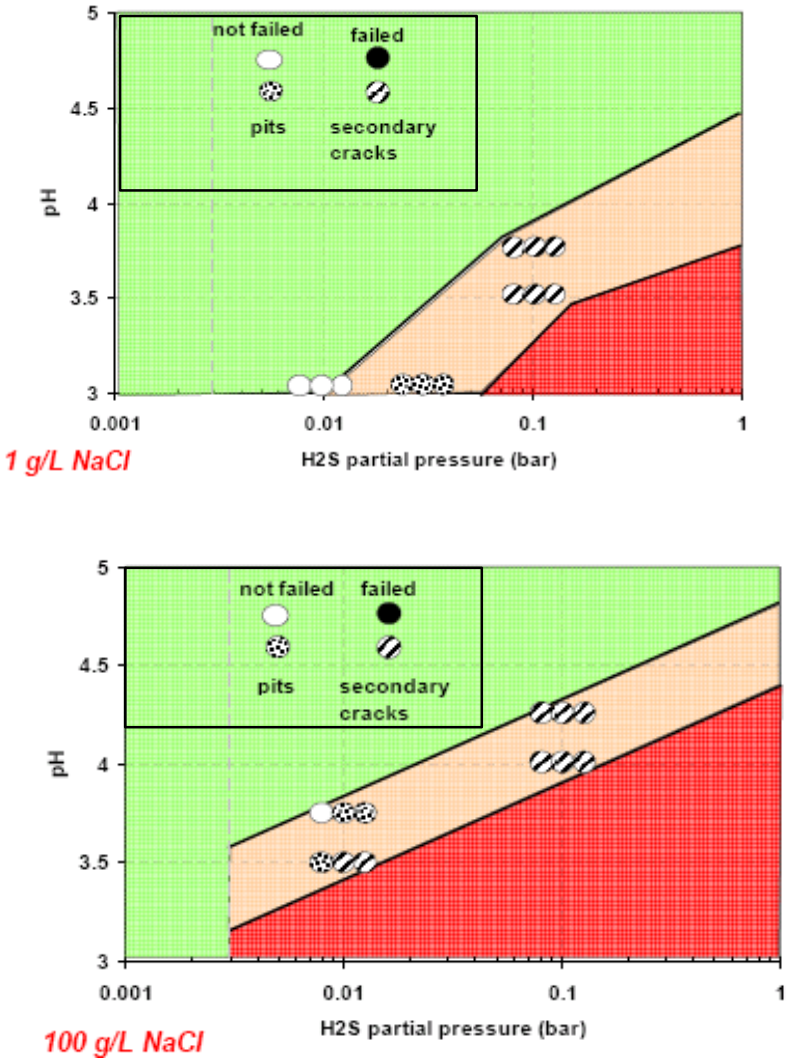


**Figure 2.27** pH-p$H_2S$ domain diagrams for 95 ksi grade (108 ksi act.) 13-5-2 super martensitic stainless steels, stressed to 90% SMYS (NACE TM0177-Method A) [15].

The Influence of chloride concentration on the SSC resistance of 110 ksi super 13Cr material was also determined by Nice et al. [18].

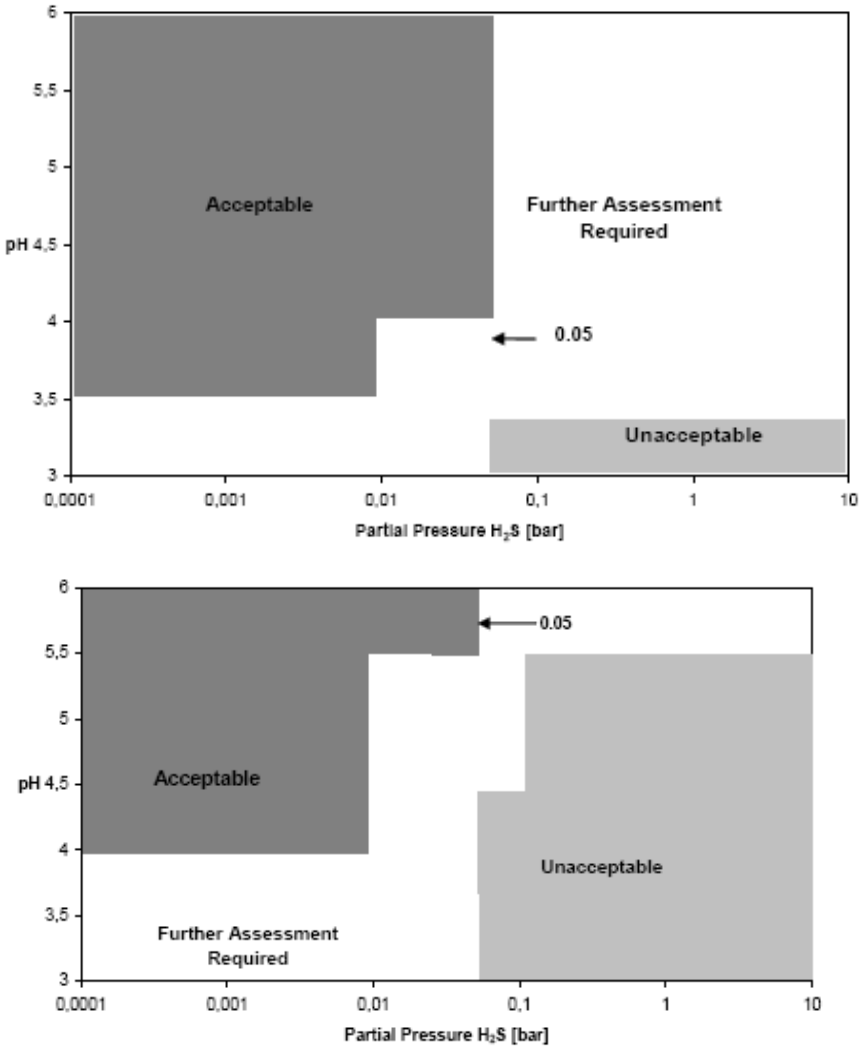


**137,000 mg/L Cl**

**Figure 2.28** pH-$pH_2S$ domain diagrams for Super 13Cr stressed to 90% AYS and tested in chloride levels of 1,000 mg/L and 137,000 mg/L (20 wt.% NaCl) [18].

A comprehensive study of the SSC and SCC resistance of the 110 ksi strength grade was presented by Takebe et al. [19] and a review of published and un-published data was conducted by Dent in 2011 and presented at the ISO 15156 maintenance panel meeting in Houston [20].

The results presented in Figures 2.29 and 2.30 clearly show the reduction in the limits of acceptability with increasing chloride ion concentration.

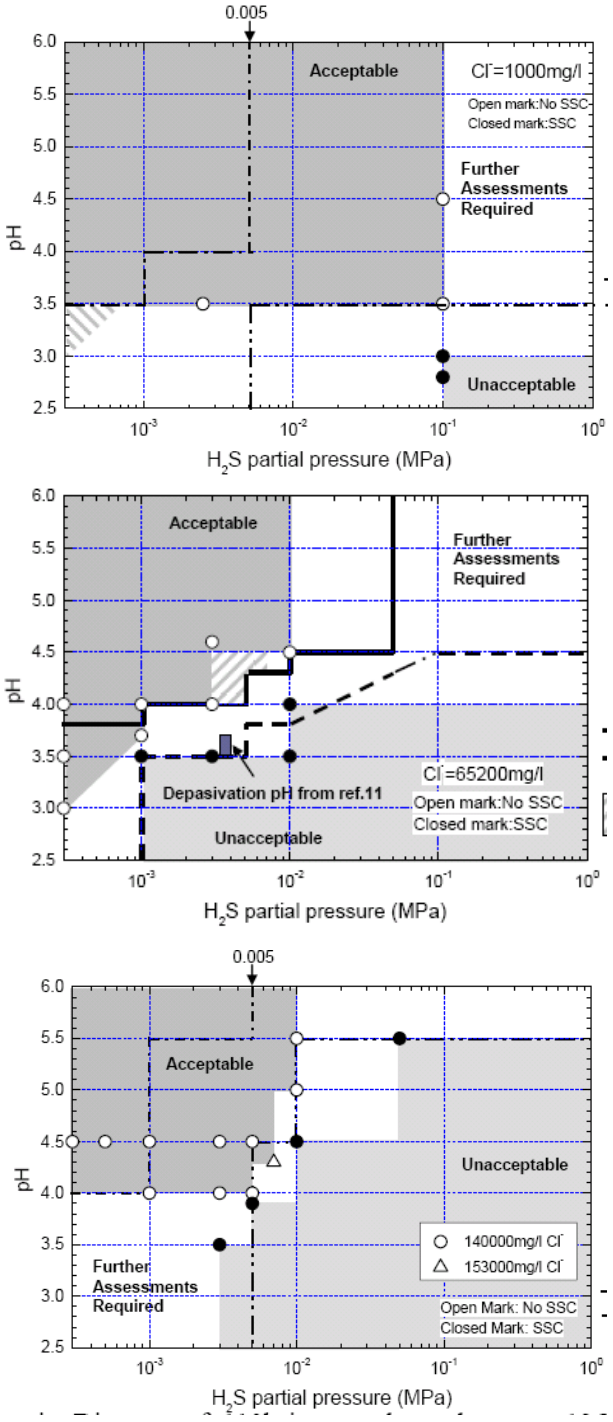


**Figure 2.29** pH-p$H_2S$ domain diagrams for 110 ksi grade 13-5-2 super martensitic stainless steels, stressed to 90% AYS (NACE TM0177-Method A) at chloride levels from 1,000 mg/L to 153,000 mg/L [19].

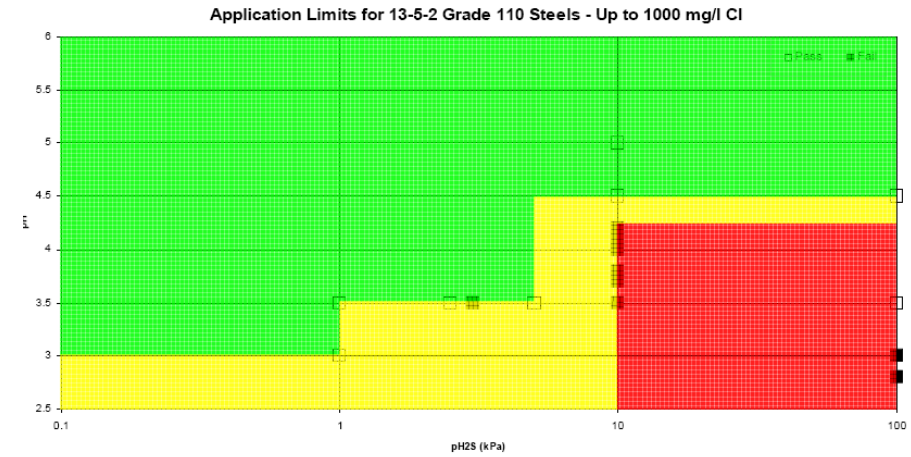


**Up to 1000 mg/L Cl**

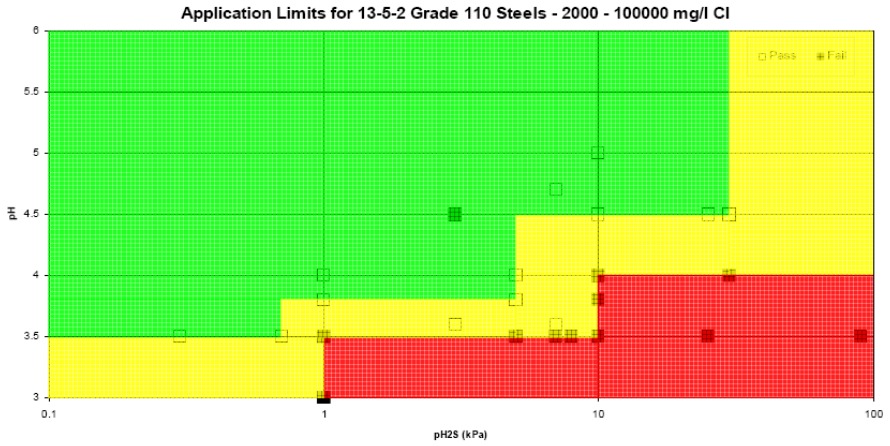


**2,000 – 100,000 mg/L Cl**

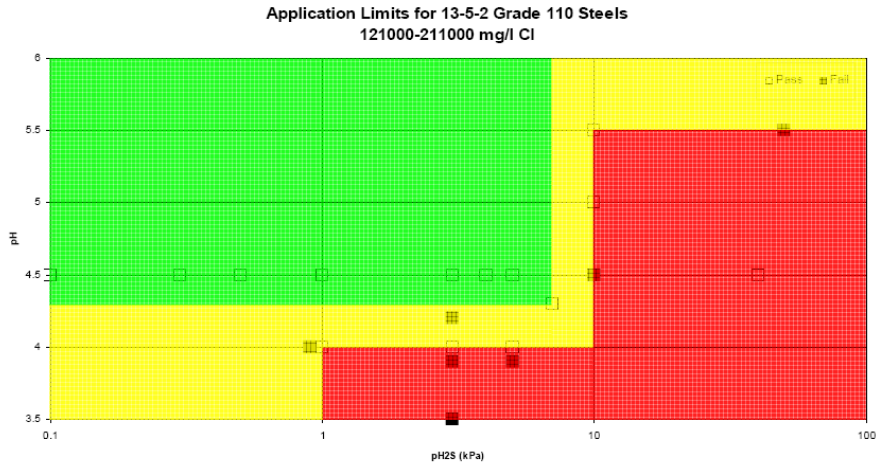


**121,000 – 211,000 mg/L Cl**

**Figure 2.30** pH-$pH_2S$ domain diagrams for 110 ksi grade 13-5-2 super martensitic stainless steels, stressed to 80% SMYS to 90% AYS (NACE TM0177-Method A) at chloride levels from 1,000 mg/L to 211,000 mg/L (Ref: Dent, Presentation to ISO 15156 Maintenance Panel, Houston [20]).

It can be seen from the previously presented pH-$pH_2S$ domain diagrams that material grade (i.e. conventional, modified or super), strength level and chloride concentration have a major Influence on the pH-$pH_2S$ threshold limits for OCTG down-hole tubular materials. pH-$pH_2S$ domain diagrams showing the Influence of the material and strength for the conventional (13Cr-L80) and super (S13 grade 95 and S13 grade 110) grades were presented by Marchebois et al. [15]. The diagrams presented in Figure 2.31 show that the acceptable pH-$pH_2S$ limits are reduced with increasing strength grade.

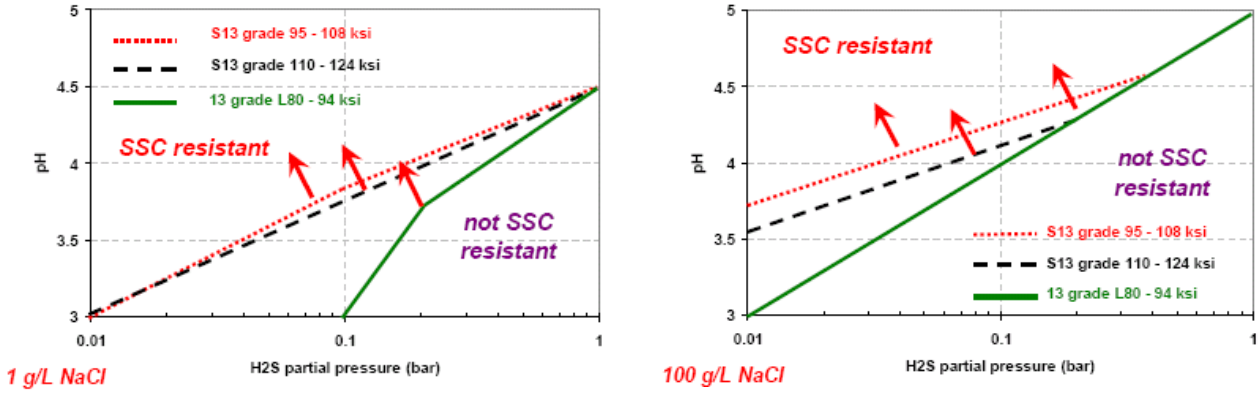


**Figure 2.31** Influence of material and strength grade on the pH-$pH_2S$ domain diagrams for 13Cr-L80, S13Cr-95 and S13Cr-110 grades of martensitic stainless steels, stressed to 90% SMYS (NACE TM0177-Method A [55]), (Ref: Marchebois et al. [15]).

The domain diagrams suggest the following acceptable limits for highly alloyed 110 ksi grade super martensitics:

- High chloride environments: 30 mbar $H_2S$ at pH 3.9, 100 mbar $H_2S$ at pH 5.0
- Low chloride environments: 10 mbar $H_2S$ at pH 3.0, 25 mbar $H_2S$ at pH 3.5, 100 mbar $H_2S$ at pH 4.0

In terms of pH, it would appear that pH 4.5 is the borderline safe limit for SSC resistance in high chloride ion content environments, and between pH 3.5-4.0 for medium to lower chloride ion content environments. There are large 'grey' areas between acceptable and unacceptable results where tests have either not been done or there are conflicting pass/fail results. For example in the high chloride ion content environment, UNS S41426 grade showed a failure at pH 4.5 and 35 mbar $H_2S$ [63] yet shows a pass at pH 4.3 and 70 mbar $H_2S$ [19]; a more severe environment. The only reported difference between these two tests was in the buffering system used.

For the failed test a sodium bicarbonate buffer was used whereas for the test that passed 0.82 g/L sodium acetate with acetic acid was used as the solution buffer. However this does not necessarily suggest that sodium bicarbonate buffer is the cause of the failure, because there is a pass at pH 4.5 and 50 mbar $H_2S$ and this test was also conducted using sodium bicarbonate. These unexpected failures could be due to a number of other causes, possibilities include: poor specimen preparation, overloading and / or oxygen contamination in the test solution. Where it is unclear whether the material passes or fails, the region is marked with 'needs further assessment'.

The 110 ksi grade UNS S41246 is a high strength super martensitic stainless steel used for down-hole tubular applications; the high strength being a desirable property for deep offshore wells. The application limits of UNS S41246 are defined in NACE MR0175/ISO 15156 [3]; allowing its use at 100 mbar $H_2S$ at pH >3.5 at a maximum yield strength of 105 ksi (27 HRc). However, no limits are specified for the chloride concentration, which clearly has an Influence on the SSC resistance when the two domain diagrams are compared.

### 2.7.4 15%Cr Grade

The higher alloyed 15%Cr grades of martensitic stainless steel provide enhanced corrosion and cracking resistance over the standard, modified and super 13%Cr grades and the material is available in a high-strength 125 ksi grade for down-hole tubular applications. The manufacturers (JFE) published data [21] on the SSC resistance in high chloride (121,200 ppm) and low chloride ion concentration (1,000 ppm) is presented in Figure 2.32.

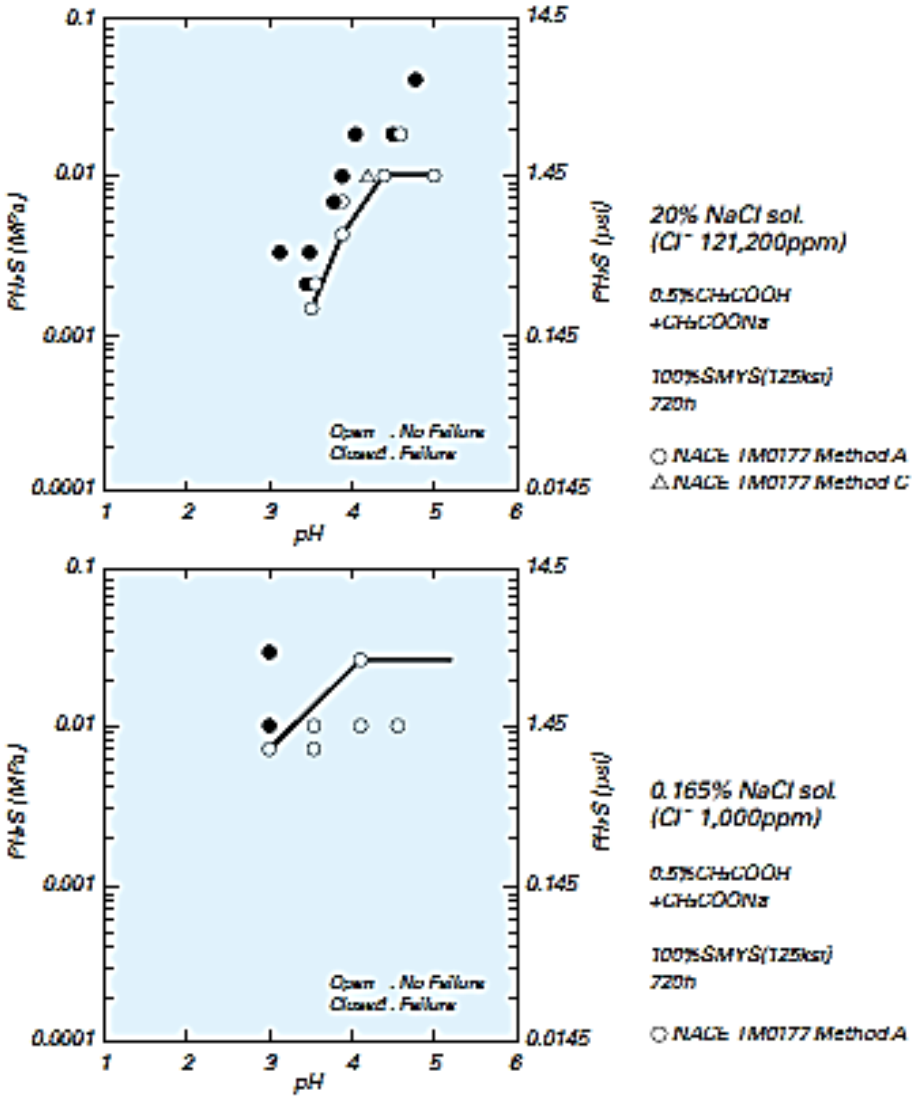


**Figure 2.32** pH – $pH_2S$ plots showing the SSC resistance of high strength 125 ksi, 15%Cr tube for down-hole tubular applications [21].

### 2.7.5 17%Cr Grade

The 17%Cr grade with the dual phase martensite-ferrite structure provides additional corrosion and cracking resistance to the 13%Cr and 15%Cr grades and is available in high strength (110 ksi and 125 ksi) grades for down-hole tubular applications. pH-pH$_2$S domain diagrams are available in the literature ([6], [22], [72]) , as shown in Figures 2.33 & 2.34.

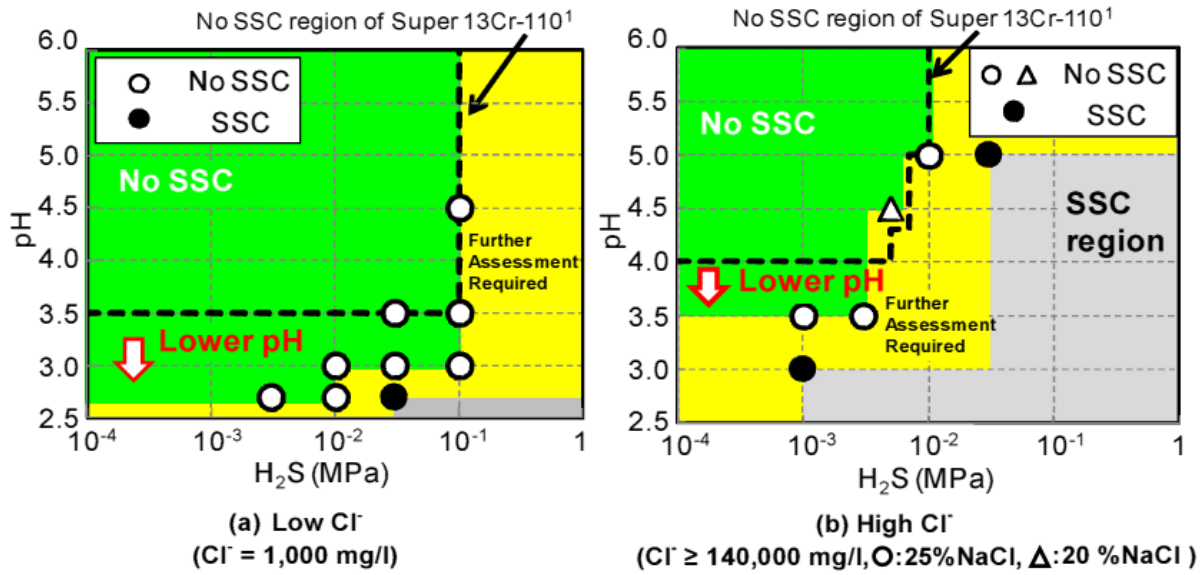


**Figure 2.33** pH – pH$_2$S domain diagrams showing the SSC resistance of super 17%Cr-125 in low and high chloride ion content environments [22].

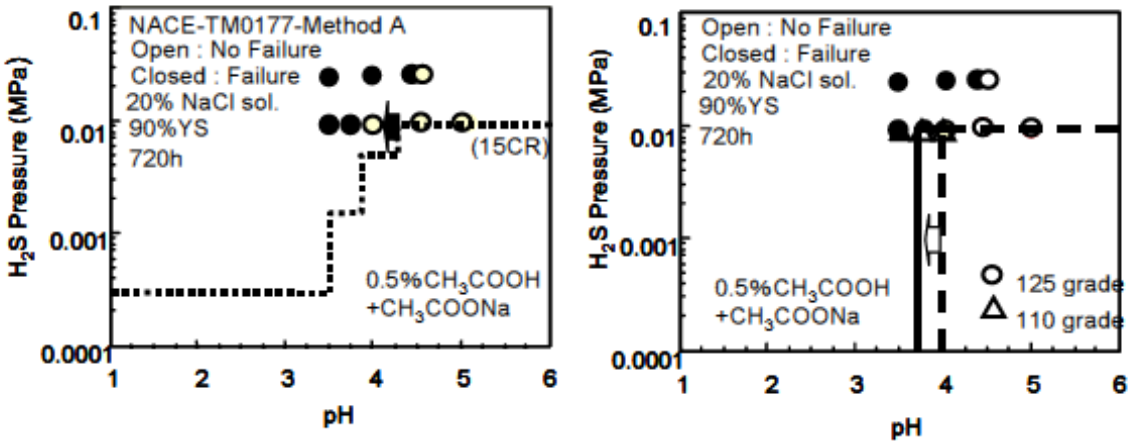


125 ksi grade 110 ksi grade

**Figure 2.34** pH – pH$_2$S domain diagrams showing the SSC resistance of 125 ksi and 110 ksi grades of 17%Cr in a high chloride ion content environment [6].

### 2.7.6 Weldable 13%Cr Martensitic Grades

The majority of published SSC data is based on 110 ksi down-hole tubular super martensitic grades and there are currently no published pH-p$H_2S$ domain diagrams for the weldable line pipe super martensitic grades. Table 2.9 summarises the SSC limits published by various authors on a range of weldable 13 %Cr martensitic stainless steels:

**Table 2.9** SSC limits of weldable 13%Cr martensitic stainless steels (room temperature)

| Reference | 13%Cr grade | Chloride level | pH | $H_2S$ limits |
|---|---|---|---|---|
| Rogne *et al*.[73] | 4-6Ni, 0.7-1.5Mo | Not specified | 3.0-3.5 | 10 mbar |
| | 4-6Ni, 2-2.5Mo | | 4.5-5.0 | 30 mbar |
| Miyata *et al*.[74] | 0.01C, 5Ni, 2Mo | 65,200 mg/L | 4.0 | >20 mbar |
| Ueda *et al*. [42] | 0.007C, 6.2Ni, 2.5Mo | 31,400 mg/L | 3.17 | >10 mbar |
| Enerhaug *et al*. [45] | 6.5Ni, 2.5Mo | 68,000 mg/L | 4.0 | >40 mbar |

From these limited data, SSC limits for weldable 13%Cr martensitic stainless steels can be summarised as:

- 40 mbar $H_2S$ at pH 4.0 for chloride levels ≤ 68,000 mg/L
- 10 mbar $H_2S$ at pH 3.17 for chloride levels ≤ 31,400 mg/L

When compared to the SSC limits defined for the higher strength super martensitics in the previous section, the results are similar, suggesting that the limits of UNS S41426 can be used as guidance for understanding the limits of the weldable grades. The main difference between the two grades is strength and carbon content, however higher strengths are known to reduce SSC resistance.

### 2.7.7 Laboratory v Service Limits

The application limits previously discussed apply to laboratory tests, which are generally considered to be more conservative than field environments. Reports show that $H_2S$ limits experienced in field environments are higher compared to laboratory tests. For example, modified 95 ksi martensitic stainless steel bent beams stressed to 90% AYS placed in a production environment did not fail after exposure for 130 to 193 days.

The production environment was a high chloride ion content (113,000 mg/L) solution with 169 psi $pCO_2$ (11.7 bara) and 278 psia (19.2 bara) $pH_2S$. Also 95 ksi and 110 ksi grades OCTG have been used in the Gulf of Mexico with 0.050 bara $pH_2S$ at temperatures ranging from 4.4°C to 93°C with no reported failures [66].

This higher resistance in service can be due to a number of reasons [66]:

- Higher or more consistent pH in the aqueous phase
- Buffering effects
- Oil wetting of the metallic surface, inhibiting corrosion effects
- Elevated service temperatures above the worst case for SSC
- More complete anaerobic conditions in production environments (i.e. Influence of oxygen contamination during laboratory testing).

## 2.8 Material Qualification for Sour Service

### 2.8.1 Background Information

For most sour-service qualification projects, materials are tested in accordance with NACE MR0175 / ISO 15156 [1]. This standard has its origins dating back from 1975 and has evolved into the current (2009) ISO standard that gives guidance on material selection and laboratory test methods for the petroleum and natural gas industries.

In 1975, the national Association of Corrosion Engineers (Now known as NACE International) published NACE standard MR0175 "*Sulphide Stress Cracking Resistant Metallic Materials for Oilfield Equipment*" [75] to provide guidelines for the selection of materials that are resistant to sulphide stress cracking in sour oilfield environments. The standard prior to 2003 was applicable when the $H_2S$ partial pressure was equal to or greater than 0.05 psi (3.4 mbar) and this was the definition of 'sour service'. However in 2003 when the standard was incorporated into the NACE MR0175 / ISO 15156 [3] document the minimum level of $H_2S$ was removed and 'sour service' was defined as "exposure to oilfield environments that contain sufficient $H_2S$ to cause cracking of materials by the mechanisms addressed by this part of ANSI/NACE MR0175/ISO 15156"

During the late 1980s, the European Federation of Corrosion (EFC) set up working party 13 to consider the qualification of materials for sour service, not covered by the NACE standard. By the mid-1990s, two guidelines were published; EFC16 [76] (for carbon and low alloy steels) and EFC17 [70] (for corrosion resistant alloys) that contained guidelines on how to test and qualify these materials for sour gas production.

The three documents (i.e. NACE MR0175-2002, EFC16 & EFC17) were eventually combined in the form of international standard NACE MR0175 / ISO15156. "*Petroleum, petrochemical and natural gas industries – Materials for use in $H_2S$ – containing environments in oil and gas production*". NACE MR0175/ISO 15156 consists of 3 parts that enable the selection and qualification of metallic materials for resistance to $H_2S$ related cracking in oil and gas production.

Part 1 [1] outlines the general principles for the selection of cracking-resistant materials and addresses *all* the mechanisms of cracking that can be caused by $H_2S$. This part gives guidance on evaluating service conditions for selecting pre-qualified SSC/SCC resistant materials; qualification and selection based on documented field experience; defining laboratory test requirements to qualify a material for $H_2S$ service; re-assessing existing alloys when service conditions change.

Part 2 [77] gives requirements and recommendations for the selection and qualification of carbon and low alloy steel. This includes the factors (such as $H_2S$ partial pressure, chloride ion content, pH etc.) that affect the behaviour of these materials in $H_2S$-containing environments; qualification against SSC; definition of sour service environments; hardness requirements in parent and welded material; laboratory testing requirements; and informative reference for calculating $H_2S$ partial pressures and determining in-situ pH.

Part 3 [3] gives requirements and recommendations for the selection and qualification of corrosion resistance alloys (CRAs) using NACE MR0175-2002 [75] rules, addressing the resistance of these materials to damage caused by SSC and other mechanisms. As with part 2, Part 3 identifies the factors that affect cracking resistance of CRAs in $H_2S$-containing environments. This part refers to EFC17 [6] and NACE TM0177 [65] for qualification of CRAs by laboratory testing. However, a key point in this standard is it stipulates that SSC testing of CRAs is carried out at ambient temperature (24°C ± 3°C) and the maximum design temperature (for SCC) for 30 days. Sub-ambient SSC testing is not a requirement of NACE MR0175 / ISO 15156 [3], as it is assumed that ambient temperature is the more sever environment for SSC susceptibility.

NACE MR0175/ISO15156 [3] refers to EFC17 [6] and NACE TM0177 [65] for SSC test method requirements. The primary methods used to load specimens are classified as *constant load*, *sustained load*, *constant total strain* and *continuously increasing strain*.

The only way to truly achieve a *constant load* for the duration of a test is by hanging a dead weight on the end of the specimen. Alternatively, spring loaded devices and proof rings can be used to apply a *sustained load* to the specimen. A proof ring is a calibrated 'ring' of material that when deflected by a given distance, applies a known load to the test specimen under uniaxial tension. *Constant strain* is achieved by deflecting the specimen to a given load and then fixing this displacement for the duration of the test. The problem with this is that a truly constant strain is difficult to achieve because of stress relaxation in the loading frame. *Continuously increasing strain* is achieved simply by loading the specimen at a constant rate until failure.

NACE TM0177 "*Laboratory Testing of Metals for Resistance to Specific Forms of Environmental Cracking in $H_2S$ Environments*" [65], originally issued in 1977 with the latest revision in 2005, covers the testing of metals subjected to a tensile stress for cracking resistance in $H_2S$-containing environments. This standard contains methods for testing metals using tensile, bent-beam, C-ring, and double-cantilever-beam (DCB) test specimens. The Slow Strain Rate Test (SSRT) method is covered in NACE standard TM0198 [78].

### 2.8.2 NACE TM0177-Method A (Tensile Test)

The uniaxial tensile test is probably the most common test for evaluating the resistance of parent materials to SSC or SCC. The method is described in NACE TM0177-Method A [55] and the standard allows the specimen to be loaded using a constant load (i.e. dead weight) or sustained load (i.e. proof ring or spring loading). It is generally recognised that the constant load method is the more severe of the two methods, since with the constant load method the stress will remain constant with any creep and the stress will increase at the site of cracks or thinning of the material due to corrosion. However the sustained-load method is more widely used due to the ease of use and small 'foot-print' of proof rings compared to constant load devices (Figure 2.35).

**Figure 2.35** NACE TM0177-Method A Standard Tensile Test (proof-ring).

### 2.8.3 NACE TM0177-Method B (Bent Beam Test)

This method is a crack initiation test using three-point loading (Figure 2.36). The test is performed under constant-strain by loading the beam to a particular deflection. The beam contains two 0.71 mm diameter holes at the mid length to assess SSC susceptibility in the presence of a stress concentration. The test solution consists of 0.5 % glacial acetic acid ($CH_3COOH$) and no sodium chloride (NaCl). Testing is performed at 24°C ± 3°C under 1 bar $H_2S$ for 30 days. The standard does not specify a loading stress level and the acceptance criteria is no cracking at ten times magnification.

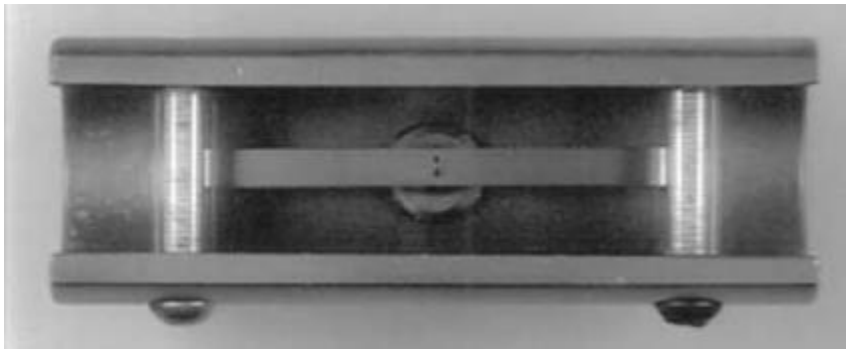

**Figure 2.36** NACE TM0177-Method B Standard Bent-Beam Test (3-point bending).

### 2.8.4 NACE TM0177-Method C (C-Ring Test)

The C-ring test is a constant strain or constant deflection type test which is referred to in NACE TM0177-Method C, EFC16 [76], EFC17 [69], ASTM G38 [79] and EN ISO 7539-5 [80].

The NACE TM0177-Method C provides a formula for stressing of the outer surface of homogeneous material within the elastic region. However the internal surface may also be stressed, where the bore surface is of particular interest, for example in the case of expanded tubular products.

For internal loading of C-Rings the deflection formula in NACE TM0177 is not valid. Also the formula is only valid in the elastic region and cannot be used to calculate the deflection required to stress CRA materials between the elastic limit and the yield stress. Under these circumstances the stress at the inner surface of the C-rings has to be monitored using strain gauges, with the strain value applied to be taken at the appropriate yield stress value, in accordance with the recommendation in section B.3.4 of ISO15156 / NACE MR0175. The yield stress is measured at the test temperature in accordance with the appropriate manufacturing specification determined from duplicate longitudinal tensile tests in accordance with ASTM A370 [81] (ASTM E8 [82]) following the recommendation in section B.3.4 of ISO 15156 / NACE MR0175 [3].

The load application on C-rings is relatively straight forward for ambient temperature SSC testing, since the presence of any cold creep can be accounted for by monitoring the strain following initial loading and adjusting to maintain the required target strain. A constant strain value would normally be achieved within 30 minutes for carbon steels, however longer stabilisation periods would be required for corrosion resistant alloys (CRAs), which show a greater tendency to exhibit cold creep. Further details on the cold creep of CRAs are provided in EFC17.

Using the constant strain or constant deflection C-ring method for elevated temperature SCC testing does present additional complications which need to be taken into consideration. Currently ISO 15156 / NACE MR0175 requires the stress (strain) to be applied to elevated temperature tests to be determined from elevated temperature test data. The specimens are then loaded at ambient temperature using the high temperature tensile data and then heated to the test temperature. At present there is no mandatory requirement in NACE TM0177-Method C to establish if there is any change in strain from room temperature to the test temperature, however the stain can indeed change due to relaxation in the loading bolt and / or creep in the material.

C-rings will show an increase in strain at the side edges, typically up to 15% higher than the mid-width strain where the strain gauge would be located and for this reason it is recommended to disregard the presence of any fine cracking which is only present within 1 mm from the edges. At the present time this recommendation is not included in NACE TM0177 or EFC 16 / EFC 17.

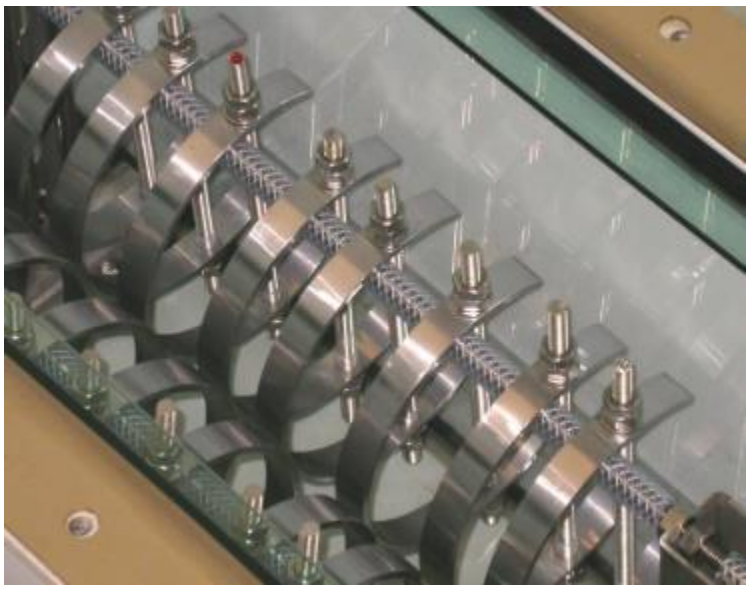

**Figure 2.37** NACE TM0177-Method C Standard C-Ring Test.

### 2.8.5 Four Point Bend (FPB) Test

The four-point bend (FPB) test is a relatively simple, 'low-tech' constant strain method for applying stress to a relatively large surface area of a test piece and is particularly suited for testing root-intact welded specimens or for materials where the retention of the as-manufactured surface is of importance. Loading is achieved by turning a bolt to displace two inner loading rollers that deflect a beam sitting on two outer support rollers (Figure 2.38). A FPB test method is currently not detailed in NACE TM0177 [55]. However a method for carbon steels is detailed in EFC16 [76] and for CRAs in EFC17. Additionally details on specimen geometry and loading are provided in ASTM G39 [83] and EN ISO 7539-2 [84]. Also NACE (TG494) and EFC working groups (WP13) are looking into some of the important issues regarding FPB testing to establish a more consistent approach across industry. Some of the issues are similar to those previously detailed for C-ring testing namely the stress relaxation / creep at elevated temperature and the increase in stress at the free edges. Other issues being discussed pertaining to parent material testing include; stress concentration at the roller locations, Influence of specimen thickness and methods for determining the applied strain (i.e. tensile v flexural bend).

If loading is carried out within the elastic limits of the material, the standards ASTM G39 [83] and ISO 7539-2 [84] can be used to calculate the stress on the tensile test surface using elastic bending theory by measuring beam deflection. However, loading becomes more complex when it is required to load CRAs to 100% of Actual Yield Strength (AYS), as stipulated in ISO 15156 / NACE MR0175 [3] and EFC 17 [69]. Under this level of load, the stress / strain response of the material moves into the plastic regime and the linear elastic equations given in ASTM G39 [83] and ISO 7539-2 [84] standards are no longer valid. The solution is to use a strain gauge bonded to the test face to directly measure loading strain. When strain gauges are used, the operator needs to know the loading strain required to achieve 100 % AYS on the test surface of the specimen.

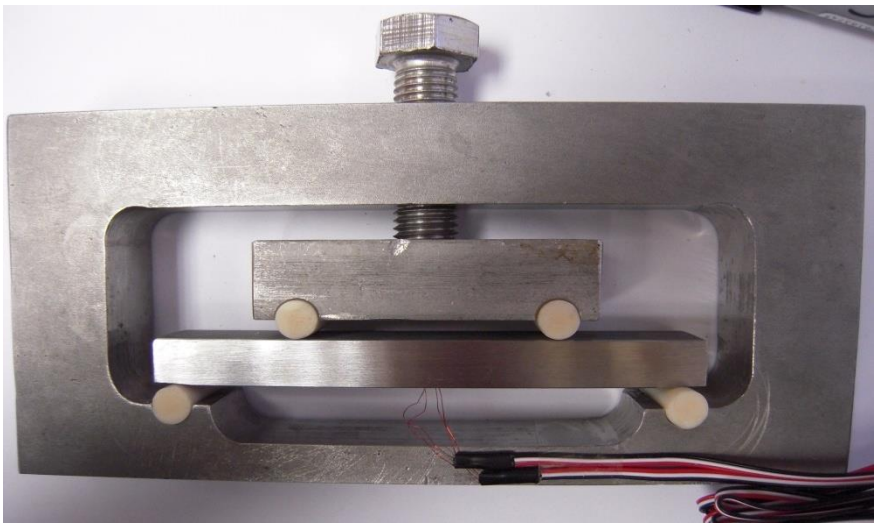

**Figure 2.38** SSC specimen loaded in Four-point bending.

NACE MR0175 / ISO 15156-3 [3] specifies that the required strain is determined from tensile stress-strain curves at the test temperature. An alternative method is to determine the strain from flexural bend tests as detailed in the NPL report [85], published in September 2009. The rationale is that stress is uniform through the thickness of a tensile tests specimen whereas there is a stress gradient through the thickness of a four-point bend specimen; stress changes from compression on the back face to tension on the test face. Therefore, the two methods are not comparable and the Influence of the stress-gradient needs to be taken into account when setting the loading strain in bending.

Recent discussions and correspondence following the NACE TG494 meeting in Orlando (March 2013) have established that the 'NPL method' is overly conservative (i.e. the applied strain / stress is too high) with regard to the level of strain applied. The increase in the strain using the flexural bend method over the tensile method was highlighted by Turnbull & Nimmo [72], who reported that a 13 %Cr super martensitic stainless steel loaded from tensile stress-strain data would be strained approximately 18 % lower than if it were loaded using flexural bend test data (a flexural bend test is a four-point bend test whereby load and strain are recorded while the test piece is deflected at a constant rate. The resulting load / strain curve is used to determine the value of strain at 0.2 % plastic strain for loading four-point bend SSC test specimens prior to exposure).

At the time of writing, there was agreement amongst the NACE TG494 members that the tensile method should be the preferred technique to use to determine the applied strain in accordance with the current requirement in ISO 15156 / NACE MR0175 [3].

### 2.8.6 Full Ring Test

The full ring test method was developed in the early 1990s, initially to qualify spiral welded pipe where it is important to retain the residual stresses from pipe manufacture and welding in order to fully characterise the cracking resistance. The initial test concept then was developed during a group sponsored project which led to the publication of a test method in 1995 (OTI 95-635) [86]. The method covers the testing of seamless and welded pipe and the qualification of girth welds.

The method does have advantages over the 'traditional' small scale tests, previously described, since the residual stresses, from pipe manufacture and welding if applicable, are retained and all forms of cracking (i.e. SSC, soft zone cracking (SZC), hydrogen-induced cracking (HIC) and stress orientated hydrogen-induced cracking (SOHIC)), as described in part 1 of NACE MR0175 / ISO 15156 [1], can be evaluated in one test.

The test is normally applied to evaluate the ambient temperature sour service resistance of carbon steels, however it has also been applied to evaluate the ambient temperature SSC resistance of weldable 13%Cr stainless line-pipe (see Figure 2.39) and the elevated temperature SCC resistance of 316L clad line-pipe [87].

The samples are tested in full thickness with the only restriction being that the length of the sample must be equal to or greater than the outside diameter in order to ensure the retention of residual stresses.

In the full ring test since all the residual stresses from the manufacturing operations are retained the design stress is applied to the bore surface, which is normally a value of 72% SMYS.

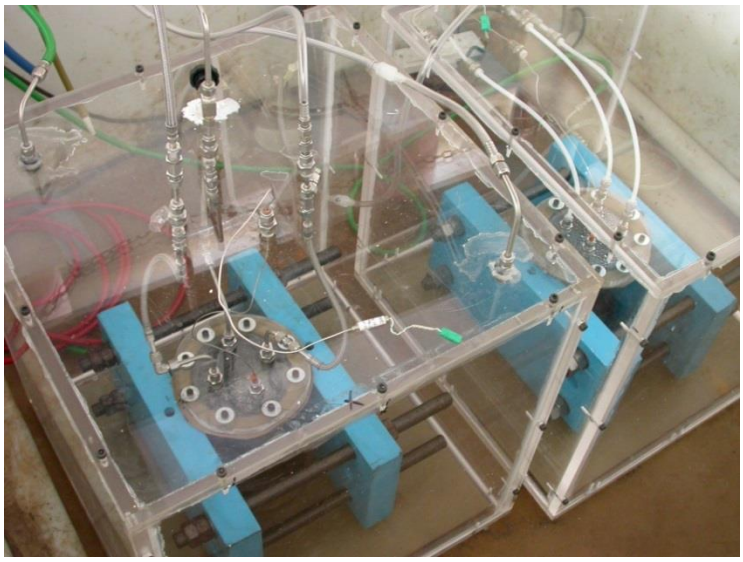

**Figure 2.39** Full Ring Testing of Weldable 13%Cr Stainless Steel line-pipe in nitrogen-purged cabinets.

### 2.8.7 Double Cantilever Beam (DCB) Test

The DCB test is detailed in Method D of NACE TM0177 [55] and describes a method to measure the resistance of materials to crack propagation and provides a value for the stress intensity factor or $K_{ISSC}$ in the case of SSC testing. The test is fundamentally different to the previous described methods since it is a crack propagation test as opposed to a crack initiation test. Therefore the method does not rely on the initiation of a crack because a crack is always initiated in a valid test. Since the test provides a numerical value of the stress intensity factor or $K_{ISCC}$ it is widely used as a quality control or release type test for down-hole tubular products and is useful for ranking materials in terms of SSC resistance.

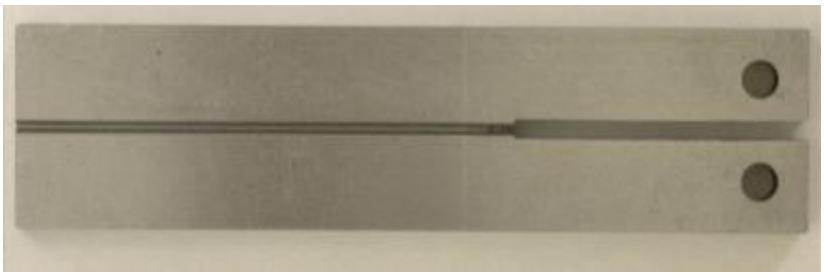

**Figure 2.40** NACE TM0177-Method D Standard Double-Cantilever-Beam test specimen.

### 2.8.8 Slow Strain Rate Testing (SSRT)

The SSRT is detailed in NACE TM1098 [78], EFC 17 [69] and ISO 7539-7 [88] and the evaluation of susceptibility to SSC or SCC is based on comparing the time to failure, % elongation and % reduction of area between specimens tested in air (inert environment) and in the corrosive environment.

For down-hole tubular products the SSRT technique has mainly be used to qualify the use of nickel alloys, where the technique can provide a rapid method to replace long term C-ring, FPB or tensile tests. The technique is particularly useful for higher temperature testing where concerns regarding creep, when using statically loaded C-ring or FPB specimens, can be eliminated. Another advantage of this technique, when testing CRAs, is that protective passive films are disrupted, thus it can be applied to applications where localised plastic strain may be encountered in service.

The disadvantage of the test is that it can be too conservative for many materials since the specimen is strained to failure, therefore the properties are changing during the test and the strain applied is unrelated to the service conditions. For these reasons the test is often used as a screening test to pass materials, since if a material 'fails' a SSRT is does not necessarily mean that the material would fail in service. Therefore materials which 'fail' an SSRT test are often tested using one of the 30-day statically loaded methods previously described.

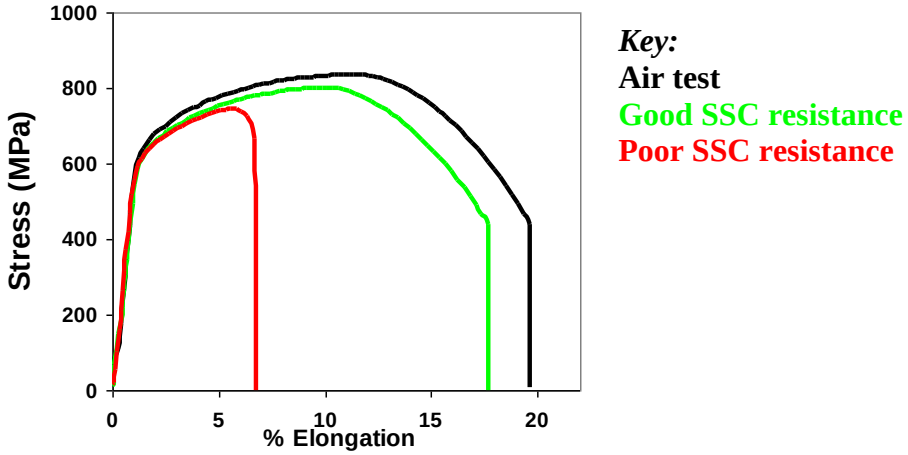


**Figure 2.41** Typical slow-strain-rate test stress v elongation curves for steels with good and poor SSC resistance.

### 2.8.9 Cyclic Slow Strain Rate Testing (CSSRT)

This CSSRT provides a dynamic method of evaluating materials which are subjected to cyclic stresses below the yield stress. The method can also be applied to cases where disruption of the passive film is considered to be important and the traditional SSRT is considered to be too severe.

The method, which is described in NACE paper 97058 [89], utilises a modified SSRT technique whereby a standard NACE TM0198 [78] specimen is cycled in the range of 80 – 100% of the 0.2% proof stress. In this region for CRAs the material will be plastically deforming, however after the first few cycles the material will be behaving elastically and therefore the properties will not be changing significantly during the test, but the passive film will be disrupted.

## 2.9 Electrochemistry

### 2.9.1 Introduction

Electrochemical testing is routinely used to evaluate the corrosion resistance and provide additional Information on the cracking mechanisms of martensitic stainless steels for applications in the oil and gas industry. The main focus of published research during the previous 10-15 years has been to investigate suitable methods to determine the intergranular corrosion susceptibility of weldable grades, to establish the Influence of artificial buffers and to obtain a better understanding on the Influence of environmental parameters (i.e. chloride ion content, pH $pH_2S$, $pCO_2$ & temperature) on the de-passivation pH, corrosion (pitting) and cracking resistance. The review will not cover the Influence of buffers which has previously been discussed (see section 2.6.5.4), and the review will only concentrate on testing conducted at ambient or low temperatures, relevant to then SSC work in the thesis.

### 2.9.2 Sensitisation / Intergranular Corrosion (IGC)

Sensitisation, defined by the local depletion of alloying elements adjacent to grain boundaries due to precipitation, has been evaluated in martensitic stainless steels by electrochemical techniques. Since parent martensitic stainless steels are subjected to a hardening and tempering heat treatment the tempering process results in the formation of chromium carbides, which may be precipitated along the grain boundaries or along the martensitic lath boundaries (intragranular precipitates). The Influence of tempering temperature on the susceptibility of a type 410 (UNS S41000) martensitic stainless steel to intergranular corrosion (IGC) has been studied by Allonso-Felleiros et al. [90] using potentiostatic, potentiokinetic and a double loop Electrochemical Potentiokinetic Reactivation (DL-EPR) techniques [91], [92] with a modified 1N $H_2SO_4$ test solution. In the DL-EPR experiments the prepared specimen was polarised from -490 mV to +500 mV and then back to -490 mV at a scan rate of 1.67 mV/min and the maximum current densities in the activation stage (i.e. forward scan) and reactivation stage (i.e. reverse scan) was measured. The degree of sensitisation (DOS) was evaluated by measuring the ratio (Ir/Ia) of the maximum reactivation current density (Ir) and the maximum activation current density (Ia). The DL-EPR test involves the measurement of the amount of charge resulting from the corrosion of the chromium-depleted regions surrounding the precipitated chromium carbide particles. In a sensitized microstructure most of these precipitates are located at the grain boundaries. However, discrete particles located within grains (referred to as intragranular precipitates) will also contribute to the total measured charge. Therefore, it is important to examine the alloy microstructure following a DL-EPR test to determine the relative proportion of corrosion sites associated with intergranular and intragranular precipitates.

The DL-EPR method was found to be the most sensitive technique in detecting chromium-depleted regions at the grain boundaries and along the martensite lath interfaces. The DL-EPR technique was also used by da Silva et al. [23] to study the Influence of heat treatment on the toughness and sensitisation of a titanium-containing super martensitic (weldable) stainless steel. The solution (1) defined in ASTM G108 [91] and a less aggressive solution (2) comprising of 0.25 $molL^{-1}$ $H_2SO_4$ and 0.01 $molL^{-1}$ KSCN were used and both solutions detected an increasing DOS above tempering temperatures of 400°C, as shown in Figure 2.42.

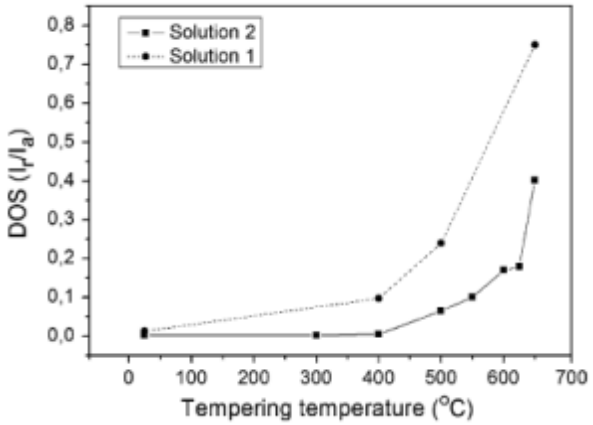


**Figure 2.42** Variation of the DOS with tempering temperature for tests with solutions 1 & 2 [23].

The DL-EPR technique was also applied to investigate [24] the Influence of 'incorrect' heat treatment on the corrosion resistance of a 13%Cr stainless steel (type 1.4006). The DL-EPR technique was compared with the results from cyclic potentiodynamic polarisation tests and both experimental methods detected a difference in the corrosion resistance of the two materials (i.e. R & T) as shown in Figure 2.43

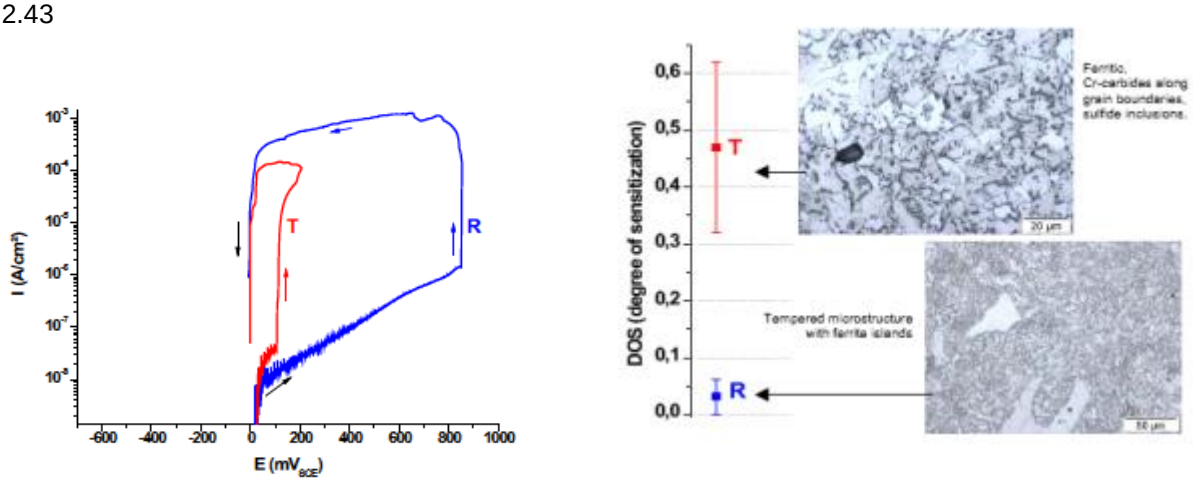


(a) (b)

**Figure 2.43** (a) - Polarisation curves for steels R & T in 100 mg/L Cl solution
(b) – Results of EPR tests and metallographic examination.
[24].

The authors concluded that compared to the potentiodynamic polarisation test the DL-EPR test was less time-consuming, simpler to apply and provided a quantitative estimation of the degree of sensitisation (DOS). However the DL-EPR test was found to be influenced by the presence of sulphide inclusions, which can lead to erroneous results.

Weldable Martensitic Stainless Steels (WMSSs) were first used for line-pipe applications in the mid-1990s and between 1996 and 2002 650 km of WMSS line-pipe was installed [93] as a cost-efficient alternative to inhibited carbon steel or 316L clad steel for sweet and mildly sour service conditions. Statoil selected the medium and high grades for their sour service Asgard and Gullfaks projects [45], [94] and NAM, in the Netherlands, selected a lean grade for their sweet onshore project [95], [96]. However in late 2001 a leak was discovered in one of the pipe-lines in the vicinity of a seam weld which had initiated at a manufacturing defect. Further investigations revealed the crack had followed an intergranular path and intergranular cracking was also discovered in the fusion-line / HAZ region of girth welds. As a result of the failures all of the 13%Cr flow lines were removed and detailed investigations followed to establish the root cause and the cracking mechanism.

Subsequent investigations [97] revealed that WMSSs in the as-welded condition were susceptible to intergranular stress corrosion cracking (IGSCC) at elevated temperatures in sweet and sour service, with the cracking being confined to the fusion-line / HAZ region. Wilms et al. [98] conducted FPB SCC testing and electrochemical testing to establish the degree of sensitisation (DOS) and correlate this to the susceptibility of the WMSS material to IGSCC. The DOS method used was based on the standard DL-EPR technique, however an electrochemical pen was used which enables the DOS in localised (i.e. 1 – 4 mm diameter) regions to be evaluated. The 'electrochemical pen' is a patented electrochemical sensor containing a counter and reference electrode integrated in a small electrochemical cell, which can make contact with the specimen (working electrode) via a porous polymer tip. Correlation between the DOS measurements using the electrochemical pen and the occurrence of IGSCC following the 3-month SCC testing was only obtained when the probe on the pen was reduced to 1 $mm^2$ which enabled the DOS in the localised fusion-line region to be measured. A micro-probe electrochemical EPR technique complimented by optical and atomic force microscopy (AFM) was also used by Maier et al. [25] to detect sensitised zones in as-welded and Gleeble simulated welded WMSS specimens.

The results, which were in agreement with the findings of Wilms et al. [98], revealed the presence of a 100 µm wide sensitised zone close to the fusion line (see Figure 2.44) and showed by AFM that the corroded region was adjacent to the prior austenite grain boundaries (see Figure 2.45).

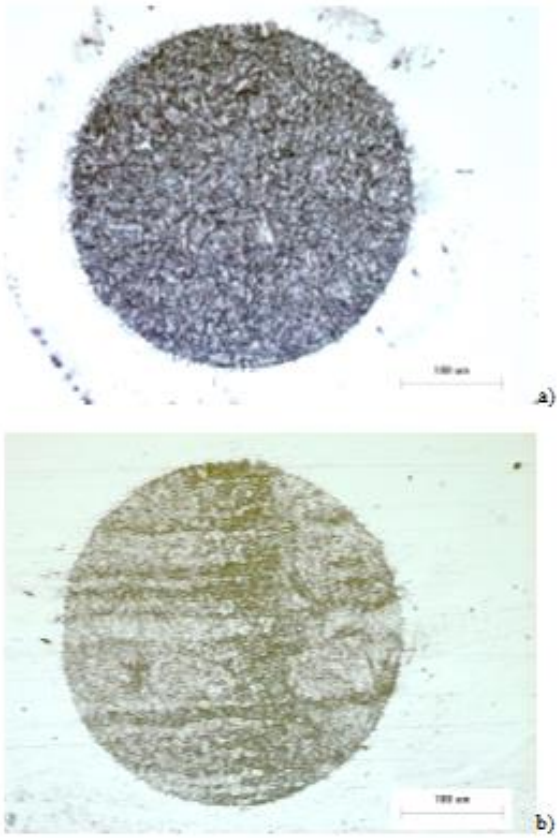


**Figure 2.44** Optical microscope images of non-sensitised base material and the sensitised zone in the welded material [25].

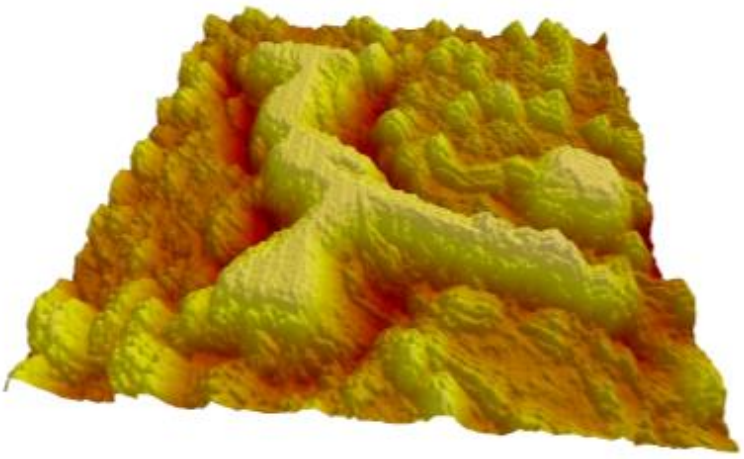

**Figure 2.45** 3-diemsional AFM image of the sensitised zone next to the fusion-line on the welded specimen (scan size 15 µm) [25].

Turnbull et al. [99] applied galvanostatic and EPR electrochemical techniques to as-welded WMSS in order to detect the presence of a sensitised zone. The galvanostatic test was not successful in detecting the sensitised zone due to pitting in areas remote from the fusion-line. The EPR technique was applied to polished specimens using a 2M $H_2SO_4$ solution and the specimens were subsequently examined optically to detect the presence of preferential grain boundary attack. Specimens were also electrolytically etched using a solution of 20% $H_2SO_4$ and $NH_4CNS$. Neither the EPR technique nor the conventional etching technique was effective, since the presence of any sensitised grain boundaries could not be distinguished from the delta-ferrite grain boundaries.

### 2.9.3 De-passivation pH

13%Cr martensitic stainless steels rely on a chromium-rich passive film for corrosion resistance in oil and gas environments. However the passive film is relatively weak compared to other CRA materials and consequently the breakdown of the passive film resulting in pitting and subsequent cracking is sensitive to the solution pH, chloride ion concentration, partial pressure of $H_2S$ and the test solution temperature. Electrochemical test methods have been used to evaluate the Influence of these parameters on the corrosion performance of 13%Cr stainless steels in sweet and sour environments.

Hashizume et al. [7] reported the de-passivation pH for 13%Cr with Mo concentrations varying from 0 – 1.9% was in the range of 3.6 – 3.8 in a 5 % NaCl + 0.5% $CH_3COOH$ solution saturated with 0.0035 MPa $H_2S$ and 0.0965 MPa $CO_2$. The solution pH was adjusted with NaOH and the de-passivation pH was evaluated by weight loss measurements and visual examination of the exposed specimens. Drugli et al. [65] and Takabe et al. [22] obtained similar de-passivation pH values to Hashizume et al. [7] in condensed water (CW) type environments.

Drugli et al. [65] applied linear polarisation resistance (LPR) measurements to determine corrosion rate of modified parent and as-welded samples in a 1 g/L NaCl+ 4 g/L $CH_3COONa$ solution, buffered with $CH_3COOH$ and saturated with 0.0008 MPa $H_2S$ and 0.1 MPa $H_2S$.

The work demonstrated that the initiation of active general corrosion occurred in the condensed water buffered to pH <3.8 with acetate buffer and the risk of active corrosion increases in buffered $CO_2/H_2S$ containing simulated condensed water compared to solutions without buffer at the same pH (see section 3.55).

Takabe et al. [22] measured the de-passivation pH of 17Cr and super 13Cr at ambient temperature, in two test solutions; one with 0.17 wt.% Cl (CW) and 0.003 MPa $H_2S$ ($CO_2$ balance) and the other with 25 wt.% NaCl (FW) and 0.001 MPa $H_2S$ ($CO_2$ balance). For the super 13Cr the de-passivation pH was 3.5 in the low chloride ion content CW type solution and approximately 4.0 in the high chloride ion content FW type solution. For the higher alloyed 17Cr material the de-passivation pH values were lower at 2.7 and 3.3 for the CW and FW solutions respectively. The work clearly illustrates (see Figure 2.46) the influence of pH, chloride concentration and the alloy compoition on the stability of the passive film in sour environments.

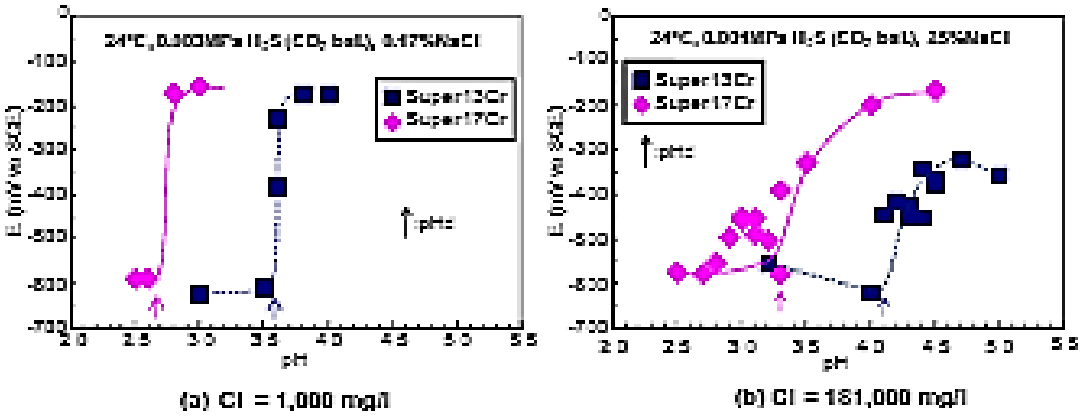


**Figure 2.46** Effect of pH on corrosion potential of Super 17Cr-125 in total 0.1 MPa gas mixtures of $H_2S$ and $CO_2$ [22].

Linne et al. [100] measured the de-passivation pH of standard 13Cr and modified 13Cr (13Cr-5Ni-2Mo) grades in a de-aerated 120 g/L NaCl (73 g/L $Cl^-$) solution and the published results revealed a de-passivation pH of 3.5 for the conventional 13Cr and a value of 1.3 for the modified 13Cr. This value of 1.3 was significantly lower than the results of Hashizume et al. [90] and Takabe et al. [16], which may have been due to the absence of $H_2S$ in the test environment.

### 2.9.4 Influence of Test Parameters (Chloride, pH and $pH_2S$)

Sirodin et al. [26] conducted potentiodynamic polarisation tests using rotating disc electrodes (RDE) on standard 13%Cr in 3% NaCl solutions, saturated with 1 bara $CO_2$ to study the Influence of acetic acid (HOAc) or sodium acetate (NaOAc) and acetic acid (HOAc) additions at in-situ pH values ranging from 3.76 – 5.68. The results obtained are summarised in Table 2-10

**Table 2.10 –** Data from the voltammetry of 3% NaCl containing NaOAc + $CO_2$ or a NaOAc/HOAc mixture [26].

| | pH[a] | [HOAc] (mM)[a] | $E_{CORR}$ vs. SCE (mV) | $R_{CORR}$ ($\Omega$ cm$^2$) | $i_{PASS}$ (mA cm$^{-2}$) |
|---|---|---|---|---|---|
| [NaOAc] (+$CO_2$) (mM) | | | | | |
| 0 | 4.00 | 0.0 | −575 | 146 | 0.25 |
| 1 | 4.60 | 0.49 | −605 | 151 | 0.28 |
| 10 | 5.17 | 2.0 | −635 | 159 | 0.12 |
| 20 | 5.34 | 2.9 | −653 | 129 | 0.14 |
| 40 | 5.49 | 4.2 | −655 | 166 | 0.18 |
| 70 | 5.61 | 5.6 | −667 | 159 | 0.17 |
| 100 | 5.68 | 6.8 | −670 | 134 | 0.12 |
| [NaOAc]:[HOAc] (mM) | | | | | |
| 1:1 | 4.60[b] | 1.0 | −586 | 426 | 0.24 |
| 5:5 | 4.55[b] | 5.0 | −595 | 437 | 0.22 |
| 10:10 | 4.55[b] | 10.0 | −584 | 250 | 0.16 |
| 1:10 | 3.76[b] | 10.0 | −560 | 140 | 0.26 |
| [NaOAc]:[HOAc] (+$CO_2$) (mM) | | | | | |
| 5:5 | 4.55 | 5 | −598 | 295 | 0.15 |

Rotation rate 1600 rpm. Temperature 333 K.
[a] Concentrations calculated using PHREEQC 2.2 [6,7].
[b] pH measured.

With increasing pH the corrosion potential increased from -560 mV $_{v\ SCE}$, at a pH of 3.76, to -670 mV $_{v\ SCE}$ at a pH of 5.68. Under all conditions the surface was passive, with a thin 20 nm film being reported and the measured passive current density ($i_{PASS}$) ranging from 0.12 – 0.28 mAcm$^{-2}$. There was no correlation between the passive current density and the solution pH, however the shape of the cathodic portion of the curves was influenced by the pH and HOAc / NaOC composition, as shown by Figure 2.47. The presence of the cathodic ‘wave’ was attributed to the reduction of acetic acid; with the size of the wave reflecting the acetic acid concentration.

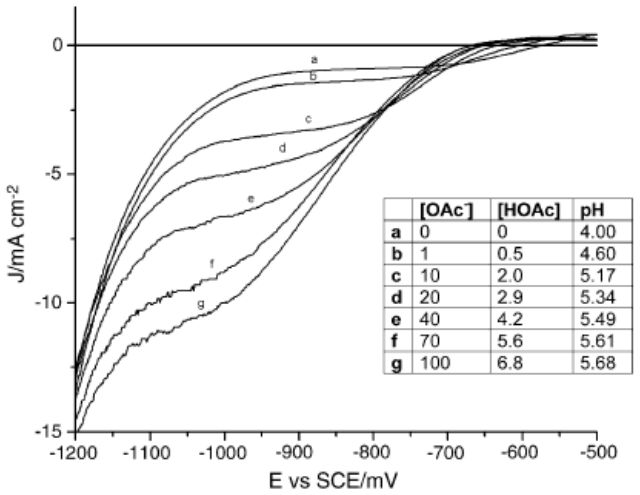


| | [OAc⁻] | [HOAc] | pH |
|---|---|---|---|
| a | 0 | 0 | 4.00 |
| b | 1 | 0.5 | 4.60 |
| c | 10 | 2.0 | 5.17 |
| d | 20 | 2.9 | 5.34 |
| e | 40 | 4.2 | 5.49 |
| f | 70 | 5.6 | 5.61 |
| g | 100 | 6.8 | 5.68 |

**Figure 2.47** Voltagrams recorded on 13%Cr stainless steel rotating disc electrodes in 3% NaCl; + various concentrations of NaOAc and saturated with $CO_2$. Rotation rate 1600 rpm. Potential scan from -1300 mV to 0 mV at 5 $mVs^{-1}$, temperature 333 K (~60°C) [26].

The Influence of solution composition and pH on the corrosion potential ($E_{corr}$) and passivity of super 13%Cr at 0.1 bara $pH_2S$ was studied by Marchebois et al. [27] using standard NACE TM0177-Method A [55] tensile specimens and polished specimens. The results from a low pH (3.50), low chloride (1 g/L NaCl), CW type solution were compared to a FW type solution with a pH of 4 and 50 g/L NaCl concentration. The corrosion potential was monitored during the 7-day tests and a significant difference in the Ecorr values were revealed; with the pH 4 solution equalising at a value of -510 mV compared to -240 mV for the lower pH, lower chloride ion content solution (see Figure 2.48).

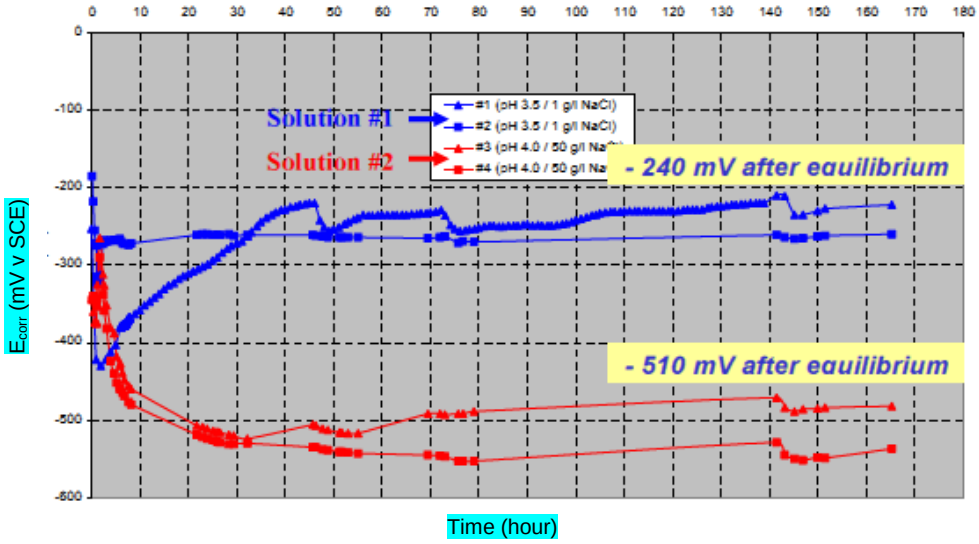


**Figure 2.48** Corrosion potential versus time recorded simultaneously during NACE TM0177 tensile tests [27].

In order to understand the corrosion behaviour of the material in the two environments and investigate the Influence on the rate of $H_2S$ saturation potentiodynamic polarisation tests were undertaken and the results are presented in Figures 2.49 & 2.50.

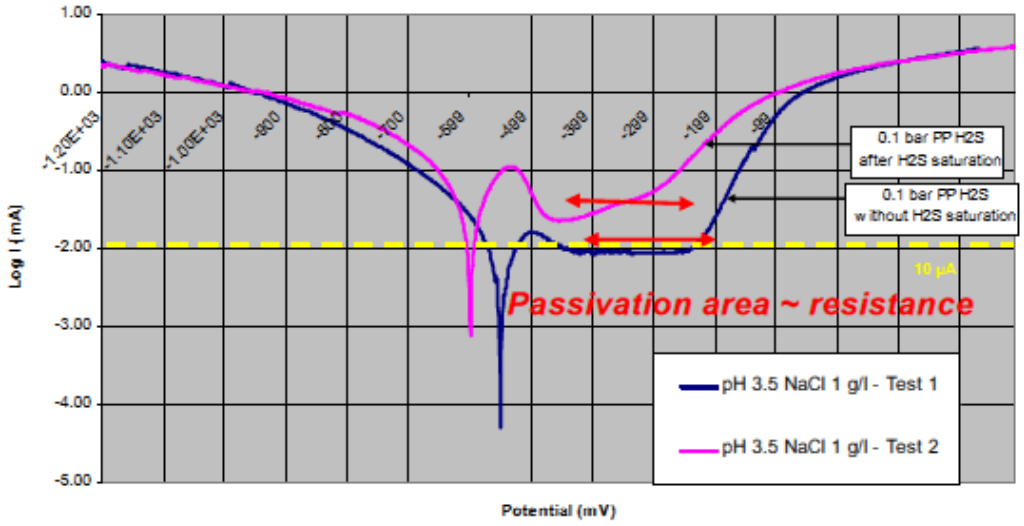


**Figure 2.49** Polarisation curves of Super 13%Cr showing the Influence of the $H_2S$ saturation of the test solution [27].

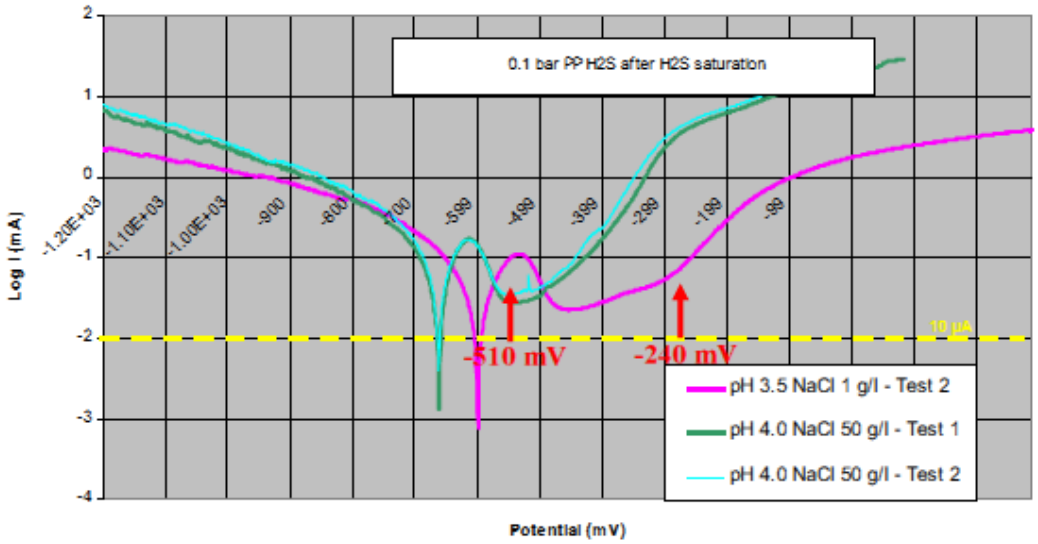


**Figure 2.50** Polarisation curves of Super 13%Cr showing the Influence of the test environment [27].

The polarisation curves in Figure 2.50 show the Influence of the rate of $H_2S$ saturation, with the specimen exposed to a rapid $H_2S$ saturation exhibiting a higher passive current density and less stable region than the specimen subjected to a slow saturation rate. Figure 2.49 illustrates the Influence the solution pH and chloride concentration on the passive film characteristics. The material in the pH 4 / 50 g/L NaCl environment exhibited a higher passive current density and a less stable passive region as compared to the pH 3.5 / 1 g/L NaCl environment,

Further cyclic polarisation tests were undertaken by Marchebois et al. [15] on standard 13Cr and super 13Cr at 24°C and 50°C in de-aerated solutions and $H_2S$ saturated (10 kPa-0.1 bara) solutions without NaCl and with1 g/L NaCl and 100 g/L NaCl concentrations. The pH was controlled to 3.5 (CW condition) by the addition of acetic acid, in the case of the chloride free solution and with 4 g/L sodium acetate, in the case of the chloride containing solutions. The corrosion potentials ($E_{corr}$) were reported together with the corrosion current density ($i_{corr}$), the breakdown potential ($E_t$) and the polarisation curves and the results are summarised in Table 2.11.

**Table 2.11** Summary of the electrochemical results for the 13Cr and S13Cr specimens in the 10 kPa $H_2S$, pH 3.5 and $H_2S$-free solutions [15]

| Material | NaCl (mg/L) | $pH_2S$ (kPa) | Temp (°C) | Ecorr (mV/SCE) | icorr ($\mu A/cm^2$) | $E_t$ (mV/SCE) |
|---|---|---|---|---|---|---|
| 13Cr | 0 | 10 | 24 | -677 | 83 | No passivity |
| S13Cr | 1 | 10 | 24 | -613 | 20 | -200 |
| | 1 | 10 | 50 | -630 | 60 | -290 |
| | 100 | 10 | 24 | -613 | 45 | No passivity |
| | 100 | 10 | 50 | -642 | 639 | No passivity |
| | | | | | | |
| 13Cr | 0 | 0 | 24 | -500 | 5 | +1350 |
| | 0 | 0 | 50 | -465 | 4 | +1250 |
| | 1 | 0 | 24 | -505 | 10 | -125 |
| | 1 | 0 | 50 | -550 | 20 | -195 |
| | 100 | 0 | 24 | -575 | 14 | -205 |
| | 100 | 0 | 50 | -550 | 23 | -275 |
| | | | | | | |
| S13Cr | 0 | 0 | 24 | -430 | 1 | +1350 |
| | 0 | 0 | 50 | -450 | 3 | +1100 |
| | 1 | 0 | 24 | -430 | 1 | +150 |
| | 1 | 0 | 50 | -510 | 6 | -75 |
| | 100 | 0 | 24 | -480 | 2 | -50 |
| | 100 | 0 | 50 | -500 | 10 | -350 |

In the presence of 10 kPa $H_2S$ the standard 13Cr was active at pH 3.5, even without the presence of chloride, whereas the S13Cr material exhibited passivity in the 1 g/L NaCl solution, however the passivity was Influenced by the chloride ion content and the passive film broke-down in the higher 100 g/L NaCl environment. In the $H_2S$-free solutions both the 13Cr and S13Cr materials demonstrated passive behaviour even in the high 100 g/L NaCl solution, although the breakdown potential ($E_t$) was sensitive to the chloride ion concentration.

Cyclic polarisation tests were conducted on the parent and HAZ regions of a WMSS in a $H_2S$-free 178,000 mg/L chloride FW water environment, saturated with 1 bara $CO_2$ at a pH of 4.5 by Lee et al. [28]. The corrosion potential in the HAZ and parent regions was approximately -530 mV v SCE, compared to the -575 mV value obtained by Sidorin [26] in the lower pH (4.0) and lower chloride concentration (approximately 30,500 mg/L $Cl^-$) solution and the -480 mV value reported by Marchabois et al. [15] in the lower pH (3.5) lower chloride concentration (approximately 61,000 mg/L $Cl^-$) solution. The differences in the values demonstrate the Influence of pH, buffer type and chloride concentration on the corrosion potential. The polarisation curves, shown in Figure 2.51 demonstrated the parent and HAZ regions exhibited passivity up to -250 to -200 mV v SCE.

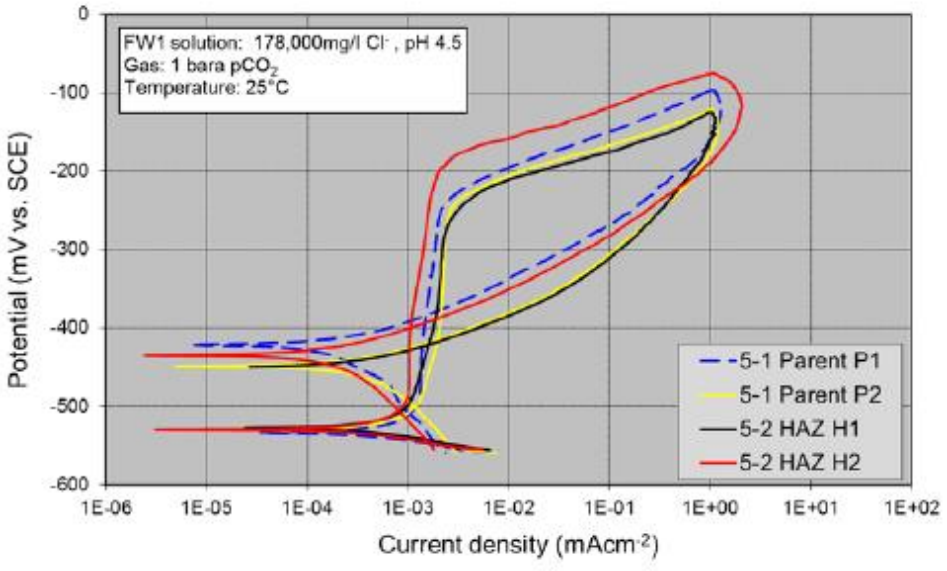


**Figure 2.51** Polarisation scans of duplicate parent and HAZ 13%Cr SMSS [28].

The stability of the passive film, particularly in the HAZ / heat-tint region in the vicinity of the weld root in weldable martensitic stainless steels (WMSSs) has been reviewed by Enerhaug et al. [29] and the results of galvanostatic and potentiodynamic tests presented. The root surfaces of WMSSs are influenced by the high temperature oxidation occurring during welding and as a consequence the surfaces are not fully passive following the welding process. If the as-received surfaces are exposed to $H_2S$ solutions during laboratory testing the break-down of the passive film in the vicinity of the welds can occur as a result of the absorption of S atoms into the passive film (S-induced pitting corrosion), leading to accelerate active dissolution of the film and premature SSC failures. Enerhaug et al. [29] proposed that the laboratory tests are too onerous for as-welded WMSS specimens because in service the welded flow line would be exposed to $H_2S$-free conditions during commissioning, which would allow the re-passivation of the surface. In the paper results were presented showing the influence of pre-exposure to $CO_2$ on the development of the passive film (see Figure 2.51). The pre-exposure to $CO_2$ reduced the passive current density and increased the range of the passive region.

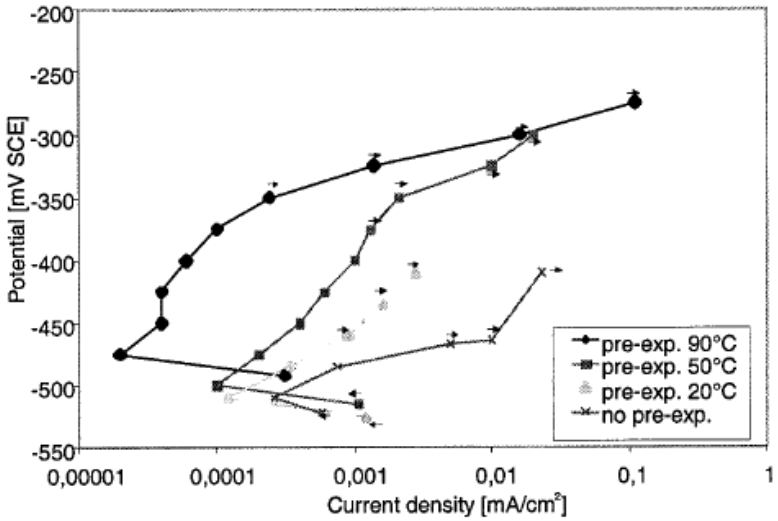


**Figure 2.52** Pitting measurements carried out by Bjordal et al and referenced by Enerhaug et al. [29], 20°C, 30,000 ppm Cl, 100 mbara $H_2S$, scan rate 12.5 mV/12hr. The specimens had been pre-exposed for 48 hrs. in a $CO_2$ saturated solution at various temperatures prior to the pitting measurements.

# CHAPTER 3: SCOPE OF WORK

The primary aim of this research project is to determine if weldable martensitic 13 %Cr stainless steel (WMSS) is more susceptible to sulphide stress cracking at 5°C compared to 24°C following the initial tests performed by Bodycote in 2005 [2] which indicated that SSC was more severe at lower test temperatures.

The tests were conducted in 2005 and subsequently testing procedures have been changed in particular with respect to the monitoring and control of the dissolved oxygen in solution and consequently a further aim of the work is to develop a standardised approach to FPB SSC testing, in particular with respect to controlling and monitoring the dissolved oxygen concentration and in-situ pH. Both of these parameters, in addition to the more controllable chloride concentration, partial pressure of $H_2S$ and temperature have an influence on the cracking susceptibility of WMSS.

A further aim of this project is to investigate the Influence of the test parameters (temperature: 5°C v 24°C and $H_2S$ partial pressure) and specimen surface preparation on the corrosion characteristics of the passive film by electrochemical techniques (i.e. by monitoring of the corrosion potential and conducting anodic potentiodynamic polarisation tests). The results should provide an insight as to whether the electrochemical character of the metal at 5°C compared to 24°C is the controlling factor for the previously observed cracking behaviour (i.e., cracking is more severe in 5°C compared to 24°C).

The work presented in this thesis addresses these aims and is presented in the following chapters:

- Chapter 5: Material Characterisation
- Chapter 6: Sulphide Stress Cracking Tests
- Chapter 7: Electrochemical Testing

## 3.1 Material Characterisation

Nippon Steel & Sumitomo Metal Corporation (NSSMC) supplied the weldable 13%Cr stainless steel pipeline material used in this investigation. Only parent material (No welded joints) was tested, since it was considered that the presence of a weld would complicate the interpretation of the results and introduce a further variable. However it was recognised that since the material tested is a weldable grade further work would be required to characterise the performance of the welded joints.

Chapter 5 presents the material characterisation tests performed on this material and include microstructure, retained austenite, tensile properties (at 5°C & 24°C), impact toughness, surface roughness and hardness. It was considered to be important to define these properties at the outset of the project as they could be influencing the SSC resistance of this material.

## 3.2 Sulphide Stress Cracking (SSC)

A test matrix shown in Table 3.1 was designed to investigate the Influence of temperature, $H_2S$ partial pressure, pH and surface condition on the susceptibility of SSC susceptibility of the material. The 69 mbara upper level of $H_2S$ was chosen to re-produce the partial pressure of $H_2S$ used in the 2005 Bodycote tests [2]. It was recognised that this level of $H_2S$ was high and beyond the upper limits of $H_2S$ which are currently used for WMSSs in the welded condition. However this high level of $H_2S$ was selected not only to reproduce the previous test conditions but also to provide a severe test environment where cracking would be expected under certain test conditions. The lower $H_2S$ level of 35 mbara was selected to produce a more benign test environment which was more in line with the upper level of $H_2S$ being currently used for WMSS flow-lines.

Two conditions were selected for the test solutions; one being a low chloride ion content (1,000 mg/L), low pH (3.5) solution representing condensed water (CW) conditions encountered in gas production and the second being a high chloride ion content (100,000 mg/L) produced water (PW) environment representing conditions which may be encountered in oil production. The condensed water (CW) was buffered with 0.4 g/L sodium acetate ($CH_4COONa$) and acetic acid ($CH_4COOH$) to achieve the in-situ pH of 3.5 and the produced water was buffered with sodium bicarbonate to achieve an in-situ pH of 4.5.

**Table 3.1** SSC Test Matrix

| Solution | pH | $H_2S$ partial pressure (mbara) | Test temperature (°C) | Surface finish |
|---|---|---|---|---|
| Produced Water: 165 g/L NaCl + sodium bicarbonate buffer | 4.5 | 69 | 24 | As-received |
| | | | | 600 SiC |
| | | | 5 | As-received |
| | | | | 600 SiC |
| | | 35 | 24 | As-received |
| | | | | 600 SiC |
| | | | 5 | As-received |
| | | | | 600 SiC |
| Condensed Water 1.65 g/L NaCl + 400 mg/L sodium acetate + acetic acid | 3.5 | 69 | 24 | As-received |
| | | | | 600 SiC |
| | | | 5 | As-received |
| | | | | 600 SiC |
| | | 35 | 24 | As-received |
| | | | | 600 SiC |
| | | | 5 | As-received |
| | | | | 600 SiC |

It was recognised that appropriate test methods would need to be developed in order to achieve the optimum test conditions. The following actions were considered to be required in the scope of work:

1. Construction of test cell in nitrogen cabinet.
2. Incorporation of oxygen probe in order to measure the in-situ oxygen values during the 30-day tests.
3. Incorporation of a method to measure and control the pH for the 30-day tests in the condensed water environment. As previously discussed in the literature review (section 2.6.5.3) the control of the pH in the type 3 environment, using an artificial buffer, can be problematic at pH values of 3.5 and below.

## 3.3 Electrochemical Testing

A test matrix, shown in Table 3.2, was designed to investigate the Influence of temperature, purge gas, $H_2S$ partial pressure and surface condition on the electrochemical behaviour of the material in the produced water (PW) environment only. For this current program of work it was not proposed to conduct electrochemical testing in the condensed water environment, since it is generally recognised that the produced water environment with a chloride ion concentration of 100,000 mg/L provides the most severe test conditions with respect to ambient or low temperature SSC. The aim of this research was to monitor the corrosion potential ($E_{corr}$) of specimens prepared with an as-received surface and a 600 SiC ground surface. The corrosion potential ($E_{corr}$) was to be monitored during saturation of the test solution with either nitrogen or carbon dioxide and then subsequently monitored during the initial (1 hr) saturation of the solution with the respective test gas. Following the solution saturation anodic potentiodynamic polarisation tests were planned in order to obtain Information on the passive current density ($i_{pass}$) and the break-down or pitting potential ($E_{bd}$) potential.

**Table 3.2** Electrochemical test matrix for the Produced Water environment with a pH of 4.5.

| Mounting compound | Specimen ref | Purge gas | Test gas | Test temperature (°C) | Surface finish |
|---|---|---|---|---|---|
| Epoxy | AR1 | $N_2$ | 35 mbara $H_2S$ | 24 | As-received |
| Epoxy | 6001 | $N_2$ | 35 mbara $H_2S$ | | 600SiC |
| Beeswax | AR6 | $N_2$ | 35 mbara $H_2S$ | | As-received |
| Beeswax | 6006 | $N_2$ | 35 mbara $H_2S$ | | 600SiC |
| Epoxy | AR9 | $N_2$ | 69 mbara $H_2S$ | | As-received |
| Epoxy | 6009 | $N_2$ | 69 mbara $H_2S$ | | 600SiC |
| Epoxy | AR2 | $CO_2$ | 35 mbara $H_2S$ | | As-received |
| Epoxy | 6002 | $CO_2$ | 35 mbara $H_2S$ | | 600SiC |
| Epoxy | AR10 | $CO_2$ | 69 mbara $H_2S$ | | As-received |
| Epoxy | 6010 | $CO_2$ | 69 mbara $H_2S$ | | 600SiC |
| Epoxy | AR8 | $N_2$ | $N_2$ | | As-received |
| Epoxy | 6008 | $N_2$ | $N_2$ | | 600SiC |
| Epoxy | AR7 | $CO_2$ | $CO_2$ | | As-received |
| Epoxy | 6007 | $CO_2$ | $CO_2$ | | 600SiC |
| Epoxy | AR3 | $N_2$ | 35 mbara $H_2S$ | 5 | As-received |
| Epoxy | 6003 | $N_2$ | 35 mbara $H_2S$ | | 600SiC |
| Beeswax | AR5 | $N_2$ | 35 mbara $H_2S$ | | As-received |
| Beeswax | 6005 | $N_2$ | 35 mbara $H_2S$ | | 600SiC |
| Epoxy | AR4 | $CO_2$ | 35 mbara $H_2S$ | | As-received |
| Epoxy | 6004 | $CO_2$ | 35 mbara $H_2S$ | | 600SiC |

It was considered that trial tests would be required in order to develop an acceptable test procedure and in particular establish suitable resins to mask the specimens.

# CHAPTER 4: EXPERIMENTAL PROCEDURE

## 4.1 Material Characterisation

### 4.1.1 Test Material

Nippon Steel & Sumitomo Metal Corporation supplied a 1 meter section of seamless pipe for this research project. The pipe is classified as an API 5LC Grade LC80-130S (NSSMC grade SM80-130S [30]) 'weldable' 13%Cr martensitic stainless steel (WMSS), with an outer diameter of 323.9mm and wall thickness of 12.7 mm. the pipe was identified as Heat no. F017024, Pipe no.1, Cert no. WYYK6485. Internal and external surfaces are alumina blasted and cleaned with a two-stage ($H_2SO_4$, $HF/HNO_3$ mix acid) pickling process. Table 4.1 shows the chemical composition of the test material, determined from Optical Emission Spectroscopy (OES) by Exova's Teesside chemical analysis laboratory (cert Ref: X903666).

**Table 4.1** Chemical composition of the LC80-130S Pipe (Heat no. F017024)

| Chemical composition (wt.%) | | | | | | | | | | | | | | |
|---|---|---|---|---|---|---|---|---|---|---|---|---|---|---|
| C | Si | Mn | P | S | Cr | Mo | Ni | Al | B | Cu | Nb | Ti | V | N |
| 0.010 | 0.23 | 0.42 | 0.015 | <0.005 | 12.0 | 2.47 | 6.41 | 0.0028 | <0.001 | 0.04 | <0.01 | 0.15 | 0.03 | 0.007 |

The API 5LC Grade LC80-130S 'weldable' 13%Cr martensitic stainless steel (WMSS) line pipe used for this research project was manufactured by NSSMC at their Wakayama steel works in Japan following the process route schematically shown in Figure 4.1 [30].

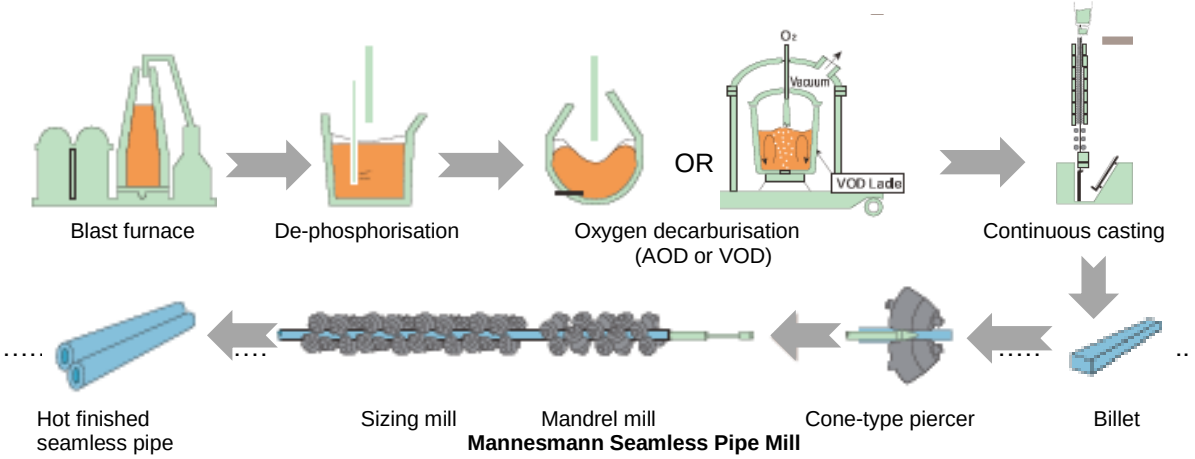


**Figure 4.1** Schematic sketch showing the manufacturing route for the seamless pipe [30].

### 4.1.2 Microstructure

Specimens were cut from transverse and longitudinal sections of the supplied pipe, wet ground to a 1200 grit finish with silicon carbide paper and polished to a 1 μm diamond finish. Microstructures were revealed using the etchants listed in Table 4.2 and examined under an optical microscope.

**Table 4.2** Etchants used in the investigation

| Etchant | Composition | Use | Procedure |
|---|---|---|---|
| Vilella's | 5 ml HCl<br>1 g Picric acid<br>100 ml Ethanol | Reveals martensite | Swabbed for one minute |
| Acidified Ferric Chloride | 300 g $FeCl_3$<br>100 ml HCl<br>1 / $H_2O$ | Reveals martensite | Swabbed for 2 seconds |

### 4.1.3 Retained Austenite[4]

Since the SSC resistance of 13%Cr stainless steels is believed to be influenced by the amount of retained austenite in the tempered martensitic microstructure, X-ray diffraction (XRD) was used to determine the volume percent of retained austenite in the test material. The tests were carried out at the University of Birmingham on a Philips X'Pert diffractometer at 24°C using Cu Kα radiation and generator settings of 40 kV and 40 mA. A 2θ scan range from 40° to 120° was employed with a 2θ step interval of 0.02°. X-ray diffraction patterns and integrated intensities were determined using Philips X'Pert "Highscore" software.

The scan range (i.e. 40° – 120° 2θ) was selected to cover five austenite peaks (111, 200, 220, 311 and 222) and five martensite peaks (110, 200, 211, 220 and 310), in order to reduce the influence of preferred orientation of the result. It is recognised that by taking into account the five austenite (γ) and five martensite ($\alpha^{-}$) peaks for calculating the retained austenite errors can be introduced due to the relatively low signal to noise ratios for the γ (220), γ (311) and γ (222) peaks.

[4] Please note that this work was performed in collaboration with Mr Matthew Walters (EngD student)

Ten specimens measuring 20 x 10 x 5 mm were prepared from transverse sections of the supplied pipe, wet-ground and polished to a 6 µm diamond finish for this investigation. Each specimen was etched in Vilella's reagent and examined under a light microscope for signs of heat effects or surface deformation which could potentially transform retained austenite to martensite near the surface. Following the visual examination, the specimens were re-polished to a 1 µm diamond finish for XRD analysis.

The volume percent of retained austenite was determined by comparing the integrated copper X-ray diffraction intensities of ferrite and austenite phases with theoretical integrated intensities. Since the theoretical intensities for martensite and ferrite are nearly the same, the theoretical intensities for martensite were calculated assuming a body-centred cubic cell (α-ferrite).

The percentage volume of retained austenite is estimated from measurements of integrated intensities (Iα & Iγ) assuming that martensite austenite are the only phases present. The method used is that outlined by Dickson [101], which extends the theory of direct comparison to correct for preferred orientation effects:

$$\frac{C_\gamma}{C_\alpha} = \frac{\frac{1}{n_\gamma}\sum_{0}^{n\gamma}\frac{I_\gamma}{R_\gamma}}{\frac{1}{n_\alpha}\sum_{0}^{n\alpha}\frac{I_\alpha}{R_\alpha}} \qquad (4.1)$$

*Where:*

γ= austenite
α = ferrite (martensite)
*C* = volume fraction of the particular phase
*I* = measured integrated intensity
*N* = number of measured (*hkl*) reflections
*R* = theoretical integrated intensity

From the calculated value of Cγ/Cα, the volume fraction of retained austenite ($C_\gamma$) was found from the relationship Cγ + Cα = 1:

$$C_\gamma = \frac{C_\gamma / C_\alpha}{\left(1 + C_\gamma / C_\alpha\right)} \qquad (4.2)$$

### 4.1.4 Tensile Tests

Uniaxial tensile tests were performed at the University of Birmingham. The tests were conducted in duplicate at 24°C on specimens machined from longitudinal and transverse orientations of the pipe using an Instron screw driven tensile testing machine. Additional tests were performed at 5°C using a DMG screw driven tensile tester fitted with a liquid nitrogen-cooled temperature controlled enclosure (Figure 4.1). All the tensile tests were performed on standard ASTM A370 [81] / ASTM E 8M [82] round section specimens to define the yield stress, ultimate tensile strength and the modulus of elasticity at the nominal test temperature. The tests were conducted at a strain rate of 0.00025 mm/mm/s ± 20%, in accordance with ASTM E8M [82].

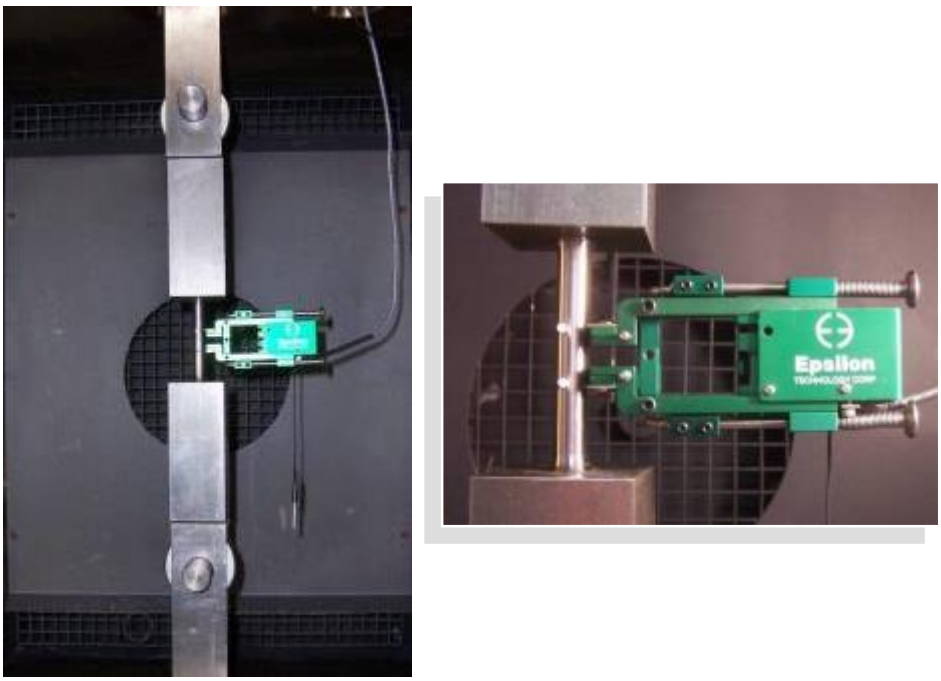


**Figure 4.2** Tensile testing in temperature controlled enclosure

### 4.1.5 Impact Toughness

Charpy impact tests were performed using the method described in ASTM E23 [102]. Thirty-three specimens measuring 55 x 10 x 10 mm were cut from a longitudinal section of the supplied pipe and wet-ground to a 600 grit finish. The notch was orientated in the through-thickness direction and the tests were performed in triplicate at each temperature in the range of -196 °C to +22 °C. Plots were made of impact energy versus temperature and percentage shear versus temperature in order to determine the ductile-brittle transition temperature (DBTT).

### 4.1.6 Flexural Bend Tests[5]

Flexural bend tests were performed at room temperature at Exova Corrosion Centre using a 50 kN Instron tensile load frame. Additional tests at 5°C were performed at the University of Birmingham using a DMG screw driven tensile tester fitted with a liquid nitrogen-cooled temperature controlled enclosure. Each flexural bend specimen (see Figure 4.3) was fitted with a biaxial strain gauge at the mid-width, mid-length position on the tensile surface to measure longitudinal and transverse strain components.

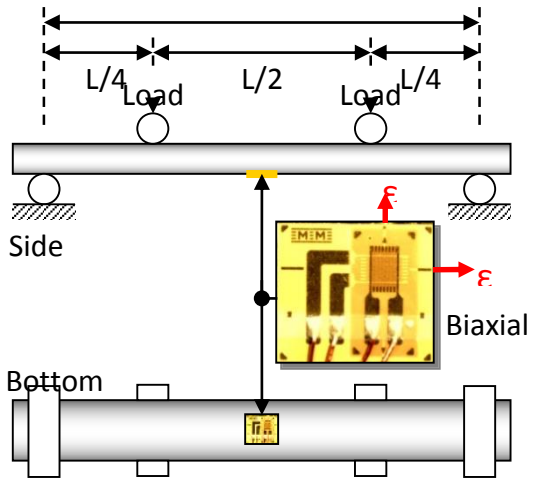


**Figure 4.3** Schematic sketch of the Four-point 'flexural' bend test sample fitted with a biaxial strain gauge

[5] Please note that this work was performed in collaboration with Mr Matthew Walters (EngD student)

Specimens were strained to approximately 1.2% and loaded at a constant rate of 1 mm per minute.

The load, strain and deflection were recorded at a rate of one sample per second using a Vishay P3 strain recorder to plot graphs of load versus strain, to determine the total strain ($\varepsilon_{tot}$) to be applied in order to achieve 0.2 % plastic strain ($\varepsilon_{pl}$) in accordance with the procedure detailed in the NPL report DEPC MPE 007 [103]. Following each test, a load-strain curve was plotted, similar to that shown in Figure 4.4.

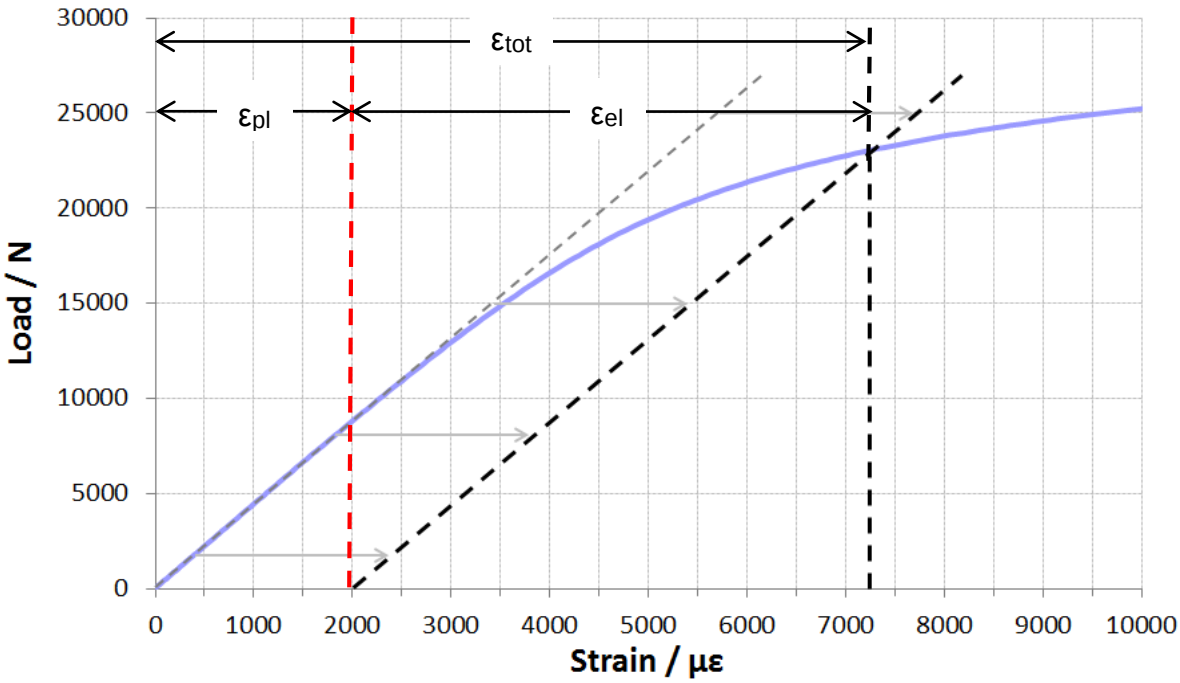


**Figure 4.4** Graph showing the determination of the total strain ($\varepsilon_{tot}$) to be applied to the flexural FPB test specimen to achieve 0.2% plastic strain ($\varepsilon_{pl}$).
The elastic strain is $\varepsilon_{el}$.

This curve was used to determine the total strain ($\varepsilon_{tot}$) to be applied to the flexural FPB specimen to achieve 0.2% plastic strain ($\varepsilon_{pl}$), by taking a line parallel to the linear elastic region of the curve from the 2000 με (0.2 %) point. Where this line intersected the curve, a vertical line was taken to the x-axis to give the total strain (i.e. plastic ($\varepsilon_{pl}$) + elastic ($\varepsilon_{el}$)) in bending. In addition to the load, strain and deflection measurements recorded during the tests, the modulus of elasticity (E) and Poisson's ratio ($\varepsilon_2/\varepsilon_1$) were also calculated for each specimen.

4.1.6.1 Room Temperature Tests

Ten flexural bend specimens were machined from the longitudinal orientation of the pipe for testing at room temperature (24°C ± 0.5°C). Four of the specimens measured 130 x 20 x 10 mm, four measured 130 x 20 x 5 mm and two measured 130 x 20 x 2.5 mm. In addition, three specimens were machined from the transverse orientation of the pipe measuring 70 x 20 x 4 mm.

All the specimens were fitted with a general-purpose, three-wire biaxial strain gauge with a grid resistance of 120 ohms. The strain gauges were a 'stacked' type with the longitudinal gauge at the bottom (closest to the specimen surface) and the transverse gauge on top. Both longitudinal and transverse gauges were wired to the P3 strain recorder.

4.1.6.2 Tests at 5°C

Four flexural FPB specimens were machined from the longitudinal orientation of the pipe for testing at 5°C ± 1°C. Room temperature (24°C ± 1°C) tests were repeated because different test apparatus were being used to achieve an ambient temperature of 5°C so it was important to ensure a valid comparison was being made between the two temperatures. All the specimens used in these tests measured 130x20x10 mm and were fitted with a general-purpose, biaxial strain gauge wired in a quarter bridge arrangement as described previously. Due to the design of the test apparatus used, beam deflection could not be measured in these tests.

### 4.1.7 Surface Roughness

Surface roughness (Ra) measurements were carried out at Exova Corrosion Centre using a Surtronic 3+ surface profiler on specimens with an as-received pipe surface (AR), a surface ground to a 120 SiC grit finish (with an automatic grinding tool) and a surface wet ground to 600 SiC grit finish. On each specimen nine measurements were taken across the surface and the average value reported.

### 4.1.8 Scanning Electron Microscopy

A JEOL 6060 scanning electron microscope (SEM) was used to image the fracture surfaces of Charpy impact specimens and the as-received, 120 SiC grit and 600 SiC grit surfaces used in the surface roughness measurements. The SEM was operated at an accelerating voltage of 20 kV, in secondary electron mode at a working distance of 10 mm.

### 4.1.9 Micro-hardness Measurements[6]

Hardness tests were conducted at the University of Birmingham using a Mitutoyo MVK-H1 hardness testing machine with a Vickers indenter and a load of 200 gf.

The Vickers hardness was determined by measuring the mean diagonal length of the indentation as defined in ASTM E384 [104].

$$Hv = 1854.4 \times P/d^2 \qquad (4.3)$$

*Where:*

Hv = Vickers hardness number
P = load (gf)
d = mean diagonal length of indentation (μm)

A sample was cut from transverse section of the supplied pipe, wet ground to a 1200 grit finish with silicon carbide paper and polished to a 1 μm diamond finish. Sixty-four micro-hardness measurements were taken across the thickness of the pipe sample at 0.2 mm intervals from the outer surface to the inner bore.

[6] Please note that this work was performed in collaboration with Mr Matthew Walters (EngD student)

# 4.2 Sulphide Stress Cracking (SSC) Testing

### 4.2.1 Test Procedure

4.2.1.1 Specimen Preparation

Four-point bend SSC test specimens were initially prepared with 'as-machined' (i.e. milled and surface ground) and 'as-received' surface finishes measuring 130 x 20 x 10 mm and 130 x 20 x 12.7 mm (full thickness of pipe) respectively.

The longitudinal edges of the test specimens were then prepared with 45° edge chamfers, except for four specimens tested at 35 mbar $H_2S$ (24°C) where the edge was left 'as-machined' in order to investigate the influence of edge preparation on the SSC resistance.

All of the 'as-machined' faces were ground to a 600 SiC grit finish and left to air-passivate for a minimum time of 48 hours before exposure to the test environment. The difference in the surface roughness (Ra) of the 600 SiC grit finished and as-received specimens is presented in section 5.7.

4.2.1.2 Specimen loading

Each of the FPB SSC test specimens was fitted with a biaxial strain gauge on the centre of the tensile face and loaded to 0.2% plastic strain (100% AYS) using the data determined from the flexural bend tests. The loading rig, shown in Figure 4.5, was manufactured from 25%Cr duplex stainless steel with 10 mm diameter alumina rollers spaced with the following dimensions:

Outer roller = 120 mm

Inner roller spacing = 60 mm

The guidelines in ASTM G39 [83] were followed with respect to the roller spacing.

Each specimen was loaded by applying small load increments whilst monitoring the longitudinal and transverse strain readings from the biaxial gauge and the equivalent uniaxial strain ($\varepsilon_{eus}$) value were calculated at each stage using the following equation:

$$\varepsilon_{eus} = [1/ (1 - \upsilon^2)]. [\varepsilon_1 + \upsilon\, \varepsilon_2] \qquad (4.4)$$

where $\varepsilon_1$ = longitudinal strain (με)

$\varepsilon_2$ = transverse strain (με)

$\upsilon$ = Poisson's ratio (taken as 0.3 for 13%Cr)

After loading, the longitudinal and transverse strain components of the bi-axial load were monitored for 2 hours to ensure the loading strain remained stable. After this stabilization period, the specimens were immersed in acetone to remove the strain gauge then thoroughly cleaned and degreased in an alkaline degreaser and in acetone preparation for exposure to the test environment.

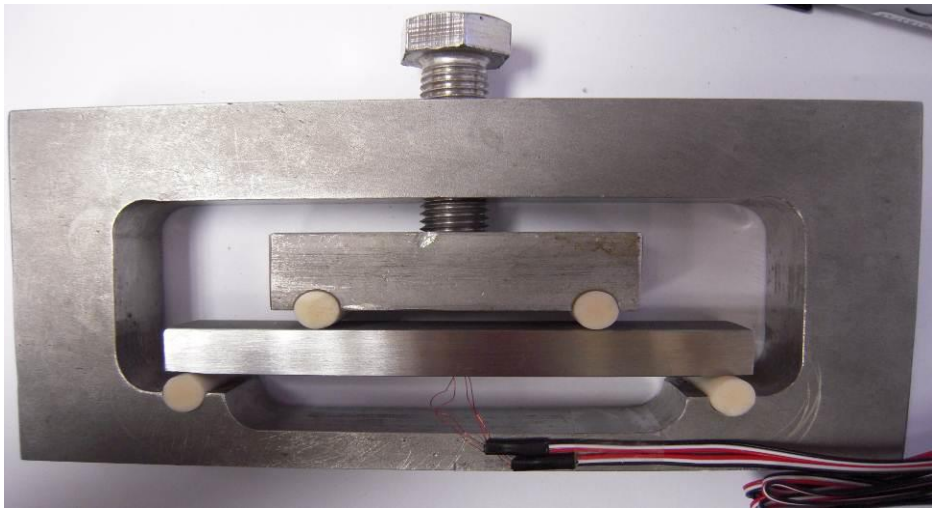

**Figure 4.5** SSC loading rig showing the alumina rollers and the specimen in position with the strain gauge attached.

4.2.1.3 Test Equipment

The SSC test rig design is shown in Figure 4.6: The idea of placing the SSC test vessel in a nitrogen chamber was developed by NPL and BP and has been shown to be effective in minimising oxygen contamination of the test solution [105].

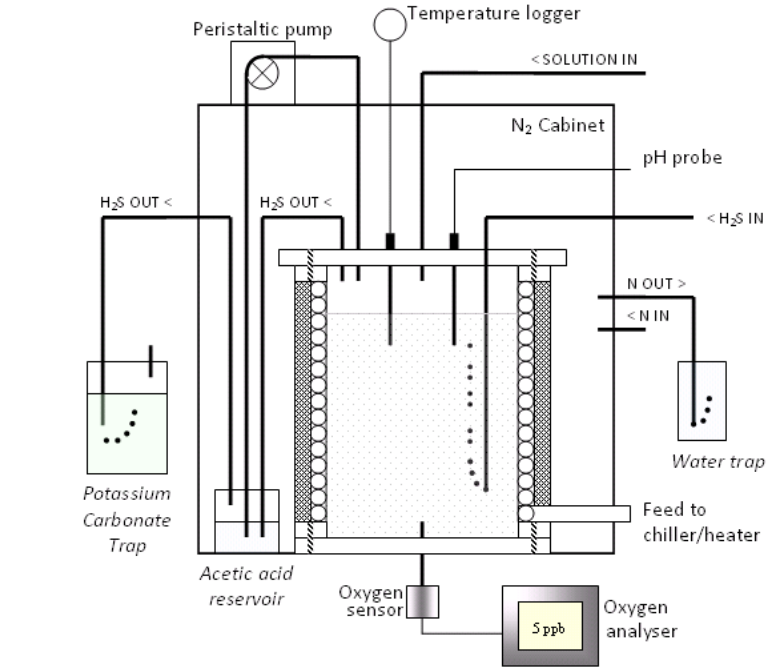


(a)

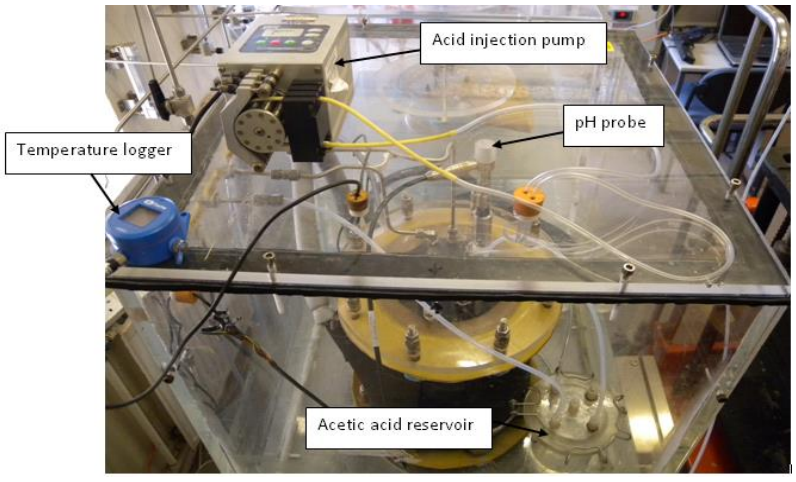


(b)

**Figure 4.6** SSC test rig design in nitrogen cabinet, with $O_2$ and pH monitoring

A 10 L ‘QVF’ glass test vessel was built inside an acrylic nitrogen cabinet to prevent oxygen contamination into the test solution. In order to monitor and record oxygen levels in the test solution, a Hach-Lange type M1100 luminescence dissolved oxygen sensor was fitted through the base of the test vessel. This sensor, which is shown in Figure 4.7, had previously been trialled at Exova Corrosion Centre and had found to be compatible with $H_2S$.

**Figure 4.7** Hach-Lange type M1100 luminescence dissolved oxygen sensor

A common problem with simulated condensed water environments, conducted at ambient pressure, is that the solution pH tends to increase during the test, as previously discussed in the literature review. To overcome this, a pH control system was developed, whereby acetic acid could be injected into the test solution under controlled de-aerated conditions. A pH sensor fitted through the lid of the vessel provided continuous pH readings of the test solution throughout the test. If the pH drifted above the 0.1 pH tolerance, then the peristaltic pump could be activated to slowly feed acetic acid into the test solution until the pH returned to within the specified range. The in-situ pH probe used for the tests is shown in Figure 4.8 and Figure 4.6 shows a photograph and schematic of the test vessel.

**Figure 4.8** Hamilton ‘ARC’ pH sensor

4.2.1.4 Test Environments

The SSC tests were performed in simulated Produced Water (PW) and Condensed Water (CW) environments at 5°C and 24°C using $H_2S$ partial pressures of 69 mbar and 35 mbar respectively. These $H_2S$ partial pressures were achieved at atmospheric pressure using certified gas mixtures of 6.9 % $H_2S$ in $CO_2$ and 3.5 % $H_2S$ in $CO_2$ respectively.

The simulated produced water was prepared by adding 165 g/L NaCl (100,000 mg/L $Cl^-$) to de-ionised water and making up to 10 litres with de-ionised water. To ensure a stable pH was achieved when exposed to the $H_2S/CO_2$ gas mixture, the solution was saturated with $CO_2$ for two hours and a small amount of sodium bicarbonate ($NaHCO_3$) buffer was added until the pH stabilised at 4.5, following the guidelines of EFC 17 [69].

10 litres of simulated condensed water solution was prepared with 1.65 g/L NaCl (1,000 mg/L $Cl^-$) and 400 mg/L sodium acetate ($CH_3COONa$) buffer, in accordance with the second edition of EFC 17 [69] and solution C of NACE TM0177 [55]. After a two-hour $CO_2$ saturation period, the solution was acidified with approximately 50 mL (0.5 % wt.) acetic acid ($CH_3COOH$) to achieve a stable pH of 3.5.

4.2.1.5 Exposure Procedure

Five loaded four-point bend test specimens (three as-received and two fully-machined specimens) were sealed inside each test vessel which in turn was sealed inside a nitrogen cabinet. A separate de-aeration vessel was used to de-aerate the test solution; the gas outlet from the test vessel was connected to the de-aeration vessel and the system was purged with nitrogen gas through both vessels. Luminescence oxygen sensors fitted to both the test vessel and the de-aeration vessel measured the oxygen content throughout the system. Once the oxygen level fell below 10 ppb in both vessels, the solution was transferred to the test vessel by creating a pressure differential between the two vessels.

Following the filling of the test vessel with the solution the nitrogen purge was continued for a further 1 hr, while the oxygen in the solution was being continuously monitored. The required $H_2S$ / $CO_2$ gas mixture was then introduced and the solution was saturated at a rate of 2L / min for a minimum duration of 2 hrs. After the solution was saturated the $H_2S$ concentration was measured together with the solution pH. The solution $H_2S$ concentration was measured using a modified iodometric titration procedure, as described in NACE TM0284 [57], taking into account the reduced $H_2S$ concentration. Also for the tests conducted at 5°C the iodine and sodium thiosulphate solutions were chilled to maintain the solubility of $H_2S$ during the titration.

During the 30 day test period, the $H_2S$ / $CO_2$ gas mixture was continuously purged through the solution at 1 bara pressure at a minimum rate of approximately 30 bubbles per minute. Solution temperature, pH and dissolved oxygen levels were monitored and recorded throughout the test.

4.2.1.6 Post-test Evaluation

At the end of the 30 day exposure period, the specimens were removed from the test vessel, flushed in de-ionised water and dried. Each specimen was inspected for cracks using a binocular microscope at magnifications up to x40 and using the red dye-penetrant examination (DPE) technique. Sections were taken through the regions containing cracks and in the absence of any visible cracking; two sections were taken through the central region at the 1/3$^{rd}$ and 2/3$^{rd}$ width locations. The sections were mounted in Bakelite, polished to a 1µm finish, etched in Vilella's reagent and examined using an optical microscope at magnifications up to x1,000. The quantity, length and depth of the cracks were measured and recorded using optical microscopy and "Image J" image analysis software.

# 4.3 Electrochemical Tests

### 4.3.1 Trial Tests -Test Cell Design - Coupon Masking Evaluation

4.3.1.1 Introduction

In order to develop an acceptable reproducible test method for the electrochemical testing it was decided to conduct trial tests to develop the optimum specimen preparation technique and test cell design.

The aim of the specimen preparation development was to develop a procedure which would be simple to apply, would retain the surfaces of interest in a clean film-free state and prevent or minimise crevice corrosion. In addition any coatings applied would need to withstand the sour test solutions at room temperature and at a temperature of 5°C.

The aim of the test cell development was to develop a cell where multiple specimens could be simultaneously exposed and the solution oxygen concentration controlled to a limit of <10 ppb and continuously monitored.

4.3.1.2 Specimen Preparation

Specimens approximately 20 mm x 20 mm x the wall thickness (approximately 12.7 mm) were cut from the parent pipe supplied by NSSMC (Heat no. F017024).

Specimens were prepared with the as-received bore surface intact.

The edges and corners of the specimens were chamfered and a 4 mm diameter hole was drilled and tapped in the one end face. A brass rod was screwed into the hole and sheathed with a glass tube which was sealed against the specimen using a Viton rubber O-ring. The sample assembly prior to coating is shown in Figure 4.8.

**Figure 4.9** Specimen, brass rod and glass tube prior to coating.

After the specimens had been assembled, as shown in Figure 4.9, the surfaces were coated with one of the five masking Compounds detailed in Table 4.3.

**Table 4.3** Details of masking compounds used for trial tests

| Number | Masking compound type | Manufacturer |
|---|---|---|
| 1 | G371 Lacomit varnish | Agar |
| 2 | Number 45 varnish | McDermid |
| 3 | Brushable Ceramic Epoxy | Devcon |
| 4 | 1 over 2 | |
| 5 | University blue lacquer | Not known |

4.3.1.3 Test Cell Development

A test cell was prepared to enable 6 specimens to be tested simultaneously so that a direct comparison could be made between the performances of the masking compounds. The cell comprised of a 10 litre glass vessel with an acrylic base and lid. In the base a fitting was made to accept the M1100 Hach-Lange Orbisphere optical probe, which has previously been described in section 4.2.1.3.

This optical probe has been successfully used by Exova to measure low oxygen values (i.e. <5 ppb) in high chloride solutions containing up to 1 bara $H_2S$. Therefore the probe was known to be acceptable to use in the particular environment. In the lid six ports were prepared to accept the specimens and a central port was made for the luggin capillary tube, which was connected to the saturated calomel reference electrode (SCE). Additional ports were prepared for the platinum wire counter electrode and for the gas in, gas out, solution fill, sampling port and data-logger. The cell was contained within a nitrogen-purged acrylic cabinet of the type shown in Figure 4.6.

#### 4.3.1.4 Test Solution Preparation

For the trial tests the 100,000 mg/L produced water composition was used, which was buffered to an in-situ pH of 4.5 by the addition of sodium bicarbonate. The solution was saturated outside of the test cell with $CO_2$ at room temperature and at 1 bara pressure in order to adjust the pH.

#### 4.3.1.5 Corrosion Potential Measurements

The prepared as-received specimens with the five different masking compounds applied (specimen numbers 1 – 5) were fitted into the cell and the cell and solution was purged with nitrogen until the oxygen level in the solution and cell fell below 10 ppb. The solution was then transferred from the purging vessel into the test cell and the potential measurements were commenced. For the initial trial the specimens were purged with nitrogen for 30 minutes, exposed to the $H_2S$ environment for approximately 1 hour and then purged with nitrogen before removing from the cell.

#### 4.3.1.6 Specimen Evaluation

Following the respective open circuit potential tests the specimens were visually examined and examined at magnifications up to 40x with the aid of a binocular microscope to evaluate the condition of the masking compound and the presence of any pitting / crevice corrosion on the specimens.

### 4.3.2 Electrochemical Measurements

#### 4.3.2.1 Introduction

Following the completion of the trial tests it was decided to use a spot welding technique to attach the copper connecting wire to the specimens and to use the ceramic epoxy coating as a masking compound on all specimens. Any differences between the electrochemical behaviour of the as-received and 600 SiC grit prepared surfaces could be directly compared using the same test parameters. The test matrix for the electrochemical tests is presented in Table 3.2 in section 3.2.

#### 4.3.2.2 Specimen Preparation

Specimens were cut from the pipe material measuring approximately 15 mm x 15 mm x the pipe wall thickness (approximately 12.7 mm). The edges and corners of the specimens were chamfered to avoid crevicing problems that could be associated with the masking compound cracking. The bore surface was prepared for the ground specimens wet grinding to a 600 SiC grit finish using successive grades of SiC papers; 60 grit - 120 grit – 240 grit – 600 grit. The bore surface on the as-received specimens was left intact. Following preparation the surfaces were degreased in an alkaline degreaser, flushed with acetone and hot air dried.

The specimens were then spot-welded to a length of copper cable and sheathed with a glass tube. The end of the tube and the welded face of the specimen were then glued together using the brushable ceramic epoxy ensuring that there was no leak path to the copper cable or spot weld. The remainder of the specimen was then coated with the brushable ceramic resin and a window was left on the test face, approximately 10 mm x 10 mm in exposed area. Care was taken to avoid contaminating the test face. The stages in the preparation of the specimens are shown in Figure 4.9.


**Figure 4.10** Stages in the preparation of the electrochemical test specimens.

Two of the as-received specimens and two of the 600 SiC ground specimens were coated with bees-wax as an alternative to the epoxy resin as previously used by Enerhaug [43]. On these specimens the surfaces of the specimens were coated with the epoxy resin with the exception of the test face (as-received or 600 SiC ground). The bees-wax was not easy to apply since it has a narrow melting temperature range, therefore it was found to be necessary to heat the specimens to approximately 50°C as well as melting the bees-wax.

4.3.2.3 Test Solution / Environment

All of the tests were conducted in the 100,000 mg/L produced water with the pH buffered to 4.5 by the addition of sodium bicarbonate. The prepared solution was saturated with 1 bara $CO_2$ at ambient temperature and the pH was adjusted to 4.5 by the addition of sodium bicarbonate.

The tests were conducted under the conditions shown in Table 3.2 as detailed in section 3.2.

4.3.2.4 Test Cell

A 1 litre glass test cell was used for all of the tests with the following ports in the lid:

i) Test specimen 1 (as-received)
ii) Test specimen 2 (600 SiC grit finish)
iii) Luggin capillary tube to saturated calomel electrode (SCE)
iv) Platinised mesh secondary electrode
v) Gas in
vi) Gas out
vii) Fill port
viii) Oxygen probe (including temperature sensor)

For the de-aeration and conditioning (either with nitrogen or carbon dioxide) of the solution prior to the Introduction into the test cell a 10 litre glass cell was used with suitable ports for the gas in, gas out, solution transfer and oxygen probe.

Since the oxygen concentration in the de-aeration vessel and test cell were monitored during the tests and the tests were of relatively short duration there was no requirement to house the vessels in a nitrogen cabinet.

4.3.2.5 Test Procedure

The test solution was prepared and purged with the respective gas (see Table 3.2). Immediately prior to starting each test the as-received and 600 SiC ground specimens were degreased using an alkaline de-greaser and propanol, which had previously been verified as an effective de-greaser against the requirements of ASTM F21. The specimens were placed in the test cell and the cell was sealed and de-aerated using the appropriate test gas (either $N_2$ or $CO_2$). The oxygen concentration of the solution and test cell was monitored and oxygen concentration in both vessels had fallen below 10 ppb the solution was transferred from the purging vessel into the test cell. The vessel was then purged with the respective purge gas at a relatively high flow rate of 1000 mL/min for 60 minutes. When the purging was commenced the corrosion potential of the two specimens was monitored using the same reference electrode and calibrated multi-meter. After the 1 hour purge period the solution was then purged with the test gas for a further 1 hour at a minimum flow rate of 1000 mL/min.

Following the 1 hour test gas purge the specimens were polarised using an ACM Instruments Gill AC potentiostat from a value -50 mV, with respect to $E_{corr}$, up to a current density value of either 0.1 $mA/cm^2$ or 1 $mA/cm^2$. For the 1st test conducted on specimens AR1 and 6001 the scan was reversed at a current density of 1 $A/cm^2$ and for tests 2 and 3 the tests were terminated at a current density of 1 $mA/cm^2$. For the remaining tests; 4 – 10, the scans were terminated at a current density of 0.1 $mA/cm^2$. Following the completion of the scans the specimens were removed, washed in water, flushed with propanol and hot-air dried.

The specimens were examined with the aid of a binocular microscope at magnifications up to 40x and the presence of any pitting and / or crevice corrosion was noted.

# CHAPTER 5: RESULTS & DISCUSSION
# Material Characterisation

## 5.1 Microstructure

Optical photomicrographs showing the microstructure of the material are presented in Figure 5.1. Etching of the parent metal revealed a tempered martensitic microstructure with a grain size of approximately 40 µm. Randomly dispersed angular, gold / orange-coloured inclusions were evident, ranging in size from 3 µm to 10 µm, as shown in Figure 5.1. The colour and shape of the inclusions indicated they were titanium nitrides (TiN) as opposed to titanium carbides (TiC) or titanium carbo-nitrides (TICN). Titanium nitrides normally appear as yellow-coloured cubic particles, whereas titanium carbides are greyish in colour with a less regular shape [106].

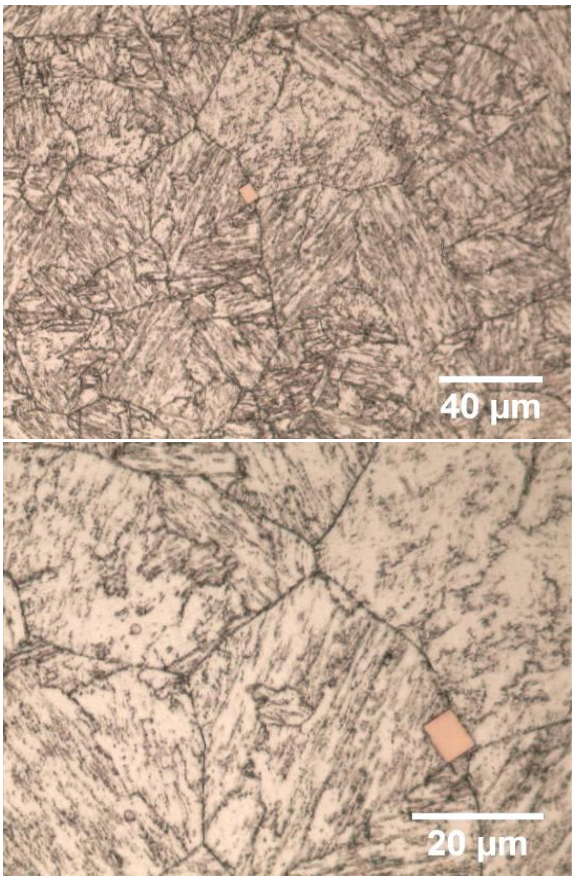


**Figure 5.1** Photomicrographs showing the microstructure of the base material, etched with acidified ferric chloride.

## 5.2 Retained Austenite

The results from the X-ray diffraction (XRD) measurements are presented in Table 5.1 and a typical trace is shown in Figure 5.2. The measured retained austenite values ranged from 9.8 % to 15.7 % with an average of 12.9 %, a standard deviation of ± 1.5% and a 95% CI of ± 2.9%.

Errors in XRD measurements of retained austenite can arise due to the, instrument limitations, calculation method used and sample condition [107]. In the case of the tests conducted the main error was considered to be due to preferred orientation

The error due to preferred orientation, calculated in accordance with the method outlined by Dickenson [101] ranged from ± 0.1% to ± 1.3% for the ten specimens with an average value of ± 0.8%. The variation in the error values can be attributed to the difference in the preferred orientation between the ten specimens, which is consistent with the fact that the specimens were taken from a wrought steel with an inhomogeneous structure.

In addition to preferred orientation other factors influence the precision in the determination of retained austenite using the X-ray diffraction method and a repeatability of ± 3% and a reproducibility of ± 4% has been reported for steels containing 15 % by volume retained austenite [108]. Also using a reference sample containing 14.7% retained austenite errors ranging from ± 0.31% to ± 2.83% have been reported by Su et al. [109], which are in a similar range to those shown in Table 5.1.

**Table 5.1** Lattice parameter and retained austenite measurements for each specimen (average used in analysis)

| Specimen | Lattice parameter ($a_o$) | | Retained austenite (%) | Preferred orientation error (±) |
|---|---|---|---|---|
| | Ferrite (martensite) | Retained austenite | | |
| 1 | 2.880 | 3.591 | 13.4 | 1.1 |
| 2 | 2.885 | 3.593 | 13.1 | 0.8 |
| 3 | 2.880 | 3.595 | 13.5 | 1.3 |
| 4 | 2.882 | 3.587 | 15.7 | 1.0 |
| 5 | 2.878 | 3.56 | 12.4 | 1.0 |
| 6 | 2.883 | 3.594 | 9.8 | 0.7 |
| 7 | 2.881 | 3.589 | 12.3 | 1.1 |
| 8 | 2.880 | 3.602 | 12.2 | 0.1 |
| 9 | 2.883 | 3.582 | 13.8 | 0.9 |
| 10 | 2.880 | 3.596 | 12.6 | 0.4 |
| **Average:** | **2.881** | **3.589** | **12.9** | **0.8** |
| Standard deviation (Sr) | 0.002 | 0.012 | 1.5 | |
| 95% CI (±) | 0.004 | 0.023 | 2.9 | |

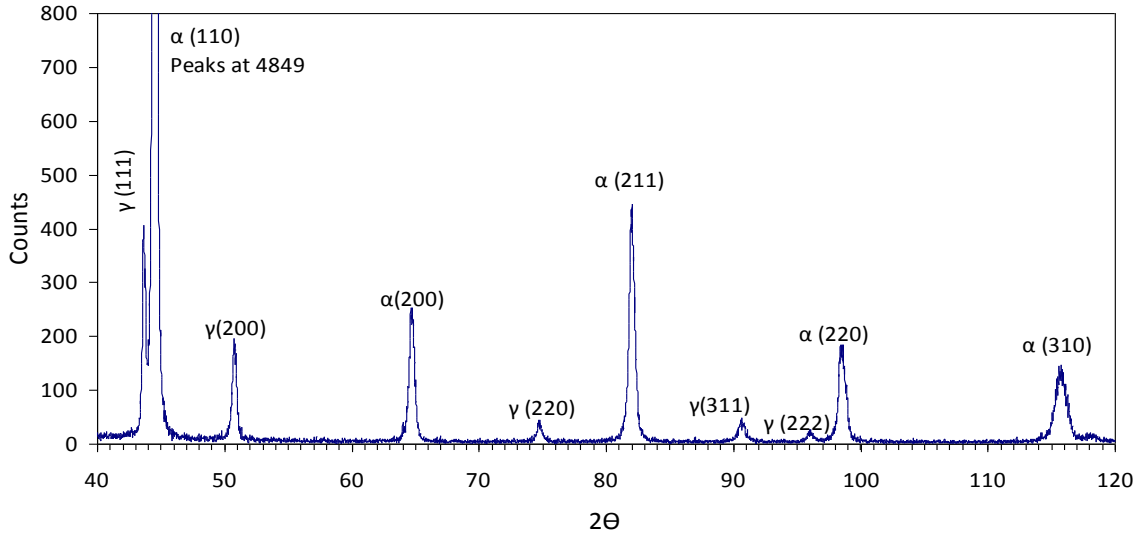


**Figure 5.2** Typical XRD trace for 13% Cr stainless steel containing approximately 12% retained austenite.

## 5.3 Tensile Tests

The tensile test results are given in Table 5.2 for the duplicate 5°C and 24°C tests. The results showed that the tensile properties did not change significantly between the two test temperatures.

**Table 5.2** 5°C and 24°C tensile test results showing the calculated strain values at 100% AYS and the modulus of elasticity values

| Temperature (°C) | $\sigma R_{p0.2}$ (MPa) | $\sigma R_{t0.5}$ (MPa) | ε @ $R_{p0.2}$ (με) | $E_{average}$ (GPa) |
|---|---|---|---|---|
| 5 | 711 | 702 | 5492 | 221 |
| 5 | 713 | 696 | 5621 | |
| 24 | 704 | 693 | 5540 | 227 |
| 24 | 704 | 697 | 5369 | |

## 5.4 Flexural Bend Tests

The flexural bend test results are given in Table 5.3 for the duplicate 5°C and 24°C tests. The results show that the flexural bend properties did not change significantly between the two test temperatures.

**Table 5.3** Flexural bend test results

| Temperature (°C) | $\varepsilon_{tot}$ (με) | $Load_{0.2}$ (kN) |
|---|---|---|
| 5 | 7329 | 21.1 |
| 5 | 7307 | 21.0 |
| 24 | 7247 | 20.9 |
| 24 | 7304 | 21.0 |

## 5.5 Tensile v Flexural Bend Tests

Table 5.4 compares the average tensile strain at 100% AYS, taken from Table 5.2, with the average total strain ($\varepsilon_{tot}$), applied to the flexural FPB specimen to achieve 0.2% plastic strain ($\varepsilon_{pl}$), taken from Table 5.3. The comparison shows that using tensile data to set the loading strain for four-point bend specimens results in the specimens being strained to a lower level (up to 25%), compared to if they were strained from flexural bend data.

**Table 5.4** Comparison of tensile and flexural bend data

| Test temperature (°C) | Average tensile 0.2% yield stress (100% AYS) (MPa) | Average strain at 100% AYS (με) | | Difference (%) |
|---|---|---|---|---|
| | | Tension | Flexure | |
| 5 | 712 | 5557 | 7318 | 24 |
| 24 | 704 | 5455 | 7276 | 25 |

## 5.6 Impact Toughness

The Charpy impact results are shown in Figure 5.3. It can be seen from Figure 5.3 that the ductile to brittle transition temperature (DBTT) is approximately -100°C, hence the SSC tests carried out at 5°C and 24°C are well within the upper shelf of this material.

The test at -115°C temperature (circled in Figure 5.3) showed a higher impact energy and % shear value than the trend line. Variations in results are often seen in Charpy impact tests and the reason for the anomalous result was likely attributable to the material inhomogeneity or variation in the test temperature.

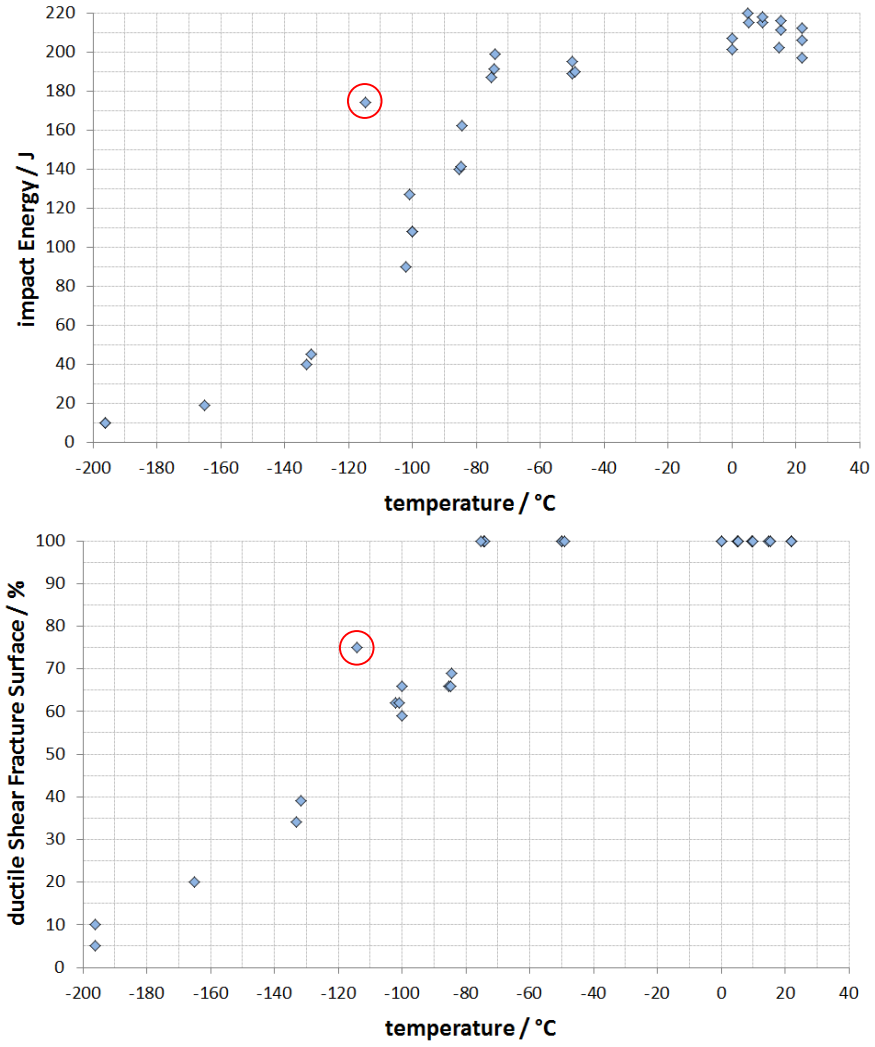


**Figure 5.3** Charpy impact energy (J) versus temperature (°C) and ductile shear fracture surface (%) versus temperature (°C) curve.

SEM images of the Charpy fracture surfaces are presented in Figure 5.4. Failures in the upper shelf region show a typical dimpled rupture fracture surface corresponding to 100 % shear. Failures at the DBT combine showed transgranular cleavage and ductile with some ductility on the ridges and around the inclusions (TiN). The fracture at the lower shelf was predominately brittle cleavage with evidence of some ductile fracture on the ridges.

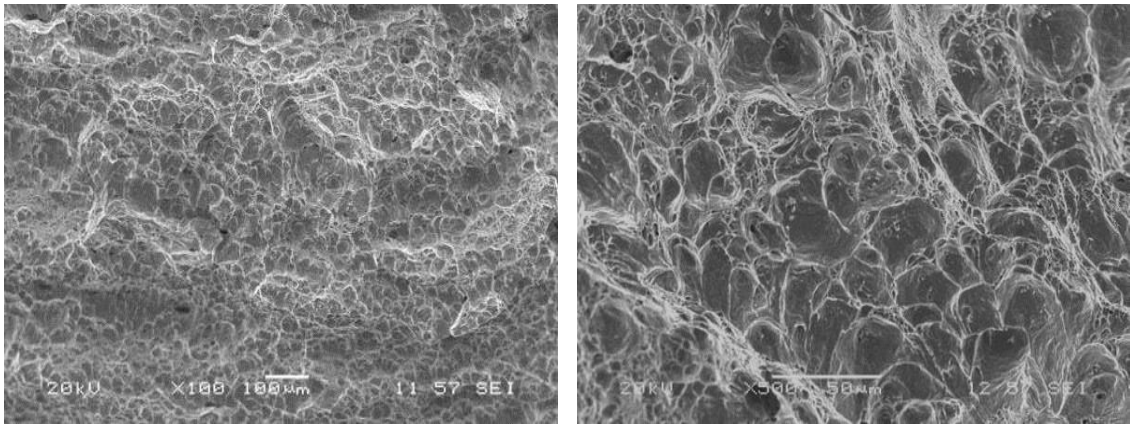


Upper shelf ductile fracture appearance

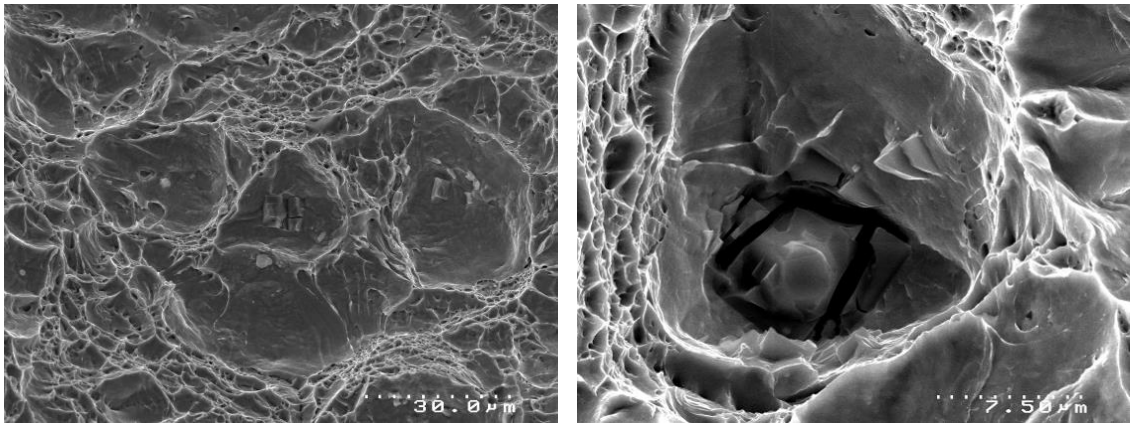


Ductile-brittle transition (DBT) region, showing example of inclusions in dimples

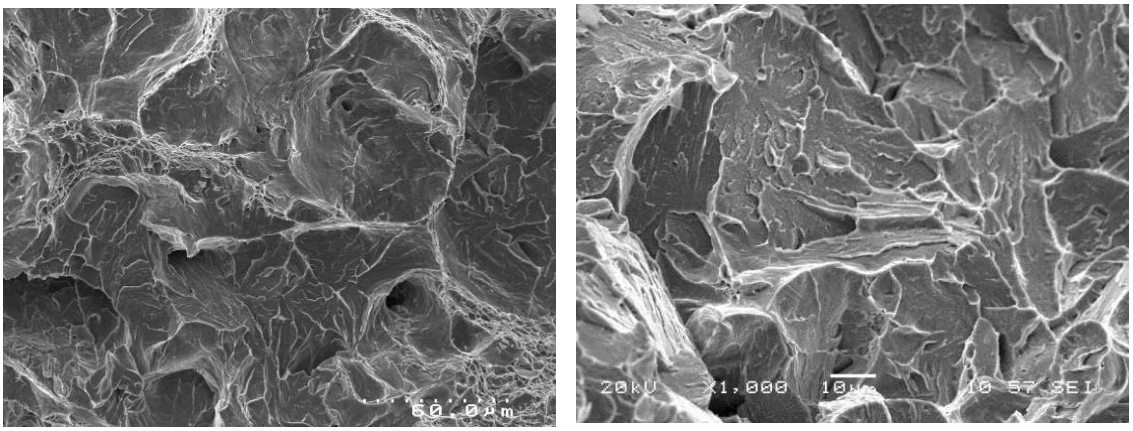


Lower shelf brittle region

**Figure 5.4** SEM images of Charpy specimen fracture surfaces at the ductile shear upper shelf region, ductile-brittle transition (DBT) region and lower-shelf brittle fracture region.

## 5.7 Surface Roughness

The average surface roughness measurements are presented in Figure 5.5. The values show that show the as-received pipe surface is the roughest with an average measurement of 4.2 µm, followed by the 120 grit finish (1.7 µm) and finally the 600 grit finish (0.1 µm). This order of roughness can be seen visually in the SEM images, presented in Figures 5.6 to 5.8.

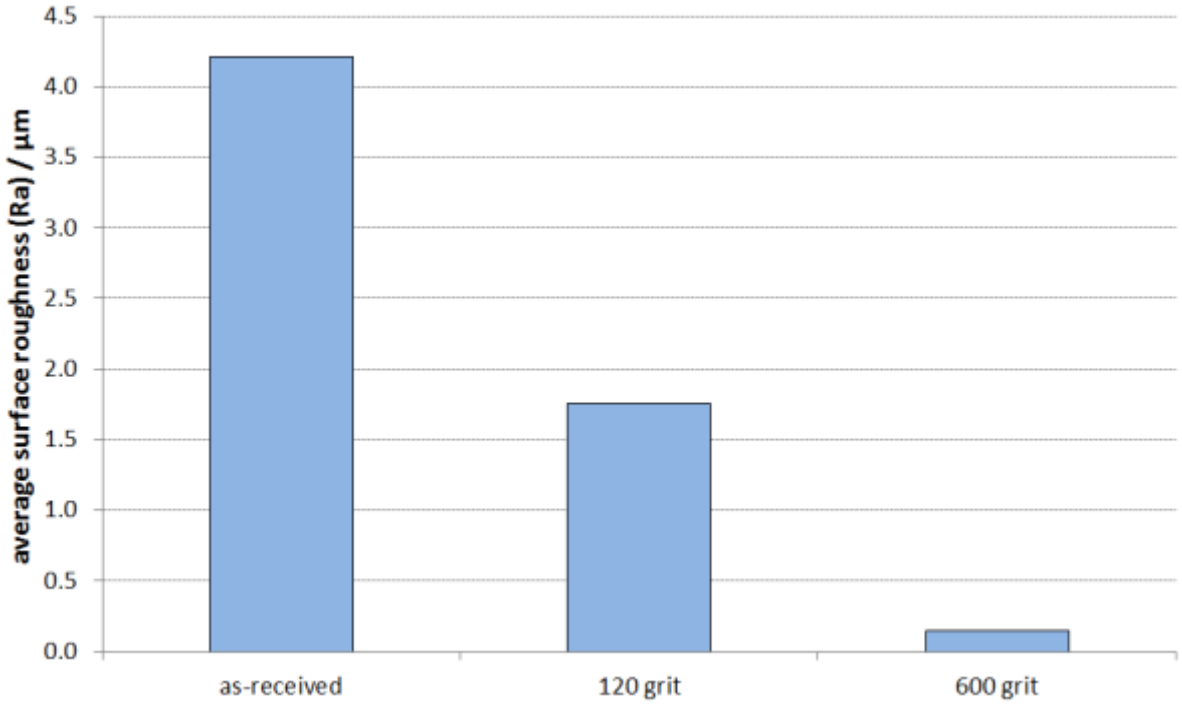


**Figure 5.5** Average surface roughness measurements

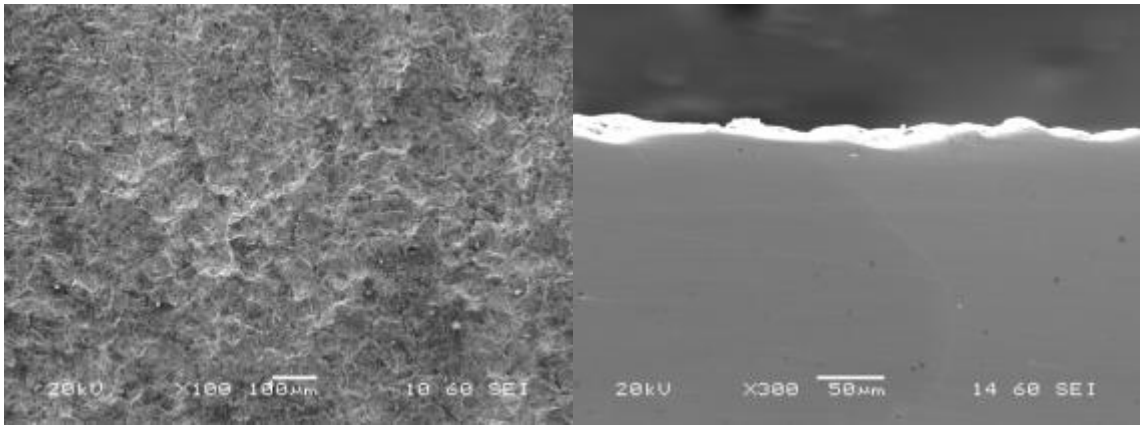


**Figure 5.6** SEM image of as-received surface: plan view (left) cross-section (right)

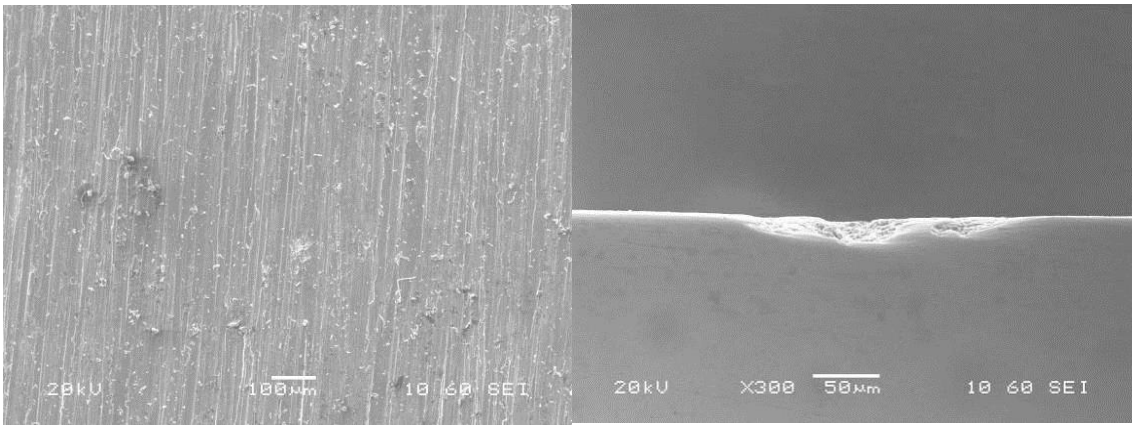


**Figure 5.7** SEM image of 120 grit surface: plan view (left) cross-section (right)

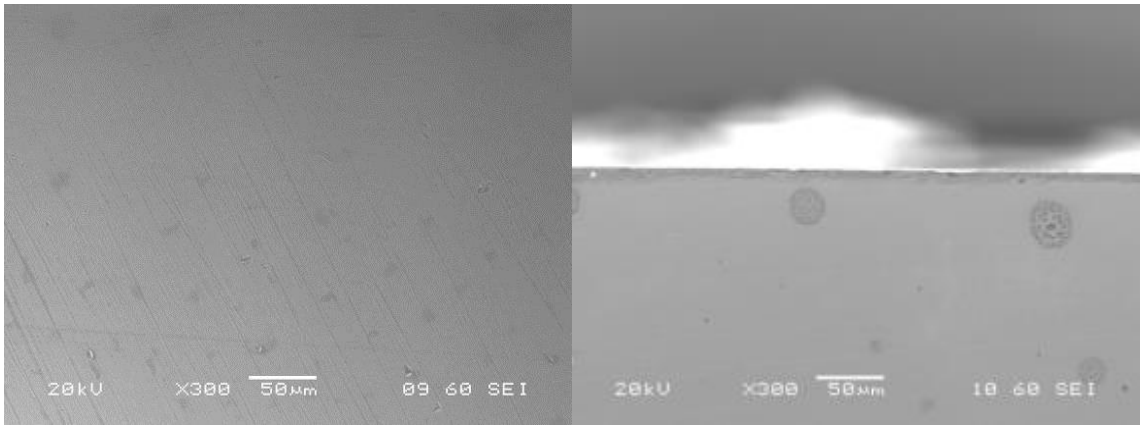


**Figure 5.8** SEM image of a 600 grit surface: plan view (left) cross-section (right)

## 5.8 Micro-hardness

The through thickness micro-hardness measurements are shown in Figure 5.9. The results reveal very little deviation in hardness as a function of through-thickness. The overall hardness of the parent metal was measured as 301 ± 6 $Hv_{0.200}$ (30 HRc) giving a standard deviation of approximately ± 2% throughout the material.

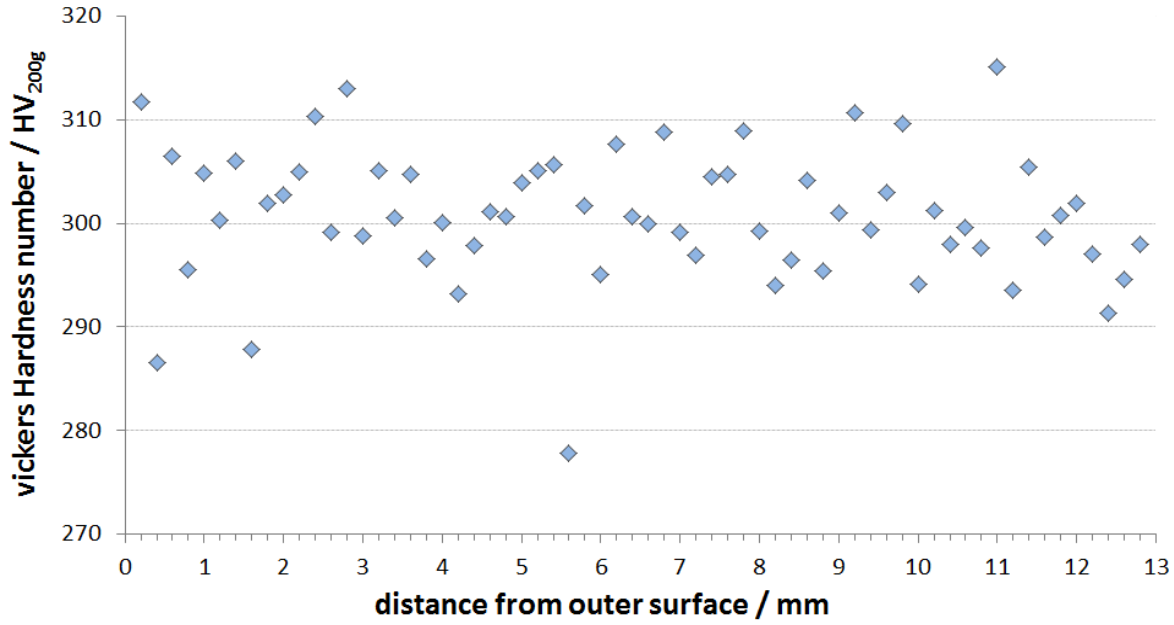


**Figure 5.9** Through-thickness hardness measurements of parent material using a 200 gf load.

# CHAPTER 6: RESULTS & DISCUSSION SSC Testing

## 6.1 Seabed Temperature SSC Investigation

### 6.1.1 Definition of Cracking Zones

ON the 4-point bend specimens tested in this study, cracking was evident in various regions in relation to the rollers and the edges. It is recognised that stress concentrations can exist close to the cut edges and there may be an Influence of the centre rollers on stress distribution. Consequently the crack locations in the following sections (i.e. chamfered edge, central region, inner rollers) were classified using the zones shown on Figure 6.1.

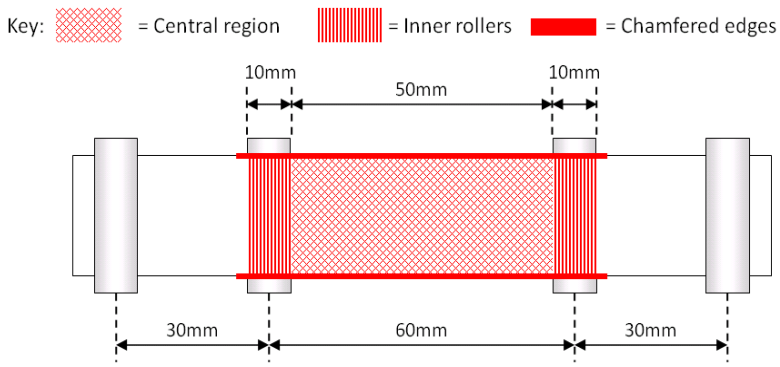


**Figure 6.1** Classification of crack location zones on the surface of the 4-point bend specimens.

### 6.1.2 Produced Water SSC Tests

The results of the produced water tests exposed to 69 mbar $H_2S$ environment are presented in Table 6.1 and a graphical representation of the crack locations are shown in Figure 6.5. At the 24°C test temperature on the as-received surface a single crack was evident on one of the specimens (P1), as shown in Figure 6.2. Since this was an isolated crack at the edge of the 4-point bend specimen's tensile surface it was considered to be an anomalous result and consequently the as-received surface was consider to exhibit acceptable SSC resistance in the test environment.

No cracks were evident on the duplicate specimens tested at 5°C with the as-received surface.

In contrast, cracks were observed on all of the fully-machined specimens and were located on the chamfered edges, in the central region between the rollers as well as above the inner loading rollers. Examples of cracking on the tensile face of the fully-machined specimens are shown in Figures 6.3 & 6.4.


**Figure 6.2** Single edge crack on as-received specimen P1 (PW, 69 mbar $H_2S$, 24°C)

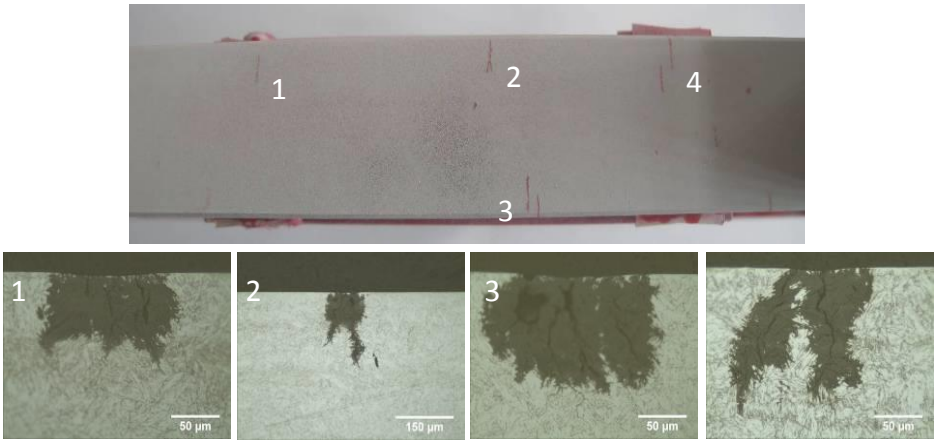


**Figure 6.3** Cracking on the fully-machined sample tested at 24°C in produced water and 69 mbar $H_2S$.

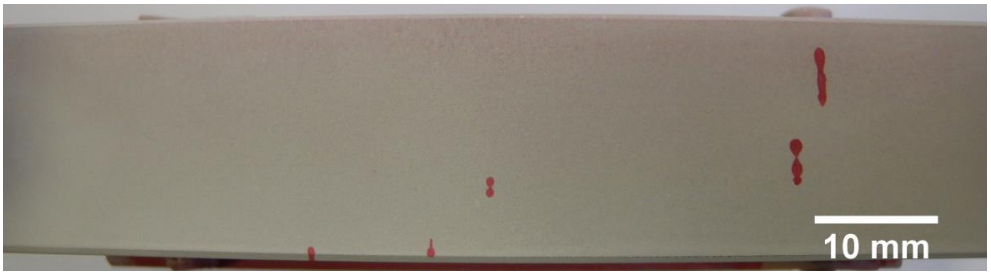


**Figure 6.4** Cracking on the fully-machined specimen P8 (PW, 69 mbara $H_2S$, 5°C)

It was noted that the largest cracks were located directly above the inner loading rollers, which indicated a higher susceptibility to SSC, probably as a result of peak stresses in the region.

**Table 6.1** SSC test results in the Produced Water environment with 69 mbara $H_2S$ (100,000 mg/L Cl, pH 4.5)

| pH | Test temp. (ºC) | Specimen reference | Surface finish | Total No. of cracks | Max. crack length (µm) | Max. crack depth (µm) | Cracking & locations | | |
|---|---|---|---|---|---|---|---|---|---|
| | | | | | | | edge | middle | rollers |
| 4.5 | 24 | P1 | As-received | 1 | 1017 | 207 | Y | N | N |
| | | P2 | As-received | 0 | 0 | 0 | N | N | N |
| | | P3 | Fully machined | 2 | 4003 | 228 | N | N | Y |
| | | P4 | Fully machined | 8 | 3408 | 860 | Y | Y | Y |
| | 5 | P5 | As-received | 0 | 0 | 0 | N | N | N |
| | | P6 | As-received | 0 | 0 | 0 | N | N | N |
| | | P7 | Fully machined | 18 | 1838 | 3000 | Y | Y | Y |
| | | P8 | Fully machined | 5 | 4188 | 844 | Y | Y | Y |

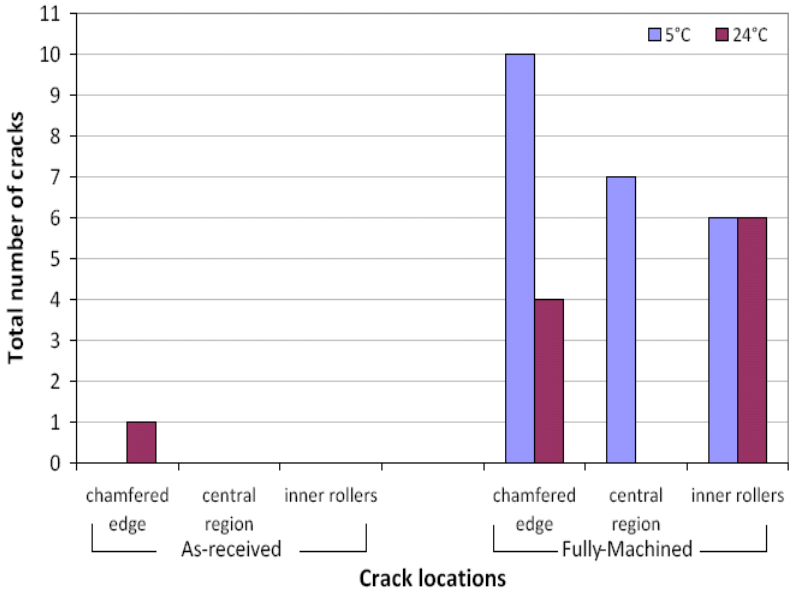


**Figure 6.5** Graphical representation of the crack frequency and locations on the specimens tested in the 69 mbara $H_2S$ environment.

It should also be noted that the cracks initiated at the site of corrosion pits (see Figure 6.3). The cracking extended away from the pits and followed a predominately intergranular path through the material, with occasional deviations along the martensitic lath boundaries.

The results for the tests conducted with the lower 35 mbara $H_2S$ partial pressure are presented in Table 6.2 and the crack frequency and locations are shown in Figure 6.6. It can be seen from Table 6.2 and Figure 6.6 that the 35 mbara $H_2S$ results, at 5°C only, also showed a higher SSC susceptibility in the fully-machined specimens, compared to the as-received specimens, which was similar to the observations at the higher 69 mbara $H_2S$ partial pressure (See Table 6.1).

**Table 6.2** SSC test results in the Produced Water environment with 35 mbara $H_2S$ (100,000 mg/L Cl, pH 4.5)

| pH | Test Temp. (°C) | Specimen reference | Surface finish | Total No. of cracks | Max. crack length (µm) | Max crack depth (µm) | Cracking & locations | | |
|---|---|---|---|---|---|---|---|---|---|
| | | | | | | | edge | middle | rollers |
| 4.5 | 24 | P9 | As-received* | 2 | 890 | 923 | Y | N | N |
| | | P10 | As-received* | 4 | 1000 | 1474 | Y | N | N |
| | | P11 | As-received | 0 | 0 | 0 | N | N | N |
| | | P12 | Fully-machined* | 0 | 0 | 0 | N | N | N |
| | | P13 | Fully-machined* | 0 | 0 | 0 | N | N | N |
| | 5 | P14 | As-received | 37 | 500 | 1175 | Y | N | N |
| | | P15 | As-received | 3 | 500 | 525 | Y | N | N |
| | | P16 | Fully-machined | 60 | 1500 | 160 | Y | Y | Y |
| | | P17 | Fully-machined | 79 | 1400 | 44 | Y | Y | Y |

*Note: all specimens were prepared with 45° edge chamfers except P9, P10, P12 & P13 where the edges were left 'as-machined'.

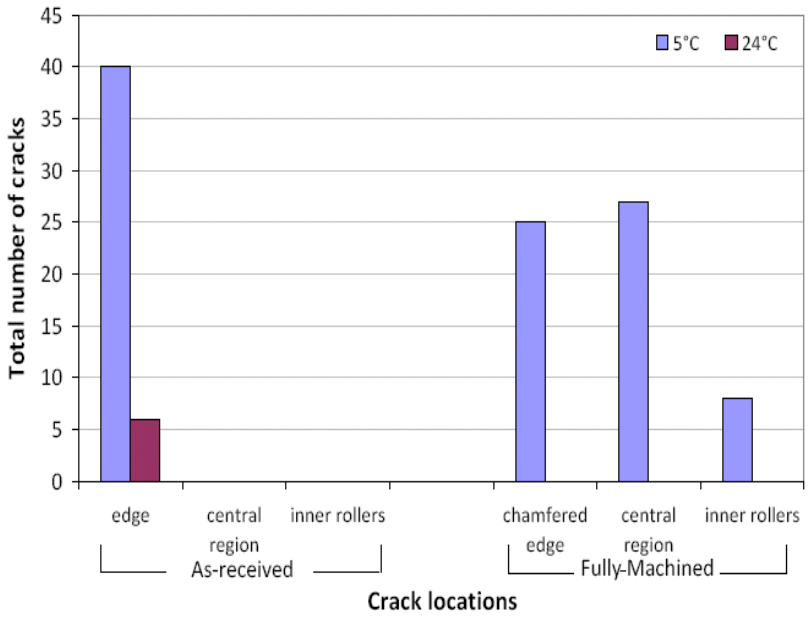


**Figure 6.6** Graphical representation of the crack frequency and locations on the specimens tested in the 35 mbara $H_2S$ environment.

The results clearly show that 5°C is a more severe environment than 24°C, since there was no cracking on the fully-machined specimens tested at 24°C, whereas both fully-machined specimens cracked at 5°C. As with the 69 mbar $H_2S$ tests, the as-received specimens only cracked along the longitudinal edges (Figure 6.7). Even though chamfering the edges appears to promote SSC, two as-received specimens (P9 & P10) tested at 35 mbar $H_2S$ and 24°C without chamfers, cracked along the edges, whereas specimen P11 (with chamfers) did not crack.

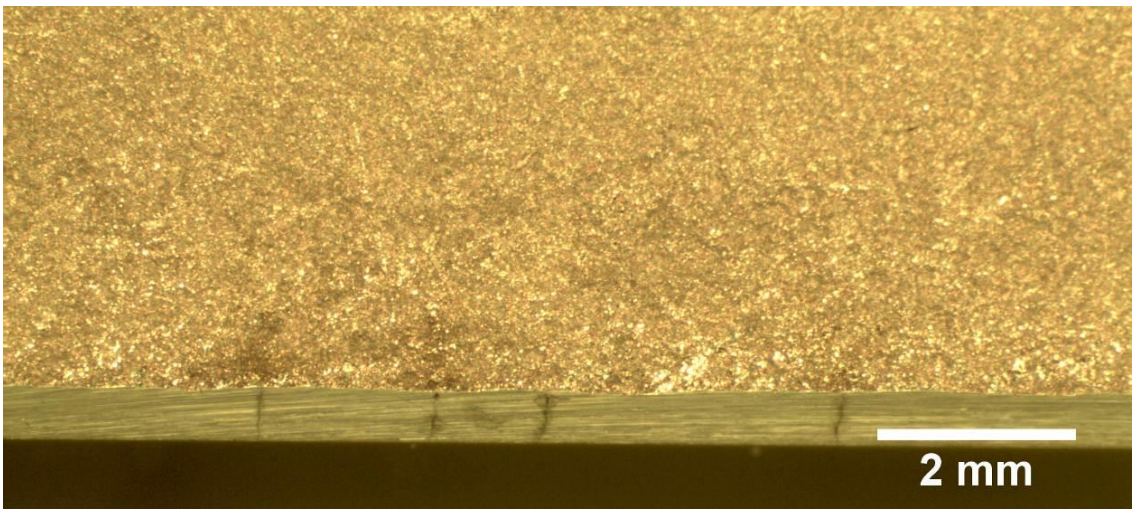


**Figure 6.7** Cracking on chamfered edge of as-received specimen P14 (PW, 35 mbara $H_2S$, 5°C).

### 6.1.3 Condensed Water SSC Tests

The results from the condensed water tests conducted at a pH of 3.5 in the 1,000 mg/L Cl solution with 69 mbara $H_2S$ are presented in Table 6.3. It can be seen from the results that none of the specimens cracked in this low chloride ion content test environment.

**Table 6.3** SSC test results in the Condensed Water environment with 69 mbara $H_2S$ (1,000 mg/L Cl, pH 3.5)

| pH | Test temp. (ºC) | Specimen reference | Surface finish | Total No. of cracks | Max. crack length (µm) | Max. crack depth (µm) | Cracking & locations | | |
|---|---|---|---|---|---|---|---|---|---|
| | | | | | | | edge | middle | rollers |
| 3.5 | 24 | C1 | As-received | 0 | 0 | 0 | N | N | N |
| | | C3 | Fully machined | 0 | 0 | 0 | N | N | N |
| | | C4 | Fully machined | 0 | 0 | 0 | N | N | N |
| | 5 | C5 | As-received | 0 | 0 | 0 | N | N | N |
| | | C6 | As-received | 0 | 0 | 0 | N | N | N |
| | | C7 | Fully machined | 0 | 0 | 0 | N | N | N |
| | | C8 | Fully machined | 0 | 0 | 0 | N | N | N |

## 6.2 Discussion

The results show that 5°C was a more severe test environment than 24°C in the high chloride ion content produced water environment. This could be attributed to an increase in the $H_2S$ solubility at lower temperatures or an increase in material susceptibility at lower temperatures. Certainly, flexural and tensile properties are not influenced by such temperature changes and the ductile to brittle transition temperature (DBTT) is well below 5°C, so this is an area for further investigation.

The results clearly show that the high chloride ion content produced water condition was a more severe test environment than the lower chloride, lower pH condensed water condition. This is in good agreement with the work done by Enerhaug et al. [45] and can be attributed to the instability of the passive film rendering the material more susceptible to pitting and subsequent cracking in the high chloride ion content environment.

Whilst the as-received surface finish provides enhanced SSC resistance, compared to the fully-machined surface, the nature of the four-point bend test means that there will always be machined surfaces exposed to the test environment. This is a limitation of the test method, which is highlighted by the cracking observed on the machined chamfered edges of the as-received specimens, whereas there was no cracking evident on the test face. Even though chamfering removes the beneficial as-received surface, it has been shown that edges left ‘as-machined’, without chamfering, were even more susceptible to SSC, due to the Influence of the stress concentration on the initiation of SSC.

One option to prevent the Influence of cut faces would be to coat the cut faces, however care would need to be taken to avoid introducing crevices. A bees-wax coating was successfully applied by Enerhaug et al. [45] to overcome the problem of SSC on the side faces of transverse weld 4PB specimens. A second option is to conduct full ring testing generally to the requirements of OTI 95 635 [86].

This full ring test method has several benefits over small scale tests, namely:

i) The as-manufactured surfaces are maintained intact so that potential anomalous laboratory test results due to surface preparation, stress concentrations and cut edges can be eliminated.

ii) All of the residual stresses from pipe manufacture and welding can be retained so that the applied stresses can be reduced, typically to 72% SMYS. This avoids problems with overstressing, which occur with small scale tests stressed to 100% AYS.

iii) A relatively large stressed area can be exposed to the test environment.

It was considered that the use of bees-wax coating on the side faces of FPB specimens or the adoption of a full ring test method would be beneficial in achieving a closer correlation between results from laboratory tests and service conditions.

In the current work, the largest cracks were observed on the tensile surface near the inner loading rollers. This is likely to be caused by the fact that specimens are plastically loaded to 100% AYS with a 'hinge' effect occurring at the rollers, thus concentrating strain in this area. Since this work was completed further discussions in NACE TG494 have established that the flexural bend approach to determine the strain to apply to FPB specimens is too severe and consequently it would be of interest in future work to repeat the tests using the strain determined from uni-axial tensile tests. The material characterisation tests on the material, reported in section 5.5, showed that the strain from the flexural bend method was 25% higher than for the tensile test method (see Table 5.5). Therefore the specimens would have been stressed well into the plastic region which would explain the reason for the hinging effect at the rollers and the observed concentration of cracks above the rollers. This high stress state, particularly highlights the beneficial effect of leaving the as-manufactured surface intact, since it demonstrates that the intact surface can withstand a high stress combined with the severe test environment with 100,000 mg/L $Cl^-$, a pH of 4.5 and a 69 mbara $H_2S$ partial pressure.

# CHAPTER 7: RESULTS & DISCUSSION
# Electrochemical Testing

## 7.1 Trial Tests – Coupon Masking Evaluation

An initial scoping study was performed in order to select the optimal masking Compound for use in the subsequent electrochemical characterisation testing. The candidate coupon masking systems were evaluated via post-test surface evaluation and via open circuit corrosion potential measurements during a 10,000 s exposure in the simulated produced water environment.

### 7.1.1 Coating Evaluation – Coupon Masking Evaluation

As-received specimens with the 5 different masking systems (see Table 7.1) were exposed to the produced water environment saturated with 35 mbara $H_2S$. The samples were visually examined and the results are provided in Table 7.2.

**Table 7.1** Details of masking compounds used for trial tests

| Specimen number | Masking compound system | Manufacturer |
|---|---|---|
| 1 | G371 Lacomit varnish | Agar |
| 2 | Number 45 varnish | McDermid |
| 3 | Brushable Ceramic Epoxy | Devcon |
| 4 | 1 over 2 | -- |
| 5 | 'University' blue lacquer | Not known |

**Table 7.2** Summary of masking compound performance

| Specimen number | Masking compound system | Performance |
|---|---|---|
| 1 | G371 Lacomit varnish | A crack was present on the back face although it did not extend through to the specimen surface. |
| 2 | Number 45 varnish | No cracking was evident. However fine pitting was evident in the coating which appeared to extend through the coating to the specimen surface. |
| 3 | Brushable Ceramic Epoxy | Some colour degradation was apparent and cracks were found at the corners, which was probably related to the inadequate chamfering of the corners. |
| 4 | 1 over 2 | A crack was evident around the O-ring seal which was believed to have occurred when the specimen was removed from the test cell. |
| 5 | University blue lacquer | Numerous cracks were evident on this coating. |

### 7.1.2 Corrosion Potential Measurements – Coupon Masking Evaluation

The results from the corrosion potential ($E_{corr}$) measurements produced during the coupon masking evaluation are presented in Figure 7.1

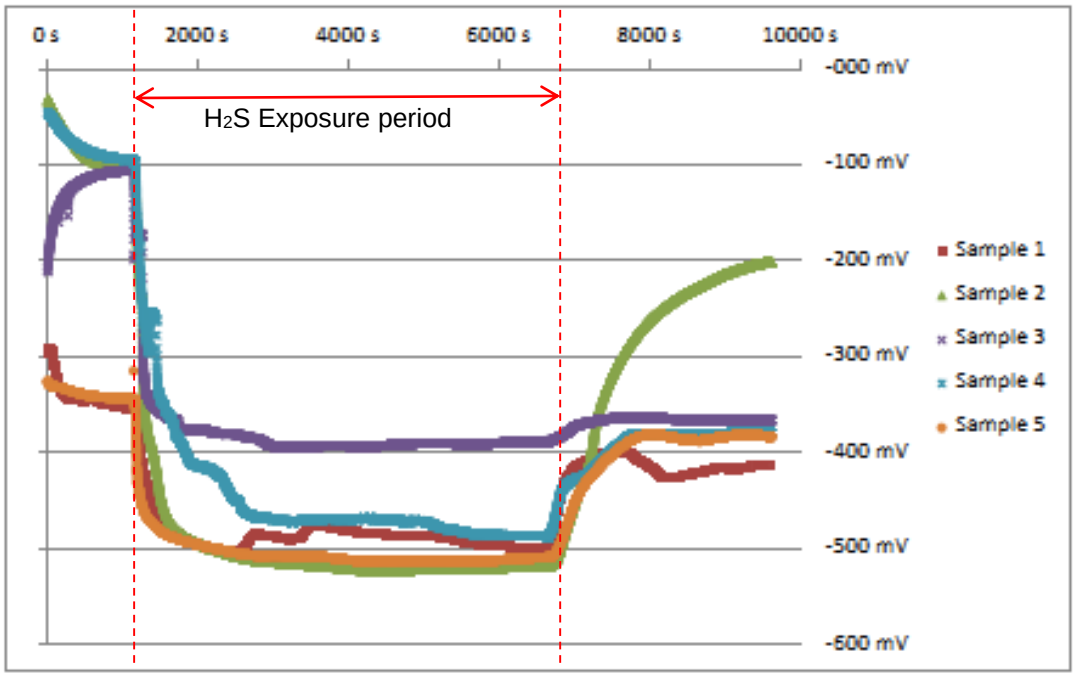


**Figure 7.1** Corrosion potential measurements for the **as-received** material coated with the 5 masking compounds, detailed in Table 7.1.
(Test Conditions: 24°C, 100,000 mg/L Cl, pH 4.5, 35 mbara $H_2S$, $N_2$ purge).

It can be seen from Figure 7.1 that the corrosion potential of the 5 specimens showed significant variations during the test. After the initial nitrogen purge three specimens (2, 3 & 4), converged on a potential of approximately -100 mV, whereas two of the specimens fell to a potential of -350 mV, indicating a difference in the surface characteristics, which could be related to contamination from the masking compounds or from variations in the initial cleaning and de-greasing. Once the $H_2S$ was introduced into the solution the potential of all of the specimens fell rapidly, with four of the five specimens converging on a potential of -500 mV ± 25 mV, whereas the one specimen (No.3) with the epoxy coating stabilised at a potential of approximately -400 mV. This coating was found to be cracked at the corners following the test which could offer an explanation on the variation in the potential. Once the nitrogen was re-introduced after the $H_2S$ exposure period the potential of all of the specimens increased although the rate of increase was variable across the five specimens.

Based on the scoping tests it was established that brushable ceramic epoxy coating (No.3) had cracked as a result of the absence of adequate chamfers on the cut edges, resulting in excessive stress concentrations. Therefore the specimen preparation procedure was modified to ensure the cut edges were chamfered and the epoxy coating was selected as the preferred choice based on ease of application and resistance to the $H_2S$ environment.

## 7.2 Electrochemical Tests

Anodic potentiodynamic scans and open circuit corrosion potential measurements were performed to characterise the electrochemical behaviour of weldable martensitic 13%Cr stainless steel (WMSS) as a function of temperature (i.e. 5°C versus 24°C) and surface condition (i.e., as-received pipe surface condition versus an 600 grit abraded finish) in a simulated produced water (PW) environment. A chloride concentration of 100,000 mg/L and a pH of 4.5 were used to provide the most severe test conditions.

### 7.2.1 Corrosion Potential (Ecorr) Measurements

The plots of corrosion potential ($E_{corr}$) versus time[7] are presented in Figures 7.2 – 7.11 and a summary of the corrosion potential results for all of the tests is shown in Table 7.3. It can be seen from the results that the corrosion potential values for the as-received (AR) specimens were consistently more positive than the specimens with the 600 SiC ground finish. This observation indicates that the passive film is more strongly developed on the as-received surface compared to the ground 600 SiC surface. When the $H_2S$ was introduced into the test cell the potentials of the as-received samples decreased and after the 1 hour saturation period all of the potentials for the samples were within ± 27 mV of the mean value of -490 mV. The potentials for the ground samples were significantly more negative than the as-received samples at the start of the $H_2S$ purge, however after the 1 hour purge the potentials stabilised to within ± 20 mV of the mean value of -516 mV, so the average was only 26 mV from the mean as-received potential, which was not considered to be significant.

[7] Please note that the frequency of recorded data for the open circuit potentials (OCP) plots presented in Figures 7.2-7.11 was on the order of one data point every 10 minutes.

The potential values were compared between the 24°C and the 5°C tests and for the 600 SiC ground samples no significant difference was observed, with the values only ranging from -497 mV to -523 mV. For the 24°C tests the average value was -500 mV compared to an average value of -464 mV for the 5°C tests. Since the values for the AR samples were changing from a relatively high value during the $H_2S$ purge it was thought that a longer purge would be required for the values to stabilise at the lower temperature, where the reaction rates at the surface would be slower.

For the 'control' tests (see Figures 7.8 and 7.9) conducted at 24°C using $CO_2$ and $N_2$, respectively, as the purge gas as well as the test gas, the difference between the corrosion potentials or open circuit potentials (OCPs) was relatively large when compared to the results from the 600 SiC ground versus the as-received surfaces, with the difference being 469 mV for the $N_2$ test and 432 mV for the $CO_2$ tests. It is also clear that the corrosion potential (OCP) of the samples in the $CO_2$ purged solutions were less negative than in the $N_2$ purged solutions. This variation could be attributed to the change in the pH from 5.6 for the $N_2$ purged solutions to 4.5 for the $CO_2$ purged tests.

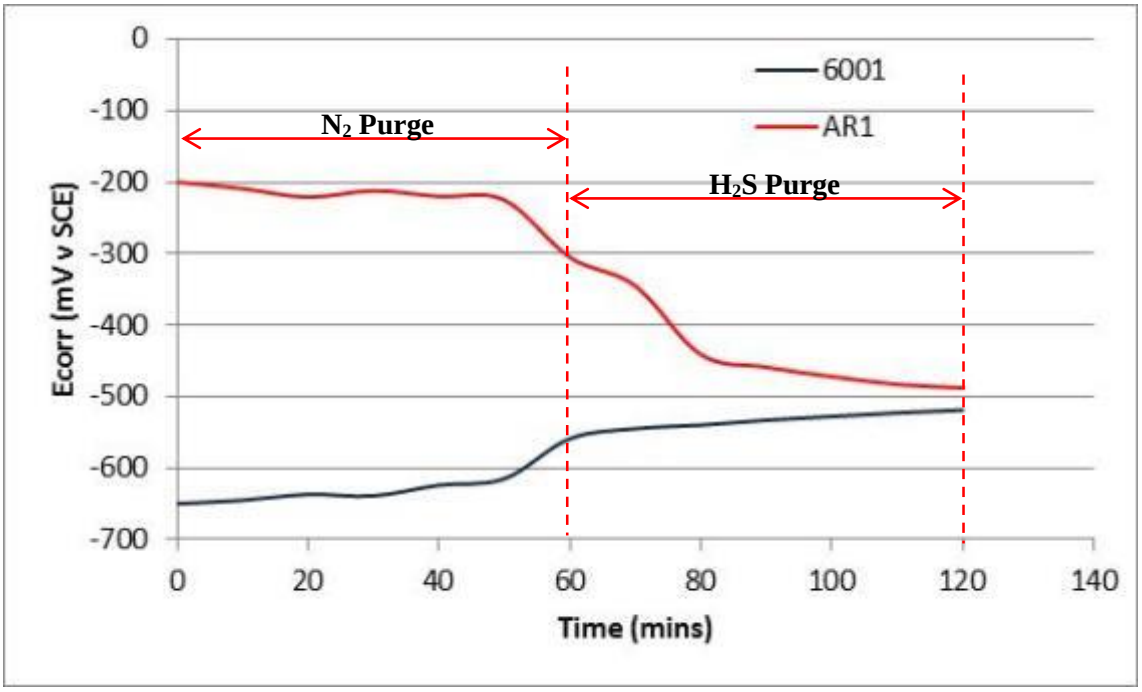


**Figure 7.2** Variation in potential with time for the as-received (AR1) and 600 SiC ground (6001) specimens. (Test conditions: 24°C, 100,000 mg/L Cl, pH 4.5, 35 mbara $H_2S$, $N_2$ purge)

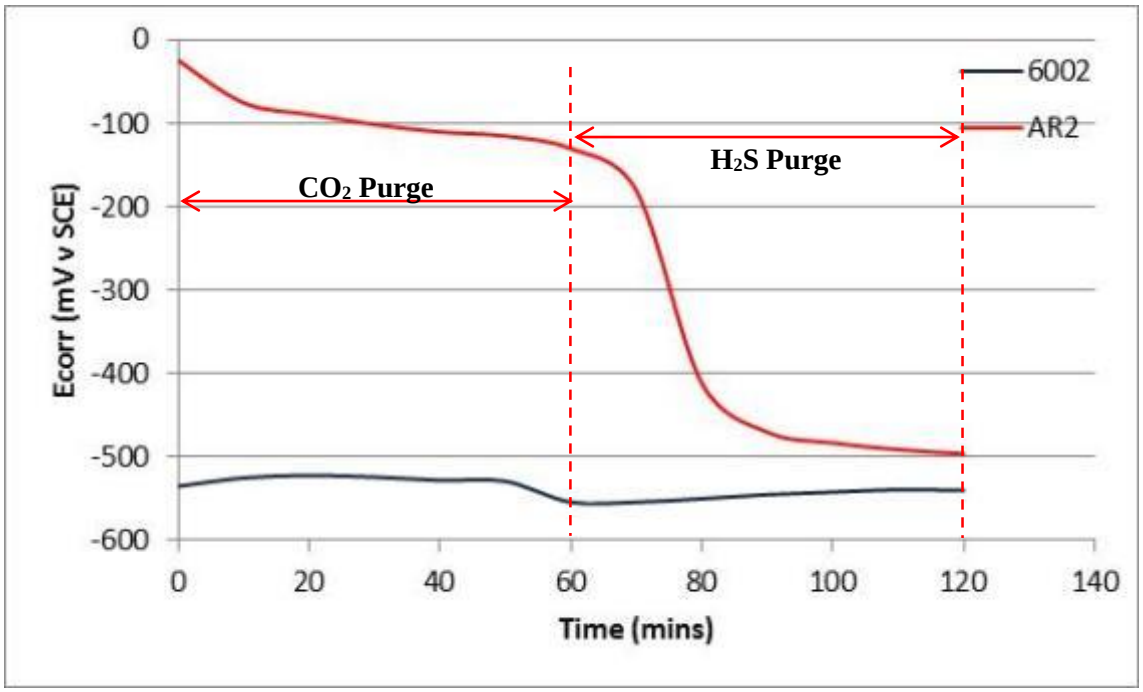


**Figure 7.3** Variation in potential with time for the as-received (AR2) and 600 SiC ground (6002) specimens. (Test conditions: 24°C, 100,000 mg/L Cl, pH 4.5, 35 mbara $H_2S$, $CO_2$ purge)

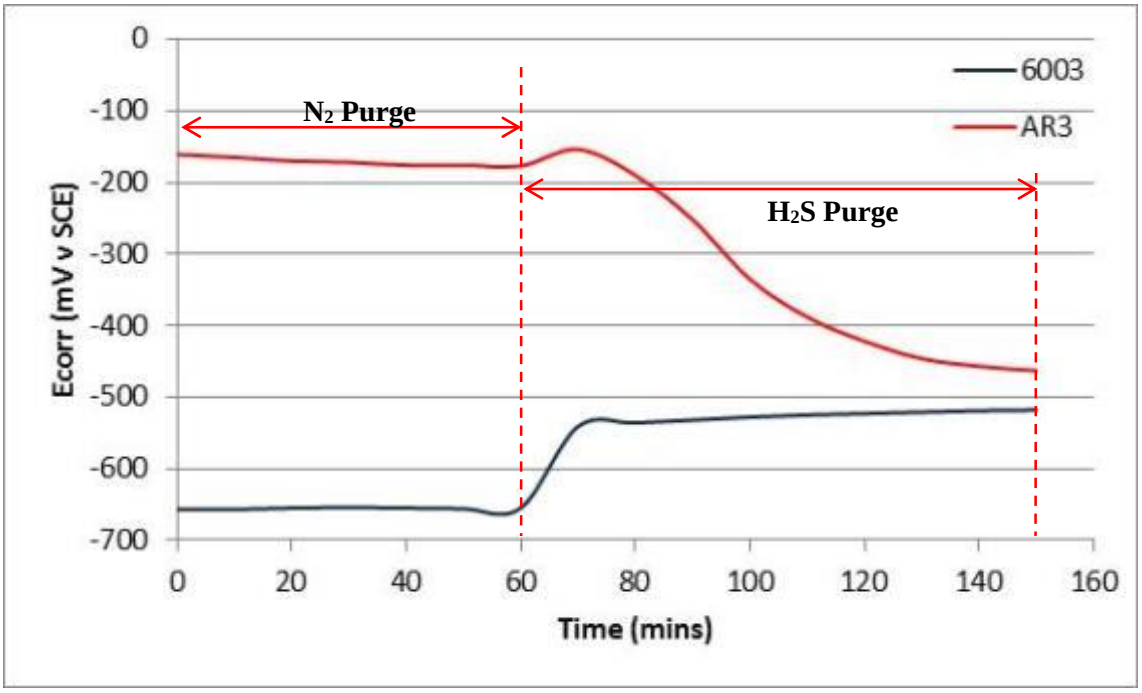


**Figure 7.4** Variation in potential with time for the as-received (AR3) and 600 SiC ground (6003) specimens. (Test conditions: 5°C, 100,000 mg/L Cl, pH 4.5, 35 mbara $H_2S$, $N_2$ purge)

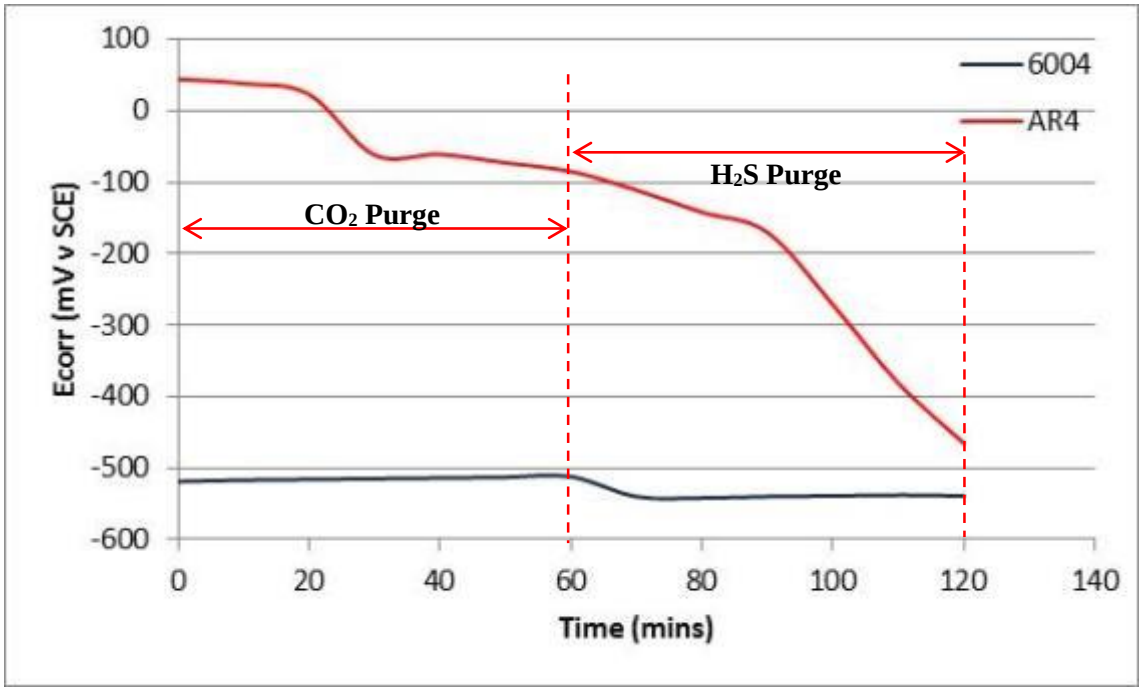


**Figure 7.5** Variation in potential with time for the as-received (AR4) and 600 SiC ground (6004) specimens. (Test conditions: 5°C, 100,000 mg/L Cl, pH 4.5, 35 mbara $H_2S$, $CO_2$ purge)

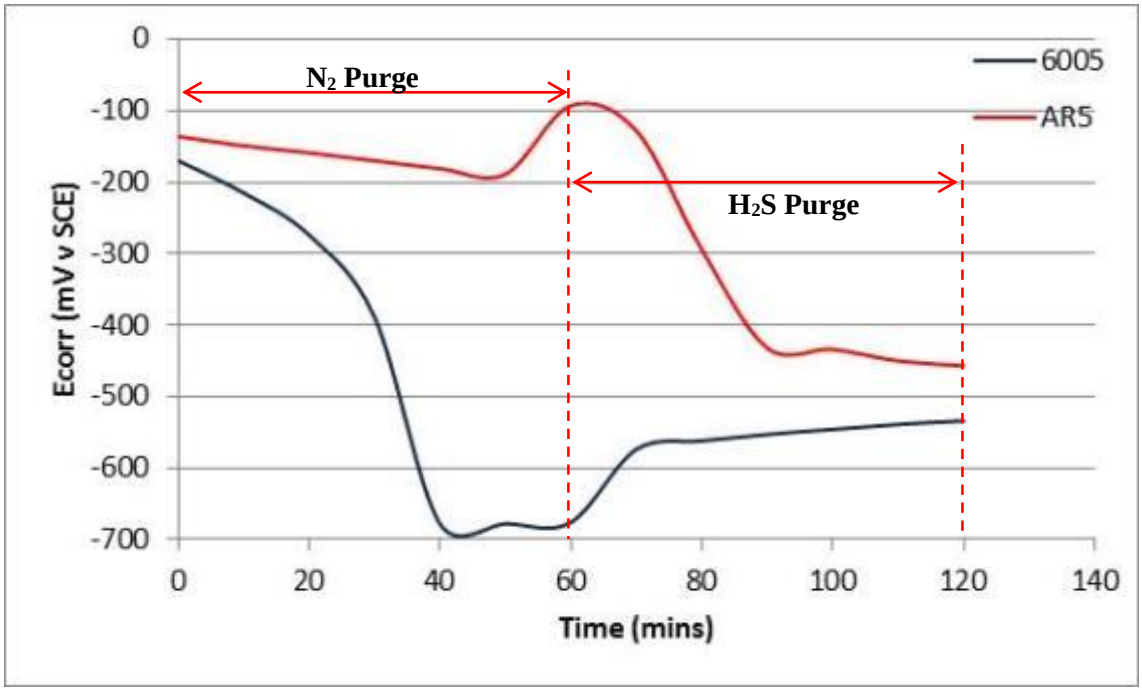


**Figure 7.6** Variation in potential with time for the as-received (AR5) and 600 SiC ground (6005) specimens. (Test conditions: 5°C, 100,000 mg/L Cl, pH 4.5, 35 mbara $H_2S$, $N_2$ purge, bees-wax coated)

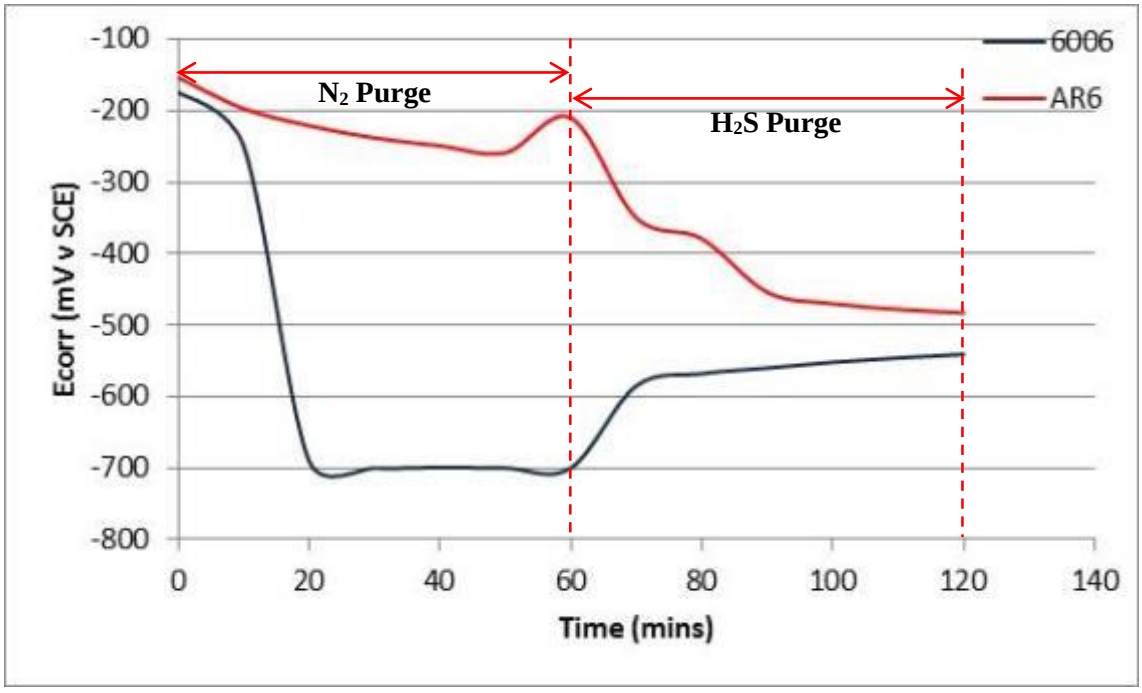


**Figure 7.7** Variation in potential with time for the as-received (AR6) and 600 SiC ground (6006) specimens. (Test conditions: 24°C, 100,000 mg/L Cl, pH 4.5, 35 mbara $H_2S$, $N_2$ purge, bees-wax coated)

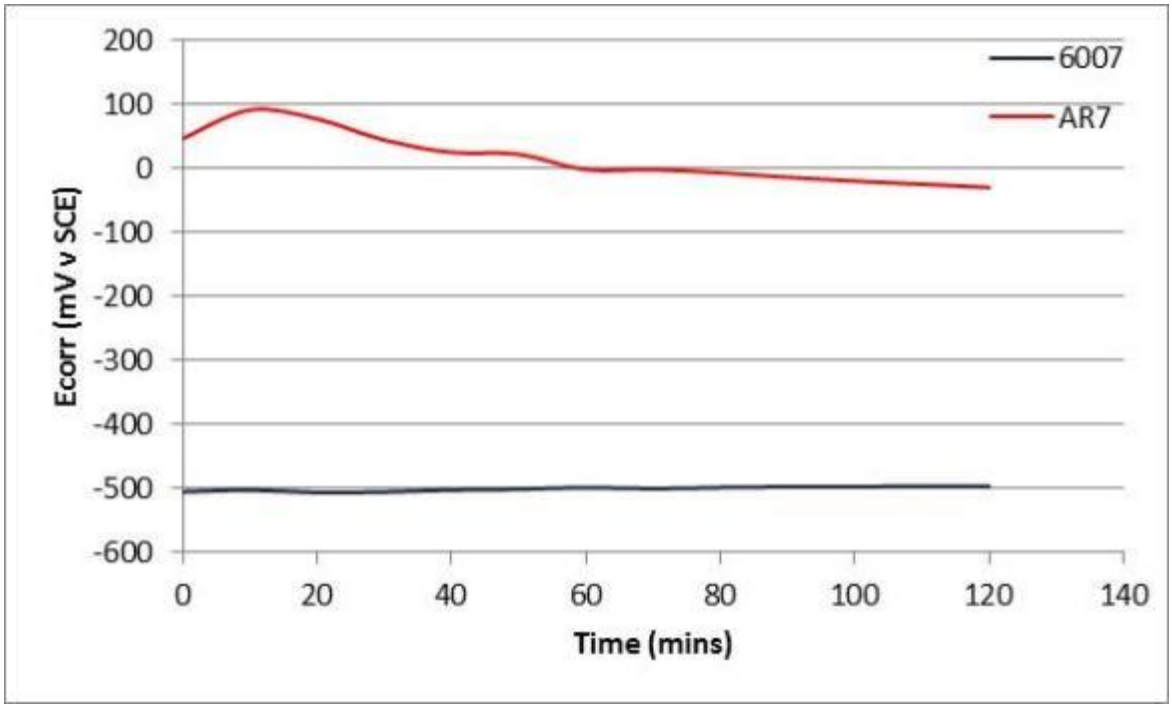


**Figure 7.8** Variation in potential with time for the as-received (AR7) and 600 SiC ground (6007) specimens. (Test conditions: 24°C, 100,000 mg/L Cl, pH 4.5, **no-$H_2S$**, $CO_2$ purge & test gas)

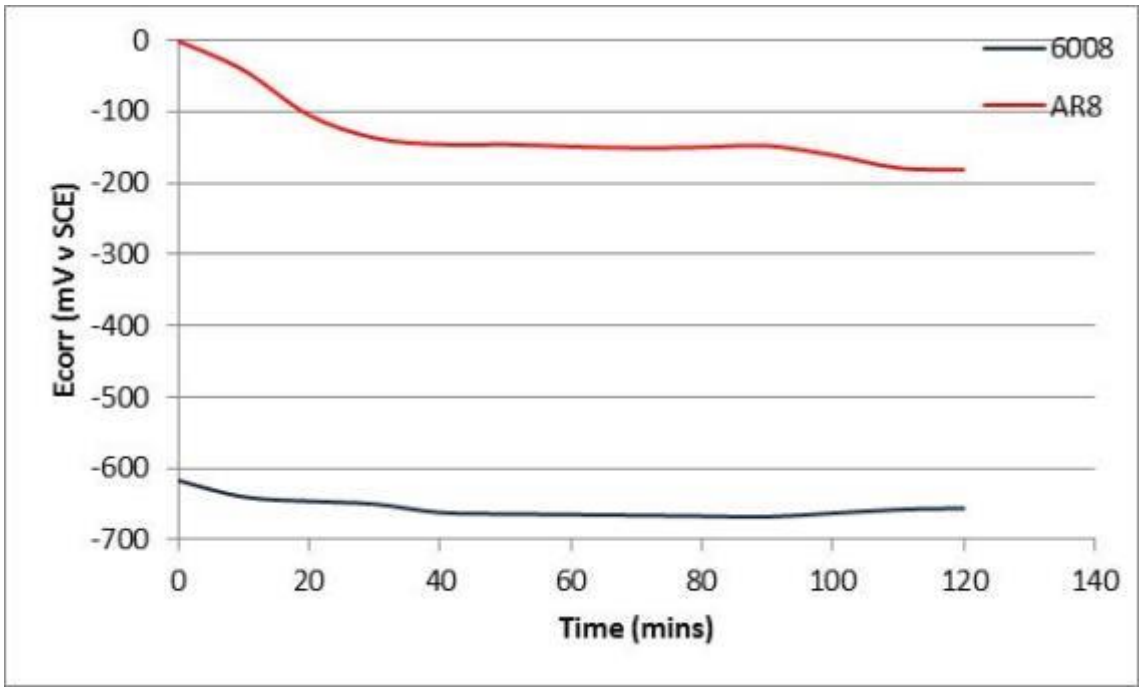


**Figure 7.9** Variation in potential with time for the as-received (AR8) and 600 SiC ground (6008) specimens. (Test conditions: 24°C, 100,000 mg/L Cl, pH 5.6, **no-$H_2S$**, $N_2$ purge & test gas)

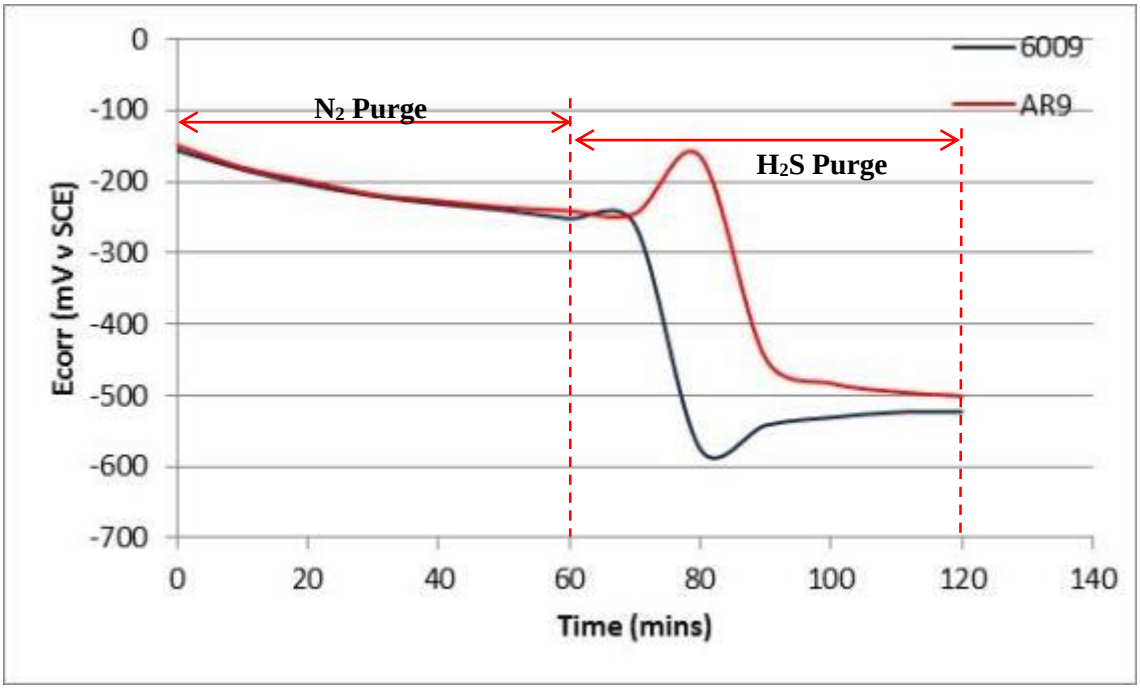


**Figure 7.10** Variation in potential with time for the as-received (AR9) and 600 SiC ground (6009) specimens. (Test conditions: 24°C, 100,000 mg/L Cl, pH 4.5, 69 mbara $H_2S$, $N_2$ purge).

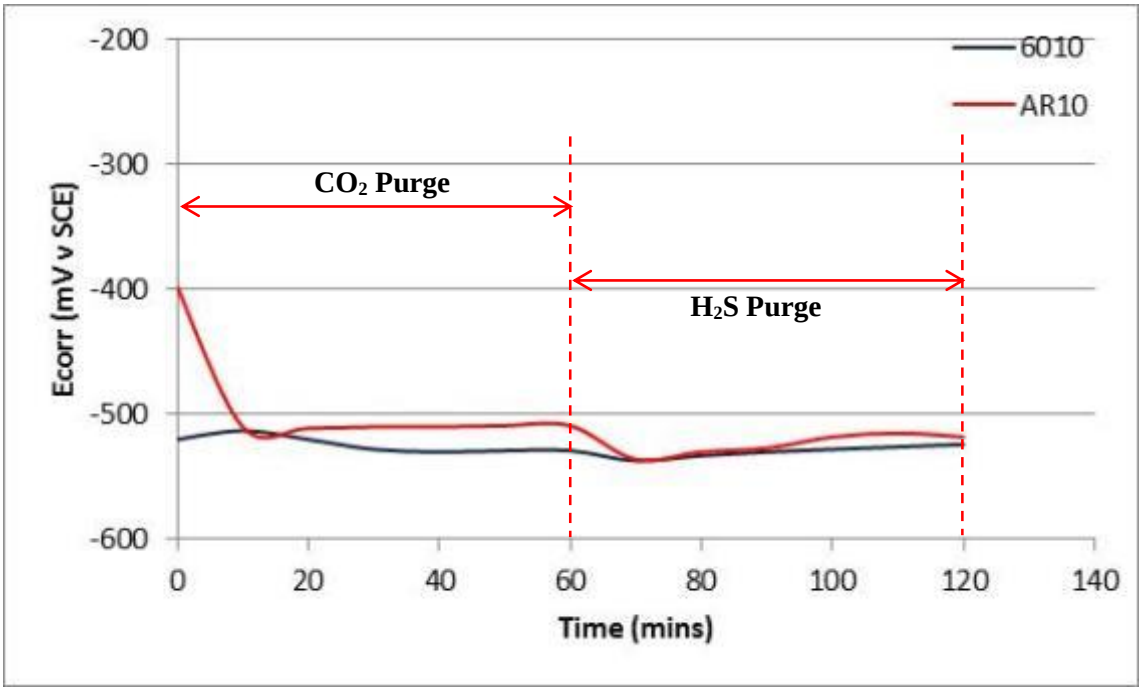


**Figure 7.11** Variation in potential with time for the as-received (AR10) and 600 SiC ground (6010) specimens. (Test conditions: 24°C, 100,000 mg/L Cl, pH 4.5, 69 mbara $H_2S$, $CO_2$ purge).

**Table 7.3** – Summary of Electrochemical Test Results

| Test | Surface condition | Masking material | Temp | Purge Gas | Test Gas | pH | Solution | Ecorr (Purge) | | | | Ecorr (scan) | Passive current density (ipass) | Breakdown potential (Ebd) | Passive film resistance |
|---|---|---|---|---|---|---|---|---|---|---|---|---|---|---|---|
| | | | | | | | | Initial purge | | Test gas purge | | | | | |
| | | | °C | | H2S-(mbara) | | $Cl^-$(mg/L) | Start (mV) | Finish (mV) | Start (mV) | Finish-1 hr (mV) | (mV v SCE) | ($\mu A/cm^2$) | (mV v SCE) | ($K\Omega$-$cm^2$) |
| | | | | | | | | | | | | | | | |
| 1 | AR | Epoxy | 24 | $N_2$ | 35 | 4.5 | 100,000 | -212 | -225 | -165 | -489 | -494 | 2.1 | -318 | 52 |
| 2 | AR | Epoxy | 24 | $CO_2$ | 35 | 4.5 | 100,000 | -23 | -115 | -123 | -497 | -498 | 2.3 | -327 | 57 |
| 3 | AR | Epoxy | 5 | $N_2$ | 35 | 4.5 | 100,000 | -3 | -176 | -60 | -464 | -463 | 1.0 | -301 | 84 |
| 4 | AR | Epoxy | 5 | $CO_2$ | 35 | 4.5 | 100,000 | 44 | -84 | -278 | -440 | -471 | 1.5 | -311 | 53 |
| 5 | AR | Beeswax | 5 | $N_2$ | 35 | 4.5 | 100,000 | -137 | -195 | -64 | -459 | -464 | 1.1 | -311 | 60 |
| 6 | AR | Beeswax | 24 | $N_2$ | 35 | 4.5 | 100,000 | -151 | -264 | -179 | -484 | -505 | 2.4 | -336 | 63 |
| | | | | | | | | | | | | | | | |
| 7 | AR | Epoxy | 24 | $CO_2$ | $CO_2$ | 4.5 | 100,000 | 56 | 0 | 0 | -31 | -59 | 0.2 | 130 | 721 |
| 8 | AR | Epoxy | 24 | $N_2$ | $N_2$ | 5.6 | 100,000 | 0 | -146 | -147 | -183 | -194 | 0.1 | 58 | 7931 |
| | | | | | | | | | | | | | | | |
| 9 | AR | Epoxy | 24 | $N_2$ | 69 | 4.5 | 100,000 | -146 | -247 | -152 | -501 | -511 | 4.4 | -315 | 18 |
| 10 | AR | Epoxy | 24 | $CO_2$ | 69 | 4.5 | 100,000 | -264 | -530 | -515 | -525 | -516 | 2.2 | -243 | 5543 |
| | | | | | | | | | | | | | | | |
| 1 | 600 SiC | Epoxy | 24 | $N_2$ | 35 | 4.5 | 100,000 | -651 | -615 | -568 | -522 | -497 | 0.6 | -278 | 784 |
| 2 | 600 SiC | Epoxy | 24 | $CO_2$ | 35 | 4.5 | 100,000 | -537 | -530 | -548 | -541 | -537 | 1.1 | -321 | 567 |
| 3 | 600 SiC | Epoxy | 5 | $N_2$ | 35 | 4.5 | 100,000 | -617 | -704 | -560 | -520 | -508 | 0.6 | -298 | 309 |
| 4 | 600 SiC | Epoxy | 5 | $CO_2$ | 35 | 4.5 | 100,000 | -522 | -514 | -534 | -541 | -532 | 1.0 | -308 | 1003 |
| 5 | 600 SiC | Beeswax | 5 | $N_2$ | 35 | 4.5 | 100,000 | -173 | -677 | -604 | -537 | -523 | 0.8 | -302 | 408 |
| 6 | 600 SiC | Beeswax | 24 | $N_2$ | 35 | 4.5 | 100,000 | -179 | -701 | -622 | -540 | -509 | 0.7 | -404 | 494 |
| | | | | | | | | | | | | | | | |
| 7 | 600 SiC | Epoxy | 24 | $CO_2$ | $CO_2$ | 4.5 | 100,000 | -507 | -502 | -498 | -497 | -491 | 1.5 | -96 | 1078 |
| 8 | 600 SiC | Epoxy | 24 | $N_2$ | $N_2$ | 5.6 | 100,000 | -617 | -666 | -666 | -658 | -663 | 0.6 | 46 | 3465 |
| | | | | | | | | | | | | | | | |
| 9 | 600 SiC | Epoxy | 24 | $N_2$ | 69 | 4.5 | 100,000 | -146 | -262 | -597 | -524 | -510 | 0.8 | -329 | 521 |
| 10 | 600 SiC | Epoxy | 24 | $CO_2$ | 69 | 4.5 | 100,000 | -530 | -510 | -524 | -518 | -519 | 1.1 | -305 | 438 |

### 7.2.2 Potentiodynamic Polarisation Tests

7.2.2.1 Influence of Temperature (24°C v 5°C)

The anodic potentiodynamic curves showing the Influence of the test temperature (i.e., 24°C v 5°C) on the electrochemical behaviour of weldable martensitic stainless steel (WMSS) specimens are presented in Figures 7.12 – 7.15 and the post-test appearance of the specimens are shown in Figures 7.16 – 7.19.

All of the tests were conducted in the 100,000 mg/L produced water (PW) environment at a pH of 4.5 with 35 mbara $H_2S$ ($CO_2$ balance) at 1 bara total pressure, with a prior $N_2$ gas purge or $CO_2$ purge gas. The material was tested in the as-received (AR) and 600 SiC ground conditions with the $N_2$ purge gas two of the four AR and 600 SiC ground specimens were tested with an epoxy coating (-E) and two with a bees-wax coating (-B).

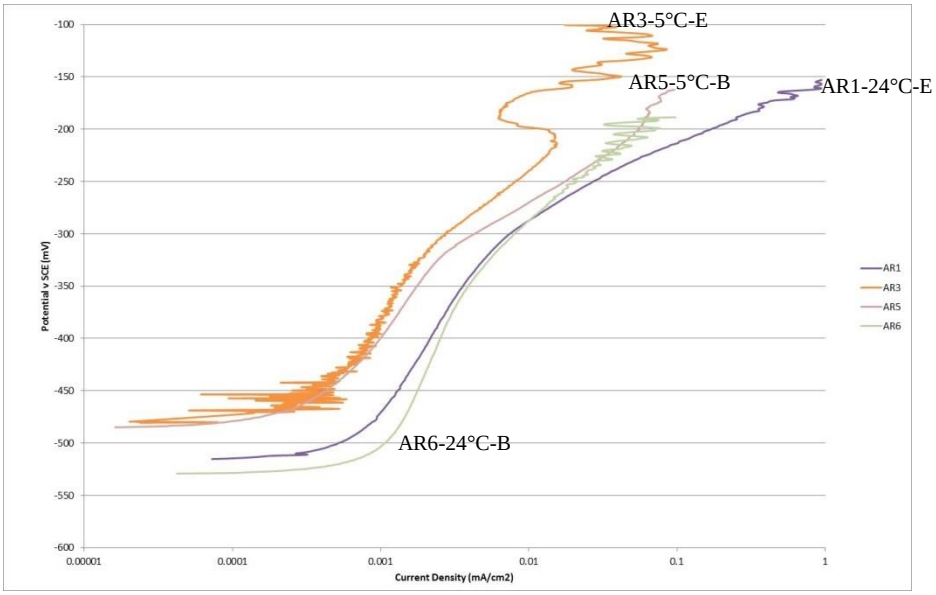


**Figure 7.12** Influence of temperature (24°C v 5°C) on the anodic potentiodynamic polarisation curves for the material in the as-received condition ($N_2$ purge).
(Test conditions: 24°C & 5°C, 100,000 mg/L Cl, pH 4.5, 35 mbara $H_2S$, $N_2$ purge).

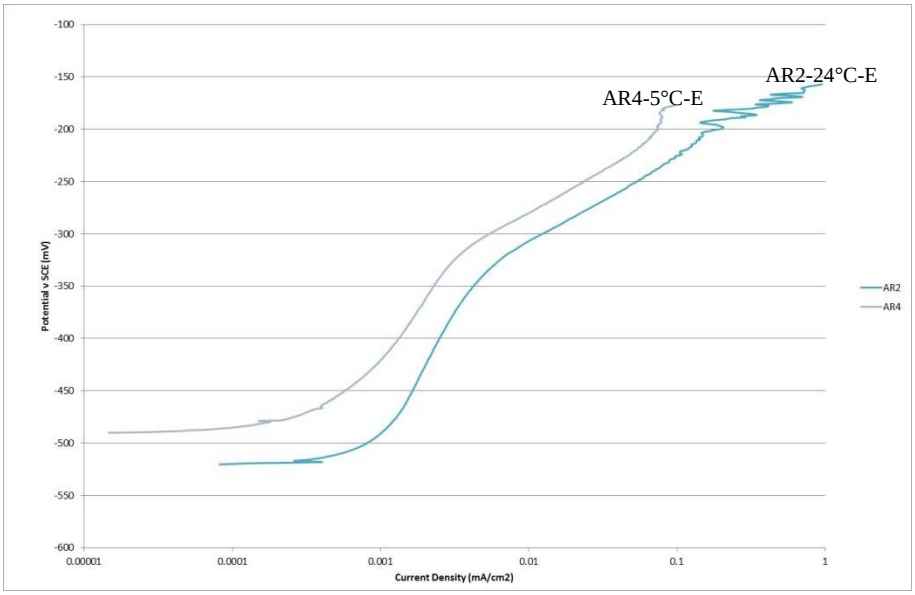


**Figure 7.13** Influence of temperature (24°C v 5°C) on the anodic potentiodynamic polarisation curves for the material in the as-received condition ($CO_2$ purge).
(Test conditions: 24°C & 5°C, 100,000 mg/L Cl, pH 4.5, 35 mbara $H_2S$, $CO_2$ purge).

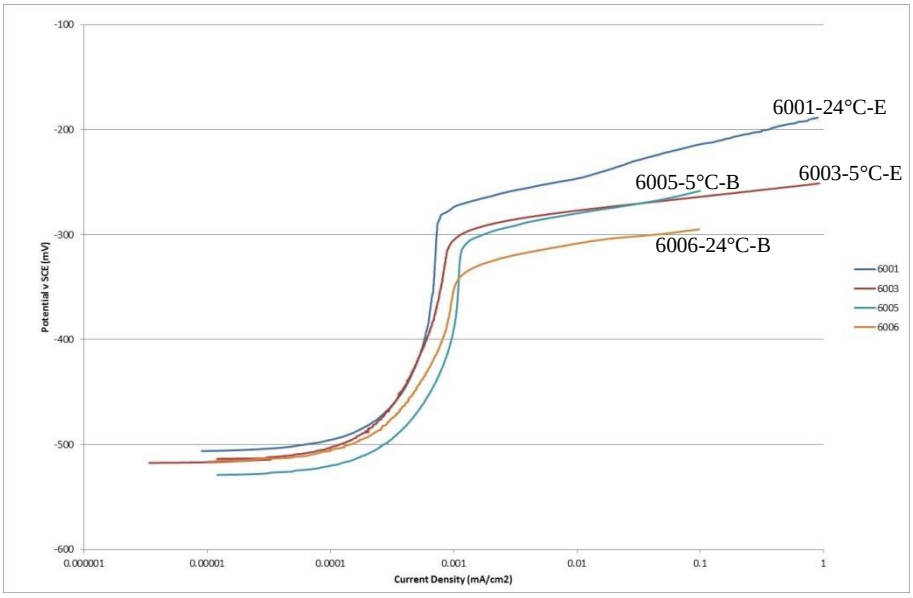


**Figure 7.14** Influence of temperature 24°C v 5°C on the anodic potentiodynamic polarisation curves for the material in the 600 SiC ground condition ($N_2$ purge).
(Test conditions: 24°C & 5°C, 100,000 mg/L Cl, pH 4.5, 35 mbara $H_2S$, $N_2$ purge).

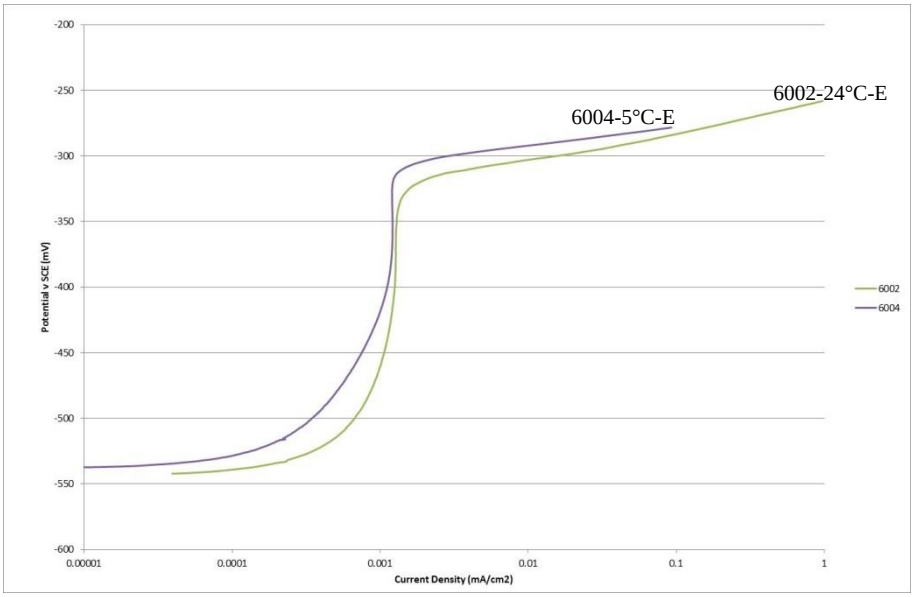


**Figure 7.15** Influence of temperature (24°C v 5°C) on the anodic potentiodynamic polarisation curves for the material in the 600 SiC ground condition ($CO_2$ purge).
(Test conditions: 24°C & 5°C, 100,000 mg/L Cl, pH 4.5, 35 mbara $H_2S$, $CO_2$ purge).

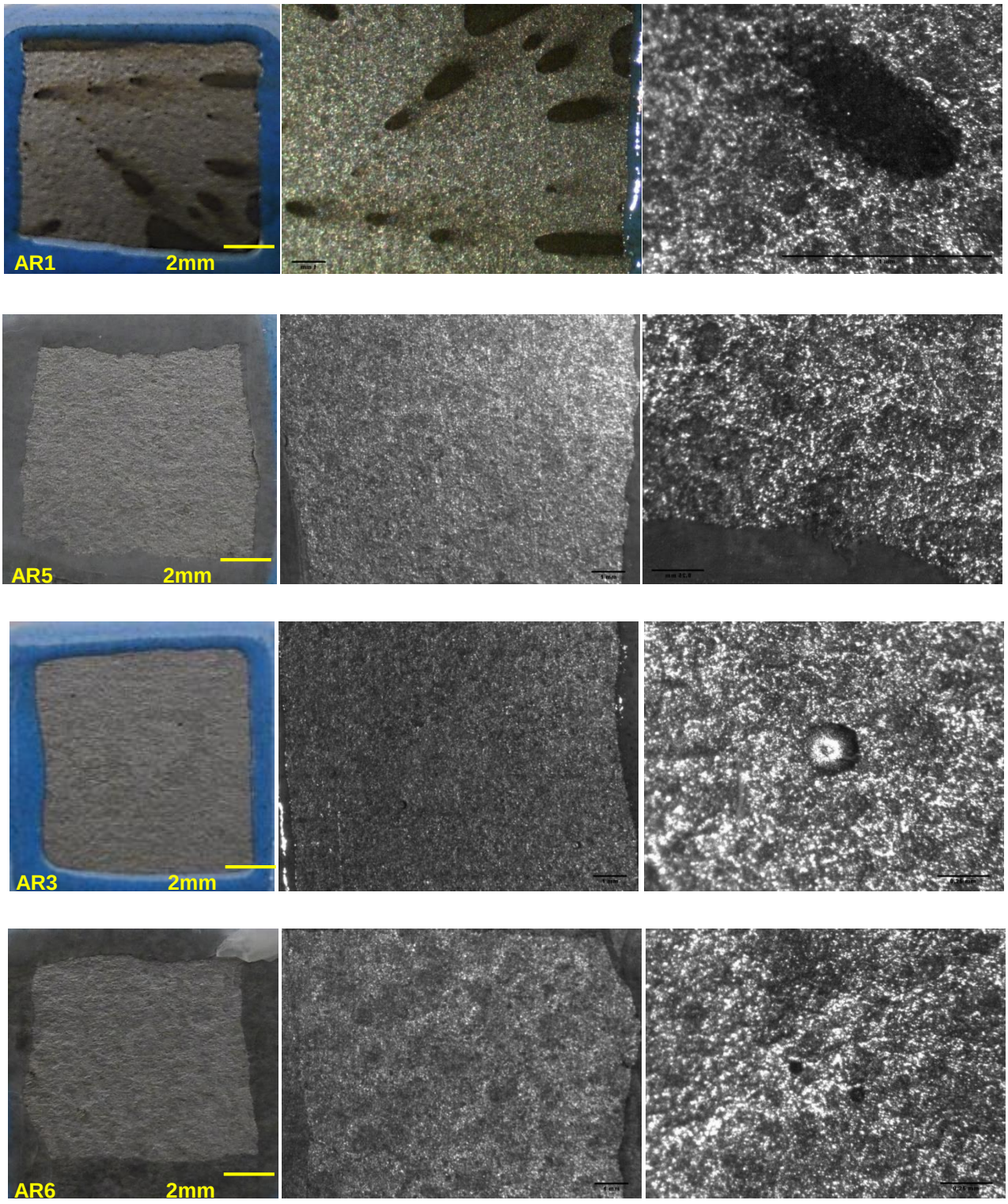


**Figure 7.16** Photomacrographs showing the appearance of the four as-received specimens and the areas of localised corrosion following the anodic potentiodynamic polarisation tests at 24°C (AR1 & AR5) and at 5°C (AR3 & AR6) with the $N_2$ purge.

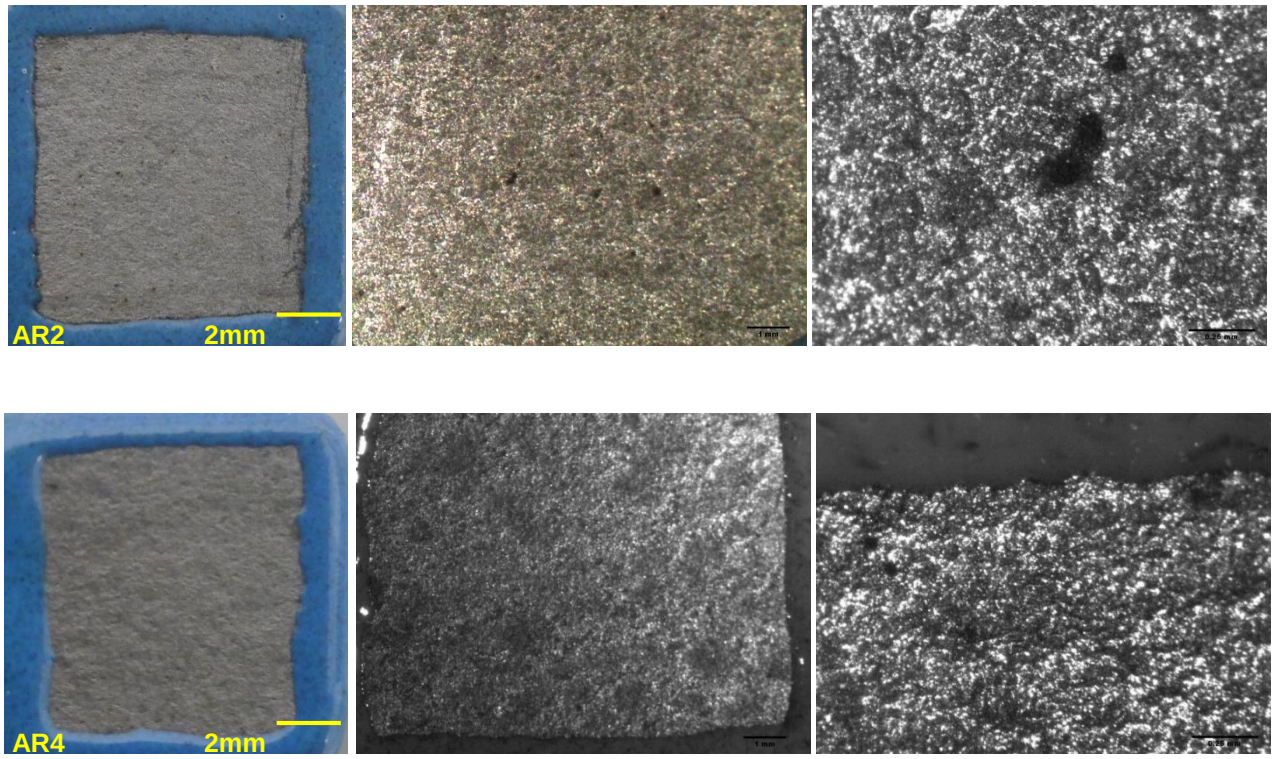


**Figure 7.17** Photomacrographs showing the appearance of the two as-received specimens and the areas of localised corrosion following the anodic potentiodynamic polarisation tests at 24°C (AR2) and at 5°C (AR4) with the $CO_2$ purge.

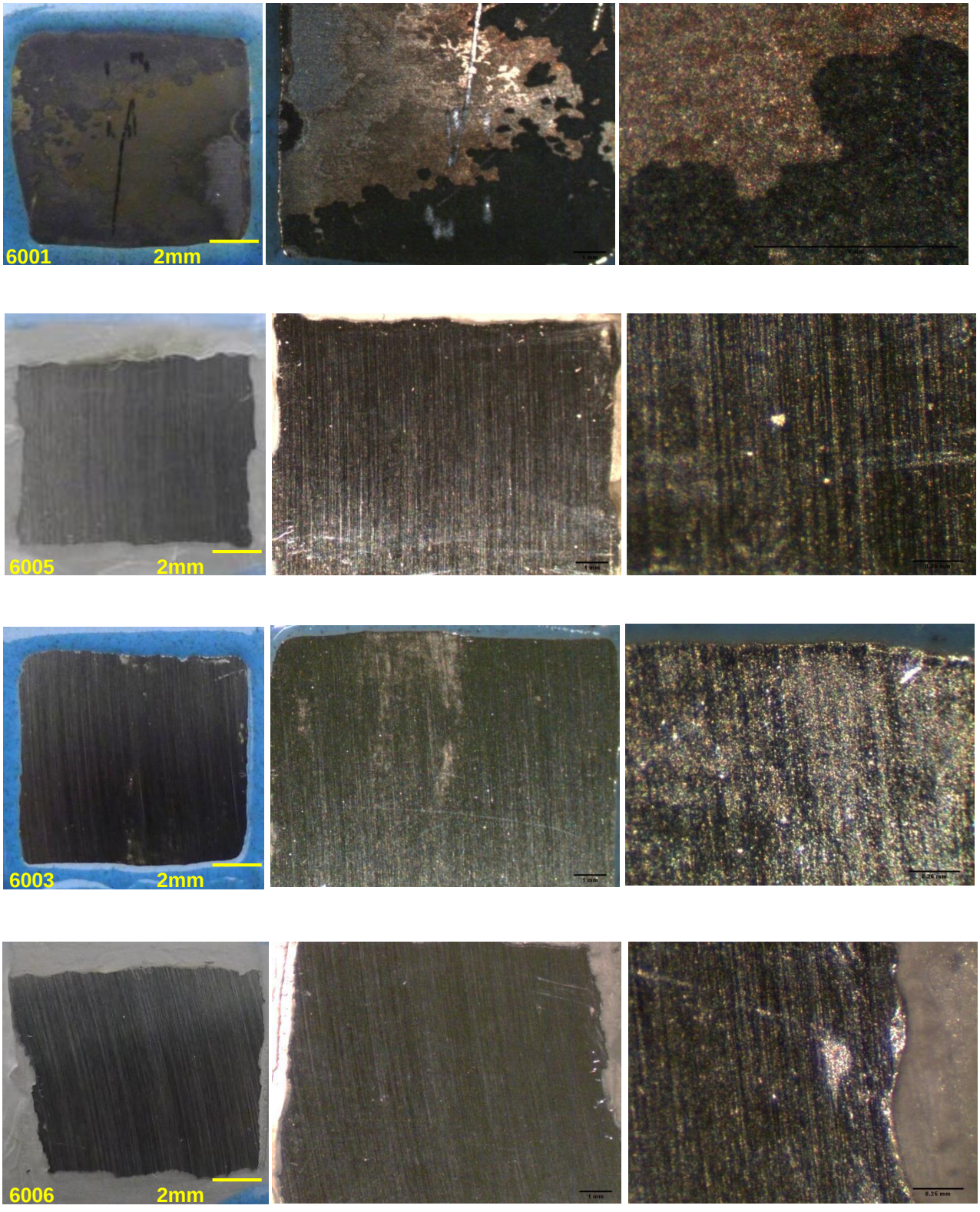


**Figure 7.18** Photomacrographs showing the appearance of the four 600 SiC ground specimens and the areas of localised corrosion following the anodic potentiodynamic polarisation tests at 24°C (6001 & 6005) and at 5°C (6003 & 6006) with the $N_2$ purge.

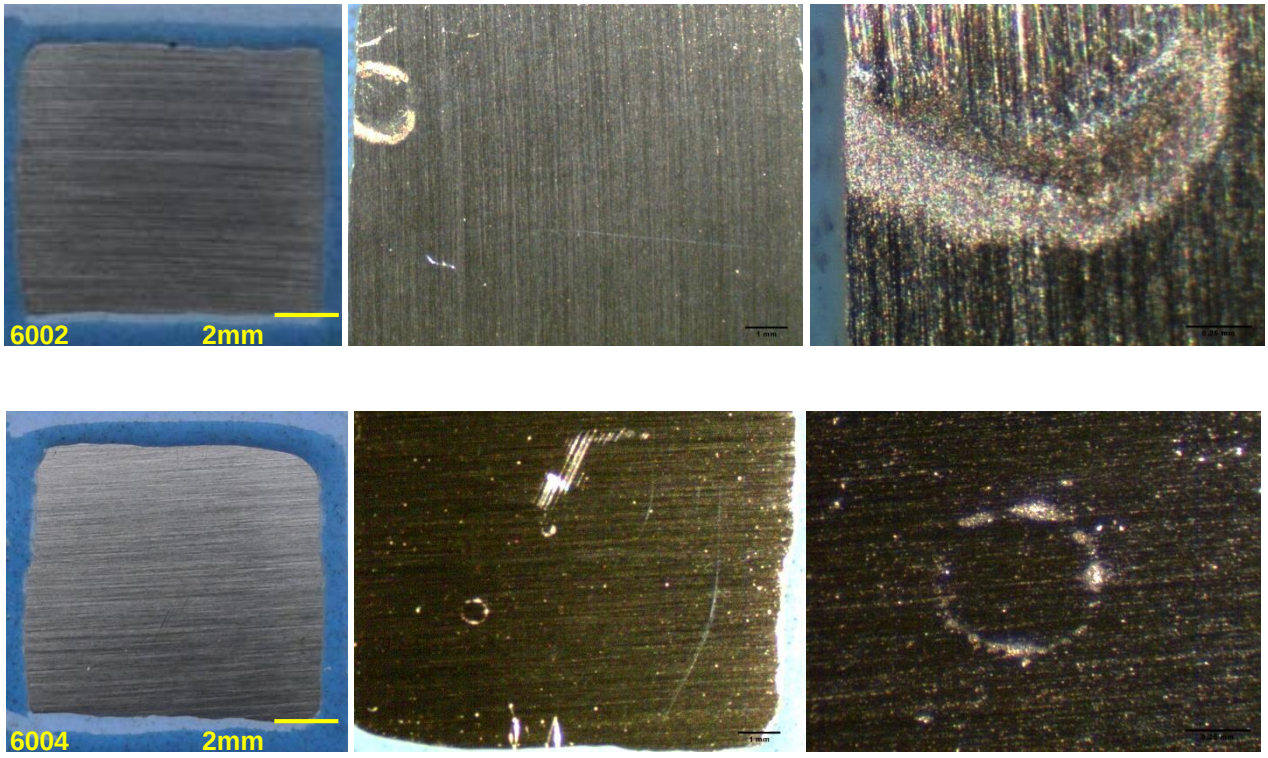


**Figure 7.19** Photomacrographs showing the appearance of the two 600 SiC ground specimens and the areas of localised corrosion following the anodic potentiodynamic polarisation tests at 24°C (6002) and at 5°C (6004) with the $CO_2$ purge.

7.2.2.2 Influence of Surface Finish (As-received v 600SiC ground)

The anodic potentiodynamic curves showing the Influence of the surface condition (i.e. as-received versus 600 SiC) on the electrochemical behaviour of the specimens tested at 24°C and 5°C are presented in Figures 7.20 – 7.21 and the post-test appearance of the specimens are shown in Figures 7.22 – 7.23.

All of the tests were conducted in the 100,000 mg/L produced water (PW) environment at a pH of 4.5 with 35 mbara $H_2S$ ($CO_2$ balance) at 1 bara total pressure, with a prior $N_2$ gas purge gas. The material was tested in the as-received (AR) and 600 SiC ground conditions and two of the four AR specimens were tested with an epoxy coating (-E) and two with a bees-wax coating (-B).

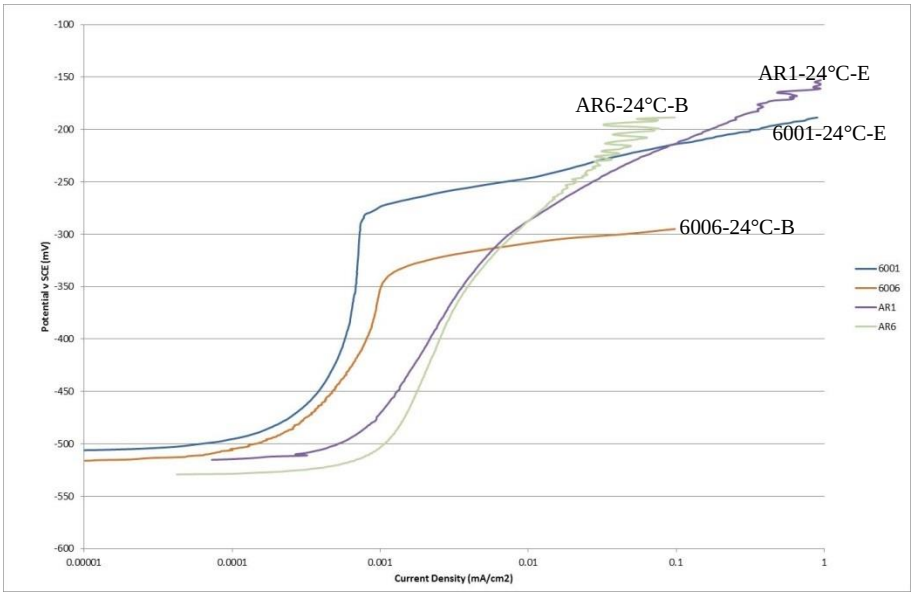


**Figure 7.20** Influence of surface finish (AR v 600 SiC ground) on the anodic potentiodynamic polarisation curves for the material tested at 24°C.
(Test conditions: 24°C, 100,000 mg/L Cl, pH 4.5, 35 mbara $H_2S$, $N_2$ purge).

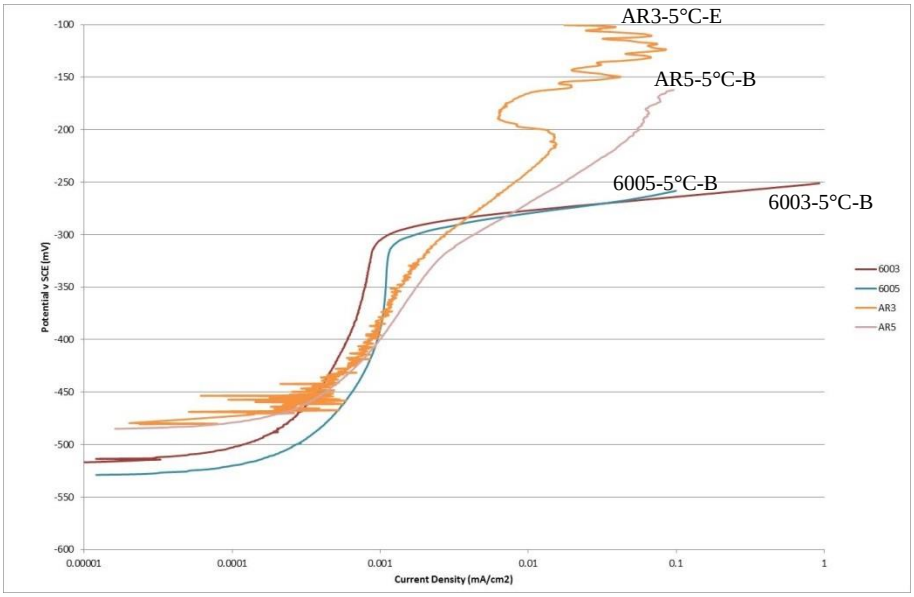


**Figure 7.21** Influence of surface finish (AR v 600 SiC ground) on the anodic potentiodynamic polarisation curves for the material tested at 5°C
(Test conditions: 5°C, 100,000 mg/L Cl, pH 4.5, 35 mbara $H_2S$, $N_2$ purge).

.

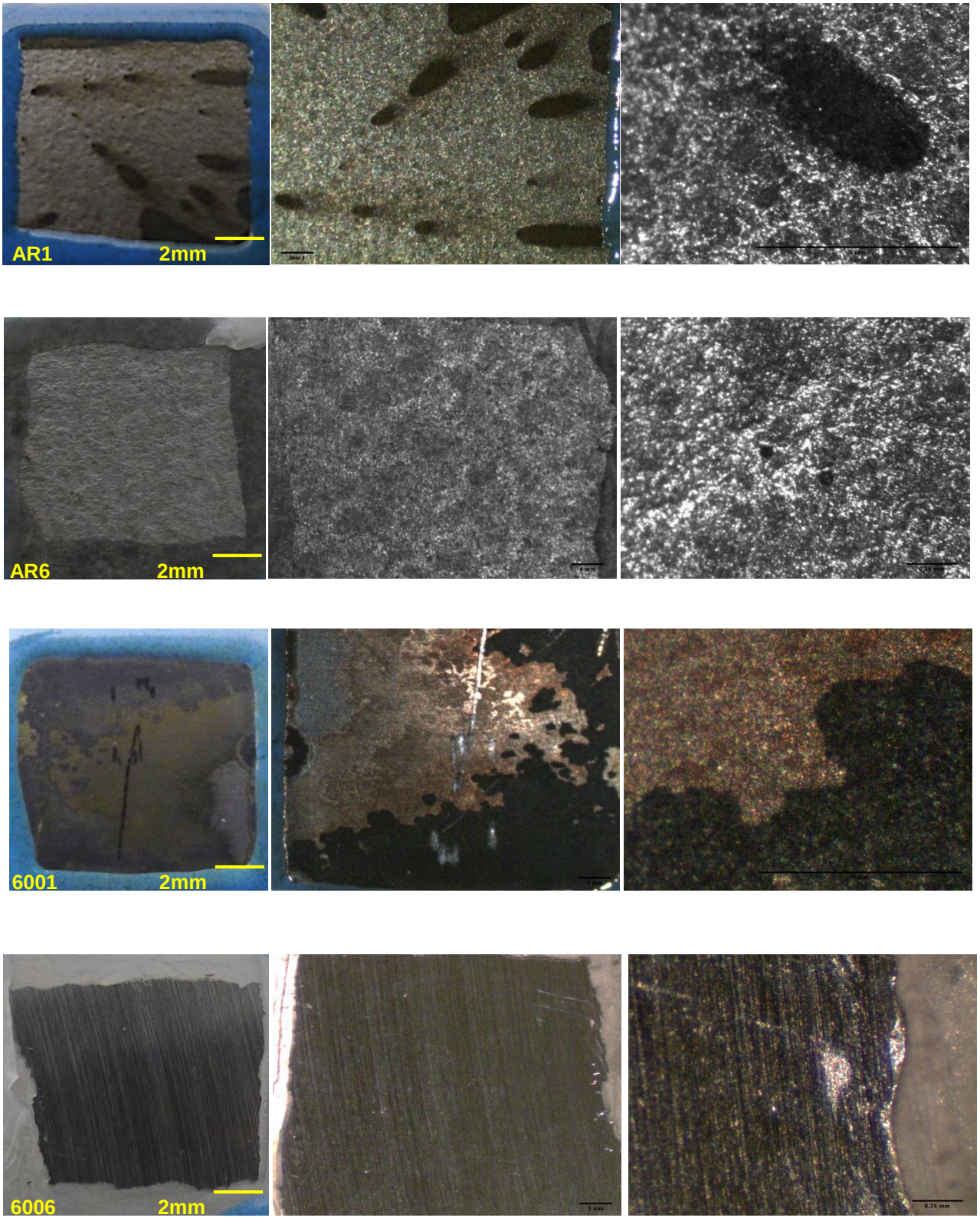


**Figure 7.22** Photomacrographs showing the appearance of the two as-received specimens (AR1 & AR6) and the two 600 SiC ground specimens (6001 & 6006) following the anodic potentiodynamic polarisation tests at 24°C with the $N_2$ purge.

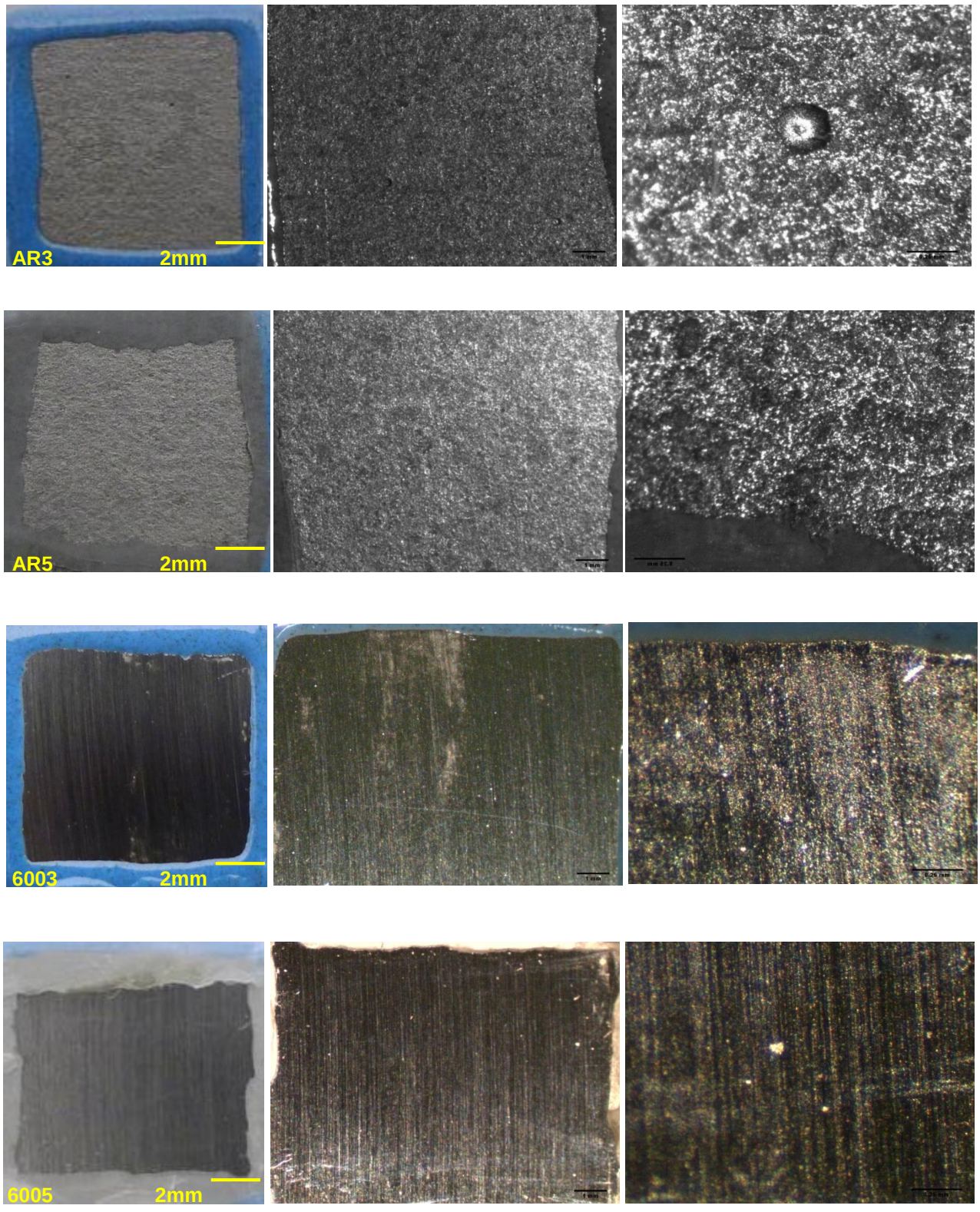


**Figure 7.23** Photomacrographs showing the appearance of the two as-received specimens (AR3 & AR5) and the two 600 SiC ground specimens (6003 & 6005) following the anodic potentiodynamic polarisation tests at 5°C with the $N_2$ purge.

7.2.2.3 Influence of $H_2S$ Concentration

The anodic potentiodynamic curves showing the Influence of the $H_2S$ concentration on the electrochemical behaviour of the specimens tested at 24°C and 5°C are presented in Figures 7.24 – 7.25 for the specimens with the as-received surface and Figures 7.26 – 7.27 for the specimens with the 600 SiC ground surface. The post-test appearance of the specimens is shown in Figures 7.28 – 7.31.

All of the tests were conducted in the 100,000 mg/L produced water (PW) environment at 1 bara total pressure. Control tests were conducted in $H_2S$-free conditions using only $N_2$ or $CO_2$ gas. For the $N_2$ test environment the pH was 5.6 and for the $CO_2$ environment the pH was 4.5. Subsequent tests (following a purge of either $N_2$ or $CO_2$) to determine the effect of $H_2S$ concentration were conducted in 35 mbara and 69 mbara $H_2S$ solutions with a balance of $CO_2$ at a pH of 4.5.The material was tested in the as-received (AR) and 600 SiC ground conditions and all specimens were tested with an epoxy coating (-E).

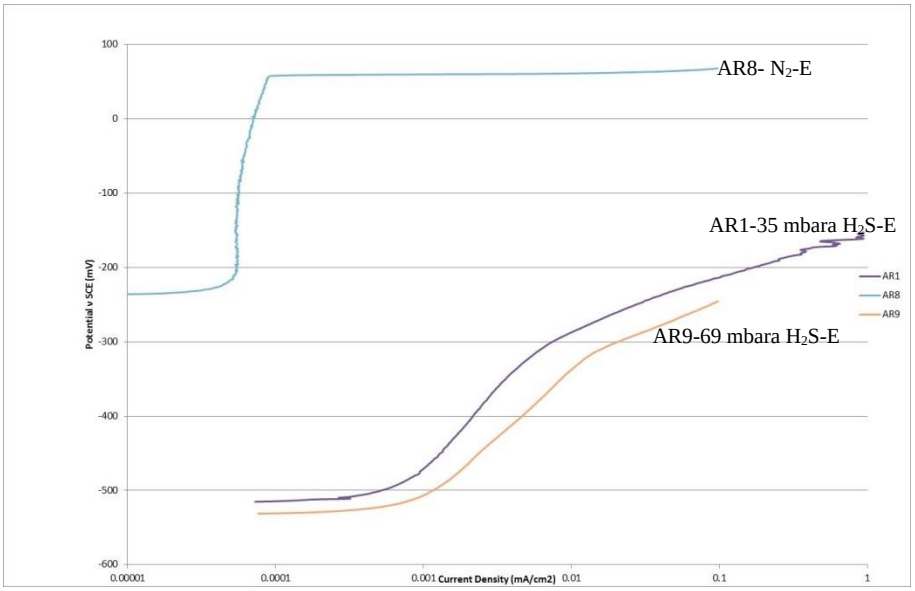


**Figure 7.24** Influence of the $H_2S$ concentration on the anodic potentiodynamic polarisation curves for the material in the as-received condition ($N_2$ purge) at 24°C.
(Test conditions: 24°C, 100,000 mg/L Cl, 0 mbara ($N_2$), 35 mbara & 69 mbara $H_2S$, $N_2$ purge, pH= 4.5 (35 mbara & 69 mbara $H_2S$ tests, 5.6 for $N_2$ test).

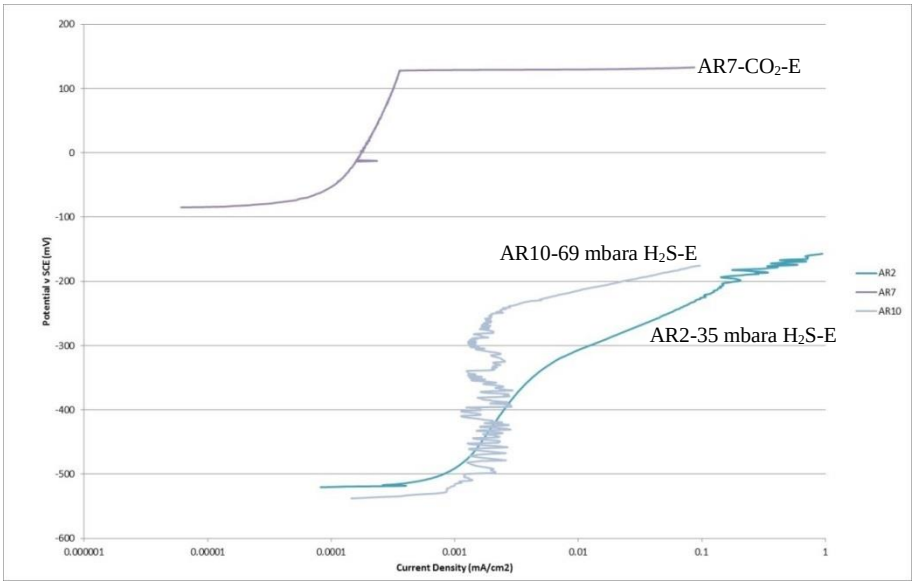


**Figure 7.25** Influence of the $H_2S$ concentration on the anodic potentiodynamic polarisation curves for the material in the as-received condition ($CO_2$ purge) at 24°C.
(Test conditions: 24°C, 100,000 mg/L Cl, 0 mbara ($CO_2$), 35 mbara & 69 mbara $H_2S$, $CO_2$ purge, pH= 4.5 for all tests).

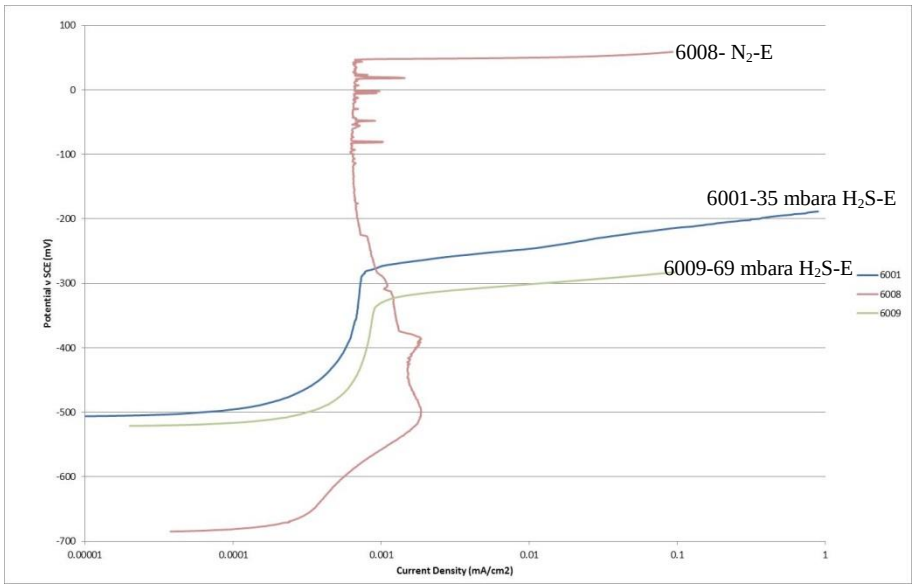


**Figure 7.26** Influence of the $H_2S$ concentration on the anodic potentiodynamic polarisation curves for the material in the 600 SiC ground condition ($N_2$ purge).
Test conditions: 24°C, 100,000 mg/L Cl, 0 mbara ($N_2$), 35 mbara & 69 mbara $H_2S$, $N_2$ purge, pH= 4.5 (35 mbara & 69 mbara $H_2S$ tests, 5.6 for $N_2$ test).

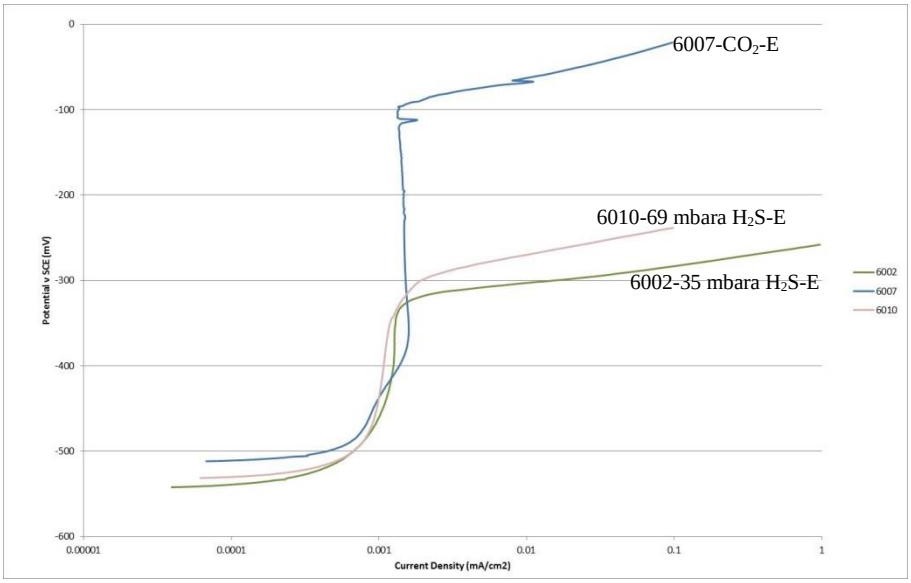


**Figure 7.27** Influence of the $H_2S$ concentration on the anodic potentiodynamic polarisation curves for the material in the 600 SiC ground condition ($CO_2$ purge).
(Test conditions: 24°C, 100,000 mg/L Cl, 0 mbara ($CO_2$), 35 mbara & 69 mbara $H_2S$, $CO_2$ purge, pH= 4.5 for all tests).

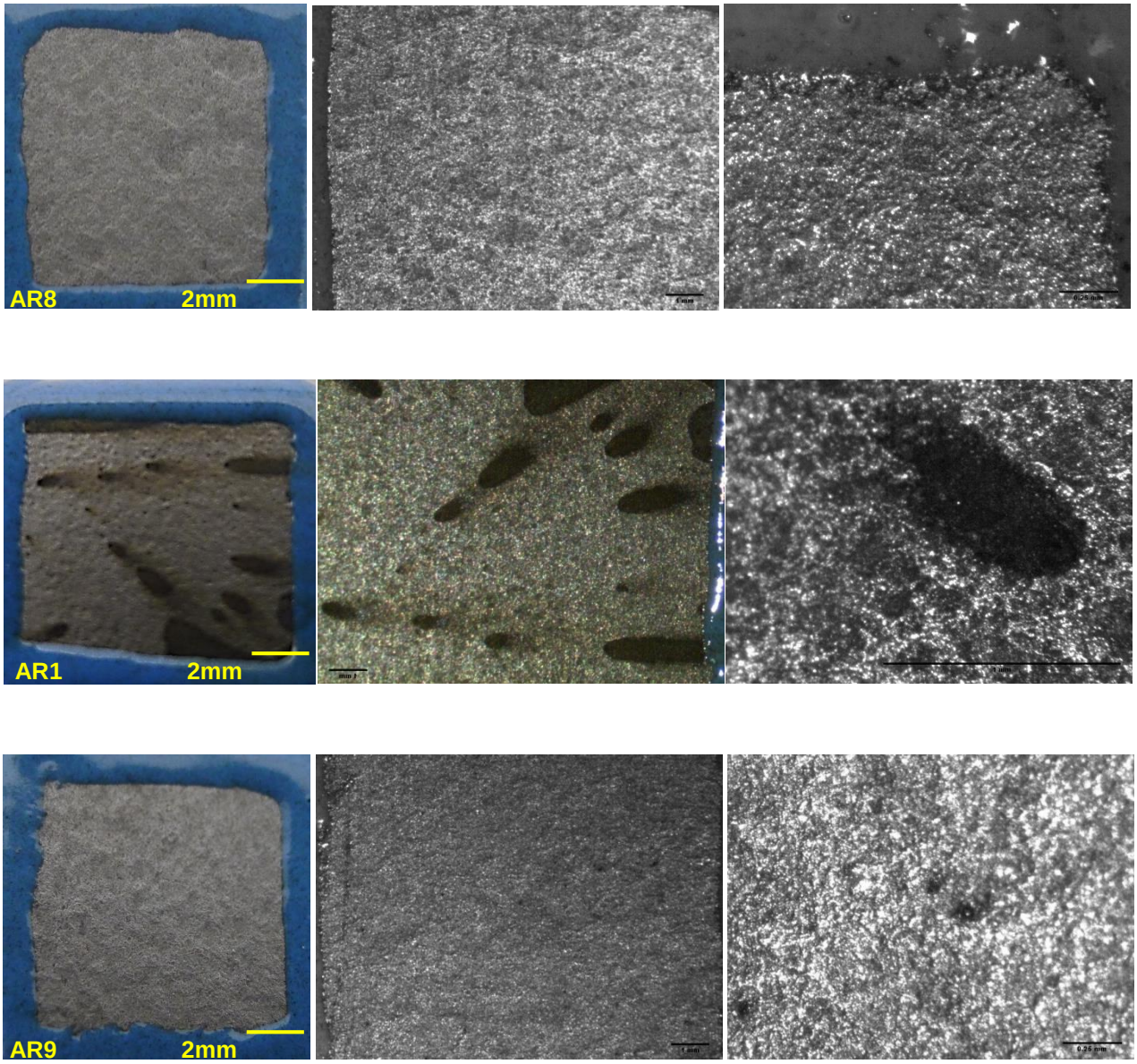


**Figure 7.28** Photomacrographs showing the appearance of the three as-received specimens AR8 ($N_2$), AR1 (35 mbara $H_2S$) and AR9 (69 mbara $H_2S$) following the anodic potentiodynamic polarisation tests at 24°C with the $N_2$ purge.

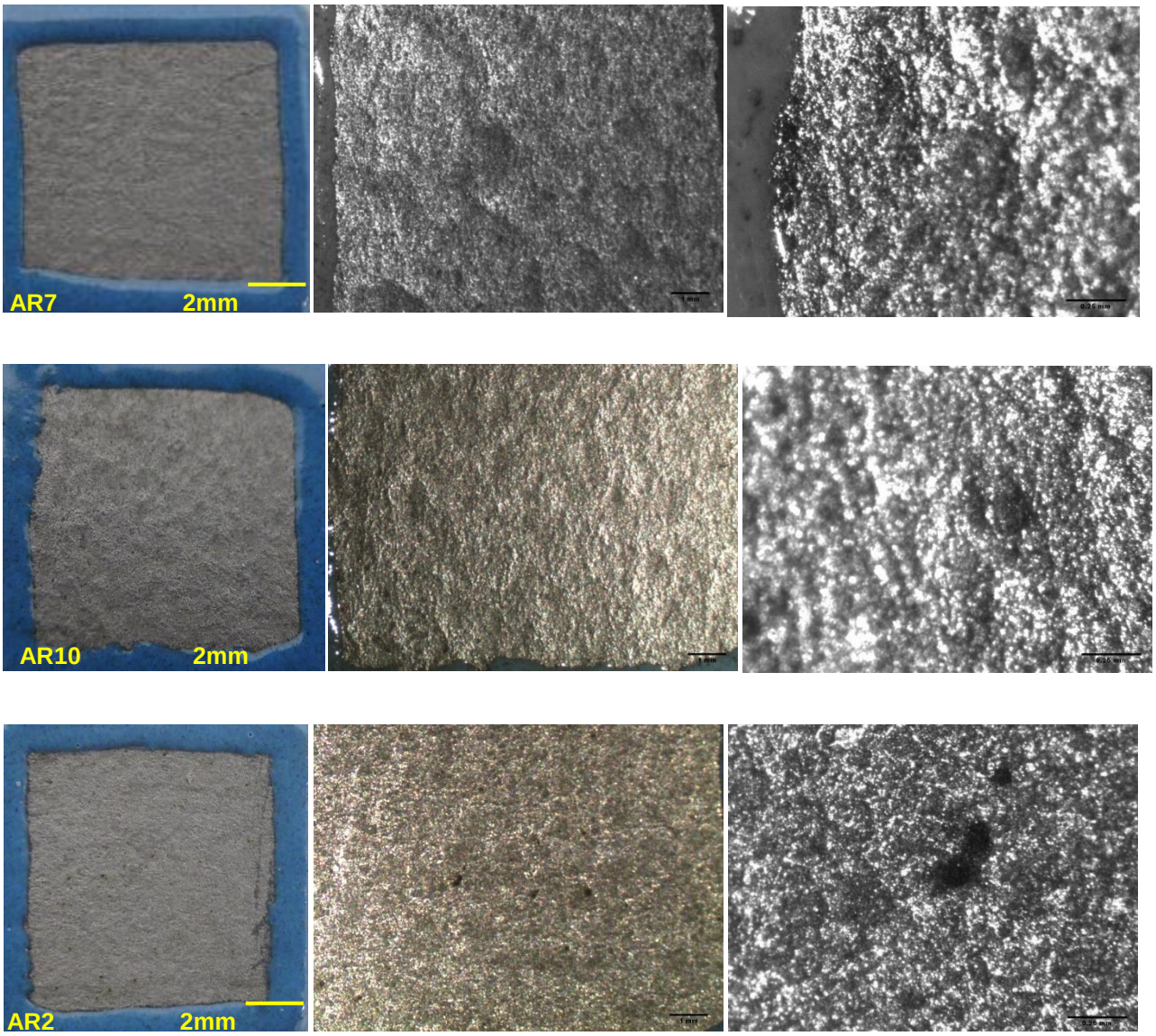


**Figure 7.29** Photomacrographs showing the appearance of the three as-received specimens AR7 ($CO_2$), AR2 (35 mbara $H_2S$) and AR10 (69 mbara $H_2S$) following the anodic potentiodynamic polarisation tests at 24°C with the $CO_2$ purge.

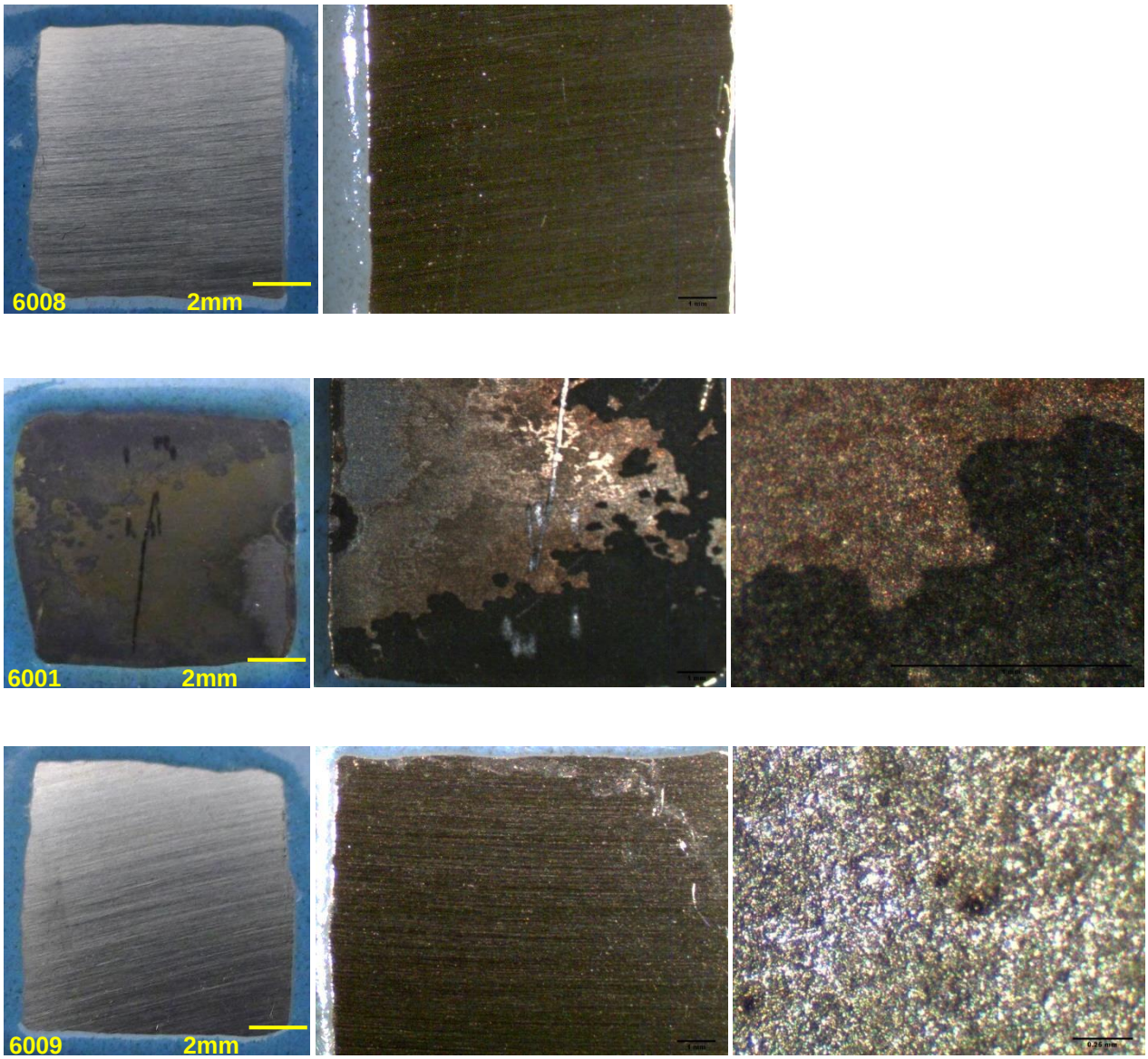


**Figure 7.30** Photomacrographs showing the appearance of the three as 600 SiC ground specimens 6008 ($N_2$), 6001 (35 mbara $H_2S$) and 6009 (69 mbara $H_2S$) following the anodic potentiodynamic polarisation tests at 24°C with the $N_2$ purge.

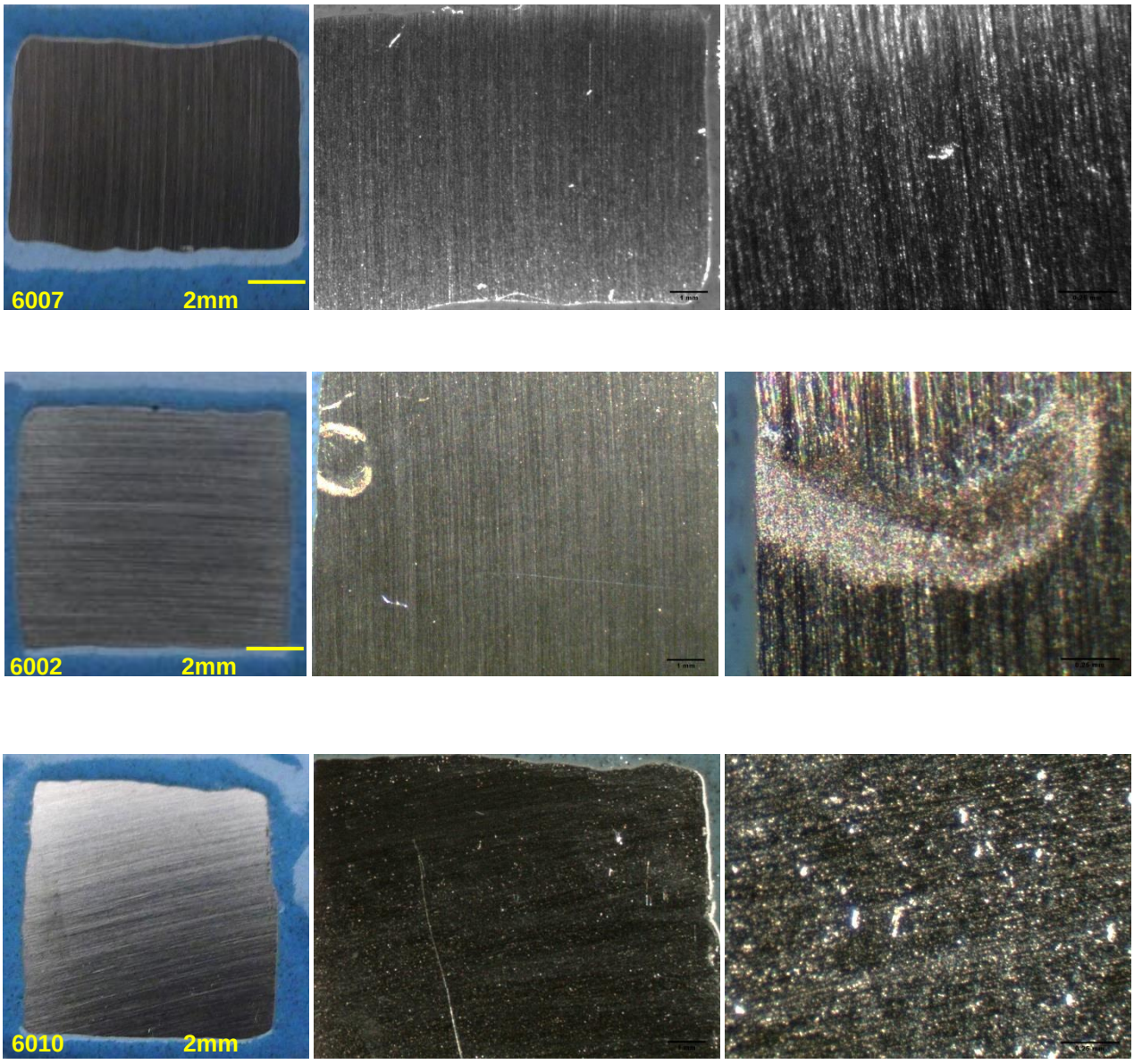


**Figure 7.31** Photomacrographs showing the appearance of the three as 600 SiC ground specimens 6007 ($CO_2$), 6002 (35 mbara $H_2S$) and 6010 (69 mbara $H_2S$) following the anodic potentiodynamic polarisation tests at 24°C with the $N_2$ purge.

7.2.2.4 Influence of Coating (Epoxy v Bees-wax)

Anodic potentiodynamic curves showing the Influence of the masking coating on the electrochemical behaviour of the AR and 600 SiC ground specimens tested at 24°C and 5°C are presented in Figures 7.32 – 7.33 and the post-test appearance of the specimens are shown in Figures 7.34 – 7.35.

All of the tests were conducted in the 100,000 mg/L produced water (PW) environment at a pH of 4.5 with 35 mbara $H_2S$ ($CO_2$ balance) at 1 bara total pressure, with a prior $N_2$ gas purge gas. The tests were conducted at 24°C and 5°C and the material was tested in the as-received (AR) and 600 SiC ground finish condition.

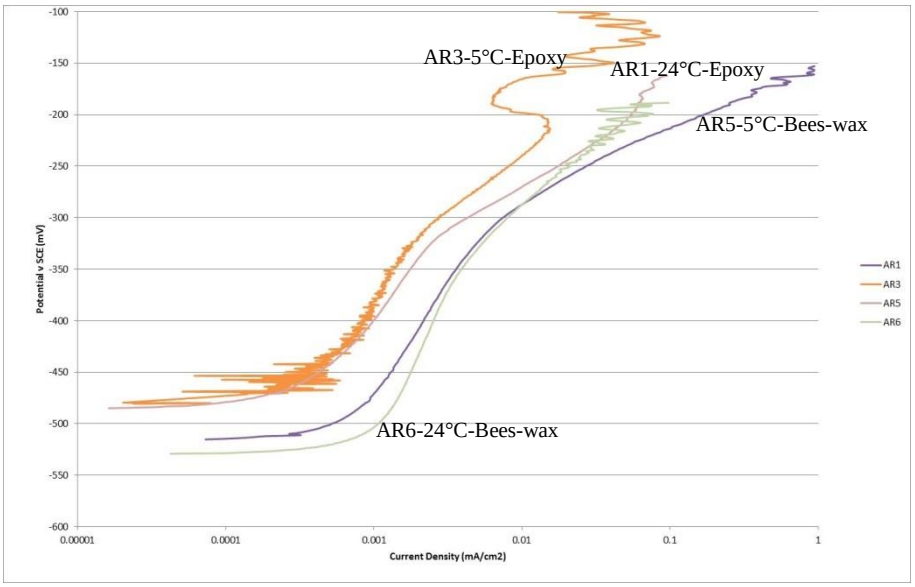


**Figure 7.32** Influence of the coating media (i.e. epoxy v bees-wax) on the anodic potentiodynamic polarisation curves for the material in the AR condition ($N_2$ purge).
(Test conditions: 24°C & 5°C, 100,000 mg/L Cl, pH 4.5, 35 mbara $H_2S$, $N_2$ purge).

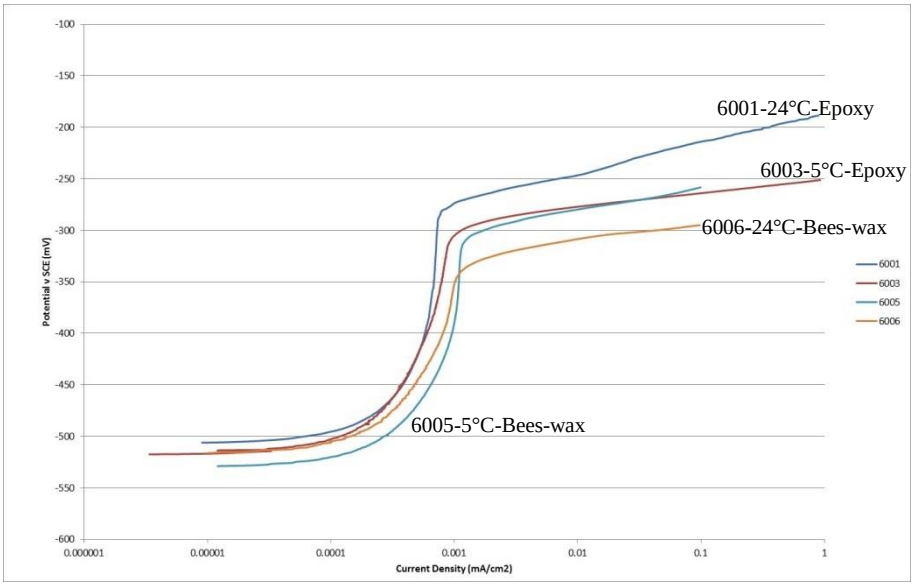


**Figure 7.33** Influence of the coating media (i.e. epoxy v bees-wax) on the anodic potentiodynamic polarisation curves for the material in the 600 SiC ground condition ($N_2$ purge). (Test conditions: 24°C & 5°C, 100,000 mg/L Cl, pH 4.5, 35 mbara $H_2S$, $N_2$ purge).

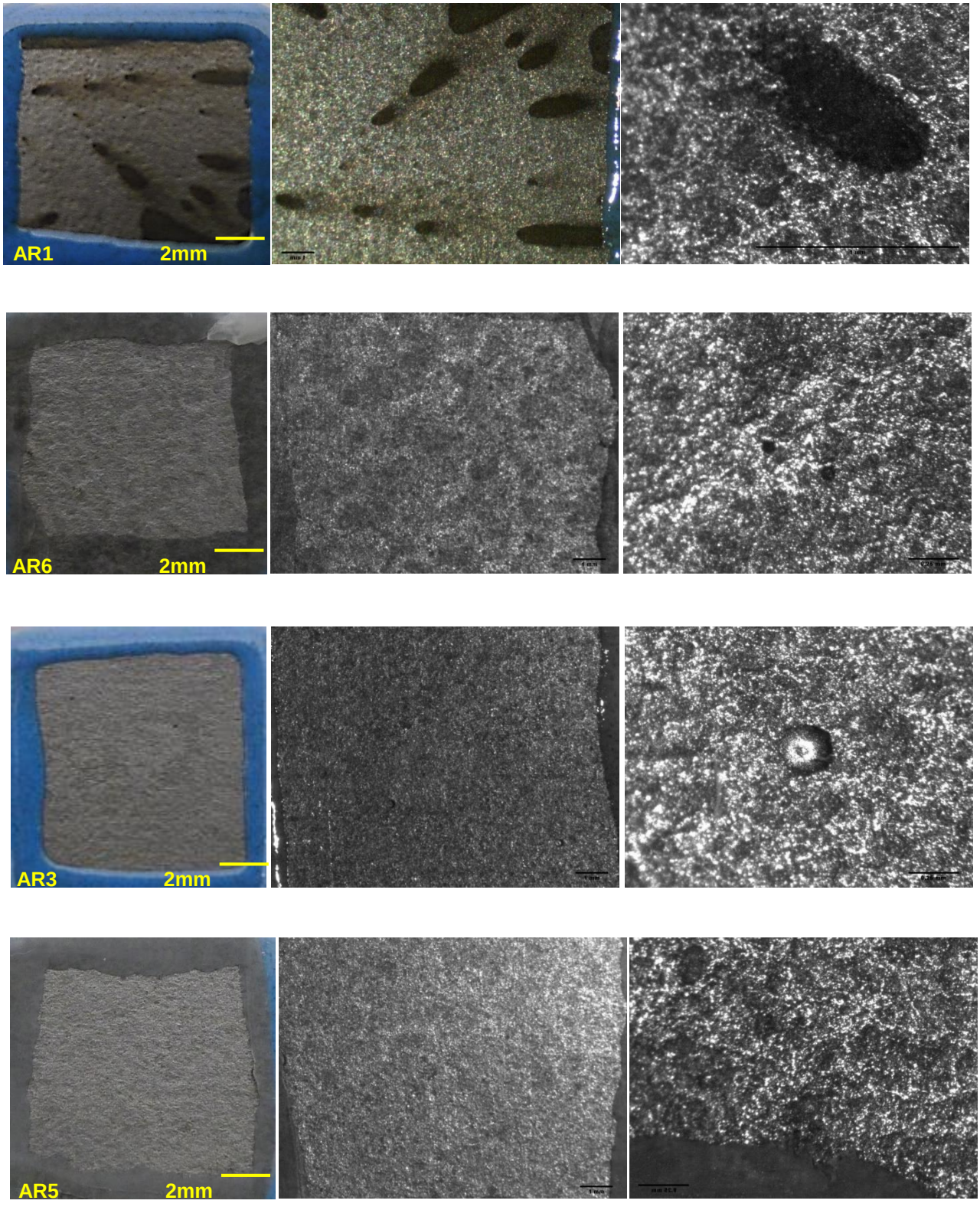


**Figure 7.34** Photomacrographs showing the appearance of the four as-received specimens AR1-Epoxy-24°C, AR6-Bees-wax @ 24°C, AR3-Epoxy-5°C, AR5-Bees-wax @ 5°C (35 mbara $H_2S$) following the anodic potentiodynamic polarisation tests with the $N_2$ purge.

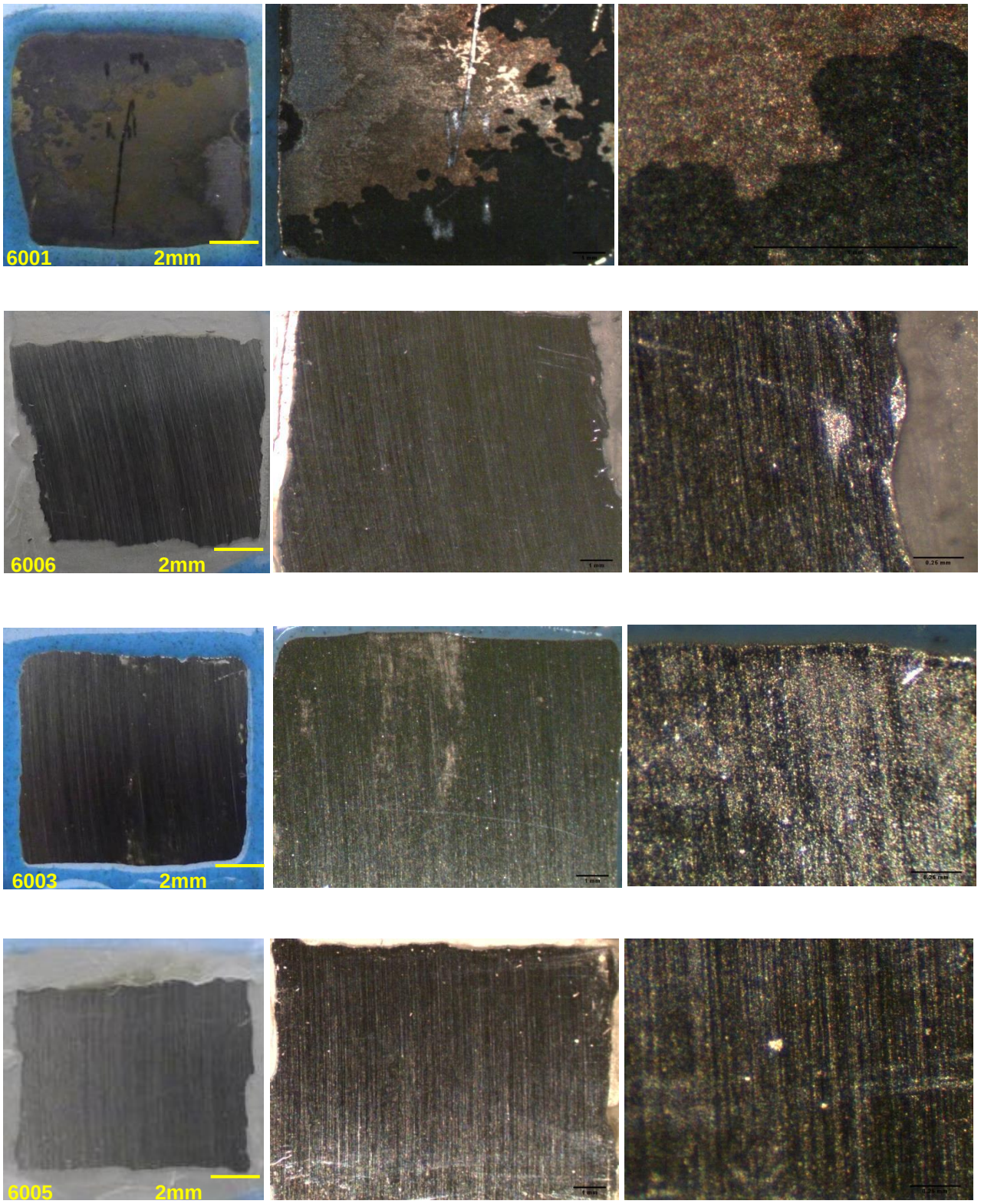


(35 mbara $H_2S$) following the anodic potentiodynamic polarisation tests with the $N_2$ purge.

7.2.2.5 Influence of Purge Gas ($N_2$ v $CO_2$)

Anodic potentiodynamic curves showing the Influence of the purge gas (i.e. $N_2$ versus $CO_2$) alone (i.e. no $H_2S$) on the electrochemical behaviour of the AR and 600 SiC ground specimens tested at 24°C are presented in Figure 7.36 and the post-test appearance of the specimens are shown in Figure 7.37.

All of the tests were conducted in the 100,000 mg/L produced water (PW) environment at 1 bara total pressure, with either $N_2$ or $CO_2$ as both the purge and test gases. The pH for the $N_2$ tests was 5.6 and for the $CO_2$ tests 4.5.

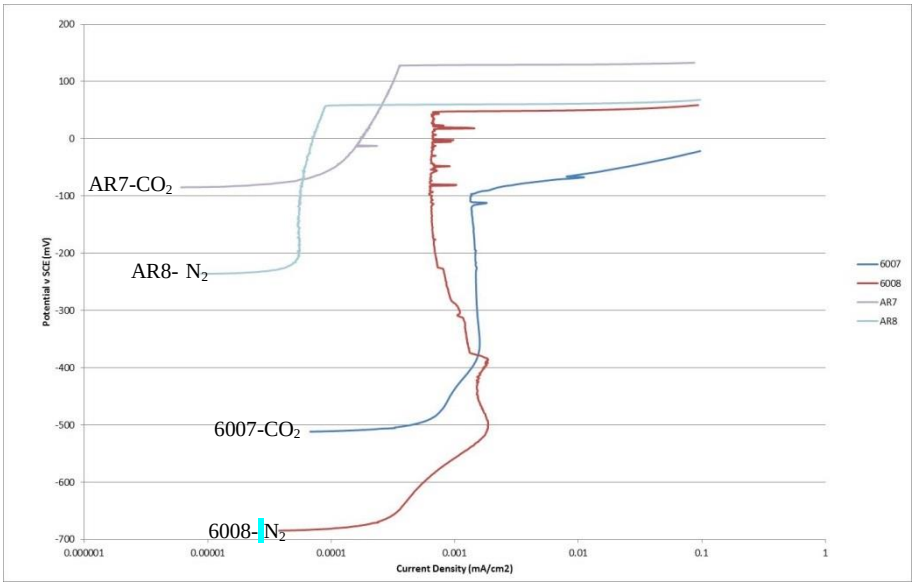


**Figure 7.36** Influence of the purge gas (i.e. $N_2$ v $CO_2$) on the anodic potentiodynamic polarisation curves for the material in the AR and 600 SiC ground conditions at 24°C.
(Test conditions: 24°C, 100,000 mg/L Cl, pH = 4.5 for $CO_2$ tests and 5.6 for $N_2$ tests)

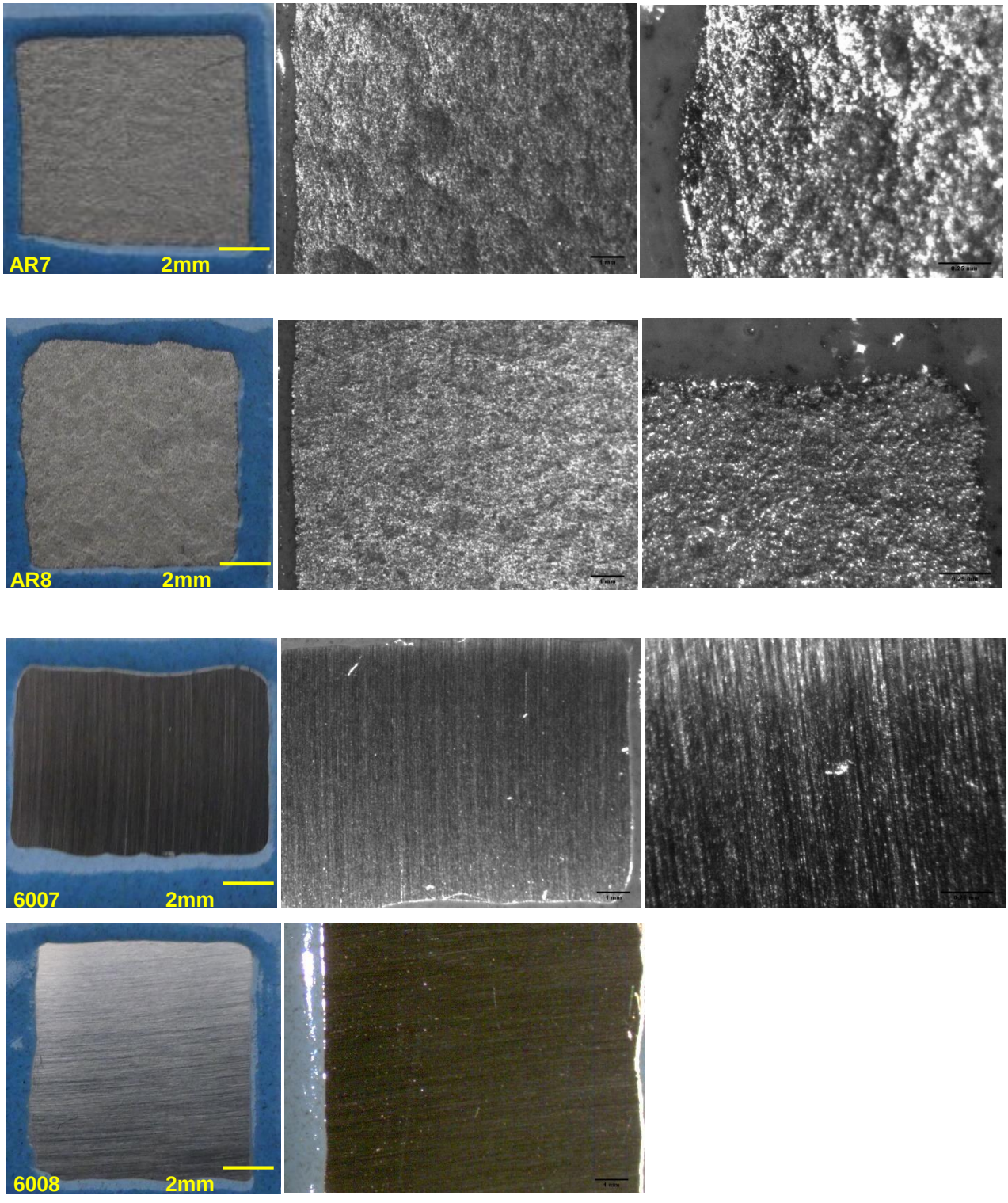


**Figure 7.37** Photomacrographs showing the appearance of the as-received specimens AR7 & AR8 and the 600 SiC ground specimens 6007 & 6008, following the anodic potentiodynamic polarisation tests at 24°C with the $N_2$ and $CO_2$ tests (**No $H_2S$**).

### 7.2.3 Repeatability & Reproducibility

Insufficient measurements were conducted under identical conditions in order to establish an accurate value for the repeatability standard deviation (Sr) for the electrochemical results. The only duplicate comparable corrosion potential measurements were made in the $N_2$ purged solution, following the 35 mbara $H_2S$ saturation period, at 24°C and 5°C using the epoxy and bees-wax coated specimens. The results from these tests were considered to be comparable, since the coating type would not influence the coating potential measurements. Based on these comparable tests the maximum repeatability standard deviation (Sr) for the corrosion potential ($E_{corr}$) measurements, tests, was 11 mV and the 95%CI value was ± 21 mV (see Table 7.11).

Information on the repeatability (closeness of agreement of measurements by the same laboratory) and reproducibility (closeness of agreement of measurements by different laboratories) for corrosion potential measurements has been published in ASTM G59 [110] and maximum 95%CI values of ± 8 mV have been reported for the repeatability and ± 36 mV for the reproducibility.

As with the corrosion potential measurements the only duplicate comparable passive current density measurements were made in the $N_2$ purged solution, following the 35 mbara $H_2S$ saturation period, at 24°C and 5°C using the epoxy and bees-wax coated specimens. The results from these tests were considered to be comparable, since the coating type would not influence the passive current density measurements. Based on these comparable tests the maximum repeatability standard deviation (Sr) for the passive current density ($i_{pass}$) measurements, tests, was 0.21 µA/cm$^2$ and the 95%CI value was ± 0.42 µA/cm$^2$ (see Table 7.11).

The breakdown potential ($E_{bd}$) measurements tend to be more stochastic than the corrosion potential and passive current measurements, which was reflected in the large variation in the Sr and 95%CI values between duplicate measurements shown in Table 7.11. From Table 7.11 it can be seen that the Sr values ranged from 3 mV to 89 mV and the 95% CI values ranged from ± 6 mV to ± 175 mV. The large variation between the values could probably be attributed to the fact that the breakdown potential is related to the onset of pitting corrosion on the ‘open’ surfaces and initiation of crevice corrosion at

the coating-specimen interface. Consequently to obtain more accurate breakdown potential measurements it was considered that a minimum of three tests should be conducted under identical conditions.

It was not possible to quantify the errors associated with the potentiodynamic polarisation curves shown in Figures 7.12 – 7.15, 7.20 – 721, 7.24 – 7.27, 7.32 – 7.33 and 7.36. However the repeatability errors were minimised by taking care to standardise the experimental parameters for comparative tests with respect to the mounting media, scan rates, potentiostat used and the specimen-luggin probe distance, since a variation in these factors are known [111] to influence the results of potentiodynamic polarisation tests.

The potentiodynamic polarisation tests conducted were considered to be reproducible and provided meaningful trends showing the influence of temperature, surface condition, masking material, purge gas and $H_2S$ concentration on the electrochemical performance. However it is recognised that insufficient identical scans were conducted in order to obtain reliable information on the standard deviation associated with the technique, due to limitations in the scope and time for this project. It should be noted that precise statistical data for potentiodynamic polarisation tests are rarely presented and the corrosion can be stochastic in nature. Information on the scatter bands for potentiodynamic polarisation tests conducted on type 430 stainless steel in sulphuric acid has been published in ASTM G5 [112] and a variation in the passive current density of ± 0.5 μA/cm$^2$ has been reported at a mean value of 1 0.5 μA/cm$^2$. Further data on the standard deviation for potentiodynamic polarisation tests has been published in ASTM G61 [113], where ± 2 standard deviation (i.e. 95%CI) values are presented for alloy C276 and type 304L stainless steel in 3.56 wt.% NaCl and the results show an order of magnitude variation in the passive current density for both materials, demonstrating the inherent variability with the test method.

# 7.3 Discussion

### 7.3.1 Influence of Temperature (24°C v 5°C)

The results from the corrosion potential measurements and anodic polarisation tests conducted at 24°C and 5°C were compared to establish the Influence of the test temperature on the corrosion characteristics and in particular the stability of the passive film.

The results of the electrochemical potential measurements conducted with the $N_2$ purge gas are summarised in Table 7.4.

**Table 7.4** Summary of corrosion potential measurements for the 24°C v 5°C comparative tests with the initial $N_2$ purge gas followed by a 35 mbara $H_2S$ test gas

| Test | Surface condition | Masking material | Temp. | Purge gas | Ecorr (Purge) | | | | Ecorr (Scan) |
|---|---|---|---|---|---|---|---|---|---|
| | | | | | Initial purge | | 35 mbara $H_2S$ Test gas | | |
| | | | (°C) | | Start (mV) | Finish (mV) | Start (mV) | Finish-1 hr (mV) | (mV v SCE) |
| | | | | | | | | | |
| 1 | AR | Epoxy | 24 | $N_2$ | -212 | -225 | -165 | -489 | -494 |
| 6 | AR | Bees-wax | 24 | $N_2$ | -151 | -264 | -179 | -484 | -505 |
| **Ave** | | | | | **-182** | **-245** | **-172** | **-487** | **-500** |
| Sr | | | | | 43 | 28 | 10 | 4 | 8 |
| 95%Cl (±) | | | | | 85 | 54 | 19 | 7 | 15 |
| 3 | AR | Epoxy | 5 | $N_2$ | -3 | -176 | -60 | -464 | -463 |
| 5 | AR | Bees-wax | 5 | $N_2$ | -137 | -195 | -64 | -459 | -464 |
| **Ave** | | | | | **-70** | **-186** | **-62** | **-462** | **-464** |
| Sr (±) | | | | | 95 | 13 | 3 | 4 | 1 |
| 95%Cl (±) | | | | | 186 | 26 | 6 | 7 | 1 |
| 1 | 600SiC | Epoxy | 24 | $N_2$ | -651 | -615 | -568 | -522 | -497 |
| 6 | 600SiC | Bees-wax | 24 | $N_2$ | -179 | -701 | -622 | -540 | -509 |
| **Ave** | | | | | **-415** | **-658** | **-595** | **-531** | **-503** |
| Sr (±) | | | | | 334 | 61 | 38 | 13 | 8 |
| 95%Cl (±) | | | | | 654 | 119 | 75 | 25 | 17 |
| 3 | 600SiC | Epoxy | 5 | $N_2$ | -617 | -704 | -560 | -520 | -508 |
| 5 | 600SiC | Bees-wax | 5 | $N_2$ | -173 | -677 | -604 | -537 | -523 |
| **Ave** | | | | | **-395** | **-691** | **-582** | **-529** | **-516** |
| Sr (±) | | | | | 314 | 19 | 31 | 12 | 11 |
| 95%Cl (±) | | | | | 615 | 37 | 61 | 24 | 21 |

Under the pre-nitrogen purged conditions, following the 1 hour $H_2S$ purge, the corrosion potential, at 24°C was -489 mV and -484 mV for the epoxy coated and bees-wax coated AR specimens, respectively, compared to -464 mV and -459 mV for the two specimens tested at 5°C.

For the 600 grit SiC ground samples $E_{corr}$ values of -522 mV and -540 mV were measured at 24°C compared to -520 mV and -537 mV at 5°C. The as-received samples did exhibit a clear difference in the potential of 25 mV at the two temperatures, whereas the 600 SiC specimens did not show any trend. The duplicate 24°C and 5°C potential values for the as-received specimens showed close agreement to within ±5 mV of the mean value however the 600 SiC ground specimens showed a greater variability of ±10 mV of the mean value. These variations are considered to be within the experimental error. However they may have been influenced by the stabilisation time required following commencement of the $H_2S$ purge period. The change in the potential during the $H_2S$ purge and the Influence of the time on the corrosion potential was reported by Marchebois et al. [27] for S13%Cr in pH 3.5 and pH 4.0, 5 wt.% NaCl solution at 0.1 bara $H_2S$. The results presented in Figure 7.38 show that although the solution would be saturated with $H_2S$ within 1 hour it could take up to 30 hr to achieve stabilisation of the Ecorr values. Consequently further work would be beneficial in order to understand the variation in the corrosion potentials with time at the two test temperatures.

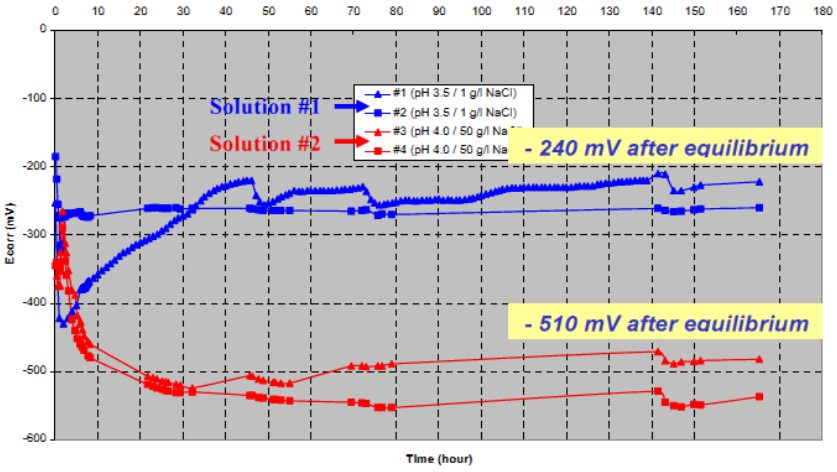


**Figure 7.38** Corrosion potential versus time recorded simultaneously during NACE TM0177 tensile tests [27].

Tests were also undertaken at the two test temperatures using a $CO_2$ purge gas and the electrochemical potential measurements are summarised in Table 7.5.

**Table 7.5** Summary of corrosion potential measurements for the 25°C v 4°C comparative tests with the initial $CO_2$ purge gas followed by a 35 mbara $H_2S$ test gas

| Test | Surface condition | Masking material | Temp. | Purge gas | Ecorr (Purge) | | | | Ecorr |
|---|---|---|---|---|---|---|---|---|---|
| | | | | | Initial purge | | Test gas purge | | (Scan start) |
| | | | (°C) | | Start (mV) | Finish (mV) | Start (mV) | Finish-1 hr (mV) | (mV v SCE) |
| | | | | | | | | | |
| 2 | AR | Epoxy | 24 | $CO_2$ | -23 | -115 | -123 | -497 | -498 |
| | | | | | | | | | |
| 4 | AR | Epoxy | 5 | $CO_2$ | 44 | -84 | -278 | -440 | -471 |
| | | | | | | | | | |
| 2 | 600 SiC | Epoxy | 24 | $CO_2$ | -537 | -530 | -548 | -541 | -537 |
| | | | | | | | | | |
| 4 | 600 SiC | Epoxy | 5 | $CO_2$ | -522 | -514 | -534 | -541 | -532 |

With the decrease in the test temperature from 24°C to 5°C the results obtained revealed an increase in the potential of 27 mV, from -498 mV to -471 mV, for the AR specimens and an increase in the potential of only 5 mV, from -537 mV to -532 mV, for the 600 grit SiC ground specimens. The results showed a similar trend to the nitrogen purged tests (see Table 7.4), with the AR specimens showing a slight increase in the potential of 31 mV, with decreasing temperature whereas the 600 SiC ground specimens only showed a small decrease in the potential of 11 mV, from -497 mV to 508 mV.

The polarisation curves for the AR specimens tested with the $N_2$ purge or $CO_2$ purge followed by a 35 mbara $H_2S$ test gas, as presented in Figures 7.12 & 7.13, showed a negative shift in the passive current density ($i_{pass}$) between the tests conducted at 24°C and 5°C, indicating a slight improvement in the passive film resistance with decreasing temperature. Passive current density values of 2.1 µA/cm$^2$, 2.4 µA/cm$^2$, and 2.3 µA/cm$^2$, (**average = 2.3 µA/cm$^2$**) were recorded at 24°C, compared to 1.0 µA/cm$^2$, 1.1 µA/cm$^2$, and 1.5 µA/cm$^2$, (**average = 1.2 µA/cm$^2$**) at 5°C. However for the material in the 600 grit SiC ground condition (Figures 7.14 & 7.15) the average passive current density was **0.8 µA/cm$^2$**at the two test temperatures. At both temperatures the material was passive and the passive current density values were significantly below the 10 µA/cm$^2$ value which has been used [27] as a threshold for the initiation of pitting or general corrosion on S13Cr material. Although the material was

considered to be passive it was noted that that the passive region showed a positive slope on the as-received (AR) specimens tested at both temperatures, whereas for the 600 SiC ground specimens the passive region was more vertical, particularly at higher potential regions, approaching the pitting potential or break-down potential.

To quantify the behaviour of the material in the passive region the passive film area resistance ($k\Omega\text{-}cm^2$) was calculated from the polarisation curves and the values are presented in Table 7.3. It is recognised that this technique will only provide semi-quantitative type results, however the results were considered to be relevant in order to highlight the difference in the shape of the polarisation curves in the passive region. For the tests conducted on the as-received surface at 24°C the values ranged from 52 – 63 $k\Omega\text{-}cm^2$ compared to 53 – 84 $k\Omega\text{-}cm^2$ for the 5°C tests, which was not considered to be significant. Overlapping values over a relatively wide range were also seen for the 600 SiC ground specimens, with the readings varying from 494 – 784 $k\Omega\text{-}cm^2$ for the 24°C tests, compared to 309 – 1003 $k\Omega\text{-}cm^2$ for the 5°C tests. The values did highlight the difference in the characteristics of the passive film between the as-received (AR) and 600 SiC ground surfaces; with the average values for the AR surface being 57 $k\Omega\text{-}cm^2$, and 66 $k\Omega\text{-}cm^2$, for the 24°C and 5°C tests compared to 615 $k\Omega\text{-}cm^2$, and 573 $k\Omega\text{-}cm^2$ for the 600 SiC ground surfaces, at the 24°C and 5°C test temperatures.

The difference between the passive film area resistance of the as-received and the 600 SiC ground surfaces was most likely related to the variation in the surface roughness, which would have increased the effective area of the as received specimen, hence leading to a discrepancy between the true area and the measured area. The area of the specimens was measured using a vernier calliper would not have taken into account the surface roughness, consequently the calculated current density values would reduce as the surface roughness increased. This difference between the true and measured areas would be greater for the as-received surface, with a roughness of 4.2 µm, than the 600 SiC ground surface, with a roughness of 0.1 µm.

The breakdown potential ($E_{bd}$) of the passive film is defined as the potential at which the passivity of the material is reduced due to the breakdown of the protective passive film. The point at which the integrity of the protective film is compromised results in an increase in the current density and this increase can be rapid, due to the onset of significant pitting / crevice corrosion, or more gradual due to more complex localised corrosion behaviour. It can be seen from Figures 7.12 - 7.15 that the breakdown potential was characterised by a change in the slope of the polarisation curve in the case of the specimens with the as-received surface, whereas for the specimens with the 600 SiC ground surface the breakdown of the passive film was more clearly defined by the rapid increase in the corrosion current density. A comparison of the $E_{bd}$ values for the tests conducted at 24°C and 5°C are presented in Tables 7.6 & 7.7.

**Table 7.6** Summary of the $E_{corr}$, $i_{pass}$ and $E_{bd}$ values for the 24°C v 5°C comparative tests with the initial $N_2$ purge gas followed by a 35 mbara $H_2S$ test gas

| Test | Surface condition | Masking material | Temp. | Purge gas | Ecorr (Scan) | Passive current density (ipass) | Breakdown potential (Ebd) | Ecorr - Ebd |
|---|---|---|---|---|---|---|---|---|
| | | | °C | | (mV v SCE) | $\mu A/cm^2$ | (mV v SCE) | (mV) |
| 1 | AR | Epoxy | 24 | $N_2$ | -494 | 2.1 | -318 | 176 |
| 6 | AR | Bees-wax | 24 | $N_2$ | -505 | 2.4 | -336 | 169 |
| **Average** | | | | | **-500** | **2.3** | **-327** | 173 |
| Sr (±) | | | | | 8 | 0.21 | 13 | 5 |
| 95%CI (±) | | | | | 15 | 0.42 | 25 | 10 |
| 3 | AR | Epoxy | 5 | $N_2$ | -463 | 1.0 | -301 | 162 |
| 5 | AR | Bees-wax | 5 | $N_2$ | -464 | 1.1 | -311 | 153 |
| **Average** | | | | | **-464** | **1.1** | **-306** | 158 |
| Sr (±) | | | | | 1 | 0.07 | 7 | 6 |
| 95%CI (±) | | | | | 1 | 0.14 | 14 | 12 |
| 1 | 600 SiC | Epoxy | 24 | $N_2$ | -497 | 0.6 | -278 | 219 |
| 6 | 600 SiC | Bees-wax | 24 | $N_2$ | -509 | 0.7 | -404 | 105 |
| **Average** | | | | | **-503** | **0.7** | **-341** | 162 |
| Sr (±) | | | | | 8 | 0.07 | 89 | 81 |
| 95%CI (±) | | | | | 17 | 0.14 | 175 | 158 |
| 3 | 600 SiC | Epoxy | 5 | $N_2$ | -508 | 0.6 | -298 | 210 |
| 5 | 600 SiC | Bees-wax | 5 | $N_2$ | -523 | 0.8 | -302 | 221 |
| **Average** | | | | | **-516** | **0.7** | **-300** | 216 |
| Sr (±) | | | | | 11 | 0.14 | 3 | 8 |
| 95%CI (±) | | | | | 21 | 0.28 | 6 | 15 |

**Table 7.7** Summary of the $E_{corr}$, $i_{pass}$ and $E_{bd}$ values for the 24°C v 5°C comparative tests with the initial $CO_2$ purge gas followed by a 35 mbara $H_2S$ test gas

| Test | Surface condition | Masking material | Temp. | Purge gas | Ecorr (Scan) | Passive current density (ipass) | Breakdown potential (Ebd) | Ecorr - Ebd |
|---|---|---|---|---|---|---|---|---|
| | | | °C | | (mV v SCE) | ($\mu A/cm^2$) | (mV v SCE) | (mV) |
| | | | | | | | | |
| 2 | AR | Epoxy | 24 | $CO_2$ | -498 | 2.3 | -327 | 171 |
| | | | | | | | | |
| 4 | AR | Epoxy | 5 | $CO_2$ | -471 | 1.5 | -311 | 160 |
| | | | | | | | | |
| 2 | 600 SiC | Epoxy | 24 | $CO_2$ | -537 | 1.1 | -321 | 216 |
| | | | | | | | | |
| 4 | 600 SiC | Epoxy | 5 | $CO_2$ | -532 | 1.0 | -308 | 224 |

It can be seen from Tables 7.6 & 7.7 that a small change in the average breakdown potential values between the two test temperatures was evident; with the 5°C temperature giving higher potential values (i.e. less negative). This would indicate improved localised corrosion resistance at 5°C as compared to 24°C, which would be the expected behaviour for stainless steels in $H_2S$-free chloride ion containing environments.

This was a valid conclusion for the specimens with both the as-received surface and the 600 grit SiC ground surface, although it should be noted that for the 600 SiC grit ground specimens there was a slightly greater spread of values (i.e. from -278 mV to -341 mV) for the 24°C test temperature.

#### 7.3.1.1 Summary

No conclusive differences in the corrosion performance of the material were established between the two test temperatures. However minor differences were detected, as summarised below:

1. The corrosion potential of the as-received surface showed only a slight decrease with decreasing temperature; of 25 mV and 27 mV for the tests conducted with the $N_2$ and $CO_2$ purge, respectively.

2. The specimens prepared with a 600 SiC ground surface did not show any significant change in the corrosion potential with temperature and average values of -531 mV and -529 mV were recorded for the $N_2$ purged solutions and -537 mV and -532 mV for the $CO_2$ purged solutions at the 24°C and 5°C test temperatures.

3. It should be noted that after the 1 hour $H_2S$ purge period although the solution is saturated the corrosion potential readings may not have been stable and consequently a 24 – 48 hour stabilisation period would be recommended for future tests.

4. For the specimens in the as-received condition the passive current density reduced with a reduction in the test temperature, indicating the lower test temperature would be beneficial to the development of the passive film.

5. The 600 SiC surface maintained a low passive current density of 0.8 $\mu A/cm^2$, which was not influenced by the test temperature.

6. The average breakdown potential of the passive film for both surface conditions increased with a reduction in the test temperature. The increase, for the $N_2$ purged tests, being 21 mV for the as-received surface and 41 mV for the 600 SiC ground surface. For the $CO_2$ purged tests the increase was 16 mV for the as-received surface and 13 mV for the 600 SiC ground surface.

### 7.3.2 Influence of Surface Finish (As-received v 600 grit SiC Ground)

The results from the corrosion potential measurements and anodic polarisation tests conducted on specimens with the as-received surface versus specimens with the 600 grit SiC ground surface were compared to establish the Influence of the surface preparation on the corrosion characteristics and in particular the stability of the passive film. This is particularly relevant to SSC tests conducted on weldable martensitic stainless steel where laboratory tests are conducted on specimens with a machined surface versus those with an as-manufactured surface finish which is typically the result of a grit blasting treatment by the steel mill. Also, although welded specimens are not being tested as part of this scope of work, grinding operations are undertaken during the welding preparation. Additionally when laboratory SSC testing is undertaken using FPB SSC specimens with the bore surface 'intact' the side and back faces are typically ground and the corners are slightly chamfered via machining to minimise stress concentrations. Consequently the surface condition is a critical parameter in SSC testing and electrochemical testing enables the interaction between the surface and the test environment to be studied with particular emphasis on the formation and stability of the passive film. The importance of the machined surfaces has been highlighted in previous sections with respect to the potential sensitivity of the machined surfaces to SSC. The possible detrimental effect of machined surfaces was also reported by Enerhaug et al. [45] in 1999 on experience with the qualification of weldable martensitic stainless steel for the Asgard field, where cracking was encountered on the side machined faces of FPB SSC specimens. It should be noted that in that study the machined side faces of the welded specimens were subsequently bees-wax coated and re-tested with acceptable SSC results.

The results of the corrosion potential measurements comparing the as-received (AR) versus the 600 SiC ground surfaces are summarised in Table 7.4 for the $N_2$ purged tests and Table 7.5 for the $CO_2$ purged tests. Under both conditions and at both test temperatures the corrosion potential after the $H_2S$ test gas purge was lower for the for the 600 grit SiC ground surfaces than the as-received surfaces, by 44 mV ($N_2$) and 44 mV ($CO_2$) for the 24°C tests and by 67 mV ($N_2$) and 101 mV ($CO_2$) for the 5°C tests. This clearly illustrates the difference in the passive film characteristics between the two prepared surfaces.

Comparison of the anodic polarisation curves presented in Figures 7.20 & 7.21 showed a clear difference in the shape of the curves, as previously discussed in section 7.3.1, with the specimens with the 600 SiC ground surface showing a steeper transition through the passive region than the specimens with the as-received surface. Also the passive current density values were lower for the 600 SiC ground specimens. At 24°C the average passive current density was 2.3 µA/cm$^2$for the as-received surface compared to 0.65 µA/cm$^2$, for the 600 grit SiC ground surface. At the 5°C test temperature the average values were also reduced from 1.05 µA/cm$^2$, for the as-received surface to 0.7 µA/cm$^2$, for the 600 SiC ground surface.

The difference in the surface roughness of the as-received and 600 SiC ground specimens would have an Influence on the exposed surface area in contact with the test environment. In section 5.7 the surface roughness was reported to be 4.2 µm for the as-received surface compared to 0.1 µm for the 600 SiC ground surface. Since the corrosion currents during the electrochemical tests are expressed as a current density, to take into account the exposed area, the current density values expressed for the as-received specimens with the relative coarse surface finish would over-estimated. It is therefore possible that higher values recorded for the as-received specimens were related to the increased area due to the surface roughness.

It was clearly evident from the majority of the corrosion potential v time plots, shown in Figures 7.2 – 7.11, that the as-received surface had a more stable passive film as a function of exposure time in solution than the 600 SiC ground surface and that the potential on the as-received specimens generally took longer to stabilise once the $H_2S$ was introduced into the test solution. The only exceptions to this behaviour were for tests 9 and 10, where similar potentials were seen for both surfaces during the initial $N_2$ and $CO_2$ purge periods, as shown in Figure 7.10 (test 9) and Figure 7.11 (test 10). The difference in the behaviour of these could not be explained and further work would be beneficial to understand the differences in the initial passive films between the two surfaces.

The passive film breakdown values ($E_{bd}$) and the difference between the corrosion potential ($E_{corr}$) and the breakdown potential values ($E_{corr} – E_{bd}$) were compared for the two surface finished and for the tests conducted at the two test temperatures with the two different purge gasses. The values are summarised in Tables 7.6 & 7.7. Taking into account the standard deviation where duplicate tests were conducted (Table 7.6) the results were comparable between the two surface finishes.

#### 7.3.2.1 Summary

The surface condition on the specimens was found to have strong Influence on the electrochemical results obtained, as summarised below:

1. The as-received surface was considered to have a more strongly developed passive film than the 600 grit SiC ground finish, which was reflected in the higher potential readings during the initial $N_2$ or $CO_2$ purge periods.

2. Following the $H_2S$ purge the corrosion potentials of the as-received and 600 grit SiC ground specimens converged to reach a value in the region of -500 mV.

3. The potentials after the initial $H_2S$ purge were generally less negative for the as-received specimens and it would be of interest to study the change in potential with time for both surfaces.

4. There was a noticeable difference in the slope of the passive region between the two surface conditions, with the inclination being steeper for the 600 SiC ground surface. This was considered to be due to the growth of the passive film being more rapid on the freshly prepared 600 SiC ground surface compared to the as-received surface which would have already formed a stable film during the prior manufacturing processes.

5. The passive film resistance to breakdown was similar for both surface conditions.

6. Both surface conditions were passive in the 100,000 mg/L Cl, pH 4, 35 mbara $H_2S$ test environment and the maximum current densities recorded (i.e. 2.4 µA/cm$^2$) were significantly below the 10 µA/cm$^2$, value which is often used as a guide to indicate active corrosion in these materials.

7. The passive current density values were generally higher on the as-received specimens and this may have been related to the difference in the roughness between the as-received surface with a roughness value (Ra) of 4.2 µm compared to the 600 SiC ground surface with a roughness value (Ra) of 0.1 µm. This roughness difference would have increased the effective area of the as-received specimens, which would reduce the reported passive current density values.

8. The tests have highlighted the difference between testing as-received and machined surfaces, which demonstrates the importance of testing the actual surfaces which will be in contact with the corrosive environment.

### 7.3.3 Influence of $H_2S$ Concentration

The Influence of $H_2S$ on the electrochemical behaviour of the as-received and 600 SiC ground surfaces has been investigated in the 100,000 mg/L Cl simulated produced water environment at a pH of 4.5 at two $H_2S$ partial pressure concentrations (i.e. 35 mbara and 69 mbara) and with the $N_2$ and $CO_2$ initial purge. The initial corrosion potential measurements, taken prior to the anodic potentiodynamic polarisation measurements are summarised in Table 7.8. The initial series of tests conducted with the $N_2$ purge gas on the AR specimens clearly showed the Influence of the two $H_2S$ concentrations on the corrosion potential of the material, with the values reducing from -194 mV for the $N_2$ test down to -494mV for the 35mbara $H_2S$ test and to -511 mV for the 69 mbara $H_2S$ test. This trend was followed for the measurements conducted with the $CO_2$ test gas and purge gas on the as-received specimens, where the potential reduced from -59 mV for the $CO_2$ test down to -498mV for the 35 mbara $H_2S$ test and down to -516 mV for the 69 mbara $H_2S$ test. These results indicated that a passive film was present on the as-received specimens and that the film had been degraded by the influence of the $H_2S$. It was interesting to note that for both the $N_2$ purged and $CO_2$ purged $H_2S$ tests the potential was lower with the higher partial pressure of $H_2S$, although the decrease was not considered to be significant.

**Table 7.8** Summary of corrosion potential measurements showing the influence of the $H_2S$ concentration

| Test | Surface condition | Masking material | Temp. | Purge gas | Test gas | pH | Ecorr (Purge) | | | | Ecorr (scan) |
|---|---|---|---|---|---|---|---|---|---|---|---|
| | | | | | | | Initial purge | | Test gas purge | | |
| | | | °C | | | | Start (mV) | Finish (mV) | Start (mV) | Finish-1hr (mV) | (mV v SCE) |
| | | | | | | | | | | | |
| 8 | AR | Epoxy | 24 | $N_2$ | $N_2$ | 5.6 | 0 | -146 | -147 | -183 | -194 |
| 1 | AR | Epoxy | 24 | $N_2$ | 35mbara $H_2S$ | 4.5 | -212 | -225 | -165 | -489 | -494 |
| 9 | AR | Epoxy | 24 | $N_2$ | 69 mbara $H_2S$ | 4.5 | -146 | -247 | -152 | -501 | -511 |
| | | | | | | | | | | | |
| 7 | AR | Epoxy | 24 | $CO_2$ | $CO_2$ | 4.5 | 56 | 0 | 0 | -31 | -59 |
| 2 | AR | Epoxy | 24 | $CO_2$ | 35mbara $H_2S$ | 4.5 | -23 | -115 | -123 | -497 | -498 |
| 10 | AR | Epoxy | 24 | $CO_2$ | 69 mbara $H_2S$ | 4.5 | -264 | -530 | -515 | -525 | -516 |
| | | | | | | | | | | | |
| 8 | 600 SiC | Epoxy | 24 | $N_2$ | $N_2$ | 5.6 | -617 | -666 | -658 | -658 | -663 |
| 1 | 600 SiC | Epoxy | 24 | $N_2$ | 35mbara $H_2S$ | 4.5 | -651 | -615 | -522 | -522 | -497 |
| 9 | 600 SiC | Epoxy | 24 | $N_2$ | 69 mbara $H_2S$ | 4.5 | -146 | -262 | -524 | -524 | -510 |
| | | | | | | | | | | | |
| 7 | 600 SiC | Epoxy | 24 | $CO_2$ | $CO_2$ | 4.5 | -507 | -502 | -497 | -497 | -491 |
| 2 | 600 SiC | Epoxy | 24 | $CO_2$ | 35mbara $H_2S$ | 4.5 | -537 | -530 | -541 | -541 | -537 |
| 10 | 600 SiC | Epoxy | 24 | $CO_2$ | 69 mbara $H_2S$ | 4.5 | -530 | -510 | -518 | -518 | -519 |

The results were different for the 600 SiC ground surface than the as-received surface and the behaviour with increasing $H_2S$ concentration was not so clear. For the $N_2$ gas test the potential fell to -663 mV, following the saturation period, which is a value to be expected for a 'freshly ground' sample under fully de-aerated $N_2$ purged conditions. Adding $H_2S$ to the solution and decreasing the pH from 5.6 ($N_2$ purged condition) to 4.5 resulted in a decrease in the potential to -497 mV and -510 mV for the 35 mbara and 69 mbara $H_2S$ partial pressures, respectively. These saturated $H_2S$ values were similar to the values recorded for the AR specimens and the same trend was observed, with the potential reducing with increasing partial pressure of $H_2S$. For the final series of tests conducted on the 600 SiC ground specimens with $CO_2$ gas, the $CO_2$ gas test stabilised at a potential of -491 mV, which was higher than for the $N_2$ gas test (i.e. -663 mV) and the difference could be explained by the change in pH from 5.6 to 4.5.Sidorin et al. [26] observed an increasing potential with decreasing pH for tests conducted at 60°C and Lee et al. [28] recorded an Ecorr value of -530 mV for a saturated $CO_2$ solution at a pH of 4.5, although the chloride content used in the later work was 178,000 mg/L compared to 100,000 mg/L for the current tests, which would explain the lower value. Also Marchebois et al. [15] reported a potential of -470 mV for a 100 g/L NaCl (approximately 60,000 mg/L Cl) solution saturated with $CO_2$ at 25°C, although the pH was only 3.5. Under the $CO_2$ purged conditions the corrosion potential of the 69 mbara $H_2S$ test was lower than the 35 mbara test, which was contrary to the other three tests. In fact the 69 mbara $H_2S$ potential was similar to the other three tests and the variation in the trend was due to 35 mbara $H_2S$ potential being higher than the previous tests at -537 mV.

The anodic potentiodynamic polarisation curves are presented in Figures 7.24 – 7.27 and a summary of the $E_{corr}$, $I_{pass}$ and $E_{bd}$ values taken from the curves are shown in Table 7.9. The difference between the corrosion potential and breakdown potential is also shown. The two series of tests conducted on the as-received surface show a significant increase in the passive current density and a decrease in the breakdown potential between the $H_2S$-free and 35 mbara $H_2S$ showing the greater susceptibility of the material to corrosion in $H_2S$-containing environments. However the material was still passive and the Ecorr-$E_{bd}$ values were 176 mV and 171 mV for the $N_2$ purged and $CO_2$ purged tests, respectively, indicating the material was in a 'safe' region regarding the breakdown of the passive film.

**Table 7.9** Summary of the $E_{corr}$, $i_{pass}$ and $E_{bd}$ values for the tests conducted to show the influence of $H_2S$ on the electrochemical test results. All tests conducted at 24°C in 100,000 mg/L Cl at a pH of 4.5 for the $CO_2$ and $H_2S$ tests and a pH of 5.6 for the $N_2$ only tests.

| Test | Surface condition | Masking material | Temp. | Purge gas | Test gas | Ecorr (scan) | Passive current density (ipass) | Breakdown potential (Ebd) | Ecorr-Ebd |
|---|---|---|---|---|---|---|---|---|---|
| | | | °C | | | (mV v SCE) | ($\mu A/cm^2$) | (mV v SCE) | (mV) |
| | | | | | | | | | |
| 8 | AR | Epoxy | 24 | $N_2$ | $N_2$ | -194 | 0.1 | 58 | 252 |
| 1 | AR | Epoxy | 24 | $N_2$ | 35mbara $H_2S$ | -494 | 2.1 | -318 | 176 |
| 9 | AR | Epoxy | 24 | $N_2$ | 69 mbara $H_2S$ | -511 | 4.4 | -315 | 196 |
| | | | | | | | | | |
| 7 | AR | Epoxy | 24 | $CO_2$ | $CO_2$ | -59 | 0.2 | 130 | 189 |
| 2 | AR | Epoxy | 24 | $CO_2$ | 35mbara $H_2S$ | -498 | 2.3 | -327 | 171 |
| 10 | AR | Epoxy | 24 | $CO_2$ | 69 mbara $H_2S$ | -516 | 2.2 | -243 | 273 |
| | | | | | | | | | |
| 8 | 600 SiC | Epoxy | 24 | $N_2$ | $N_2$ | -663 | 0.6 | 46 | 709 |
| 1 | 600 SiC | Epoxy | 24 | $N_2$ | 35mbara $H_2S$ | -497 | 0.6 | -278 | 219 |
| 9 | 600 SiC | Epoxy | 24 | $N_2$ | 69 mbara $H_2S$ | -510 | 0.8 | -329 | 181 |
| | | | | | | | | | |
| 7 | 600 SiC | Epoxy | 24 | $CO_2$ | $CO_2$ | -491 | 1.5 | -96 | 395 |
| 2 | 600 SiC | Epoxy | 24 | $CO_2$ | 35mbara $H_2S$ | -537 | 1.1 | -321 | 216 |
| 10 | 600 SiC | Epoxy | 24 | $CO_2$ | 69 mbara $H_2S$ | -519 | 1.1 | -305 | 214 |

Increasing the $H_2S$ partial pressure from 35 mbara to 69 mbara on the tests conducted with the $N_2$ gas purge resulted in a significant increase in the passive current density from 2.1 $\mu A/cm^2$ to 4.4 $\mu A/cm^2$, which would be indicative of a weakening of the passive film. However the breakdown potential remained unchanged and the $E_{corr} - E_{bd}$ value increased over the 35 mbara $H_2S$ test indicating the overall effect of increasing the $H_2S$ partial pressure was not significant with regard to the stability of the passive film. For the second test conducted with a $CO_2$ purge gas the 69 mbara $H_2S$ test was not considered to be valid, since it can be seen from Figure 7.25 that the initial trace appeared normal and followed the shape of the 35 mbara $H_2S$ test at a lower potential. The trace then increased rapidly in a vertical direction indicating the formation of the passive film although the trace was unstable and was not in line with the other 69 mbara $H_2S$ tests.

For the two series of tests conducted with the 600 SiC ground prepared surface the passive current densities remained relatively low for the tests conducted in the $H_2S$-free, 35 mbara $H_2S$ and 69 mbara $H_2S$ conditions and in-fact the passive current density reduced from 1.5 $\mu A/cm^2$ to 1.1 $\mu A/cm^2$ for the $CO_2$ tests and remained at 1.1 $\mu A/cm^2$ even when the $H_2S$ partial pressure was increased from 35 mbara to 69 mbara.

7.3.3.1 Summary

1. A rapid change in corrosion potentials was seen for the majority of the tests when the $H_2S$ was introduced with the potentials stabilising in the region of -500 mV. At this potential the material is passive.

2. The recorded potentials were similar for both of the $H_2S$ concentrations and the effect of the increase in the $H_2S$ partial pressure from 35 mbara to 69 mbara was not found to be significant.

### 7.3.4 Influence of Coating

The Influence of the coating or masking material on the on the electrochemical behaviour of the as-received and 600 SiC ground surfaces has been investigated in the 100,000 mg/L Cl simulated produced water environment at a pH of 4.5 with a $N_2$ initial purge.

The initial corrosion potential measurements taken prior to the anodic potentiodynamic polarisation measurements are summarised in Table 7.10. It can be seen from the table that there were variations in the initial nitrogen purge potentials between the samples, however this was considered to be related to the time required for the potentials to stabilise and was not a function of the coating. Following the $H_2S$ saturation period the corrosion potential of the epoxy and bees-wax coated samples showed close agreement with a maximum standard deviation (Sr) of 13 mV (± 25 mV 95%CI) being measured. It is recognised that this is not a good statistical method being based on two tests, however all of the tests showed relatively low Sr (95%CI) values and therefore it was considered to be a valid approach.

**Table 7.10** Summary of corrosion potential measurements showing the influence of the masking material (epoxy v bees-wax). Test conditions: 100,000 mg/L PW, pH 4.5, 35 mbara $H_2S$, $N_2$ purge gas.

| Test | Surface condition | Masking material | Temp. (°C) | Purge gas | Ecorr (purge) | | | | Ecorr (scan) |
|---|---|---|---|---|---|---|---|---|---|
| | | | | | Initial purge | | Test gas purge | | |
| | | | | | Start (mV) | Finish (mV) | Start (mV) | Finish-1 hr (mV) | (mV v SCE) |
| | | | | | | | | | |
| 1 | AR | Epoxy | 24 | $N_2$ | -212 | -225 | -165 | -489 | -494 |
| 6 | AR | Bees-wax | 24 | $N_2$ | -151 | -264 | -179 | -484 | -505 |
| **Ave** | | | | | **-182** | **-245** | **-172** | **-487** | **-500** |
| Sr (±) | | | | | 43 | 28 | 10 | 4 | 8 |
| 95%CI (±) | | | | | 85 | 54 | 19 | 7 | 15 |
| 3 | AR | Epoxy | 5 | $N_2$ | -3 | -176 | -60 | -464 | -463 |
| 5 | AR | Bees-wax | 5 | $N_2$ | -137 | -195 | -64 | -459 | -464 |
| **Ave** | | | | | **-70** | **-186** | **-62** | **-462** | **-464** |
| Sr (±) | | | | | 95 | 13 | 3 | 4 | 1 |
| 95%CI (±) | | | | | 186 | 26 | 6 | 7 | 1 |
| 1 | 600 SiC | Epoxy | 24 | $N_2$ | -651 | -615 | -568 | -522 | -497 |
| 6 | 600 SiC | Bees-wax | 24 | $N_2$ | -179 | -701 | -622 | -540 | -509 |
| **Ave** | | | | | **-415** | **-658** | **-595** | **-531** | **-503** |
| Sr (±) | | | | | 334 | 61 | 38 | 13 | 8 |
| 95%CI (±) | | | | | 654 | 119 | 75 | 25 | 17 |
| 3 | 600 SiC | Epoxy | 5 | $N_2$ | -617 | -704 | -560 | -520 | -508 |
| 5 | 600 SiC | Bees-wax | 5 | $N_2$ | -173 | -677 | -604 | -537 | -523 |
| **Ave** | | | | | **-395** | **-691** | **-582** | **-529** | **-516** |
| Sr (±) | | | | | 314 | 19 | 31 | 12 | 11 |
| 95%CI (±) | | | | | 615 | 37 | 61 | 24 | 21 |

The anodic potentiodynamic polarisation curves are presented in Figures 7.32 – 7.33 and a summary of the $E_{corr}$, $I_{pass}$ and $E_{bd}$ values taken from the curves are shown in Table 7.11.The polarisation curves were generally similar between the epoxy and bees-wax coated samples and the measured parameters (i.e. $E_{corr}$, $I_{pass}$ and $E_{bd}$) were all in close agreement.

**Table 7.11** Summary of the $E_{corr}$, $i_{pass}$ and $E_{bd}$ values for the tests conducted to show the influence of the masking material on the electrochemical test results.
Test conditions: 100,000 mg/L PW, pH 4.5, 35 mbara $H_2S$, $N_2$ purge gas.

| Test | Surface condition | Masking material | Temp. | Purge / test gas | Ecorr (scan) | Passive current density (ipass) | Breakdown potential (Ebd) | Ecorr-Ebd |
|---|---|---|---|---|---|---|---|---|
| | | | °C | | (mV v SCE) | ($\mu A/cm^2$) | (mV v SCE) | (mV) |
| | | | | | | | | |
| 1 | AR | Epoxy | 24 | $N_2$ | -494 | 2.1 | -318 | 176 |
| 6 | AR | Bees-wax | 24 | $N_2$ | -505 | 2.4 | -336 | 169 |
| **Average** | | | | | **-500** | **2.3** | **-327** | **173** |
| Sr (±) | | | | | 8 | 0.21 | 13 | 5 |
| 95%CI (±) | | | | | 15 | 0.42 | 25 | 10 |
| 3 | AR | Epoxy | 5 | $N_2$ | -463 | 1.0 | -301 | 162 |
| 5 | AR | Bees-wax | 5 | $N_2$ | -464 | 1.1 | -311 | 153 |
| **Average** | | | | | **-464** | **1.1** | **-306** | **158** |
| Sr (±) | | | | | 1 | 0.07 | 7 | 6 |
| 95%CI (±) | | | | | 1 | 0.14 | 14 | 12 |
| 1 | 600 SiC | Epoxy | 24 | $N_2$ | -497 | 0.6 | -278 | 219 |
| 6 | 600 SiC | Bees-wax | 24 | $N_2$ | -509 | 0.7 | -404 | 105 |
| **Average** | | | | | **-503** | **0.7** | **-341** | **162** |
| Sr (±) | | | | | 8 | 0.07 | 89 | 81 |
| 95%CI (±) | | | | | 17 | 0.14 | 175 | 158 |
| 3 | 600 SiC | Epoxy | 5 | $N_2$ | -508 | 0.6 | -298 | 210 |
| 5 | 600 SiC | Bees-wax | 5 | $N_2$ | -523 | 0.8 | -302 | 221 |
| **Average** | | | | | **-516** | **0.7** | **-300** | **216** |
| Sr (±) | | | | | 11 | 0.14 | 3 | 8 |
| 95%CI (±) | | | | | 21 | 0.28 | 6 | 15 |

7.3.4.1 Summary

1. The results were generally comparable between the epoxy coated and bees-wax coated specimens. However it was considered that the epoxy coating was easier to apply and the samples could be de-greased after the application of the coating. Adequate degreasing was more difficult with the bees-wax coating since the coating was softer and more sensitive to solvents.

2. The masking / coating medium should not Influence the corrosion potential or passive current density values, however the medium can Influence the breakdown potential, in particular by promoting crevicing, which may lead to lower values. It should be noted that the tested specimens did exhibit evidence of crevicing although this was generally not severe. However further work would be beneficial to develop an optimised test method, in particular where the as-manufactured or as-received surface are required to be left intact.

### 7.3.5 Influence of Purge Gas

The Influence of the purge gas (i.e. $N_2$ v $CO_2$) on the on the electrochemical behaviour of the as-received and 600 grit SiC ground surfaces has been investigated in the 100,000 mg/L Cl simulated produced water environment at a pH of 4.5 for $CO_2$ and 5.6 for $N_2$.

The initial corrosion potential measurements taken prior to the anodic potentiodynamic polarisation measurements are summarised in Table 7.12. It can be seen from the table that there were significant differences between the corrosion potential measurements for both the AR and the 600 grit SiC ground specimens. For the AR specimens after the 2 hr purge period with the two respective test gases (i.e. $N_2$ and $CO_2$) the potential was 152 mV higher with the $CO_2$ gas purge compared with the $N_2$ gas purge. A similar trend was evident on the 600grit SiC ground specimens, with the potential being 161 mV higher with the $CO_2$ gas purge.

**Table 7.12** Summary of corrosion potential measurements showing the influence of the purge gas Test conditions: 100,000 mg/L PW at 24°C, $N_2$ purge (pH 5.6) and $CO_2$ purge (pH 4.5).

| Test | Surface condition | Masking material | Temp | Purge gas | Test gas | pH | Ecorr (purge) | | | | Ecorr (scan) |
|---|---|---|---|---|---|---|---|---|---|---|---|
| | | | | | | | Initial purge | | Test gas purge | | |
| | | | °C | | | | Start (mV) | Finish (mV) | Start (mV) | Finish-1 hr (mV) | (mV v SCE) |
| | | | | | | | | | | | |
| 8 | AR | Epoxy | 24 | $N_2$ | $N_2$ | 5.6 | 0 | -146 | -147 | -183 | -194 |
| | | | | | | | | | | | |
| 7 | AR | Epoxy | 24 | $CO_2$ | $CO_2$ | 4.5 | 56 | 0 | 0 | -31 | -59 |
| | | | | | | | | | | | |
| 8 | 600 SiC | Epoxy | 24 | $N_2$ | $N_2$ | 5.6 | -617 | -666 | -666 | -658 | -663 |
| | | | | | | | | | | | |
| 7 | 600 SiC | Epoxy | 24 | $CO_2$ | $CO_2$ | 4.5 | -507 | -502 | -498 | -497 | -491 |

The anodic potentiodynamic polarisation curves are presented in Figure 7.36 and a summary of the $E_{corr}$, $I_{pass}$ and $E_{bd}$ values taken from the curves are shown in Table 7.13. From Figure 7.36 and Table 7.13 it can be seen that there was a large variation in the anodic polarisation behaviour between the two test gases (i.e. $N_2$ & $CO_2$) and in particular between the as-received (AR) and 600 SiC ground surfaces.

The surface / test gas showing the highest corrosion resistance was the as-received surface with the $CO_2$ test gas, where the passive current density was very low at 0.2 µA/cm$^2$ and the breakdown potential was highest out of all of the tests at 130 mV. The corrosion potential for this sample was also high at -59 mV, demonstrating that the as-received surface had a 'protective' passive film, which compared to the nitrogen purged test with a corrosion potential of -194 mV, appeared to have been enhanced by the $CO_2$ gas purge. It was interesting to note that when the same conditions were applied to the 600 SiC ground surface any beneficial effects of the $CO_2$ were not seen in the results, since the test on sample 6007 had the highest passive current density and the lowest breakdown potential of -96 mV. Consequently from the limited results the enhancement of the passive film in the presence of $CO_2$ was only seen on the as-received surface.

**Table 7.13** Summary of the $E_{corr}$, $i_{pass}$ and $E_{bd}$ values for the tests conducted to show the influence of the purge gas on the electrochemical test results.
Test conditions: 100,000 mg/L PW, pH 4.5, 35 mbara $H_2S$.

| Test | Surface condition | Masking material | Temp | Purge gas | Ecorr (scan) | Passive current density (ipass) | Breakdown potential (Ebd) | Ecorr-Ebd |
|---|---|---|---|---|---|---|---|---|
| | | | °C | | (mV v SCE) | (µA/cm$^2$) | (mV v SCE) | (mV) |
| | | | | | | | | |
| 8 | AR | Epoxy | 24 | $N_2$ | -194 | 0.1 | 58 | 252 |
| 7 | AR | Epoxy | 24 | $CO_2$ | -59 | 0.2 | 130 | 189 |
| | | | | | | | | |
| 8 | 600 SiC | Epoxy | 24 | $N_2$ | -663 | 0.6 | 46 | 709 |
| 7 | 600 SiC | Epoxy | 24 | $CO_2$ | -491 | 1.5 | -96 | 395 |

The potential beneficial effects of $CO_2$ on the corrosion and SSC resistance have previously been shown by Enerhaug et al. [29]. The authors demonstrated the beneficial effects of a short-term treatment with $CO_2$ in order to provide a mild oxidising agent to develop the passive films in the heat tint region of weldable martensitic stainless steel girth welds. Following the treatment the passive film potential increased from -470 mV up to approximately -200 mV where it was reported to remain stable. This value is significantly lower than the -59 mV value recorded for the test on the as-received surface and similar to the -194 mV value recorded for the as-received surface in the $N_2$ purge gas. Enerhaug et al. [29] reported the passive film broke down and led to pitting at a potential in the region of 100 mV, which was similar to the 130mV value measured for the AR specimen 7 which had been exposed to the $CO_2$ purge for 2 hrs. at 24°C before the polarisation test.

It should be noted that Statoil now include a 48 hr pre-exposure to $CO_2$ at 90°C in their test procedures for SSC testing of weldable martensitic stainless steel girth welds. The reasoning behind the treatment is that the bore surfaces of pipelines may see fresh water or produced water conditions (without the presence of $H_2S$) during commissioning or early production and as a consequence these conditions provide a mildly oxidising environment thus allowing the strengthening of passive films in the heat tint region. However the same reasoning would apply to the parent pipe surfaces and the passive films from the manufacturing operations may also benefit from pre-exposure to a mildly oxidising environment before exposure to the aggressive $H_2S$ conditions. Purging with nitrogen for a long period would not be beneficial, since it would not provide the mild oxidising conditions required for passivation.

7.3.5.1 Summary

1. For both the $N_2$ and $CO_2$ purge gases there was a difference of approximately 160 mV (152 mV / 161 mV) in the corrosion potential values, for both the AR and the 600 SiC ground specimens, with the $N_2$ purge gas generating more negative potentials. The potential difference between the two gases was most likely due to the pH variation, with the $CO_2$ pH being 4.5 compared to 5.6 for the $N_2$ test environment.

2. The purge gas used for the tests did have a significant Influence on the polarisation curves.

3. The use of the $CO_2$ purge as opposed to the $N_2$ purge had a beneficial effect on the development of a more stable passive film (as indicated by the breakdown potential) on the as-received surface only. On the 600 SiC ground sample the reverse was found with the passive current density being higher and the breakdown potential lower for the $CO_2$ purge condition compared to the $N_2$ purge condition.

4. The beneficial effects of a $CO_2$ purge gas pre-treatment of weldable 13%Cr stainless steels has previously been reported [29] and is currently being adopted by Statoil AS [114] for their SSC tests on welded 13%Cr martensitic stainless steel.

# CHAPTER 8: SUMMARY DISCUSSION

One aim of the thesis was to establish if any correlation existed between the SSC behaviour of the material and the results from the laboratory electrochemical tests. It has been demonstrated that the material does exhibit a greater susceptibility to SSC at the typical seabed temperature of 5°C compared to ambient temperature (i.e. 24°C). In addition to the temperature factor the susceptibility of the material to SSC was found to be influenced by the surface condition, with the as-manufactured surface providing enhanced resistance to SSC, at both temperatures compared to the 600 grit SiC ground surface. The Influence of the stress concentration, at the edges and over the central rollers was also found to be a factor in the crack initiation. Finally the environment was another factor with cracking being observed in the pH 4.5, 100,000 mg/L $Cl^-$ PW environment but not in the pH 3.5 1,000 mg/L $Cl^-$ CW environment.

Electrochemical testing using corrosion potential measurements and anodic potentiodynamic polarisation scans were conducted under the same conditions as for the SSC tests (the CW environment was not used for the electrochemical tests since no SSC cracking was observed). The electrochemical measurements conducted did not show any correlation with the SSC cracking trend as a function of the test temperature. Consequently the electrochemical tests could not explain the increased cracking susceptibility with decreasing temperature. If the increased susceptibility to cracking is not related to any changes in passivity then it may be related to changes in the solution chemistry (i.e. increased solubility of oxygen and $H_2S$), a decrease in the pitting resistance or an increase in the amount of trapped hydrogen. For the SSC tests conducted, the oxygen was continuously monitored so oxygen was not thought to be the problem. The solubility of $H_2S$ does increase significantly at low temperatures and the measurements taken at Exova, shown in Figure 2.13 revealed the $H_2S$ solubility for the PW solution nearly doubled from 24°C to 5°C. Consequently this could be a factor due to the significant increase in the concentration of $H_2S$ available to disrupt the passive film. If the passive film remains relatively unchanged with the decreasing temperature it is unlikely that the hydrogen concentration would increase since active corrosion, localised corrosion or plastic straining would be required to allow hydrogen to enter the material. However it was evident that

the cracking observed was associated with pitting corrosion at the surface which is the more typical nature of the crack initiation in the high chloride ion content produced waters. The presence of the localised corrosion would allow hydrogen to enter the surface and combined with the high stresses applied to the specimens could result in the low temperature SSC. However the difference in the amount of hydrogen entering the steel between 24°C and 5°C is unlikely to be significant. This assumption was supported by the work of Hinds *et al.* [31]. Their research showed that over the temperature range of 5°C to 70°C the concentration of reversibly trapped hydrogen was not significantly Influenced in a charged super martensitic stainless steel with 12 % retained austenite. Also Turnbull et al. [60] reported that for a AISI 410 martensitic stainless steel over a temperature range of 23 – 80°C the increase in the reversibly trapped hydrogen with decreasing temperature is counterbalanced by the decrease in the lattice hydrogen concentration, so the cracking resistance is not temperature dependent.

It is a possibility that the passive film on the SSC specimens was being disrupted during the test as a result of the high surface strain (i.e. 7300 με). The disruption of the film would increase the likelihood of local pit initiation, leading to cracking. This theory would tie in with the fact that the majority of the cracks were located in areas of high plastic strain, at the edges of the specimens and above the inner rollers. However this theory would not fully explain the reason for the increased cracking at 5°C compared to 24°C and it would be of interest to conduct further work to repeat the electrochemical testing on specimens which had been strained in the same manner as the FPB SSC tests to address this question.

The mechanical tests conducted on the material showed a low ductile-brittle transition temperature of -100°C and similar tensile and flexural bend properties at the two test temperatures, therefore the influence of the mechanical properties on the low temperature cracking can be discounted.

The SSC tests revealed that the material was more susceptible to cracking in the 600 SiC ground condition, which could be related to the differences in electrochemical test results since the as-received surface was considered to have a more strongly developed passive film than the 600 SiC ground finish, which was reflected in the higher potential readings during the initial $N_2$ or $CO_2$ purge periods.

# CHAPTER 9: CONCLUSIONS

1. In the high chloride produced water environment at a pH of 4.5 the material was found to be more susceptible to SSC at 5°C compared to 24°C.

2. The as-received surface provided improved SSC resistance compared to the 600 SiC ground surface. Therefore the material should be tested with the as-received surface intact whenever possible in order to optimise the SSC resistance and provide a more representative test sample.

3. Cracking was observed on the specimens along the edges of the stressed face and directly above the centre rollers and these cracks were considered to have been influenced by stress (strain) concentration effects.

4. The stress (strain) applied to the FPB specimens was determined from flexural bend test data which resulted in the application of surface strains 24 – 25% higher than for strains calculated by the tensile test method. These high strains were considered to have Influenced the results and it is recognised that the application of strains from flexural bend data is too severe, particularly at the 100% AYS values applied for CRA testing.

5. The PW solution with the 100,000 mg/L $Cl^-$ concentration and a pH of 4.5 provided a more aggressive environment than the 1,000 mg/L $Cl^-$ / pH 3.5 CW solution.

6. The ductile to brittle transition temperature was -100°C and there were no significant differences between the 24°C and 5°C tensile and flexural bend results, therefore it was not considered the SSC results had been influenced by any changes in material properties with temperature.

7. The retained austenite content of the material was 12.9% (9.8 – 15.7%), which was considered to be typical for this type of martensitic stainless steel.

8. The corrosion potential and passive film characteristics were not found to be significantly influenced by the change in temperature and consequently the electrochemical testing conducted could not explain the reason for the difference in the SSC behaviour between 24°C and 5°C. However it is recognised that further electrochemical testing would be beneficial on stressed specimens, where the passive film would be influenced by the surface stress.

9. The electrochemical test results did highlight differences between the as-received and the 600 SiC ground surfaces:
    a. The as-received surface was considered to have a more strongly developed passive film than the 600 SiC ground surface, which was reflected in the higher potential readings during the initial $N_2$ or $CO_2$ purge periods.
    b. The corrosion potentials after the initial $H_2S$ purge were generally lower for the as-received specimens and it would be of interest to study the evolution in potential with time for both surfaces.
    c. There was a noticeable difference in the slope of the passive region between the two surface conditions, with the inclination being steeper for the 600 SiC ground surface. This was considered to be due to the growth of the passive film being more rapid on the freshly prepared 600 SiC ground surface compared to the as-received surface which would have already formed a stable film during the prior manufacturing processes.

10. The as-received and 600 SiC ground surface conditions were passive in the 100,000 mg/L $Cl^-$, pH 4, 35 mbara $H_2S$ test environment and the maximum current densities recorded (i.e. 2.4 $\mu A/cm^2$) were significantly below the 10 $\mu A/cm^2$ value, which is often used as a guide to indicate active corrosion in these materials.

11. The use of the $CO_2$ purge as opposed to the $N_2$ purge had a beneficial effect on the development of a more stable passive film (as indicated by the increased value of the breakdown potential) on the as-received surface only. On the 600 SiC ground sample the reverse was found with the passive current density being higher and the breakdown potential lower for the $CO_2$ purge condition compared to the$N_2$ purge condition.

# CHAPTER 10: FURTHER WORK

It was considered that the following further work would be beneficial in order to obtain a clearer understanding on the Influence of the specimen and test conditions on the SSC susceptibility and passive film characteristics:

1. Conduct full ring tests at the 24°C and 5°C test temperatures in the PW solution with 69 mbara $H_2S$ to eliminate the Influence of cut faces and stress concentrations on the crack initiation.

2. Repeat the PW tests at the two test temperatures and with the two test surface conditions using the lower strain value obtained from tensile test data, in accordance with ISO 15156 / NACE MR0175 [3], to establish the Influence of stress.

3. Repeat the electrochemical test work on stressed FPB specimens to investigate the Influence of stress on the stability of the passive film during the initial gas purge (i.e. $N_2$ or $CO_2$), during the $H_2S$ gas purge and the during the anodic polarisation scans. This work will provide a better understanding of the relationship between the passive film and the initiation of pitting / cracking at the two test temperatures and in the two surface conditions.

4. Investigate alternative masking materials and procedures to eliminate the likelihood of crevice corrosion.

5. Conduct Electrochemical Impedance Spectroscopy (EIS) measurements during the initial gas purge (i.e. $N_2$ or $CO_2$) and during the $H_2S$ purge periods on un-stressed coupons to better characterise the passive film development.

6. Investigate the Influence of ‘pre-conditioning’ of the surfaces on the SSC resistance as well as on the electrochemical behaviour by exposure to $CO_2$ saturated solutions.

# REFERENCES


[1] *NACE MR0175 / ISO 15156-1: Petroleum and Natural Gas industries — Materials for use in $H_2S$-Containing Environments in Oil & Gas Production - Part 1: General Principals for Selection of Cracking-Resistant Materials*. 2009.

[2] A. J. Bishop, "Investigation of Sour Duty Stability and Tolerance to Hydrogen Generated from a Cathodic Protection Ststem for Weldable Super-Martensitic Stainless Steel for Pipeline Applications," 2005.

[3] *NACE MR0175 / ISO 15156-3: Petroleum and Natural Gas industries — Materials for use in $H_2S$-Containing Environments in Oil & Gas Production - Part 3: Cracking-Resistant CRAs (Corrosion-Resistant Alloys) and Other Alloys*. 2009.

[4] *API Specification 5CT - Specification for Casing and Tubing*, no. 9. www.api.org/publications, 2011.

[5] "FMC Technologies, Woodside Echo Yodel Australia." www.fmctechnologies.com.

[6] M. Kimura and K. Shimamoto, "Development of New 17Cr Stainless Steel OCTG with Superior Corrosion Resistance," in *Eurocorr 2011*, 2011, no. 10, p. Paper No.4538.

[7] S. Hashizume, Y. Inohara, and K. Masanura, "Effects of pH and $pH_2S$ on SSC Resistance of Martensitic Stainless Steel," *NACE Corros. 2000*, no. 00130.

[8] T. Hara and H. Asahi, "Effect of δ-ferrite on sulfide stress cracking in a low carbon 13 mass% chromium steel," *ISIJ Int.*, vol. 40, no. 11, pp. 1134–1141.

[9] K. Kondo, H. Amaya, T. Ohmura, and K. Moriguchi, "Effect of Cold Work on Retained Austenite and on Corrosion Performance in Low Carbon Martensitic Stainless Steels," *NACE Corros. 2003*, no. 03094, 2003.

[10] M. Kimura, Y. Miyata, T. Toyooka, and Y. Kitahaba, "Effect of Retained Austenite on Corrosion Performance for Modified 13 % Cr Steel Pipe," *Corrosion*, vol. 57, no. 5, pp. 433–439, 2001.

[11] M. Walters, "Determination of $H_2S$ Concentration by Iodometric Titration - Unpublished work conducted at Exova Corrosion Centre." 2011.

[12] S. Sakamoto, K. Maruyama, H. Asahi, and H. Kaneta, "Effects of Environmental Factors on SSC Property of Modified 13Cr Steels In Oil and Gas Fields," *NACE Corros. 97*, no. 21, 1997.

[13] M. Meng, J; Skogsberg, J; Chambers, B; Kimura, "Environmentally Assisted Cracking Testing of High Strength 15Cr Steel in Sour Well Environments," in *Corrosion 2011*, 2011, no. 11100, pp. 9–16.

[14] H. Amaya and M. Ueda, "Effect of Test Solution Compositions on Corrosion Resistance of 13Cr Materials in a Little Amount of $H_2S$ Environment," in *CORROSION 99*, 1999, no. 585.

[15] H. Marchebois, H. El Alami, J. Leyer, and A. Gateaud, "Sour Service Limits of 13%Cr and Super 13%Cr Stainless Steels for OCTG: Effect of Environmental Factors," in *NACE Corrosion 2009*, no. 09084.

[16] M. Cayard and R. Kane, “Serviceability of 13Cr Tubulars in Oil and Gas Production Environments,” *Corros. 98*, no. 112, 1998.

[17] R. D. Kane, “Safe Operating Windows for Martensitic & Duplex Stainless Steels,” *Present. to ISO 15156 Maint. Panel Meet.*, 2007.

[18] P. I. Nice and J. W. Martin, “Application Limits for Super Martensitic and Precipitation Hardened Stainless Steel Bar-Stock Materials,” in *NACE corrosion 2005*, 2005, no. 05091.

[19] H. Takabe, M. Ueda, J. W. Martin, and P. I. Nice, “Application Limits for 110 ksi Strength Grade Super 13Cr Steel in $CO_2$ Environments Containing Small Amounts of $H_2S$,” in *NACE Corrosion 2009*, 2009, no. 09083.

[20] P. Dent, “Review of SSC Limits for 110ksi High Strength 13-5-2 Martensitic Stainless Steels,” *Presentation to ISO 15156 Maintenane Panel*, 2011. .

[21] JFE, “JFE-UHP-15CR-125.” pp. 28–30, 2013.

[22] H. Takabe, H. Amaya, Y. Otome, M. Ueda, K. Kondo, T. Ohe, and S. Nakatsuka, “The Effect of Alloying Elements on Environmental Cracking Resistance of Stainless Steels in $CO_2$ Environments with and without Small Amount of $H_2S$,” in *NACE Corrosion 2012*, 2012, pp. C2012–0001277.

[23] G. F. Silva, S. S. M. Tavares, J. M. Pardal, M. R. Silva, and H. F. G. Abreu, “Influence of Heat Treatments on Toughness and Sensitization of a Ti-alloyed Supermartensitic Stainless Steel,” *J. Mater. Sci.*, vol. 46, no. 24, pp. 7737–7744, Jul. 2011.

[24] P. Linhardt, G. Ball, S. Strobl, and R. Haubner, “Application of the EPR-Test to 13 % Chromium Stainless Steels,” in *Eurocorr 2011*, 2011, p. 4925.

[25] J. Maier, B. Kinsella, S. Bailey, T. Becker, and T. Ladwein, “Local Electrochemistry and Scanning Probe Microscopy Techniques to Clarify Intergranular Cracking Phenomena in Weldable Martensitic Stainless Steels,” in *CORROSION 2009*, 2009, p. 09088.

[26] D. Sidorin, D. Pletcher, and B. Hedges, “The electrochemistry of 13% chromium stainless steel in oilfield brines,” *Electrochim. Acta*, vol. 50, no. 20, pp. 4109–4116, Jul. 2005.

[27] H. Marchebois, J. Leyer, and B. Orlans-Joliet, “SSC Performance of a Super 13% Cr Martensitic Stainless Steel for OCTG: Three-Dimensional Fitness-for-Purpose Mapping According $pH_2S$, pH and Chloride Content,” in *NACE Corrosion 2007*, 2007, no. 07090.

[28] C.-M. Lee, P. E. Kvaale, S. L. Stome, S. Bond, and R. E. Lye, “Corrosion Testing of Weldable 13%Cr Supermartensitic Stainless Steel For Weld Procedure Qualification,” *NACE Corros. 2012*, no. C2012–0001245, 2012.

[29] J. Enerhaug, S. Olsen, U. Steinsmo, and O. Grong, “A New Approach to the Evaluation of Pitting Corrosion of Supermartensitic Weldments,” in *NACE Corrosion 2002*, 2002, p. 02039.

[30] “Nippon Steel & Sumitomo Metal, Seamless Steel Line Pipe.” Nippon Steel & Sumitomo Metal Corporation, http://www.nssmc.com, 2012.

[31] A. Hinds, G; Zhao, J; Griffith, A, J; Turnbull, “Hydrogen Diffusion in Super 13% Chromium Martensitic Stainless Steel,” *Corrosion*, vol. 61, no. 4, pp. 348–354, 2005.

[32] A. Turnbull, “Effect of Sodium Acetate Buffer on Electrochemistry and Corrosion - Unresolved Issues,” in *Private communication*, 2005.

[33] “ISO 11960 - Petroleum and Natural Gas Industries - Steel Pipes for use as Casing or Tubing for Wells.” ISO, 2011.

[34] “ISO 15156 Maintenance Panel meeting Minutes,” Stockholm, 2011.

[35] “Sumitomo Metals, SM17CRS-125.” Sumitomo Metal Industries Ltd, http://www.sumitomo-tubulars.com, pp. 4–7.

[36] S. Huizinga and R. Ohm, “Qualification and Application Limits of Weldable Supermartensitic 13Cr Linepipe Steels,” *Corros. 2001*, no. 01093, 2001.

[37] JFE Steel Corporation, “JFE OCTG,” *JFE Data Sheet*, vol. Cat.No E1E, 2012.

[38] Tenaris, “Tenaris 13Cr Grades - Data Sheet.” 2013.

[39] “Nippon Steel & Sumitomo Metal, Seamless Casing & Tubing.” Nippon Steel & Sumitomo Corporation, http://www.nssmc.com/, 2012.

[40] Vallourec, “OCTG product selection guide,” 2010.

[41] A. Bojack, L. Zhao, P. F. Morris, and J. Sietsma, “In-situ Determination of Austenite and Martensite Formation in 13Cr6Ni2Mo Supermartensitic Stainless Steel,” *Mater. Charact.*, vol. 71, pp. 77–86, Sep. 2012.

[42] M. Ueda, T. Mori, H. Amaya, K. Kondo, and K. Ueda, “Corrosion Resistance of Weldable Super 13Cr Stainless Steel in $H_2S$ Containing $CO_2$ Environments,” *Corros. 96*, p. Paper No. 58, 1996.

[43] J. Enerhaug, “A Study of Localised Corrosion in Super Martensitic Steel Weldments,” The Norwegian University of Science and Technology (NTNU), Trondheim, Norway., 2002.

[44] A. Turnbull and A. Griffiths, “NPL Report MATC(D)83 - Corrosion and cracking of weldable 13 Cr martensitic stainless steels: a review,” 2002.

[45] J. Enerhaug, P.-E. Kvaale, M. Bjordal, J. M. Drugli, and T. Rogne, “Qualification Of Welded Super 13%Cr Martensitic Stainless Steels for the Asgard Field,” *NACE Corros. 99*, no. Paper No.587, 1999.

[46] S. Olsen and J. Enerhaug, “Common Pitfalls During SSC and Pitting Testing of Supermartensitic Stainless Steels for Use in Pipelines,” in *NACE Corrosion 2002*, p. Paper 02038.

[47] R. Kane, J. Skogsberg, J. Meng, and B. Chambers, “New Evaluation and Qualification Protocol for Stainless Steel Tubulars for $H_2/CO_2$ Service,” *EuroCorr09, Sept.*, p. Paper No. 8065, 2009.

[48] A. Smirnova, R. Johnsen, and K. Nisancioglu, “Influence of Temperature and Hydrostatic Pressure on Hydrogen Diffusivity and Permeability in 13%Cr Super Martensitic Stainless Steel Under Cathodic Protection,” in *NACE Corrosion 2010*, 2010, no. 10292, pp. 1–10.

[49] P. D. Bilmes, M. Solari, and C. L. Llorente, “Characteristics and Effects of Austenite Resulting from Tempering of 13Cr–NiMo Martensitic Steel Weld Metals,” *Mater. Charact.*, vol. 46, no. 4, pp. 285–296, Apr. 2001.

[50] J. Ramirez, “Effect of PWHT on The Heat-Affected Zone Properties of Super-Martensitic Stainless Steel Pipes,” *NACE Corros. 2004*, no. 04136.

[51] J. Ramirez, “Mechanical Properties and Hydrogen Induced Stress Corrosion Cracking of Super 13Cr Steel Welded Joints,” *Corros. 2006*, no. 06140, pp. 1–28, 2006.

[52] K. Kondo, K. Ogawa, H. Amaya, M. Ueda, and H. Ohtani, “Development of Weldable Super 13Cr Martensitic Stainless Steel for Flowline,” in *International Offshore and Polar Engineering Conference*, 2002, vol. 3, pp. 303–309.

[53] K. Nose and H. Asahi, “Effect Of Microstructure On Corrosion Resistance of a Martensitic Stainless Linepipe,” in *NACE Corrosion 2000*, no. 00145.

[54] P. D. Bilmes, C. L. Llorente, L. Saire Huamán, L. M. Gassa, and C. A. Gervasi, “Microstructure and Pitting Corrosion of 13CrNiMo Weld Metals,” *Corros. Sci.*, vol. 48, no. 10, pp. 3261–3270, Oct. 2006.

[55] “NACE TM0177-2005-Standard Test Method - Laboratory Testing of Metals for Resistance to Sulphide Stress Cracking and Stress Corrosion Cracking in $H_2S$ Environments.” NACE International, Houston, Texas, 2005.

[56] A. Smirnova, R. Johnsen, and K. Nisancioglu, “Effect of tensile stress on hydrogen permeation in 13% Cr supermartensitic stainless steel,” in *Eurocorr 2010*, 2010, p. Paper No.9474.

[57] “NACE TM0284-11-Standard Test Method Evaluation of Pipeline and Pressure Vessel Steels for Resistance to Hydrogen-Induced Cracking.” NACE International, Houston, Texas, 2011.

[58] P. J. Cooling, M. B. Kermani, J. W. Martin, and P. I. Nice, “The Application Limits of Alloyed 13%Cr Tubular Steels for Downhole Duties,” *NACE corriosion 98*, no. 94, 1998.

[59] M. Kimura, Y. Miyata, T. Toyooka, Y. Nakano, F. Murase, and K. Takojima, “Effect Of Test Method On SSC Performance Of Modified 13Cr Steel,” *NACE Corros. 98*, no. 114.

[60] A. Turnbull and A. Griffiths, “Review: Corrosion and Cracking of Weldable 13 wt-%Cr Martensitic Stainless Steels for Application in the Oil and Gas Industry,” *Corros. Eng. Sci. Technol.*, vol. 38, no. 1, pp. 21–50, Mar. 2003.

[61] R. Case, R. Newman, S. Olsen, and G. Rorvik, “Pit Growth Behavior of Modified 13 Cr Steel in Sour Environments,” *Eurocorr 2000*, 2000.

[62] P. Dent, C. Fowler, M. Walters, B. Connolly, M. Ueda, M. Amaya, and H. Takabe, “Evaluation of the Seabed Temperature Corrosion and Sulphide Stress Cracking Resistance of Weldable Martensitic 13% Chromium Stainless Steel,” *Corros. 2013*, p. Paper No. 2589, 2013.

[63] B. Chambers, R. Kane, and M. Yunovich, “Implications Of Temperature And Buffering Systems For Laboratory Testing Of Alloy Steel And 13Cr Materials In Oil And Gas Production Environments,” in *Corrosion 2011*, 2011, no. 11096, p. Paper no. 11096.

[64] J. Crolet and J. Leyer, “Use and abuse of artificial acetate buffering in standardized and application specific testing,” *Corros. 2004*, no. 04140, p. Paper No. 04140, 2004.

[65] J. Drugli, M. Svenning, and S. Axelsen, “The Effect of Using Buffered Solutions in Corrosion Testing of Alloyed 13% Cr Martenistic Stainless Steels for Mildly Sour Applications,” *Corros. 99*, no. 586, p. Paper No. 586, 1999.

[66] J. Meng, J. Chambers, M. Yunovich, and R. Kane, “What is Really Known About Using 13Cr Tubulars in Sour Service ?,” *Mater. Perform.*, vol. 50, no. 8, pp. 72–78, 2011.

[67] T. Sunaba, H. Honda, and Y. Tomoe, “Localised Corrosion Performance Evaluation of CRAs in Sweet Environments with Acetic Acid at Ambient Temperature and 180degC,” in *Corrosion 2010*, 2010, no. 10335, p. Paper No. 10335.

[68] A. Griffiths and A. Turnbull, “Issues in Testing Corrosion and Environmentally Assisted Cracking of Super 13Cr Stainless Steel,” in *Supermartensitics 2002*, 2002, p. Paper No. 010.

[69] *EFC 17-2nd Edition, Corrosion Resistant Alloys for Oil and Gas Production: Guidance and Test Methods for $H_2S$ Service*, 2nd ed., no. May. Maney, 2002.

[70] *EFC17-1st Edition, Corrosion Resistant Alloys for Oil and Gas Production: Guidance and Test Methods for $H_2S$ Service*. Maney, 2002.

[71] *NACE TM0177-1996-Standard Test Method - Laboratory Testing of Metals for Resistance to Sulphide Stress Cracking and Stress Corrosion Cracking in $H_2S$ Environments*. Houston, Texas: NACE International, 1996.

[72] Y. Ishiguro, Y. Miyata, T. Nakahashi, T. Suzuki, M. Kimura, H. Sato, and K. Shimamoto, “Enhanced Corrosion-Resistant Stainless Steel OCTG of 17Cr for Sweet and Sour Environmnets,” in *NACE Corrosion 2013*, pp. 51313–02436–SG.

[73] T. Ronge, H. I. Lange, Svenning, A. Aldstedt, S. J-K, E. Ladanova, S. Olsen, R. Howard, and R. Leturno, “Intergranular Corosion / Cracking of weldable 13% Cr Steel at Elevated Temperature,” in *NACE Corrosion 2002*, no. 02428.

[74] Y. Miyata, M. Kimura, T. Koseki, T. Toyooka, and F. Murase, “Martensitic Stainless Steel Seamless Linepipe with Superior Weldability and $CO_2$ Corrosion Resistance,” *NACE Corros. 97*, no. 19, 1997.

[75] *NACE Standard MR0175-2002, Sulphide Stress Cracking Resistant Metallic Materials for Oilfield Equipment*. Houston, Texas: NACE International, 2002.

[76] *EFC 16-3rd Edition, Guidelines on Materials Requirements for Carbon and Low Alloy Steel for $H_2S$-Containing Environments in Oil and Gas Production*, no. July. Maney, 2009.

[77] *NACE MR0175 / ISO 15156-2: Petroleum and Natural Gas industries — Materials for use in H2S-Containing Environments in Oil & Gas Production - Part 2: Cracking-Resistant Carbon and Low-Alloy Steels, and the use of Cast Irons*. 2009.

[78] “NACE TM0198-11-Standard Test Method Slow Strain Rate Test Method for Screening Corrosion- Resistant Alloys for Stress Corrosion Cracking in Sour Oilfield Service,” no. 21232. NACE International, Houston, Texas, 2011.

[79] *ASTM G38 - Standard Practice for Making and Using C-Ring Stress Corrosion Specimens*. West Conshohocken, PA, USA: ASTM International, 2013.

[80] “ISO 7539-5: Corrosion of Metals and Alloys - Stress Corrosion Testing - Part 5: Preparation and use of C-ring Specimens.” ISO, 1989.

[81] *ASTM A370-Standard Test Methods and Definitions for Mechanical Testing of Steel Products*. West Conshohocken, PA, USA: ASTM International, 2012.

[82] *ASTM E8 - Standard Test Methods for Tension Testing of Metallic Materials*. West Conshohocken, PA, USA: ASTM International, 2013.

[83] *ASTM G39-99 - Standard practice for preparation and use of Bent-Beam stress-corrosion test specimens*, vol. 99, no. Reapproved 2011. West Conshohocken, PA, USA: ASTM International, 2011.

[84] *ISO 7532-2, Corrosion of metals and alloys - Stress corrosion testing - Part 2: Preparation and use of bent-beam specimens*. ISO, 1989.

[85] "BP ETP Guidance Note, GN 36-018, Standardised Test Method for Four-Point Bend Stress Corrosion Cracking Tests," 2009.

[86] "OTI 95 635, A Test Method to Determine the Susceptiblity to Cracking of Linepipe Steels in Sour Service." Her Majesty's Stationary Office, Norwich, UK, 1996.

[87] S. Nodland, K. D. Fatehi, and P. Dent, "Large and Small Scale SSC/SCC Testing of 316L Clad at 135degC," *Corros. 2009*, no. 09364, pp. 1–15.

[88] *ISO 7539-7 : 2005, Corrosion of metals and alloys - Stress corrosion testing - Part 7: Method for slow strain rate testing*, 2nd ed. ISO, 2005.

[89] V. Nisbet, W, J, R; Hartman, R, H, C; Handel, G, "Rippled Strain Rate Test For CRA Sour Service Materials Selection," in *NACE Corrosion 97*, 1997, no. 58, p. Paper No. 58.

[90] N. Alonso-Falleiros, M. Magri, and I. G. S. Falleiros, "Intergranular Corrosion in a Martensitic Stainless Steel Detected by Electrochemical Tests," *Corrosion*, vol. 55, no. 8, pp. 769–778, Aug. 1999.

[91] *ASTM G108 - 94 (2010), Standard Test Method for Electrochemical Reactivation (EPR) for Detecting Sensitisation of AISI Type 304 and 304L Stainless Steels*, vol. 94, no. 2010. West Conshohocken, PA, USA: ASTM International, 2010.

[92] *ISO 12732 : 2006 Corrosion of Metals and Alloys - Electrochemical Potentiokinetic Reactivation Measurement using the Double Loop Method (based on Cihal's Method )*. ISO, 2006.

[93] L. Smith and M. Celant, "Martensitic Stainless Steels in Context," *Supermartensitic 2002*, 2002.

[94] J. Enerhaug, S. L. Eliassen, and P. E. Kvaale, "Qualification of Welded Super 13%Cr Martensitic Stainless Steels for Sour Service Applications," in *NACE Corrosion 97*, 1997, no. 60, p. Paper No. 60.

[95] H. Van der Winden, P. Toussaint, and L. Coudreuse, "Past , Present and Future of Weldable Supermartensitic Alloys," in *Stainless Steel World Conference & Exhibition*, 2005.

[96] W. Van Gestel, "Girth weld failures in 13Cr sweet wet gas flow lines," *Corros. 2004*, no. 04141, p. Paper No. 04141, 2004.

[97] S. Huizinga and R. Ohm, "Experiences with Qualification of Weldable Martensitic Stainless Steel Pipe," *Corros. 2003*, no. 03092, 2003.

[98] M. E. Wilms, S. Huizinga, J. G. de Jong, W. E. Liek, and G. A. M. Radrum, "Susceptibility of Weldable Martensitic Stainless Steel (13Cr) Pipelines to Internal Cracking," in *NACE Corrosion 2006*, no. 06493.

[99] A. Turnbull and B. Nimmo, "Stress Corrosion Testing of Welded Supermartensitic Stainless Steels for Oil and Gas Pipelines," *Corros. Eng. Sci. Technol.*, vol. 40, no. 2, pp. 103–109, Jun. 2005.

[100] C. P. Linne, F. Blanchard, G. C. Guntz, and B. J. Orlans-Joliet, “Corrosion Performances of Modified 13Cr for OCTG in Oil And Gas Environments,” in *NACE Corrosion 97*, no. 28.

[101] M. Dickson, “The significance of texture parameters in phase analysis by X-ray diffraction,” *J. Appl. Crystallogr.*, pp. 176–180, 1969.

[102] *ASTM E23-Standard Test Methods for Notched Bar Impact Testing of Metallic Materials*. West Conshohocken, PA, USA: ASTM International, 2012.

[103] A. Turnbull and W. Nimmo, “NPL REPORT DEPC MPE 007 Methodology for Determining the Resistance of Welded Corrosion Resistant Alloys to Stress Corrosion using the Four-Point Bend Method,” 2004.

[104] *ASTM E384 - Standard test method for knoop and vickers hardness of materials*. West Conshohocken, PA, USA: ASTM International, 2010.

[105] P. I. Nice and J. W. Martin, “Sulphide Stress Cracking (SSC) Resistance Limits For A 125 ksi Grade High Strength Low Alloy OCTG Developed For Mildly Sour Service,” *Corros. 2010*, no. 10307, pp. 1–13, 2010.

[106] R. T. Kiepura and B. R. Sanders, *Metals Handbook Ninth Edition, Volume 9, Metallography and Microstructures*, December 1. Ohio 44073: American Society for Metals, 1985.

[107] L. Zhao, N. H. Van Dijk, and E. Bru, “Magnetic and X-ray diffraction measurements for the determination of retained austenite in TRIP steels,” *Mater. Sci. Eng.*, vol. 313, pp. 145–152, 2001.

[108] *ASTM E975-13, Standard Practice for X-Ray Determination of Retained austenite in Steel with Near Random Crystallographic Orientation*, vol. 1. West Conshohocken, PA, USA: ASTM International, 2013.

[109] Y. Su, L. Chiu, T. Chuang, C. Huang, C. Wu, and K. Liao, “Retained austenite amount determination comparison in JIS SKD11 steel using quantitative metallography and X-ray diffraction methods,” *Adv. Mater. Res.*, vol. 482–484, pp. 1165–1168, 2012.

[110] *ASTM G59, Standard Test Method for Conducting Potentiodynamic Polarization Resistance Measurements*, vol. 97, no. 2014. West Conshohocken, PA, USA: ASTM International, 2014.

[111] N. G. Thompson and J. H. Payer, *DC Electrochemical Test Methods*. Houston, Texas: NACE International, 1998.

[112] *ASTM G5-Standard Reference Test Method for making Potentiodynamic Anodic Polarisation Measurements*. West Conshohocken, PA, USA: ASTM International, 2013.

[113] *ASTM G61 - Standard Test Method for Conducting Cyclic Potentiodynamic Polarization Measurements to Determine the Corrosion Susceptibility of Irin-, Nickel-, or Cobalt-Based Alloys*. West Conshohocken, PA, USA: ASTM International, 1986.

[114] *TR2023-Version 4, $H_2S$ Cracking Resistant Materials*, Version 4. Statoil, 2012.